This is to certify that the
dissertation entitled

THE ROLE OF HYPOXIA INDUCIBLE FACTORS IN LUNG DEVELOPMENT AND COBALT-INDUCED LUNG INJURY

presented by

YOGESH SAINI

has been accepted towards fulfillment
of the requirements for the

Ph.D. degree in Genetics

Major Professor's Signature

December 18, 2009

Date

THE ROLE OF HYPOXIA INDUCIBLE FACTORS IN LUNG DEVELOPMENT AND COBALT-INDUCED LUNG INJURY

By

Yogesh Saini

A DISSERTATION

Submitted to
Michigan State University
in partial fulfillment of the requirements
for the degree of

DOCTOR OF PHILOSOPHY

Genetics

2009

ABSTRACT

THE ROLE OF HYPOXIA INDUCIBLE FACTORS IN LUNG DEVELOPMENT AND COBALT-INDUCED LUNG INJURY

By

Yogesh Saini

The increasing use of disposable electronics and growing industrialization of nation's economies have drastically raised the risk of exposure to toxic metals. One of these metals, cobalt, is used widely in several industries involved in the production of coloring agent for ceramics, hard metal alloys, sintered carbides, drilling and grinding tools. Cobalt (or hard metal) asthma caused by the inhalation of cobalt containing dust is characterized by airway constriction, alveolitis, fibrosis and associated giant cell interstitial pneumonitis. The characterization of cobalt-induced toxicities demands comprehensive understanding of the effects of toxicants on cell signaling and the downstream changes in gene expression. It is well established that cobalt is a hypoxia mimic due to its ability to induce hypoxia-like gene expression responses. To enhance our understanding of cobalt-induced toxicity and determine the role of its ability to mimic hypoxia signaling in the process, we generated a doxycycline inducible lung-specific Hypoxia inducible factor 1α (HIF1α) deficient system in mice.

In utero, lung specific deletion of HIF1α resulted in altered surfactant metabolism and defects in alveolar epithelial differentiation that led to premature death due to respiratory distress. In contrast, the *in utero* deletion of HIF2α (another prominent form of HIFα) from the lungs did not affect the viability

of neonates. Interestingly, the removal of both HIF1α and HIF2α from the lungs during development led to the birth of phenotypically normal pups, suggesting that the loss of HIF2α can rescue the lethal phenotype associated with the loss of HIF1α from the lungs. Microarray analysis of the lungs from HIF1αΔ/Δ, HIF2 αΔ/Δ and HIF1/2 αΔ/Δ identified sets of genes, involved in various cellular pathways such as surfactant metabolism and vesicular trafficking that were specifically affected in the HIF1αΔ/Δ neonates and these results suggest possible mechanistic information for the role of HIFs in lung development.

In order to elucidate the role of epithelial derived-HIF1α signaling in cobalt-induced lung injury, we deleted the transcription factor postnatally. These mice were exposed to cobalt chloride via oropharyngeal aspiration. Compared to control mice, mice that were HIF1α deficient in their lungs exhibited airway infiltration of eosinophils associated with airway epithelial changes, including mucus cell metaplasia and increased levels of the chitinase-like proteins YM1 and YM2. These results suggested that airway epithelial-derived HIF1α plays a critical role in modulating the inflammatory response of the lung. Moreover, its disruption leads to a tissue that is biased towards a Th2-like response and exhibits an asthma-like phenotype following cobalt challenge. Taken together, the striking differences observed following cobalt exposure in the two mice suggests that they will be a powerful tool to understand the relationship between allergy-induced asthma, hypoxia, and inflammation.

ACKNOWLEDGMENTS

I would like to take this opportunity to express my profound gratitude to my advisor Dr. John J. LaPres who gave me the opportunity to work in his lab under his quality mentorship. I want to thank him for his sincere guidance, generous time, patience, encouragement and continuous support throughout my research work. His precious scientific advice and great attitude towards science compelled me to adopt those elite qualities in my developing scientific career which I will take with me through my entire career. I feel extremely fortunate to have Dr. LaPres as my major advisor.

I greatly appreciate my guidance committee members; Dr. Jack R Harkema, Dr. A. Daniel Jones, Dr. Robert A Roth, and Dr. Susan L Ewart for their great help, insightful comments and constructive discussions. I am indebted to them for their valuable suggestions and continued inputs to improve my research progress as well as my scientific career.

I am thankful to the Genetics Program and Dr. Barbara Sears (Director, Genetics Program) for accepting me in to the program which gave me great opportunity to enhance my scientific career. I sincerely thank Jeannine Lee for all her help from the day I submitted my application for admission to the program. I would also like to thank Environmental and Integrative Toxicology Program executive committee for providing me opportunity to gain expertise in Toxicology as my second PhD major.

I am obliged to Kyung Y. Kim, Christian Merrill and Krista Greenwood for their help in my research work. I would like to thank all the lab members from Dr. Harkema's laboratory, especially Lori Bramble, Ryan Lewandowski, Dr. Daher I Aibo, Dr. Neil Birmingham, Dr. James Wagner and Dr. Daven Jackson for their endless help during my research work.

My sincere thanks are extended to all current and former colleagues in Dr. LaPres's laboratory, especially Dr. Ajith Vengellur, Dr. Scott G Lynn, Dorothy M Tappenden, Heyjin Hwang, Kyunghee Burkitt, Steven Proper, Amy Bays and Dr. Kang Ae Lee for all their kind help, cooperation, and friendly atmosphere. I also want to thank all my friends and colleagues in Genetics Program, Integrative Toxicology Program and Biochemistry and Molecular Biology Department. I also want to thank my friends Vishal, Shipra, Ram and Anita for their kind help and providing me a very friendly atmosphere.

I greatly appreciate ULAR and Human Histopathology Division for their help in my research work.

I thank with all my heart to my parents for their encouragements, love and support which motivated me to accomplish all my educational aims. Finally, my special thanks go to my dear wife, Sonika Patial who has been a source of motivation during all those tough moments. It is a very special year of my life as we were blessed with our baby boy, Krish on 15th November.

TABLE OF CONTENTS

LIST OF TABLES

LIST OF FIGURES

Images in this dissertation are presented in color

KEY TO ABBREVIATIONS

ANOVA	Analysis of Variance
ARNT	Aryl hydrocarbon receptor nuclear translocator
ATP	Adenosine triphosphate
C/EBP	CAAT/enhancer-binging protein
CBP	CREB binding protein
CCSP	Clara cell secretory protein
COPD	Chronic obstructive pulmonary disease
CRE	Cyclization recombination
CREB	cAMP response element binding
DFO	Desferrioxamine
DMOG	Dimethyloxaloglutarate
DPPC	Dipalmitoylphosphatidylcholine
DTT	Dithiothreitol
EDTA	Ethylenediaminetetraacetic acid
EMT	Epithelial-mesenchymal transition
EPO	Erythropoietin
ETC	Electron transport chain
Foxa2	Forkhead box A2
H&E	Hematoxylin and eosin

HAPE	High-altitude pulmonary edema
HGPRT	hypoxanthine guanine phosphoribosyl transferase
HIF	Hypoxia inducible factor
HNF	Hepatocyte nuclear nactor
HO-1	Haemoxygenase-1
HRE	Hypoxia responsive element
IgE	Immunoglobulin isotype E
IgG	Immunoglobulin isotype G
IL	Interleukin
Lb	lamellar bodies
LoxP	Locus of crossover in P1
MEF	Mouse embryonic fibroblast
MTF-1	Metal transcription factor-1
mv	Microvilli
NFκB	Nuclear factor-kappa B
ODD	Oxygen-dependent degradation domain
PAS	Per/Arnt/Sim
PAS	Periodic acid Schiff
PFK-1	Phosphofructokinase-1
PHD	Prolyl hydroxylase domain protein
PMSF	Phenylmethylsulphonyl fluoride

PN	Postnatal
pO_2	Partial pressure of oxygen
pVHL	von Hippel-Lindau protein
RDS	Respiratory distress syndrome
RIPA	Radioimmunoprecipitation assay
ROS	Reactive oxygen species
RT-PCR	Reverse transcriptase-polymerase chain reaction
rtTA	Reverse tetracycline transactivator
SDS-PAGE	Sodium dodecyl sulfate polyacrylamide gel electrophoresis
SEM	Standard error of mean
SP-C	Surfactant protein C
TAD	Transactivation domain
TEM	Transmission electron microscopy
TF	Transferrin
TGF-β1	Transforming growth factor-beta 1
TNF-α	Tumor necrosis factor-alpha
VEGF	Vascular endothelial growth factor
μm	Micrometer

Introduction

1. Oxygen

Oxygen is the third most abundant element, after hydrogen and helium, in the universe and makes up nearly 21% of the earth's atmosphere. Oxygen is the most important factor for the viability of living systems, except for obligate anaerobes. Oxygen acts as the ultimate electron acceptor in aerobic respiration and therefore, is critical for energy production in the form of adenosine triphosphate (ATP). Oxygen also acts as a substrate in various biosynthetic reactions as well as breakdown product in catabolic reactions [1].

The indispensable involvement of oxygen in energy generation and other critical cellular processes made it important to evolve sensing mechanisms for changes in oxygen availability. Evolutionary adaptation has selected various pathways to deal with oxygen tension fluctuations. These pathways regulate short- and long-term responses. Every organism, either unicellular or multicellular, possesses the ability to sense changes in the ambient oxygen and respond through alterations in metabolism and gene expression [2].

For strict aerobic unicellular organisms or cells in culture, oxygen comes from the atmosphere, either directly or dissolved in the surrounding medium. In multicellular organisms, however, oxygen is supplied by tissue bathing fluids containing dissolved or protein-bound oxygen delivered by

specialized respiratory organs or tissue systems to allow gas exchange. These respiratory systems consist of conducting zones leading to the gas exchange area where oxygen diffuses into the tissue bathing fluid (blood in mammals). Different organisms have evolved varying anatomical structures to obtain and circulate oxygen, including very simple structures (e.g. gills and trachea) to complex specialized structures (e.g. lungs). The mammalian respiratory system represents one of the most complex respiratory structures.

2. Anatomy and Development of the Respiratory System

2.A. Development of the lung

Human lung development initiates at third week of gestation (corresponds to E9.5 of mouse gestation) and proceeds through three chronological periods: embryonic, fetal period proper and postnatal periods. The fetal period proper is further divided in to three stages called pseudoglandular, canalicular and saccular. Since the process of differentiation proceeds from the center to the periphery of the lung asynchronously between lobes, there is significant overlap between these stages [3].

In humans, the embryonic period corresponds to 4-7 weeks after fertilization and represents the beginning of organ development. The lung appears, towards the end of the fourth week, as a bud ventral to the

prospective esophagus. As the laryngotracheal groove deepens, lung bud grows in to the surrounding mesenchymal matrix by successive dichotomous branching. By the end of the seventh week, the lobar, segmental and subsegmental portion of airway tree with high columnar epithelium is already formed [3].

Starting from the eighth week, the lung resembles a small tubuloacinar (epithelial) gland, hence, the stage is called as a pseudoglandular stage which runs from fifth week to seventeenth week (corresponds to E9.5 to E16.5 of mouse gestation). It is in this stage that continuous growth and branching of the peripheral portion of epithelial tube leads to the formation of prospective conductive airways and appearance of acinar outline. Epithelial-mesenchymal interactions regulate this growth and branching pattern. Removal of mesenchyme from the tip of a sprouting tube prevents further branching whereas plantation of mesenchyme alongside of a lower order tube results in the appearance of new branch [4, 5]. Moreover, the presence of collagen and mesenchyme is needed for branching and epithelial differentiation [6, 7]. By the twelfth week, mucous glands are present as solid sprouts from the epithelial layer and acquire canal and secretory activities by the fourteenth week [8]. At the end of seventeenth week, acini are composed of stem tubule (prospective terminal bronchiole), 2-4 future respiratory bronchioles and small clusters of short tubules and buds.

The canalicular stage of lung development spans from week 17 to week 26 in humans (corresponds to E16.5 to E17.5 of mouse gestation). At this stage compact acinar clusters grow by three processes: peripheral branching, elongation of each tubular branch, and widening of the distal airspaces. Thus, the tubules until about three orders of branching are referred to as canaliculi. It is at this stage that capillarization starts taking place around the airspaces to establish close contact with the overlaying cuboidal epithelium lined with Type II cells. These contact points are the sites where the cuboidal epithelial cells decrease in height and transform into Type I cells. These type I cells have attenuated cytoplasmic processes and form the future air-blood barrier. The two processes, close apposition of capillary epithelium to the epithelial cells and the epithelial flattening are intimately related, but it is unclear which of the two processes induces the other. The air blood barrier transformation starts peripherally as the cuboidal (undifferentiated) epithelial cells (Type II cells) towards the center are needed for further growth and branching [3]. It has been shown that Type II cells can incorporate tritiated thymidine (cell division) and lose their granules to differentiate eventually into Type I cells [9]. A similar pattern of transformation has also been observed in damaged alveolar epithelium suggesting the stem cell role of Type II cells [10]. Similarly, it has been shown that the Clara cells, secretory cell type of the bronchioles, represents the progenitor cells of the bronchiolar epithelium [11].

Saccular stage of lung development represents period from week 24 to week 36 in humans (corresponds to E17.5 to PN6 of mouse gestation). In the terminal phase of the canalicular stage, the airways consist of clusters of relatively thin-walled terminal saccules and is referred to as saccular or terminal sac. These saccules give rise to the last generation of airways, some prospective alveolar ducts, and the alveolar sacs at the outermost periphery. Thus each canalicule, except the last branch, goes through the stages of being a saccule, then a smooth-walled channel, and after birth, when alveoli have formed, a typical alveolar duct. The vast elaboration of the air space coupled with marked decrease in interstitial tissue has an important consequence on the alveolar capillary arrangement. The capillaries network form a mesh round the airway channels and within the intersaccular septa as the airspaces approach each other. It is in the saccular stage that the pulmonary surfactant system matures (between week 29 and week 32 in humans).

At birth, the lung parenchyma structure is still in an immature state despite the complete branching pattern and number of airway generations. Neonatal human lung contains only 20 million alveoli, which represents approximately 10 % of the full population of 300 million observed in adult lung [12]. At birth, the rat lung consists of smoothly contoured ducts and saccules having thick primary septa and relatively thick layer of connective tissues. It

takes two postnatal weeks to transform these immature structures into alveolar ducts and alveoli lined with thin inter-alveolar septa [13, 14].

2.B. Anatomy of the Respiratory System

The mammalian respiratory system is composed of two major components: the conducting portion and the respiratory portion. The conducting portion, situated both outside and within the lungs, conveys air from the external milieu to the lungs whereas the respiratory portion, located strictly within the lungs, functions in the actual exchange of oxygen for carbon dioxide (external respiration). The conducting portion of the respiratory system is composed of the nasopharynx, trachea, primary bronchi, secondary bronchi (lobar bronchi), tertiary bronchi (segmental bronchi), bronchioles, and terminal bronchioles. The bronchial tree, stemmed from trachea, divides 15 to 20 times before reaching the level of the terminal bronchioles. The left and right lobes have 2 and 3 secondary bronchi (branches of the primary bronchi), also known as lobar bronchi, respectively. As these secondary bronchi enter the lobes of the lung, they subdivide into smaller branches, tertiary (segmental) bronchi. Each tertiary bronchus arborizes and leads to the formation of bronchioles. Each bronchiole supplies air to a pulmonary lobule. It is generally accepted that the bronchioles represent the 10^{th} to 15^{th} generation of dichotomous branching of the bronchial tree. Their diameter can vary among authors from 0.3mm to 5mm.

The epithelial lining of larger bronchioles is primarily ciliated simple columnar with occasional goblet cells whereas the smaller bronchioles have simple cuboidal (many with cilia) with occasional Clara cells and no goblet cells. Clara cells are columnar cells with dome-shaped apices that have short, blunt microvilli. Clara cell cytoplasm houses numerous secretory granules containing glycoproteins that protect bronchiolar epithelium. Additionally, these cells degrade toxins in the inhaled air via cytochrome P-450 enzymes in their smooth endoplasmic reticulum [15]. Some investigators suggest that Clara cells produce a surfactant-like material that reduces the surface tension of bronchioles and facilitates the maintenance of their patency [16]. It has been shown that Clara cells divide to regenerate the bronchiolar epithelium [17-20]. Thus, Clara cells forms a very important cell population lining the bronchiolar epithelium.

The respiratory portion of the respiratory system is composed of respiratory bronchioles, alveolar ducts, alveolar sacs, and alveoli. Terminal bronchiole branch to give rise to respiratory bronchioles and forms the first region of the respiratory system where exchange of gases can occur. Respiratory bronchioles are similar in structure to terminal bronchioles except that their walls are interrupted by the presence of thin-walled, pouch-like structures known as alveoli, where efficient gaseous exchange occurs. As respiratory bronchioles branch, they become narrower in diameter and their population of alveoli increases. Subsequent to several branchings, each

respiratory bronchiole terminates in an alveolar duct. Alveolar ducts do not have walls of their own; they are merely linear arrangements of alveoli. An alveolar duct that arises from a respiratory bronchiole branches, and each of the resultant alveolar ducts, usually ends as a blind outpouching composed of two or more small clusters of alveoli, known as an alveolar sac. Each alveolus is a small outpouching, about 200μm in diameter, of respiratory bronchioles, alveolar ducts, and an alveolar sac that is composed of highly attenuated type I pneumocytes (also known as type I alveolar cells or squamous alveolar cells) and larger type II pneumocytes (also known as great alveolar cells, septal cells, and type II alveolar cells). Approximately 95% of the alveolar surface is lined by type I pneumocytes which are highly flattened with cytoplasm thickness of approximately 80nm. The type II pneumocytes are more numerous than type I pneumocytes, however, they occupy only about 5% of the alveolar surface. The most distinguishing feature of these cells is the presence of membrane-bound lamellar bodies that contain pulmonary surfactant, the secretory product of these cells.

Pulmonary surfactants, heterogenous phospholipoproteinaceous material consisting of 90% lipids and 10% proteins, that are synthesized on the rough endoplasmic reticulum (RER) of type II pneumocytes. The surfactants are composed primarily of two phospholipids (dipalmitoylphosphatidylcholine (DPPC) and phosphatidylglycerol) a neutral lipid, and four unique proteins (surfactant apoproteins SP-A, SP-B, SP-C, and

SP-D). The surfactants are modified in the golgi apparatus and are then released from the *trans* golgi network into secretory vesicles, known as composite bodies, the immediate precursors of lamellar bodies. The lamellar body-bound surfactants are released via exocytosis into the lumen alveolar lumen where it forms a lattice-like network known as tubular myelin. The surfactants decrease surface tension, thus preventing atelectasis, namely the collapse of the alveolus. The surfactants are continuously manufactured by type II pneumocytes and are phagocytosed and recycled by type II pneumocytes and, less frequently, by alveolar macrophages. In addition to producing and phagocytosing surfactants, type II pneumocytes also act as precursor of type I pneumocytes.

Alveolar macrophages, also known as Dust Cells, phagocytize particulate matter in the lumen of the alveolus as well as in the interalveolar spaces. The circulating blood monocytes, after infiltrating into the pulmonary interstitium, become alveolar macrophages and migrate between Type I pneumocytes into the alveolar spaces. These cells phagocytose particulate matter, such as dust and bacteria, and thus maintain a sterile environment within the lungs. Alveolar macrophages also assist Type II pneumocytes in the recycling of surfactants. Approximately 100 million macrophages migrate to the bronchi each day and are transported from there by ciliary action to the pharynx to be eliminated by being swallowed or expectorated. Some alveolar

macrophages, however, reenter the pulmonary interstitium and migrate into lymph vessels to exit the lungs.

3. Mammalian Gas exchange

Mammals have one of the most advanced respiratory systems. In animal physiology, respiration is defined as the transport of oxygen from the outside air to the cells within tissues, and the simultaneous transport of carbon dioxide in the opposite direction. This is different from cellular respiration, which is a biochemical oxidation pathway by which cells release energy from the chemical bonds of food molecules (e.g. glucose) and provide that energy for the essential processes of life.

In humans and other mammals, physiological respiration involves four steps: Ventilation, the process of moving ambient air in to and out of alveolar space. Pulmonary gas exchange or external respiration, the process of gaseous exchange between the alveoli and the pulmonary capillaries. Gas transport, movement of gases throughout the circulatory system to deliver oxygen to peripheral tissues and to transport carbon dioxide back to the pulmonary gas exchange site. Peripheral gas exchange, the transfer of gases between the tissue capillaries and the tissues/cells.

The respiratory and cardiovascular systems work in concert to carry gases to and from the tissues. Veins carry deoxygenated blood from

peripheral tissues to the right atrium of the heart that transfers the blood to the right ventricle. The right ventricle pumps blood through the pulmonary artery towards the lungs. The pulmonary artery branches out to form capillary beds around the alveoli in close apposition to Type I pneumocytes to form 200-600 nm thick blood-gas barrier (alveolar-capillary barrier) [21]. Blood oxygenated at the blood-gas barrier is carried via the pulmonary vein to the left heart from where oxygenated blood (pO_2: 100mmHg) is pumped into the aorta and eventually to the whole body.

The pO_2 in capillaries varies among different tissues and within the tissues depending upon the location and physiological state. For example, within the liver lobules, the pO_2 varies depending on the proximity to the blood carrying vessels. The pO_2 of hepatic artery is 95-105 mmHg whereas the pO_2 of vena cava is approximately 40-45 mmHg [22]. At normal oxygen concentration, oxygen levels within the body vary between tissue and cell types. For instance, oxygen concentration required for normal brain function is uniformly higher than that for the muscles. Thus, a range of pO_2 is found in different tissues makes some tissues or organs more prone to oxygen deficit, a condition known as hypoxia.

4. Hypoxia

4.A. Biological Significance

The normal pO_2 state is known as normoxia and when the pO_2 in the cell or tissue drops below this normal level, a state of hypoxia is said to exist. In the systemic context, hypoxia is categorized into four subcategories: hypoxic, anemic and circulatory hypoxia. Hypoxic hypoxia arises due to decrease in ambient oxygen partial pressure attributed to hypoventilation or altitude. Anemic hypoxia results from decreased hemoglobin concentration that leads to declined oxygen-carrying capacity of the blood. Circulatory hypoxia arises because of impaired tissue perfusion [23].

In systemic or organ system context, the hypoxic conditions arise in normal physiological process as well as in pathological conditions. It is well known that mammalian embryos develop in a state of partial hypoxia (pO_2 = 20–30 mmHg) and hypoxic conditions within the embryo have been characterized in the neural tubes, heart, and intersomitic mesenchyme at an early stage of organogenesis [24]. This decreased oxygen availability is an important regulator of proper angiogenesis and tubulogenesis [25]. Studies have shown that fluctuation in oxygen tension within the uteroplacental environment is an important determinant of cellular events during trophoblastic invasion and the placental remodeling process [26]. In the pathological settings, hypoxia is a critical feature in several diseases, including cancer,

myocardial ischemia, cerebral ischemia, atherosclerosis, rheumatoid arthritis, and chronic obstructive pulmonary disease (COPD).

The lung's integral role in oxygen uptake and supply does not preclude it from being negatively impacted by hypoxia. Conditions like airway obstruction, intra-alveolar exudates, septal thickening by edema, inflammation, fibrosis, or damage to alveolar capillaries can induce localized hypoxic conditions within the lung. In airway inflammatory diseases like asthma, lung structure changes due to persistent inflammation pose obstruction to air flow, which leads to a hypoxic condition in the affected pulmonary tissue [27]. There is a correlation between allergic airway inflammatory diseases and the upregulation of hypoxia sensitive proteins such as glycolytic enzymes, prolyl-4-hydroxylase, peroxiredoxin 1, and arginase [28]. In the current discussion on hypoxia, it is clear that hypoxia and hypoxia induced downstream processes have both beneficial as well as detrimental roles in the biological system.

4.B. Cellular Responses to hypoxia

An active cell might use as much as 2×10^6 molecules of ATP per second. Many fundamental cellular processes, such as transcription, translation, metabolic reactions, cytoskeletal movements, and ion transport require ATP as a primary source of energy. Maintenance of a cellular homeostatic environment using ATP-dependent ion pumping systems such as the Na^+/K^+ ATPase requires 20 to 80% of the cellular metabolic energy.

Reduced ATP generation results in the loss of the cell's ability to maintain ionic and osmotic balance. Failure of these ion-motive ATPase leads to membrane depolarization, uncontrolled Ca^{2+} influx through voltage-gated Ca^{2+} channels, and subsequent activation of calcium-dependent phospholipases and proteases. These events result in uncontrolled cell swelling, hydrolysis of biomolecules, leakage of cellular compartments and eventually, to cell necrosis [29]. Since oxygen is the primary requirement in efficient ATP generation in mitochondria, hypoxia exhibit its affect through a compromised electron transport chain and reduced ATP generation. Cells have developed selective bypass processes responsible for alternate but efficient energy conservation or generation. These adaptive and pro-survival processes include anaerobic glycolysis and reallocation of cellular energy between essential and nonessential ATP demand processes.

Under hypoxia, cells switch to anaerobic glycolysis, a less efficient ATP generating process to meet their energy demands. This switch is turned on through allosteric regulation of phosphofructokinase-1 (PFK-1) activity and the overexpression of enzymes involved in anaerobic glycolysis [30]. PFK-1 catalyzes the conversion of fructose 6-phosphate to fructose 1,6-bisphosphate and is considered a major regulatory enzyme that controls carbon flux through glycolysis. PFK-1 is allosterically regulated by a number of metabolites. ADP, AMP and fructose-2,6-biphosphate are allosteric activators, whereas ATP and

citrate are the allosteric inhibitors of PFK-1. Under energy deficit (e.g. hypoxic conditions), the cellular AMP/ATP ratio is elevated which results in the activation of PFK-1 via an AMP activated protein kinase (AMPK) dependent process. AMPK activation has also been reported to recruit Glut-4 (glucose transporter) to the plasma membrane and to increase the expression of hexokinase as well as some mitochondrial enzymes involved in TCA cycle and electron transport chain (ETC) [31].

Another strategy adopted by cells to survive or adapt under hypoxic stress is reallocation of cellular energy between essential and nonessential ATP demand processes. Protein synthesis and ion motive ATPases account for more than 66% and 90% of ATP consumption in rat thymocytes and rat skeletal muscles, respectively [32]. The ATP consumption hierarchy is rearranged in energy deficit circumstances whereby Na^{+}/K^{+} pumping and Ca^{2+} cycling processes become the higher ATP consumers instead of replication, transcription, or translation [33].

Most of the adaptive hypoxic responses take place with in seconds through the activation or inhibition of already synthesized structural or regulatory proteins. However, some adaptive responses take place or are fine-tuned at the level of gene transcription or translation. As discussed in the

Figure 1.1. Domain structure of human HIFs.

HIF-α (HIF-1α, HIF-2α, HIF-3α), HIF-1β (ARNT), and ARNT2 belong to Per-ARNT-Sim (PAS) protein superfamily. HIF-α consists of four structural domains: basic Helix-Loop-Helix (bHLH) domain (blue), Per-ARNT-Sim (PAS) domain (green), oxygen-dependent degradation domain (ODD) (purple), and transactivation (TAD) domain (yellow). HIF-1β and ARNT2 lacks ODD but shares all the other three domains present in HIF-α. The presence of the ODD that makes HIF-α oxygen-labile. "Images in this dissertation are presented in color."

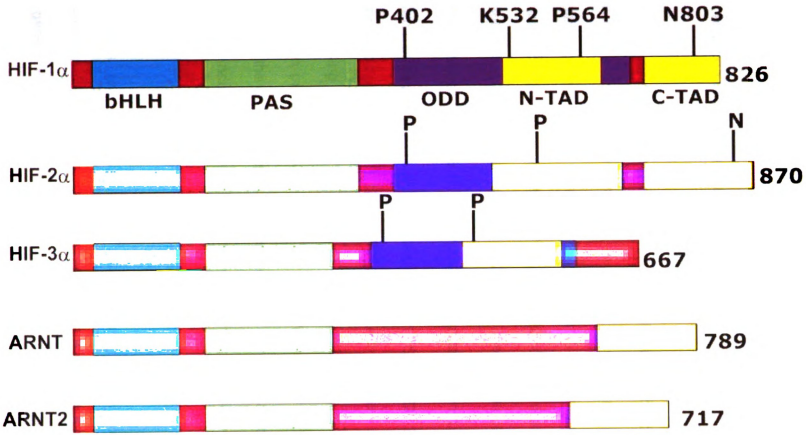
P402
K532
P564
N803
HIF-1α
826
bHLH
PAS
ODD
N-TAD
C-TAD
P
P
N
HIF-2α
870
P
P
HIF-3α
667
ARNT
789
ARNT2
717

next section, hypoxia-responsive transcription factors function at the hub of oxygen sensing machinery.

4.C. Hypoxia-responsive transcription factors

The oxygen sensing system consists of several hypoxia-responsive transcription factors that mediate regulation of genes responsible for maintaining or rescuing tissue perfusion and ATP generation, including vascular endothelial growth factor (VEGF), glycolyic enzymes, and glucose transporters. Several transcription factors are also influenced by hypoxia, including nuclear factor-κB (NFκB), cAMP response element binding (CREB), activator protein 1 (AP-1), p53, Stable Protein 1 (SP-1), SP-3, Early growth response factor 1 (EGR-1), CCAAT/enhancer-binding protein beta (C/EBPβ), GATA binding protein-2 (GATA-2) and signal transducers and activators of transcription protein (STAT5) [34]. Although these transcription factors are involved in the cellular response to decreases in oxygen availability, the family of hypoxia-inducible factors (HIFs) comprises the principal regulators of the transcriptional response to hypoxia.

HIFs are the most widely studied family of hypoxia responsive transcription factors and they directly influence the expression of more than 150 genes. HIFs belong to the basic Helix-Loop-Helix (bHLH)-Per/Arnt/Sim

Figure 1.2. Structure of human HIF1α protein and oxygen-dependent modification of HIF1α.

The stability and transcriptional activity of HIF1α is regulated in oxygen-dependent manner. The oxygen-dependent degradation domains contain conserved prolyl residues (P) 402 and 564 that undergo hydroxylation in the normoxia conditions. The hydroxylated prolyl residues, including acetylated lysyl (K-532) residue, form a binding site for von Hippel-Lindau tumor suppressor protein (pVHL). The oxygen-dependent hydroxylation of asparagyl residue (N-803) blocks the binding of CBP and p300 transcriptional regulators and consequently inhibits HIF1 mediated transcription. "Images in this dissertation are presented in color."

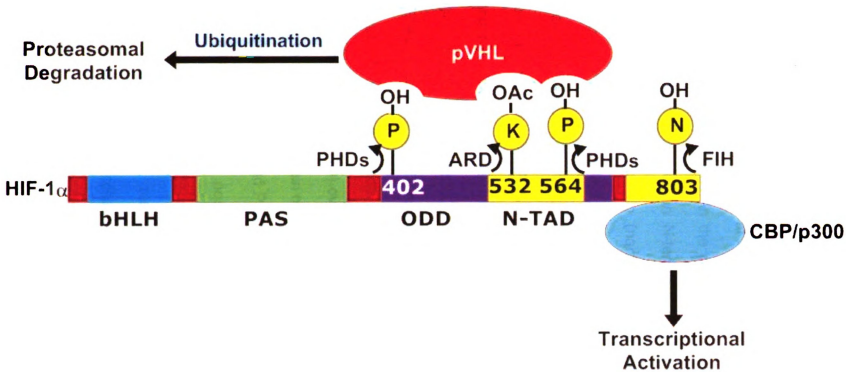
Proteasomal Degradation
Ubiquitination
pVHL
OH
OAc
OH
OH
P
K
P
N
PHDs
ARD
PHDs
FIH
HIF-1α
402
532 564
803
bHLH
PAS
ODD
N-TAD
CBP/p300
Transcriptional Activation

(PAS) superfamily of transcription factors [35] (Fig. 1.1). HIFs are heterodimeric factors consisting of α (HIF1α, HIF2α, and HIF3α) and β subunits (HIF1β (also known as aryl hydrocarbon nuclear translocator, ARNT) and ARNT2 [36]. These heterodimers bind at A/(G)CGTG consensus sites in the hypoxia response elements (HREs) in the promoter regions of hypoxia responsive genes. HIFs consists of an N-terminal basic helix-loop-helix (bHLH) domain, a central PAS domain (named for the three founding members of the family, Per, ARNT, and Sim) and two C-terminal transactivation domains (TADs) (Fig. 1.1). The bHLH acts to bind DNA and is a primary dimerization surface. The PAS domain is a secondary dimerization surface, dictating specificity of the interactions between various PAS proteins. The TAD closest to the C-terminus (C-TAD) is the primary activator of transcription. The interior TAD (N-TAD) has lower transactivation activity. The unique feature that sets HIFαs apart from HIFβs is the presence of an oxygen-dependent degradation domain (ODD) overlapping the N-TAD. These ODDs are responsible for rendering the protein oxygen labile. The ODD contains two conserved prolyl residues (Pro402 and Pro564 in human HIF1α; Pro402 and Pro577 in murine HIF1α) which are post-translationally hydroxylated under normoxic conditions [37] (Fig. 1.2). The family of enzymes, prolyl hydroxylase domain containing proteins (PHDs), responsible for this modification are related to the hydroxylase involved in collagen synthesis [38]. PHDs were first identified in *C. elegans* as egg laying abnormal nine homologs (EGLN) and

Figure 1.3. Hypoxia Signaling in normoxic and hypoxic conditions.

The hypoxia signaling in the normoxic conditions begins in the cytosol where PHDs continuously respond to the changes in oxygen concentrations. Under normoxic conditions, PHDs hydroxylate HIFα that, in turn, leads to the pVHL mediated proteasomal degradation thus inhibition of HIF1 mediated transcription (A). Under hypoxic conditions, PHDs activity is inhibited leading to the stabilization of HIF1α. Stabilized HIF1α translocates into the nucleus where it binds to HIF1β to form active HIF1heterodimer. "Images in this dissertation are presented in color."

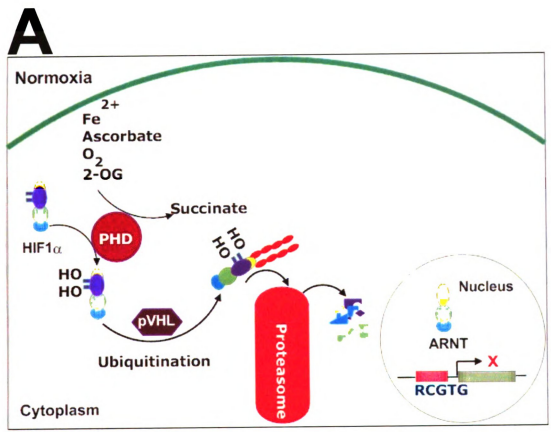
A
Normoxia
2+
Fe
Ascorbate
O2
2-OG
Succinate
PHD
HIF1α
HO
HO
pVHL
Ubiquitination
Proteasome
Nucleus
ARNT
X
RCGTG
Cytoplasm

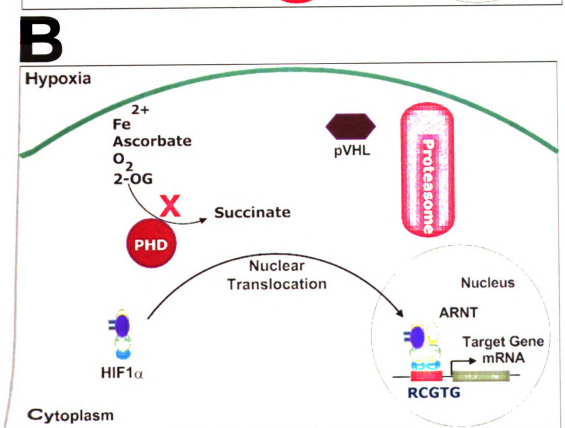
B
Hypoxia
2+
Fe
Ascorbate
O2
2-OG
X
Succinate
PHD
pVHL
Proteasome
Nuclear
Translocation
Nucleus
ARNT
Target Gene
mRNA
HIF1α
RCGTG
Cytoplasm

later shown to have three mammalian homologs (PHD1-3) [39]. PHDs are Fe(II)-, ascorbate-, and 2-oxoglutarate-dependent dioxygenases that utilize oxygen as a co-substrate. One oxygen atom of the oxygen molecule is used in the hydroxylation of the HIFα prolyl residue (within a consensus LXXLAP amino acid sequence) and the other reacts with 2-oxoglutarate, yielding succinate and CO_2 as products [40]. Once hydroxylated, the HIFα is recognized by the tumor suppressor protein, von-Hippel Lindau (pVHL), which acts as the recognition component of E3-ubiquitin ligase complex and targets HIFα for proteolysis by the ubiquitin–proteasome pathway [41] (Fig. 1.3A).

Under hypoxic conditions, the PHDs are unable to hydroxylate the cytoplasmic HIFα, which results in its stabilization and accumulation in the cytoplasm (Fig. 1.3B). There are two proposed mechanisms underlying the inhibition of PHDs under hypoxic stress. First, direct loss of substrate (i.e oxygen) decreases the enzymes activity. The second involves hypoxia-induced changes in reactive oxygen species (ROS) levels within the cytoplasm that impacts various aspects of PHD's function, including iron redox cycling.

Regardless of mechanism, it has been established that hypoxia leads to PHD inhibition and subsequent stabilization of HIFα that initiates the adaptation responses through gene expression [37]. Besides hypoxia, PHDs can also be inhibited by certain compounds referred to as hypoxia mimics. These mimics include cobalt (competes with Fe(II)), desferrioxamine (DFO, an

iron chelator), and dimethyloxalylglycine (DMOG, an αKG analog). Exposure to these compounds results in HIF1α stabilization and subsequent transcriptional response [42].

4.D. HIF signaling and regulation of gene expression

More than 150 genes are directly regulated by HIF-mediated transcription following exposure to hypoxia. It has been estimated that more than 2% of human arterial endothelial cell genome is regulated by HIF-1, directly or indirectly [43]. These genes are involved in a wide variety of functions including cellular energy metabolism, cell proliferation, angiogenesis, matrix and barrier functions, hormonal regulation, cytoskeletal integrity, cell migration, vasomotor regulation, growth and apoptosis [44].

Switching to anaerobic glycolysis is probably the first pro-survival step that cells choose under hypoxic stress (Pasteur effect). Several genes involved in glycolysis and glucose uptake have been identified as HIF1 target genes [45, 46]. Genes involved in cell proliferation such as transforming growth factor-α and β3 (TGF-α and β3), insulin-like growth factor-2 (IGF-2), IGF binding protein 1, 2, and 3 (IGF-BP), cyclin G2 and WAF1 are some of the known HIF target genes.

At the systemic and tissue level, exposure to hypoxia leads to changes in HIF-responsive genes that regulate important processes such as erythropoiesis, angiogenesis, and vascular remodeling. HIF regulated genes, including erythropoietin (EPO), transferrin (TF), transferrin receptor, ceruloplasmin (CP), haemoxygenase-1 (HO-1), VEGF, Flt-1 (VEGF receptor 1), PAI-1, adrenomedullin, endothelin 1 (END-1), inducible nitric oxide synthase (NOS2A), endothelial nitric oxide synthase (NOS3) and ferrochelatase (FECH) are all involved in enhanced oxygen supply [47].

4.E. HIF signaling and development

Perhaps, the most obvious physiological role of HIF signaling is observed in mammalian embryonic and fetal development. Hypoxia is a consistent feature during gestational development, with pO_2 ranging from 55 mmHg (conception) to 12 mmHg (late gestation). Despite the placental formation, the late gestational pO_2 values in umbilical artery, umbilical vein and amniotic fluid remains below approximately 23, 30 and 12 mmHg, respectively [48]. Under these hypoxic conditions, embryonic and fetal stages rely on the mechanisms dedicated to maintain oxygen supply and using the pO_2 as a developmental cue.

4.E.1. Placentation and hypoxia signaling

During oocyte release and fertilization the oxygen delivery is diffusion mediated. These stages are the most anaerobic stage of fetal development due to several factors, including increase in the diffusion distance of oxygen to the mitochondria and poor vascularization and low intrauterine pO_2. In order to meet the increasing oxygen demands of the growing conceptus, the process of placentation is very important. The first phase of placentation is characterized by cytotrophoblastic proliferation into the endometrial stroma followed by cell fusion and formation of syncytium. The mass formed by the fusion of invading cytotrophoblasts is called the syncytiotrophoblasts and it massively increases the surface area available for nutrient exchange between the mother and the fetus. The second phase of placentation includes the differentiation of remaining (non-syncytial) cytotrophoblasts to form primary villi that penetrate the maternal decidua, myometrium and vasculature which ultimately develop to form true placental gas exchange interface.

During placentation, the morphogenesis of placental gas exchange interface is regulated by oxygen tension in two different forms of cytotrophoblasts. The proliferative form of cytotrophoblasts is undifferentiated which is characteristically prominent at the low pO_2 (fetal pO_2) whereas the other non-proliferative (differentiated, motile and invasive) form appears at arterial pO_2 [49]. The formation of placental gas exchange interface is thus,

precisely controlled by oxygen tension surrounding the tissues through an oxygen sensor mechanism.

The oxygen sensor involved in the transduction of change in oxygen tension to the physiological signal (placental gas exchange interface establishment) has been recognized as PHDs, with the effector pathway as HIF signaling [50]. It has been demonstrated that HIF1α mRNA is expressed maximally between 5 to 8 weeks of gestation and falls abruptly at 12 weeks (corresponds to E9.5 and E10.5 of mouse fetus) with the establishment of placental gas exchange process [51]. This finding suggested the possible role of HIF responsive genes in the process of placentation. Later it was shown that antisense mediated knockdown of HIF1α in the cultured villous implants at fetal pO_2 resulted in the adoption of the differentiated, non-proliferative, motile, and invasive form of cytotrophoblasts, which normally appears at arterial pO_2. It suggested that HIF1α stabilization at low pO_2 signals the retention of undifferentiated and proliferative form of cytotrophoblasts that is relieved after the pO_2 is raised to arterial levels leading to HIF1α degradation [52, 53]. It has also been shown that the knockdown of HIF1α results in the suppression of TGFβ3 (HIF1 target gene) which is responsible for the switch from the proliferative to the invasive form. This switch was reversed on the addition of recombinant TGFβ3 [49, 54, 55]. Further, to explore the HIF

signaling underlying the roles of hypoxia in placental development, various murine models with disrupted HIF pathways have been generated [50, 54, 56].

Disruption of all the three PHDs (PHD1, PHD2 and PHD3) in the murine model has shown that mice lacking PHD1 (*Phd1* $^{-/-}$) and PHD3 (*Phd3* $^{-/-}$) had apparently normal placental development whereas *Phd2* $^{-/-}$ exhibited several placental defects such as abnormal distribution of trophoblast giant cells, reduced villous branching in the labyrinth, and widespread penetration of the labyrinth by syncytiotrophoblasts. Due to these defects, *Phd2* $^{-/-}$ embryos exhibit lethality on day E 12.5 [50]. The disruption of PHD2 led to the upregulation of HIF1α as well as HIF2α in the placenta and embryonic tissues [50]. Contrary to *Phd2* $^{-/-}$ mice, *Vhl* $^{-/-}$ mice exhibited more severe defects in the placental development such as failure to develop syncytiotrophoblasts, lack of invasion of maternal blood vessels leading to embryonic lethality at E9.5 to E10.5 (stage of placental dysgenesis) [57, 58]. The roles of HIF1β (ARNT) in the placental development were reported in three different studies showing embryonic mortality at day E9.5 due to defective vascularization of labyrinth of placenta and yolk sac, an increased number of trophoblast giant cells and defective cell fate determination [54, 59-61]. These differences suggest additional roles of PHD2 and VHL other than mediation of HIF stabilization or additional mechanism of regulation of HIFs activity [57].

A detailed study on the effect of different allelic dosage combinations of either or both HIFα (HIF1α$^{+/-}$/2α$^{+/+}$, HIF1α$^{-/-}$/2α$^{+/+}$, HIF1α$^{+/-}$/2α$^{+/-}$, HIF1α$^{-/-}$/2α$^{-/-}$, HIF1α$^{+/+}$/2α$^{+/-}$, HIF1α$^{+/+}$/2α$^{-/-}$) on the placental development have been undertaken. HIF1α$^{-/-}$/2α$^{-/-}$ mice showed absence of placental vasculature, increase in trophoblastic giant cells, poor invasive efficiency and defective placental structure thus representing phenocopy of ARNT deficient mice [56]. The defective phenotype of HIF1α$^{-/-}$ were further aggravated by deleting either or both alleles of HIF2α, which suggested that the phenotypes among different dosage combinations showed allele-specificity. HIF1α$^{-/-}$ mice exhibited defective chrioallantoic fusion with maternal lacunae and fewer and defective placental vascularization that were normal in E 9.5 HIF2α$^{-/-}$ embryos [56]. These results suggest that hypoxia and its signaling is also important in the embryonic development of organ systems.

4.E.2. Hypoxic regulation of organogenesis

It is clear from above studies that murine germ line inactivation of either HIF1α, HIF2α, ARNT, PHD2 or the VHL tumor suppressor results in embryonic or perinatal lethality. To overcome embryonic lethality, conditional

alleles for HIF1α, HIF2α, ARNT and VHL have been generated that now allow tissue and cell type specific knock down. Several murine knockouts of HIF, pVHL, PHD, and VEGF have demonstrated the essential role of hypoxia-responsive pathway proteins in organogenesis.

4.E.2.a. Vascular System

Embryonic vasculature development is a crucial process contributing to the survival of the fetus and development of the other organ systems. Disruption studies for different members of HIF signaling pathways have contributed vastly towards our understanding of embryonic vascularization events. Homozygous deficiency of ARNT leads to defective angiogenesis of the yolk sac [61]. Homozygous deficiency of HIF2α in murine embryo results in vascular disorganization in yolk sac and failure to assemble and maintain vascular tubular structure and leading eventually to death between day E9.5 and E13.5 [62, 63]. Similarly, the HIF1α knockout mouse displayed disorganized yolk sac vascularization with disorganized branching pattern. HIF1α deficient embryos exhibited only a few capillaries in the neural fold with complete absence of vascular network and also reduced size of dorsal aorta [64]. Current insights in to the role of different HIFs in the vascularization clearly define the importance of oxygen tension, hypoxia and HIF signaling.

4.E.2.b. Cardiac System

The role of HIF signaling in cardiac development has been extensively studied by various groups using systemic, as well as, tissue specific mice models. Systemic HIF1α knockout mice display cardiac defects such as myocardial hyperplasia, pericardial obliteration of ventricular lumen, increased number of myocardial cells and cardia bifida (bilateral heart tubes that develop in to two hearts) [64-67]. Inactivation of single allele of HIF1α ($HIF1\alpha^{+/-}$) had no observable developmental phenotype, however, further analysis of these partially deficient adult mice revealed abnormal physiological responses to chronic hypoxic exposures. As compared to control animals, $HIF1\alpha^{+/-}$ mice exhibited impaired physiological responses to hypoxia such as weight loss, polycythemia, right ventricular hypertrophy, pulmonary hypertension and pulmonary vascular remodeling [68]. The cardiac myocytes specific HIF1α deletion do not exhibit any lethality phenotypes or abnormalities, however, these mice exhibited physiological abnormalities in cardiac function, vascularity, energy availability, and calcium handling even under normoxia conditions, suggesting that HIF-1α coordinates gene expression at all oxygen levels [69].

Although systemic HIF2α null progeny from congenic C576BL/6J strain failed to survive due to embryonic or perinatal lethality, progeny from isogenic 129S6/SvEvTac strain survived with multi-organ pathologies. The surviving $HIF2\alpha^{-/-}$ progenies exhibited cardiac mitochondrial hypertrophy but no

hyperplasia. Cardiac myocytes from HIF2$\alpha^{-/-}$ mice contained many degenerating mitochondria with intact inner mitochondrial membranes [70]. In conclusion, deletion of hypoxia signaling proteins results in the defective cardiac development and compromised functioning.

4.E.2.c. Lung

Lung morphogenesis proceeds in a consistently low pO_2 environment characterized by shallow gradients of oxygen from the fetal vasculature into the tissue mass. Several studies have demonstrated that the hypoxic condition that a fetus faces is an important determinant in lung development. It has been well documented that low fetal pO_2 serves to maintain epithelial lumen fluid secretion and lung expansion [71]. Land et al. have shown that rat lung explants display increased airway surface complexity (complex branching pattern) at fetal pO_2 (23 mmHg) as compared to ambient (142 mmHg) steady-state pO_2. The observed difference in branching pattern was confined towards the periphery suggesting the hypoxia dependency of mesenchyme differentiation and airway bifurcation events [72]. Fisher et al. have demonstrated that the ROS produced under hypoxic conditions interferes with the airway branching morphogenesis, and N-acetylcysteine (antioxidant) treatment afforded protection against hyperoxia [73]. Similarly, several other

studies have shown the consequences of redox modulation on airway morphogenesis [74, 75].

Hypoxia and HIF signaling pathway activation have been studied through investigation of the spatial and temporal expression of HIF/VEGF pathway proteins in the developing human lung. Expression analysis of staged human embryo at third trimester showed consistent HIF1α expression, and there was no observable increase in the expression of proteins of HIF1α degradation pathway [76]. This finding suggests the continually activated hypoxia signaling in the post-placentation lung. HIF1α expression was restricted to branching epithelium, whereas HIF2α appeared to be present in the vascular structures as well as branching epithelium, reflecting their different roles in pulmonary development. HIF1β was shown to be present in the mesenchymal as well as epithelial structures, providing a basis for downstream activation of both HIF1α and HIF2α [76].

All of the systemic knockout mice models for genes involved in the HIF signaling die *in utero* from various defects in organogenesis. However, some of the HIF2α knockout embryos that survived full term exhibited postnatal respiratory distress due to insufficient surfactant production [77]. The midgestational lethalities of the systemic knockout models has made it challenging to study the role of HIFs in fetal lung development.

5. Hypoxia and its effects on the lung

Alveolar epithelial cells require normal oxygenation to run their high energy demanding processes like surfactant biosynthesis, fluid uptake, and maintenance of alveolocapillary barrier. Several clinical conditions involve hypoxic challenge to the alveolar epithelial cells resulting in functional changes [78]. Alveolar epithelial cells survive hypoxia through several adaptive mechanisms like increased glycolysis, increased vasculogenesis, downregulation of high energy consuming Na,K-ATPase activity and protein synthesis. Alveolar edema clearance requires active Na,K-ATPase. Thus, downregulation of this protein in hypoxia results in the altered fluid uptake and edema clearance. The most well studied hypoxia-affected processes in alveolar epithelium are the activity and maintenance of Na,K-ATPase and amiloride-sensitive epithelial sodium channel (ENaC) pumps. Acute hypoxemic respiratory failure is associated with the flooding of the alveolar spaces with fluid and the resorption of this fluid into the interstitial and vascular spaces depends on these two ion pumps. The amiloride-sensitive ENaC pump actively uptakes sodium ions at the apical surface of alveolar epithelial cells, whereas at the basolateral surface sodium ions are actively transported against a gradient in exchange for potassium ions into the interstitium, predominantly by Na,K-ATPase. The development of ion gradient due to the movement of sodium ions results in the movement of water into the epithelial cells and eventually in to the interstitium via aquaporins [79-82]. High-altitude

pulmonary edema (HAPE), a life-threatening condition characterized by alveolar flooding that occurs in predisposed individuals at high altitudes, has been linked to hypoxic pulmonary vasoconstriction [83].

A direct role of hypoxia in alveolar epithelium is not well characterized. Hypoxia (1.5% O_2 for 60 min) induced Na,K-ATPase trafficking out of the plasma membrane into the intracellular membranes, which suggests a role for hypoxia in the regulation of topological distribution of these pumps [84]. It has also been shown that hypoxia downregulates plasma membrane specific Na,K-ATPase activity without affecting the whole cell protein expression levels [85]. These effects are observed under short-term severe hypoxic exposure and are reversible. In contrast, prolonged hypoxic conditions results in reduction in the cellular pool of Na,K-ATPase [78]. A549 cells exposed to 1.5% O_2 for 2 hours displayed approximately a 50% loss of the plasma membrane bound ATP-driven Na^+ pumps. These findings suggest that the cells undertake this adaptive strategy to save energy and reduce oxygen consumption through the inhibition and/or degradation of energy consuming metabolically active molecules [86].

6. Hypoxia Mimics and HIF signaling

HIFα stabilizers are also known as hypoxia mimics. Agents such as metals (Ni(II), Co(II), Mn(II), and V(V)), desferroxamine (DFO) and dimethyloxallyl glycine (DMOG) are commonly studied hypoxia mimics. It has been shown that cobalt can stabilize HIFα, and HIFα modulates cobalt induced cell toxicity [87]. Additionally, occupational exposure of metals like cobalt (Co(II)) are known to cause lung injury. Hence, it is rational to use cobalt-induced lung injury models to understand the role of HIF signaling in various respiratory diseases involving hypoxia such as respiratory distress syndrome, HAPE and COPD.

7. Metals

7.A. History of metals

It was in the new Stone Age that ancient man started using metal rich rocks as weapons and tools. The Bronze Age (3000-1000 BC) began with the advent of metallurgical technique of mixing tin ore with copper ore to produce bronze. Bronze proved to be a very useful alloy in the production of new tools for farming and hunting. It was not until the start of Iron Age (1500-800 BC) that bronze was displaced as the most widely used metal and brought the advent of the steel industry. The New Metal Age has also posed several health concerns especially for the workers who are involved in mining and metal industries [88-90].

7.B. Biological significance of metals

The metal's property to donate its electrons to become cations and hence, electrophiles, makes these cations an important component of the active site of enzymes with redox reaction mechanisms. In addition, some metal ions form an integral part of nonenzyme proteins including hemoglobin, ferritin, ceruloplasmin, rubredoxin, cytochromes, and cyanocobalamin. Proteins containing bound metal ions are referred as metalloproteins (metalloenzymes). The metal ion forms coordinated bonds with nitrogen, sulfur or oxygen atoms of amino acids in the polypeptide chain. Approximately 25-33% of proteins require metals for proper function or maintenance of structural integrity. Metalloproteins such as cytochromes play important roles in cellular energy production via their role in the electron transport chain (ETC). In addition, metalloproteins play critical roles in processes such as signal transduction (calmodulin), metabolism (cyanocobalamin), antioxidation (superoxide dismutase), and transport (ceruloplasmin). Not all the metals are biologically beneficial. Metals such as lead and mercury are toxic to the cellular machinery. Another group of metals known as trace metals (Mn, Fe, Co, Ni, Cu, Zn, and Cd), are required in minute concentrations for cellular functions but at higher concentrations they pose health hazards .

7.C. Toxicity of Metals

Metals are probably the oldest known toxicants in human medicine. For many, the mechanism of action that leads to toxicity is not well characterized for many of them. Biogeological cycles and industrialization have redistributed metals in the environment and lead to the appearance of new metals in the food chain, soil, air, and water. When injected into the atmosphere, gaseous or particulate metals may be transported to distant places [91]. The toxicological effects of metals depend on the time, dose and route of exposure [92]. Toxicities are further determined by other factors such as half-life in the tissues (varies among tissues), valence state, and ligand binding. Hexavalent chromium is highly toxic whereas its trivalent form functions as an essential trace element. Finally, organometallic forms of some metals differ in their toxic properties. For instance, non ionized alkyl compounds such as methyl mercury Is a neurotoxin, whereas mercuric chloride is a nephrotoxic compound [92].

A majority of transition metals are characterized as nonessential to the cellular machinery and are toxic at minimal doses. The few, such as cobalt, that are required for cellular functions, show toxic phenotypes at higher concentrations. These toxic phenotypes fall under three categories: disturbance of normal metal ion equilibrium, damage to biomolecules, and alteration in gene expression patterns. Increased concentrations of divalent cobalt interfere with iron metabolism and compete for the iron-binding site on metalloproteins and metalloenzymes. Certain metal exposures result in

damage to biomolecules such as proteins and nucleic acids. Elements such as As, Hg and Cd form covalent bonds with the –SH group of proteins. For example, arsenic can inactivate the pyruvate dehydrogenase complex through covalently binding to the –SH group of dihydrolipoic acid [93]. Some redox active transition metals including cobalt generate reactive ROS that, in turn, oxidize cellular proteins, nucleic acid and lipids [94, 95].

Metals regulate and alter the activity and/or stability of various metal-responsive transcriptional factors that cause changes in the level of gene expression and activate various signaling pathways. Metals and metal-induced ROS generation have been demonstrated to affect a number of receptors and genes, including growth factor receptors, src kinases, ras signaling, mitogen-activated protein kinases, and nuclear transcription factors such as NFκB, AP-1, p53, MTF-1, NFAT, and HIF-1 [96]. NFκB is an important redox sensitive transcription factor that is affected by metal exposure resulting in oxidative stress. It has been shown that divalent nickel and cobalt exposure causes NFκB induced upregulation of adhesion molecules ICAM-1, VCAM-1, and E-selectin in endothelial cells [97]. AP-1 is another nuclear transcription factor that is stimulated by metal induced oxidative stress. Arsenic(II), vanadium(V), chromium(VI), nickel(II), cadmium(II), lead, cobalt, and iron are known to activate AP-1 in a variety of cells [96]. Metallothioneins (MTs) are a class of cysteine-rich proteins that play a critical roles in the heavy metal metabolism and detoxification. Metal-

induced expression of MTs depends on the zinc-finger transcription factor, metal transcription factor-1 (MTF-1) which acts as a cellular stress-sensor protein [98]. MTF-1 binding to the metal responsive element on the MTF-1 targeted genes is allosterically regulated by zinc leading to elevated MTs expression [99, 100]. Certain metals such as Co(II), Ni(II), V(II), Mn(II) are referred as "hypoxia mimics" due to their ability to stabilize HIFα.

Cobalt has been known to induce the expression of erythropoietin and thus this metal was used to treat anemia. [101, 102]. Cobalt also activates angiogenic responses through VEGF expression [103]. These responses are known to be mediated through HIFα stabilization. Several different mechanisms have been proposed for the cobalt-mediated stabilization of HIF1α however; the exact mechanism is still not well understood. It has been shown that cobalt inhibits pVHL binding to the ODD domain of HIFα [104]. In addition, cobalt-induced ROS generation leading to ferrous oxidation, chelating of ascorbic acid and replacing non-covalently held iron atom from the PHDs have also been suggested as mechanisms for the metal's ability to stabilize HIFα [105].

8. Cobalt

8.A. Occurrence and uses

Cobalt is a rare magnetic transition metal and falls in period four of the periodic table with nickel, iron and manganese. It primarily occurs in nature as

oxides, arsenides and sulfides, and its cobaltous (Co(II)) state is predominantly used in the chemical industry [106, 107]. Historically, it has been used as a dye in pottery, oil paints, high speed drills and cutting machines as a component of hard metal (tungsten carbide (80-95%) combined with cobalt (5-20%) and nickel (0-5%)). In present industrial settings, it is primarily used in the production of superalloys, corrosion resistant alloys, high speed steels, batteries, magnets, wear resistant coatings and various metallurgical applications [95]. Other industrial uses include diamond polishing with cobalt containing disks, radioactive isotopes in medicine and the production of drying agents, pigments, and catalysts [107].

8.B. Cobalt metabolism and Exposure

Cobalt is an essential trace element for humans and is consumed as cobalamin (essential component of vitamin B_{12}). Cobalamin is required for the production of red blood cells and the prevention of pernicious anemia. In addition, cobalamin is also required in the methionine and nucleic acid biosynthesis pathways. For the general population, diet is the main source of exposure and the average daily dietary intake ranges from 5 to 45 μg. Major dietary sources of cobalt are seafoods, bran, cocoa, and certain meats [108]. Generally, the concentration of cobalt in the drinking water is low (less than 5 μg/L) [107].

Cobalt salts are well absorbed in the jejunum and without significant accumulations, 80% of ingested cobalt is excreted in the urine while 15 % is excreted in feces via enterohepathic pathway. In the human body, the total amount of cobalt is estimated to be approximately 1.1 mg. It has been shown that muscles contain the largest fraction whereas its highest concentration is found in fat tissues. The normal levels in human urine and blood are about 1.0 and 0.18 μg/L, respectively.

Cobalt is found to be present in urbanized air in the range between 0.5 to 60 ng/m^3 [109]. Tobacco smoke contains 0.3-2.3 mg Co/kg dry weight, which puts smokers at higher risk of cobalt-induced lung injury [110]. In industrial settings, metal refinery workers and those involved in the production of certain alloys, such as tungsten carbide, are at greatest risk for cobalt-induced toxicity.

8.C. Cobalt toxicity

Despite its use for treatment of anemic patients, associated toxic effects were reported to be goitrogenic due to hypothyroidism and thyroid hyperplasia [111]. Epidemiological studies have shown an association between goiter prevalence and the elevated cobalt levels in water and soil. Cobalt induced cardiomyopathy was observed in brewery workers who consumed cobalt-contaminated beer. Postmortem findings included pericardial effusion,

myofibrillar loss and congestive heart failure [112]. Excessive erythrocytosis (polycythemia) has been reported in cobalt miners [113]. In humans, gastrointestinal effects such as vomiting, diarrhea, liver injury and allergic dermatitis were also reported in case of oral exposure to cobalt [114].

Acute inhalation exposure of cobalt in humans results in respiratory problems such as congestion, edema, and hemorrhage of the lung. Chronic exposure to cobalt through inhalation leads to respiratory irritation, coughing, shortness of breath, wheezing, asthma, pneumonia, and fibrosis [107]. Inhalation exposure of hard metal workers has been shown to cause hard metal lung disease that is interchangeably used in literature with cobalt lung, hard metal asthma, and giant cell interstitial pneumonitis. Ambient concentrations of 0.002 to 0.01 mg/m^3 have been shown to cause respiratory irritation, and higher concentrations (0.1 mg Co/m^3 or higher) can cause hard metal lung disease [92].

8.D. The role of HIFs in cobalt-mediated toxicity

The role of hypoxia signaling in cobalt-induced cellular toxicities has been studied in various in vitro models. Cobalt chloride induced toxicity has been tested in mouse embryonic fibroblasts (MEFs) and the *in vitro* role of HIF1α has already been established in cobalt-induced toxicity [87]. The cobaltous chloride-induced oxidative stress mechanism has been investigated

in skeletal muscle cell lines, where exposure to $CoCl_2$ resulted in elevated intracellular oxidants, the accumulation of HIF1α protein, and the expression of VEGF [115]. In addition, $CoCl_2$-induced astrocyte toxicity is mediated through HIF1α regulated apoptosis [116].

Hypothesis and Specific Aims

Cobalt exposure leads to pathological conditions such as airway constriction, alveolitis, fibrosis and associated giant cell interstitial pneumonitis. There is little known, however, about the role of hypoxia signaling in these conditions. Several *in vitro* studies have shown that HIF1α is an important mediator of the toxic responses observed upon cobalt exposure. Previous studies in our lab, using an immortalized mouse embryonic fibroblast (MEFs) cell line lacking HIF1α, established the correlation between HIF1α removal and protection against $CoCl_2$ toxicity. Validation of our *in vitro* understanding of cobalt-induced HIFs signaling necessitates the *in vivo* studies of cobalt toxicity in HIFs null animals. Based on these previous findings, I propose the following hypothesis.

Hypothesis: Cobalt-induced lung toxicity is mediated by HIF stabilization and transcription and the subsequent changes in inflammatory mediators and cellular response.

Each of the chapters in this dissertation is dedicated to address following specific aims.

Aim 1: Create and characterize a lung specific inducible HIF1α deficient mouse model.

To validate *in vitro* data, a lung-specific inducible HIF1α deficient mouse model was generated. The generated mice were characterized using techniques such as histopathology, western blotting, real-time PCR and electron microscopy.

Aim 2: Determine the role of HIF1α in cobalt-induced lung injury in mice.

A postnatal strategy to delete HIF1α from the lung epithelial cells was adopted. HIF1α deficient mice were used to study the time-dependent progression of cobalt-induced lung inflammation.

Aim 3: Create and characterize combined HIF1α and HIF2α lung specific inducible knockout model (quadruple transgenic model).

To investigate the role of HIF2α in the lung development, another prominent isoform of HIFα in lungs, lung-specific inducible HIF2α deficient mice were generated. To further enhance our understanding of the collective role of these two HIFs in lung development, mice with a lung-specific deletion

of HIF2α (termed HIF2α$^{\Delta/\Delta}$) and HIF1/2α (termed HIF1/2α$^{\Delta/\Delta}$) were generated.

Importance:

The findings from these studies will have a great impact on our current understanding on the roles of HIF1α and HIF2α in the lung development. The studies on cobalt exposures in HIF-deficient mice will provide a mechanistic understanding on the roles of these transcription factors in airway inflammatory responses.

REFERENCES

1 Wagner, P. D. (2008) The biology of oxygen. Eur Respir J. **31**, 887-890

2 Bunn, H. F. and Poyton, R. O. (1996) Oxygen sensing and molecular adaptation to hypoxia. Physiological reviews. **76**, 839-885

3 Burri, P. H. (1984) Fetal and postnatal development of the lung. Annual review of physiology. **46**, 617-628

4 Alescio, T. and Cassini, A. (1962) Induction in vitro of tracheal buds by pulmonary mesenchyme grafted on tracheal epithelium. The Journal of experimental zoology. **150**, 83-94

5 Wessells, N. K. (1970) Mammalian lung development: interactions in formation and morphogenesis of tracheal buds. The Journal of experimental zoology. **175**, 455-466

6 Spooner, B. S. and Faubion, J. M. (1980) Collagen involvement in branching morphogenesis of embryonic lung and salivary gland. Developmental biology. **77**, 84-102

7 Masters, J. R. (1976) Epithelial-mesenchymal interaction during lung development: the effect of mesenchymal mass. Developmental biology. **51**, 98-108

8 Bucher, U. and Reid, L. (1961) Development of the mucus-secreting elements in human lung. Thorax. **16**, 219-225

9 Kauffman, S. L. (1980) Cell proliferation in the mammalian lung. International review of experimental pathology. **22**, 131-191

10 Crapo, J. D., Barry, B. E., Foscue, H. A. and Shelburne, J. (1980) Structural and biochemical changes in rat lungs occurring during exposures to lethal and adaptive doses of oxygen. The American review of respiratory disease. **122**, 123-143

11 Evans, M. J., Cabral-Anderson, L. J. and Freeman, G. (1978) Role of the Clara cell in renewal of the bronchiolar epithelium. Laboratory

investigation; a journal of technical methods and pathology. **38**, 648-653

12 Davies, G. and Reid, L. (1970) Growth of the alveoli and pulmonary arteries in childhood. Thorax. **25**, 669-681

13 Burri, P. H. (1974) The postnatal growth of the rat lung. 3. Morphology. The Anatomical record. **180**, 77-98

14 Burri, P. H., Dbaly, J. and Weibel, E. R. (1974) The postnatal growth of the rat lung. I. Morphometry. The Anatomical record. **178**, 711-730

15 Ji, C. M., et al. (1995) Pulmonary cytochrome P-450 monooxygenase system and Clara cell differentiation in rats. Am J Physiol. **269**, L394-402

16 Mason, R. J. (1987) Surfactant synthesis, secretion, and function in alveoli and small airways. Review of the physiologic basis for pharmacologic intervention. Respiration; international review of thoracic diseases. **51 Suppl 1**, 3-9

17 Hong, K. U., et al. (2004) Basal cells are a multipotent progenitor capable of renewing the bronchial epithelium. The American journal of pathology. **164**, 577-588

18 Nettesheim, P., et al. (1990) Pathways of differentiation of airway epithelial cells. Environmental health perspectives. **85**, 317-329

19 Park, K. S., et al. (2006) Transdifferentiation of ciliated cells during repair of the respiratory epithelium. American journal of respiratory cell and molecular biology. **34**, 151-157

20 Stripp, B. R. and Reynolds, S. D. (2008) Maintenance and repair of the bronchiolar epithelium. Proceedings of the American Thoracic Society. **5**, 328-333

21 Richard Harding, K. P., Charles Plopper. (2004) The Lung: Development, Aging and The Environment. Academic Press

22 Jiang, J., et al. (1996) Measurement of PO_2 in liver using EPR oximetry. J Appl Physiol. **80**, 552-558

23 Scheufler, K. M. (2004) Tissue oxygenation and capacity to deliver O2 do the two go together? Transfus Apher Sci. **31**, 45-54

24 Lee, Y. M., et al. (2001) Determination of hypoxic region by hypoxia marker in developing mouse embryos in vivo: a possible signal for vessel development. Dev Dyn. **220**, 175-186

25 Land, S. C. (2003) Oxygen-sensing pathways and the development of mammalian gas exchange. Redox Rep. **8**, 325-340

26 Cartwright, J. E., Keogh, R. J. and Tissot van Patot, M. C. (2007) Hypoxia and placental remodelling. Advances in experimental medicine and biology. **618**, 113-126

27 Guzman, G. J., Cueto, A. H. and Yepez, S. H. (2008) Contribution of hypoxia in pulmonary tissue remodeling in asthmatic processes. Rev Alerg Mex. **55**, 18-32

28 Fajardo, I., Svensson, L., Bucht, A. and Pejler, G. (2004) Increased levels of hypoxia-sensitive proteins in allergic airway inflammation. American journal of respiratory and critical care medicine. **170**, 477-484

29 Michiels, C. (2004) Physiological and pathological responses to hypoxia. The American journal of pathology. **164**, 1875-1882

30 Bartrons, R. and Caro, J. (2007) Hypoxia, glucose metabolism and the Warburg's effect. Journal of bioenergetics and biomembranes. **39**, 223-229

31 Hardie, D. G. and Hawley, S. A. (2001) AMP-activated protein kinase: the energy charge hypothesis revisited. Bioessays. **23**, 1112-1119

32 Rolfe, D. F. and Brown, G. C. (1997) Cellular energy utilization and molecular origin of standard metabolic rate in mammals. Physiological reviews. **77**, 731-758

33 Buttgereit, F. and Brand, M. D. (1995) A hierarchy of ATP-consuming processes in mammalian cells. The Biochemical journal. **312 (Pt 1)**, 163-167

34 Cummins, E. P. and Taylor, C. T. (2005) Hypoxia-responsive transcription factors. Pflugers Arch. **450**, 363-371

35 Wang, G. L., Jiang, B. H., Rue, E. A. and Semenza, G. L. (1995) Hypoxia-inducible factor 1 is a basic-helix-loop-helix-PAS heterodimer regulated by cellular O2 tension. Proceedings of the National Academy of Sciences of the United States of America. **92**, 5510-5514

36 Semenza, G. L., et al. (1997) Structural and functional analysis of hypoxia-inducible factor 1. Kidney international. **51**, 553-555

37 Weidemann, A. and Johnson, R. S. (2008) Biology of HIF-1alpha. Cell death and differentiation. **15**, 621-627

38 Kaelin, W. G., Jr. and Ratcliffe, P. J. (2008) Oxygen sensing by metazoans: the central role of the HIF hydroxylase pathway. Molecular cell. **30**, 393-402

39 del Peso, L., et al. (2003) The von Hippel Lindau/hypoxia-inducible factor (HIF) pathway regulates the transcription of the HIF-proline hydroxylase genes in response to low oxygen. The Journal of biological chemistry. **278**, 48690-48695

40 Epstein, A. C., et al. (2001) C. elegans EGL-9 and mammalian homologs define a family of dioxygenases that regulate HIF by prolyl hydroxylation. Cell. **107**, 43-54

41 Cockman, M. E., et al. (2000) Hypoxia inducible factor-alpha binding and ubiquitylation by the von Hippel-Lindau tumor suppressor protein. The Journal of biological chemistry. **275**, 25733-25741

42 Groenman, F. A., et al. (2007) Effect of chemical stabilizers of hypoxia-inducible factors on early lung development. Am J Physiol Lung Cell Mol Physiol. **293**, L557-567

43 Manalo, D. J., et al. (2005) Transcriptional regulation of vascular endothelial cell responses to hypoxia by HIF-1. Blood. **105**, 659-669

44 Chowdhury, R., Hardy, A. and Schofield, C. J. (2008) The human oxygen sensing machinery and its manipulation. Chemical Society reviews. **37**, 1308-1319

45 Wenger, R. H. (2002) Cellular adaptation to hypoxia: O2-sensing protein hydroxylases, hypoxia-inducible transcription factors, and O2-regulated gene expression. Faseb J. **16**, 1151-1162

46 Wenger, R. H. (2000) Mammalian oxygen sensing, signalling and gene regulation. The Journal of experimental biology. **203**, 1253-1263

47 Rocha, S. (2007) Gene regulation under low oxygen: holding your breath for transcription. Trends in biochemical sciences. **32**, 389-397

48 Land, S. C. (2004) Hochachka's "Hypoxia Defense Strategies" and the development of the pathway for oxygen. Comparative biochemistry and physiology. **139**, 415-433

49 Caniggia, I., et al. (2000) Hypoxia-inducible factor-1 mediates the biological effects of oxygen on human trophoblast differentiation through TGFbeta(3). The Journal of clinical investigation. **105**, 577-587

50 Takeda, K., et al. (2006) Placental but not heart defects are associated with elevated hypoxia-inducible factor alpha levels in mice lacking prolyl hydroxylase domain protein 2. Molecular and cellular biology. **26**, 8336-8346

51 Rodesch, F., Simon, P., Donner, C. and Jauniaux, E. (1992) Oxygen measurements in endometrial and trophoblastic tissues during early pregnancy. Obstetrics and gynecology. **80**, 283-285

52 Cowden Dahl, K. D., et al. (2005) Hypoxia-inducible factors 1alpha and 2alpha regulate trophoblast differentiation. Molecular and cellular biology. **25**, 10479-10491

53 Fryer, B. H. and Simon, M. C. (2006) Hypoxia, HIF and the placenta. Cell cycle (Georgetown, Tex. **5**, 495-498

54 Adelman, D. M., et al. (2000) Placental cell fates are regulated in vivo by HIF-mediated hypoxia responses. Genes & development. **14**, 3191-3203

55 Schaffer, L., et al. (2003) Oxygen-regulated expression of TGF-beta 3, a growth factor involved in trophoblast differentiation. Placenta. **24**, 941-950

56 Cowden Dahl, K. D., et al. (2005) Hypoxia-inducible factors 1 alpha and 2 alpha regulate trophoblast differentiation. Molecular and cellular biology. **25**, 10479-10491

57 Gnarra, J. R., et al. (1997) Defective placental vasculogenesis causes embryonic lethality in VHL-deficient mice. Proceedings of the National Academy of Sciences of the United States of America. **94**, 9102-9107

58 Tang, N., et al. (2006) pVHL function is essential for endothelial extracellular matrix deposition. Molecular and cellular biology. **26**, 2519-2530

59 Kozak, K. R., Abbott, B. and Hankinson, O. (1997) ARNT-deficient mice and placental differentiation. Developmental biology. **191**, 297-305

60 Abbott, B. D. and Buckalew, A. R. (2000) Placental defects in ARNT-knockout conceptus correlate with localized decreases in VEGF-R2, Ang-1, and Tie-2. Dev Dyn. **219**, 526-538

61 Maltepe, E., et al. (1997) Abnormal angiogenesis and responses to glucose and oxygen deprivation in mice lacking the protein ARNT. Nature. **386**, 403-407

62 Peng, J., Zhang, L., Drysdale, L. and Fong, G. H. (2000) The transcription factor EPAS-1/hypoxia-inducible factor 2alpha plays an important role in vascular remodeling. Proceedings of the National Academy of Sciences of the United States of America. **97**, 8386-8391

63 Patel, S. A. and Simon, M. C. (2008) Biology of hypoxia-inducible factor-2alpha in development and disease. Cell death and differentiation. **15**, 628-634

64 Ryan, H. E., Lo, J. and Johnson, R. S. (1998) HIF-1 alpha is required for solid tumor formation and embryonic vascularization. The EMBO journal. **17**, 3005-3015

65 Semenza, G. L. (2006) Regulation of physiological responses to continuous and intermittent hypoxia by hypoxia-inducible factor 1. Experimental physiology. **91**, 803-806

66 Iyer, N. V., et al. (1998) Cellular and developmental control of O2 homeostasis by hypoxia-inducible factor 1 alpha. Genes & development. **12**, 149-162

67 Compernolle, V., et al. (2003) Cardia bifida, defective heart development and abnormal neural crest migration in embryos lacking hypoxia-inducible factor-1alpha. Cardiovascular research. **60**, 569-579

68 Yu, A. Y., et al. (1999) Impaired physiological responses to chronic hypoxia in mice partially deficient for hypoxia-inducible factor 1alpha. The Journal of clinical investigation. **103**, 691-696

69 Huang, Y., et al. (2004) Cardiac myocyte-specific HIF-1alpha deletion alters vascularization, energy availability, calcium flux, and contractility in the normoxic heart. Faseb J. **18**, 1138-1140

70 Scortegagna, M., et al. (2003) Multiple organ pathology, metabolic abnormalities and impaired homeostasis of reactive oxygen species in Epas1-/- mice. Nature genetics. **35**, 331-340

71 Baines, D. L., et al. (2001) Oxygen-evoked Na+ transport in rat fetal distal lung epithelial cells. The Journal of physiology. **532**, 105-113

72 Land, S. C. and Darakhshan, F. (2004) Thymulin evokes IL-6-C/EBPbeta regenerative repair and TNF-alpha silencing during endotoxin exposure in fetal lung explants. Am J Physiol Lung Cell Mol Physiol. **286**, L473-487

73 Fisher, J. C., Kling, D. E., Kinane, T. B. and Schnitzer, J. J. (2002) Oxidation-reduction (redox) controls fetal hypoplastic lung growth. The Journal of surgical research. **106**, 287-291

74 Kramer, B. W., Kramer, S., Ikegami, M. and Jobe, A. H. (2002) Injury, inflammation, and remodeling in fetal sheep lung after intra-amniotic endotoxin. Am J Physiol Lung Cell Mol Physiol. **283**, L452-459

75 Young, S. L., Evans, K. and Eu, J. P. (2002) Nitric oxide modulates branching morphogenesis in fetal rat lung explants. Am J Physiol Lung Cell Mol Physiol. **282**, L379-385

76 Groenman, F., et al. (2007) Hypoxia-inducible factors in the first trimester human lung. J Histochem Cytochem. **55**, 355-363

77 Compernolle, V., et al. (2002) Loss of HIF-2alpha and inhibition of VEGF impair fetal lung maturation, whereas treatment with VEGF prevents fatal respiratory distress in premature mice. Nature medicine. **8**, 702-710

78 Jain, M. and Sznajder, J. I. (2005) Effects of hypoxia on the alveolar epithelium. Proceedings of the American Thoracic Society. **2**, 202-205

79 Matthay, M. A., Robriquet, L. and Fang, X. (2005) Alveolar epithelium: role in lung fluid balance and acute lung injury. Proceedings of the American Thoracic Society. **2**, 206-213

80 Matthay, M. A., Folkesson, H. G. and Verkman, A. S. (1996) Salt and water transport across alveolar and distal airway epithelia in the adult lung. Am J Physiol. **270**, L487-503

81 Canessa, C. M., et al. (1994) Amiloride-sensitive epithelial Na+ channel is made of three homologous subunits. Nature. **367**, 463-467

82 McCann, J. D. and Welsh, M. J. (1990) Basolateral K+ channels in airway epithelia. II. Role in Cl- secretion and evidence for two types of K+ channel. Am J Physiol. **258**, L343-348

83 Scherrer, U., et al. (1999) High-altitude pulmonary edema: from exaggerated pulmonary hypertension to a defect in transepithelial sodium transport. Advances in experimental medicine and biology. **474**, 93-107

84 Dada, L. A., et al. (2003) Hypoxia-induced endocytosis of Na,K-ATPase in alveolar epithelial cells is mediated by mitochondrial reactive oxygen species and PKC-zeta. The Journal of clinical investigation. **111**, 1057-1064

85 Carpenter, T. C., et al. (2003) Hypoxia reversibly inhibits epithelial sodium transport but does not inhibit lung ENaC or Na-K-ATPase expression. Am J Physiol Lung Cell Mol Physiol. **284**, L77-83

86 Comellas, A. P., et al. (2006) Hypoxia-mediated degradation of Na,K-ATPase via mitochondrial reactive oxygen species and the ubiquitin-conjugating system. Circulation research. **98**, 1314-1322

87 Vengellur, A. and LaPres, J. J. (2004) The role of hypoxia inducible factor 1alpha in cobalt chloride induced cell death in mouse embryonic fibroblasts. Toxicol Sci. **82**, 638-646

88 Chandler, H. (1998) Metallurgy for the Non-Metallurgist. ASM International

89 Gunnar F. Nordberg, B. A. F., Monica Nordberg, Lars Friberg (2007) Handbook of the Toxicology of Metals Academic Press

90 Nordberg, G. (2007) Handbook on the toxicology of metals. Academic Press, Amsterdam ; Boston

91 Morel, F. M. and Price, N. M. (2003) The biogeochemical cycles of trace metals in the oceans. Science (New York, N.Y. **300**, 944-947

92 Casarett, L. J., Doull, J. and Klaassen, C. D. (2008) Casarett and Doull's toxicology : the basic science of poisons. McGraw-Hill, New York

93 Hu, Y., Su, L. and Snow, E. T. (1998) Arsenic toxicity is enzyme specific and its affects on ligation are not caused by the direct inhibition of DNA repair enzymes. Mutation research. **408**, 203-218

94 Stohs, S. J. and Bagchi, D. (1995) Oxidative mechanisms in the toxicity of metal ions. Free radical biology & medicine. **18**, 321-336

95 Vengellur, A. (2007) The role of HIF1[alpha] signalling in metal-induced toxicity. ed.)^eds.). pp. xiii, 227 leaves, Michigan State University. Dept. of Genetics, 2007.

96 Leonard, S. S., Harris, G. K. and Shi, X. (2004) Metal-induced oxidative stress and signal transduction. Free radical biology & medicine. **37**, 1921-1942

97 Goebeler, M., et al. (1995) Activation of nuclear factor-kappa B and gene expression in human endothelial cells by the common haptens nickel and cobalt. J Immunol. **155**, 2459-2467

98 Lichtlen, P. and Schaffner, W. (2001) The "metal transcription factor" MTF-1: biological facts and medical implications. Swiss Med Wkly. **131**, 647-652

99 Westin, G. and Schaffner, W. (1988) A zinc-responsive factor interacts with a metal-regulated enhancer element (MRE) of the mouse metallothionein-I gene. The EMBO journal. **7**, 3763-3770

100 Heuchel, R., et al. (1994) The transcription factor MTF-1 is essential for basal and heavy metal-induced metallothionein gene expression. The EMBO journal. **13**, 2870-2875

101 Goldwasser, E., Jacobson, L. O., Fried, W. and Plzak, L. (1957) Mechanism of the erythropoietic effect of cobalt. Science (New York, N.Y. **125**, 1085-1086

102 Goldberg, M. A., Dunning, S. P. and Bunn, H. F. (1988) Regulation of the erythropoietin gene: evidence that the oxygen sensor is a heme protein. Science (New York, N.Y. **242**, 1412-1415

103 Ladoux, A. and Frelin, C. (1994) Cobalt stimulates the expression of vascular endothelial growth factor mRNA in rat cardiac cells. Biochemical and biophysical research communications. **204**, 794-798

104 Yuan, Y., Hilliard, G., Ferguson, T. and Millhorn, D. E. (2003) Cobalt inhibits the interaction between hypoxia-inducible factor-alpha and von Hippel-Lindau protein by direct binding to hypoxia-inducible factor-alpha. The Journal of biological chemistry. **278**, 15911-15916

105 Salnikow, K., et al. (2004) Depletion of intracellular ascorbate by the carcinogenic metals nickel and cobalt results in the induction of hypoxic stress. The Journal of biological chemistry. **279**, 40337-40344

106 Malard, V., et al. (2007) Global gene expression profiling in human lung cells exposed to cobalt. BMC genomics. **8**, 147

107 Barceloux, D. G. (1999) Cobalt. Journal of toxicology. **37**, 201-206

108 Cobb, A. G. and Schmalzreid, T. P. (2006) The clinical significance of metal ion release from cobalt-chromium metal-on-metal hip joint arthroplasty. Proceedings of the Institution of Mechanical Engineers. **220**, 385-398

109 Morgan, G. B., Ozolins, G. and Tabor, E. C. (1970) Air pollution surveillance systems. Science (New York, N.Y. **170**, 289-296

110 Wehner, A. P., Busch, R. H., Olson, R. J. and Craig, D. K. (1977) Chronic inhalation of cobalt oxide and cigarette smoke by hamsters. American Industrial Hygiene Association journal. **38**, 338-346

111 Kriss, J. P., Carnes, W. H. and Gross, R. T. (1955) Hypothyroidism and thyroid hyperplasia in patients treated with cobalt. Journal of the American Medical Association. **157**, 117-121

112 Centeno, J. A., Pestaner, J. P., Mullick, F. G. and Virmani, R. (1996) An analytical comparison of cobalt cardiomyopathy and idiopathic dilated cardiomyopathy. Biological trace element research. **55**, 21-30

113 Jefferson, J. A., et al. (2002) Excessive erythrocytosis, chronic mountain sickness, and serum cobalt levels. Lancet. **359**, 407-408

114 Lauwerys, R. and Lison, D. (1994) Health risks associated with cobalt exposure--an overview. The Science of the total environment. **150**, 1-6

115 Ciafre, S. A., et al. (2007) CoCl(2)-simulated hypoxia in skeletal muscle cell lines: Role of free radicals in gene up-regulation and induction of apoptosis. Free radical research. **41**, 391-401

116 Karovic, O., et al. (2007) Toxic effects of cobalt in primary cultures of mouse astrocytes. Similarities with hypoxia and role of HIF-1alpha. Biochemical pharmacology. **73**, 694-708

Chapter 2

HIF1α is essential for normal intrauterine differentiation of alveolar epithelium and surfactant production in the newborn lung of mice

This chapter is the edited version of a research article that was published in The Journal of Biological Chemistry, Volume 283, No. 48 (33650-33657), November 28, 2008.

Authors: Yogesh Saini, Jack R. Harkema and John J. LaPres.

Abstract

Neonatal respiratory distress syndrome (RDS) is mainly the result of perturbation in surfactant production and is a common complication seen in premature infants. Normal fetal lung development and alveolar cell differentiation is regulated by a network of transcription factors. Functional loss of any of these factors will alter the developmental program and impact surfactant production and normal gas exchange. During development, the fetus is exposed to varying oxygen concentrations and must be able to quickly adapt to these changes in order to survive. Hypoxia-inducible factor 1α (HIF1α) is the primary transcription factor that is responsible for regulating the cellular response to changes in oxygen tension and is essential for normal development. Its role in lung maturation is not well defined and to address this knowledge gap, a lung-specific HIF1α knockout model has been developed. Loss of HIF1α early in lung development leads to pups that die within hours of parturition, exhibiting symptoms similar to RDS. Lungs from these pups display impaired alveolar epithelial differentiation and an almost complete loss of surfactant protein expression. Ultrastructural analysis of lungs from HIF1α deleted pups had high levels of glycogen, aberrant septal development, and changes in several factors necessary for proper lung development, including HIF2α, β-catenin and vascular endothelial growth factor. These results suggest that HIF1α is essential for proper lung maturation and alteration in its normal signaling during premature delivery might explain the pathophysiology of neonatal RDS.

Introduction

During development an embryo is exposed to varying levels of oxygen as a balance is created between vascularization and tissue growth. Localized hypoxia, a decrease in available oxygen, is a normal part of this process. The programmed responses to these decreases in available oxygen are essential for viability [1, 2]. *In utero*, the embryo is supplied with oxygen and nutrients through the placental barrier. Following parturition, oxygen is supplied by the neonatal lungs and therefore, proper intrauterine development of the alveolar gas exchange regions of the lung is essential for the newborn's first breath and for sustaining life outside the womb [3].

Lung morphogenesis is a complex process that is orchestrated by several transcription factors, growth factors, and extracellular cues [4]. For example, thyroid transcription factor-1 regulates the expression of the genes for Clara cell secretory protein (CCSP) produced in Clara cells in the tracheobronchial airways and various surfactants produced by alveolar type II cells in the lung parenchyma [5, 6]. CCAAT-enhancer binding protein α (CEBPα) is essential for proper regulation of alveolar Type II cell differentiation, and Forkhead box A2 (Foxa2) controls various cellular programs involved in lung development (e.g. surfactant expression) (6-8). Ablation of any of these factors results in major structural and functional abnormalities ranging from undeveloped alveolar structure and/or improper airway branching to the faulty processing of various secretory components [7, 8]. One of the extracellular cues that is

important for fetal vascular growth and lung morphogenesis is the physiologically low O_2 environment of the fetus. The ability to cope with this developmental "hypoxia" is not only important for lung maturation but essential for the viability of the fetus [1, 2].

Cellular responses to decreased oxygen availability are regulated by a family of proteins called hypoxia-inducible factors (HIFs). The ability of HIFs to respond to hypoxia is controlled by oxygen-dependent post-translational hydroxylation. The prolyl hydroxylases, PHDs, modify HIFs on essential residues in an oxygen-, iron- and α-ketoglutarate-dependent manner. Once hydroxylated, the HIF is quickly degraded in a proteasomal-dependent process that involves the Von Hippel Lindau (VHL) tumor suppressor. HIF1α, the most ubiquitously expressed HIF, has been shown to play a critical role in normal development. HIF1α regulates the expression of genes important for cellular adaptation to hypoxia, including glycolytic enzymes and angiogenic factors [9]. Gene deletion studies have established that HIF1α is indispensable during fetal development as

HIF1α$^{-/-}$ mice die at midgestation, in association with defects in VEGF expression and vascularization [10-12]. In addition, HIF1$^{+/-}$ mice developed pulmonary hypertension and pulmonary vascular remodeling under hypoxic conditions [13]. PHD inhibitor-induced HIF stabilization has been shown to improve lung growth in prematurely born baboon neonates, predominantly through enhanced expression of VEGF [14]. Finally, loss of HIF2α has been

shown to perturb normal lung development through loss of VEGF expression and to subsequently decrease alveolar type II cell production of pulmonary surfactants [15].

Previous studies using systemic HIF1α deletions have demonstrated its central role in development and partial HIF1α deletions resulted in disrupted normal functioning of tissues such as heart and lung [13, 16, 17]. The present study was aimed at elucidating the role(s) of HIF1α in the *in utero* differentiation of the alveolar epithelium. To this aim, mice with a lung-specific deletion of HIF1α (termed $HIF1\alpha^{\Delta/\Delta}$) were generated. Lung specific embryonic deletion of HIF1α earlier than 3 days prior to parturition led to $HIF1\alpha^{\Delta/\Delta}$ neonates exhibiting cyanosis and respiratory failure soon after birth. The expression of surfactant proteins was significantly lower in $HIF1\alpha^{\Delta/\Delta}$ pups as compared to littermate control pups. Examination of the lungs from $HIF1\alpha^{\Delta/\Delta}$ pups via light and transmission electron microscopy confirmed defects in both alveolar epithelial differentiation and septal development that resulted in the observed respiratory distress.

Material and methods

Transgenic mice and genotyping: $HIF1\alpha^{flox/flox}$ and SP-C-rtTA$^{-/tg}$/$(tetO)_7$-CMV-Cre$^{tg/tg}$ transgenic mice were generous gifts of Randall Johnson (UCSD) and Jefferey Whitsett (Cincinnati Children's Hospital Medical Center),

respectively [10, 17-19]. HIF1α$^{flox/flox}$ mice were mated to SP-C-rtTA$^{-/tg}$/ (tetO)$_7$-CMV-Cre$^{tg/tg}$ transgenic mice to generate SP-C-rtTA$^{-/tg}$/(tetO)$_7$-CMV-Cre$^{tg/tg}$/HIF1α$^{flox/flox}$ mice line capable of respiratory epithelium specific conditional recombination in the floxed HIF1α gene. In this model, depending on the day doxycycline is administered to the dam, various cell populations within the lung undergo recombination in HIF1α$^{flox/flox}$ alleles (20). Genotyping screening of the mice progeny was performed by PCR for all the three loci using previously published primer sequences (Table 1). Genomic DNA extraction from tail clipping was performed using Direct PCR extraction system (Viagen Biotech, CA) via manufacturer's instructions. PCR conditions were standardized for all the three alleles: denaturation at 94°C for 3 min; 38 cycles of denaturation at 94°C for 45 sec, annealing at 60°C for 45 sec and polymerization at 72°C for 60 sec. followed by a 7 min extension at 72°C. Size of the amplified products obtained were approx 210 bp for HIF1α (wild type); 244bp for HIF1α$^{flox/flox}$; 370 for *Cre* transgene; 350 for *rtTA* transgene (Fig. 1B).

Doxycycline treatment and animal husbandry: Dams bearing triple (SP-C-rtTA$^{-/tg}$/(tetO)$_7$-CMV-Cre$^{tg/tg}$/HIF1α$^{flox/flox}$) and double ((tetO)$_7$-CMV-Cre$^{tg/tg}$/HIF1α$^{flox/flox}$) transgenic embryos were maintained on doxycycline

feed (625 mg doxycycline/Kg; Harlan Teklad, Madison, WI) and drinking water (0.8 mg/ml: Sigma chemicals Co.). The day of parturition was taken as reference point to calculate the duration of doxycycline exposure. Control and $HIF1\alpha^{\Delta/\Delta}$ pups exposed to doxycycline treatment for 0 to14 Days *in utero* were sacked within one hour of parturition. All pups were sacrificed by decapitation. Mice used in this study were kept at the animal housing facility under the strict hygienic and pathogen free conditions approved by the university laboratory animal resource (ULAR) regulatory unit.

Lungs harvesting and processing: 3-8 pups were analyzed from each genotype and doxycycline treatment. Pups were assessed for total body and lung weight. Lung tissues were isolated and left lung lobe was fixed in 10% neutral buffered formalin (NBF) or 4% glutaraldehyde for morphological analysis. The remaining lung tissue was divided; half was snap frozen for Western blotting, half was stored in RNA*later* RNA Stabilization Reagent (Qiagen) for RNA isolation and qRT-PCR analysis.

Western blotting: Snap frozen lung tissue (10 mg) was lysed and homogenized in RIPA buffer (50 mM Tris HCl, 1% NP-40, 0.25% sodium deoxycholate, 150 mM NaCl, 1 mM each of EDTA, PMSF, sodium vandate, sodium fluoride, 1 M DTT) containing protease inhibitors (1µg/ml each of aprotinin, leupeptin, pepstatin) using a bead beater system (45 seconds at 30 Hz frequency). Insoluble material was removed by centrifugation (10,000 x g

for 10 min.) and protein concentration was measured in supernatant using Bradford protein assay [20]. Protein samples (30 µg) were separated by SDS-PAGE (NuPage 4-12% Bis-Tris gradient gel, Invitrogen, CA) and transferred to a nitrocellulose membrane. Western blots were performed with rabbit or goat antibodies against surfactant associated proteins (SP-A (sc 13977, Santa Cruz, CA), SP-B (AB 3780, Chemicon), SP-C (sc-13979, Santa Cruz, CA) and SP-D (SC 7709, Santa Cruz, CA), and β–actin (loading control; SC-7210, Santa Cruz, CA). Proteins were visualized with HRP-conjugated goat anti-rabbit IgG (sc-2004, Santa Cruz, CA) or rabbit anti-goat (sc-2768, Santa Cruz, CA) and ECL western blot system (Pierce, USA).

Histopathology and immunohistochemistry: At least four to six pups of each genotype and doxycycline treatment were analyzed for histopathological changes. Formalin fixed left lung lobe tissues were paraffin embedded and 5-micron thick sections were mounted on glass slides and stained with hematoxylin and eosin (H&E), periodic acid Schiff (PAS), or immunostained with SP-B (1: 500 dilution, AB3780, Chemicon, MA), SP-C (1:4000 dilution, antibody kindly provided by Jeffrey Whitsett) and CRE (1:100 dilution, AB24608; Abcam, Cambridge, MA). Briefly, tissue sections were deparaffinized and endogenous peroxidase activity was quenched by incubation with 6% H_2O_2 for 30 min. Immunostaining was performed using Rabbit Vector Elite ABC kit (Vector Laboratories, CA), according to the manufacturer's recommendations.

Transmission electron microscopy: Neonatal lung sections were fixed in 4% buffered glutaraldehyde overnight at 4°C, stored in the 10% NBF fixative until postfixation with 1% phosphate-buffered osmium tetroxide. Tissues were dehydrated through a graded series of ethanol and propylene oxide, and embedded in Poly/Bed-Araldite resin (Polysciences, Inc., Warrington, PA). One µm-thick sections were cut and stained with toluidine blue for light microscopic identification of specific tissue sites for transmission electron microscopy (TEM). Ultrathin tissue sections for TEM were cut at approximately 75 nm and stained with lead citrate and uranyl acetate. Sectioning was performed with an LKB Ultratome III (LKB Instruments, Inc., Rockville, MD). Ultrastructural tissue examination and photography were performed with a JEOL JEM 100CXII electron microscope (JEOL Ltd., Tokyo, Japan).

RNA isolation and real-time PCR analysis: 10 mg lung tissue stored in RNA*later* RNA Stabilization Reagent was homogenized in RLT buffer (RNeasy RNA isolation Kit, Qiagen, Maryland) using a Retsch MM200 bead beater system (Retsch, Haan, Germany). Total RNA quantification was performed spectrophotometrically (NanoDrop ND-1000 UV-Vis Spectrophotometer). Total RNA (1 µg) was reverse transcribed using superscript II reverse transcriptase kit (Invitrogen, CA). Expression level of selected genes involved in surfactant metabolism and lung development were analyzed by Real-Time PCR using SYBR green (Applied Biosystems, Foster City, CA) as previously

described [21]. Gene specific primers are listed Table 2. Copy number was determined by comparison with standard curves of the respective genes. This measurement was controlled for RNA quality, quantity, and RT efficiency by normalizing it to the expression level of the hypoxanthine guanine phosphoribosyl transferase (HGPRT) gene. Statistical significance was determined by use of normalized relative changes and ANOVA.

Quantitative analysis: qRT-PCR analysis was performed using unpaired two-tailed Student's *t*-test on GraphPad Prism. Results were considered significant at the 5% level.

Results

Conditional inactivation of HIF1α in the lung:

The HIF1α gene was inactivated in the lung by mating HIF1α conditional null mice ($HIF1\alpha^{flox/flox}$) [10] to an inducible bitransgenic mouse, SPC-rtTA, that expresses the reverse tetracycline transactivator (rtTA) under the control of the human surfactant protein C (SP-C) promoter and the Cre recombinase gene with a tetracycline operon (Fig. 2.1A) [18]. SPC-rtTA mice have been shown to express Cre recombinase specifically in the epithelial cells of the primordial lung buds as well as in the alveolar and bronchiolar epithelium of postnatal mice in the presence of an inducer (i.e. doxycycline) [19]. In the present study, compound litters from reciprocal matings between SP-C $-rtTA^{-/tg}$/ $(tetO)_7$-$CMV\text{-}Cre^{tg/tg}$/ $HIF1\alpha^{flox/flox}$ and $(tetO)_7$-$CMV\text{-}Cre^{tg/tg}$/

Figure 2.1. Lung specific, doxycycline-inducible deletion of HIF1α in triple transgenic mice.

(A) Triple transgenic mice were generated to induce expression of rtTA protein in the epithelial cells of the lung. rtTA expression is controlled by human *SP-C* promoter. Another transgene is *(tetO)7-CMV-Cre recombinase* transgene in which Cre recombinase expression is controlled by *(tetO)7-CMV* promoter in the presence of doxycycline, and rtTA protein. Cre recombinase recognizes the loxP sites flanking exon 2 of HIF1α locus and facilitates homologous recombination and thus inactivation of HIF1α locus. (B) Genotyping of transgenes. Gel shows the genotyping results for all the combinations of three transgenes. Floxed HIF1α size is 274 bp and wild type HIF1α is 240 bp. C, qRT-PCR results for HIF1α mRNA from triple transgenic mice in the absence (Control) and presence ($HIF1\alpha^{\Delta/\Delta}$) of doxycycline (14 day in *utero* exposure). Values are the average of five separate animals per group. D, Western blot analysis for HIF1α from lungs of triple transgenic mice in the absence (Control) and presence ($HIF1\alpha^{\Delta/\Delta}$) of doxycycline (14 day *in utero* exposure). Blots were also probed with a tubulin-specific antibody to demonstrate equal loading. Two independent animals from both groups are shown (1–4). "Images in this dissertation are presented in color."

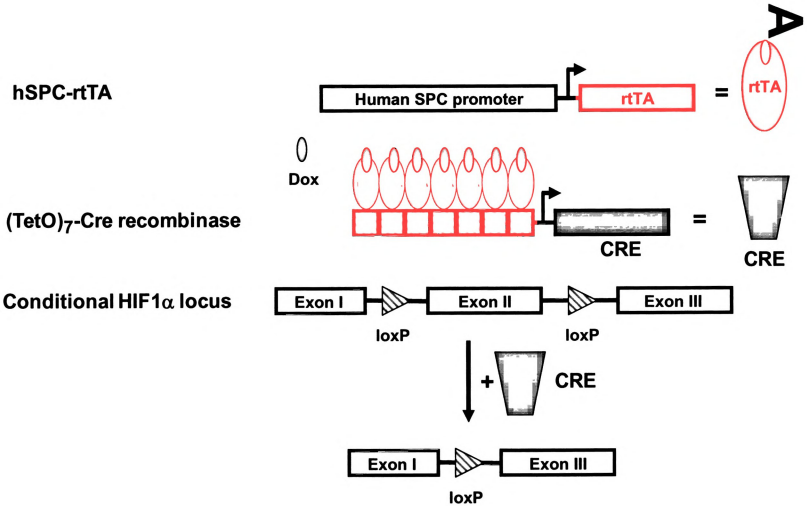
hSPC-rtTA
Human SPC promoter
rtTA
=
rtTA
Dox
(TetO)7-Cre recombinase
CRE
=
CRE
Conditional HIF1α locus
Exon I
Exon II
Exon III
loxP
loxP
+
CRE
Exon I
Exon III
loxP

Figure 2.1. Continued.

Figure 2.1 Continued.

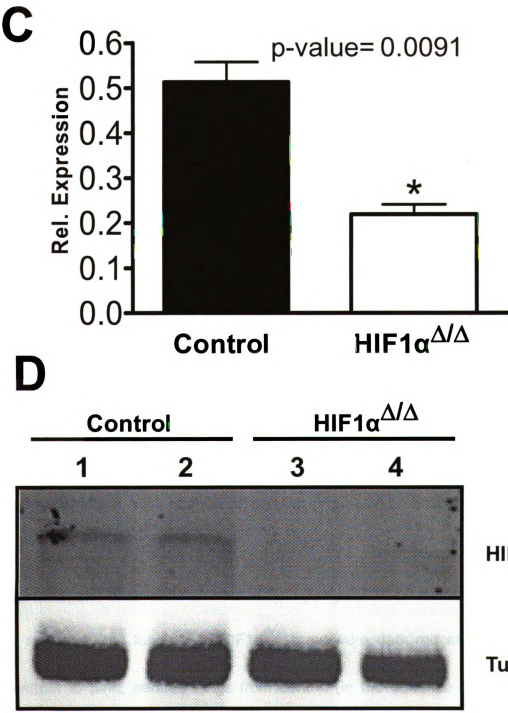

HIF1α$^{flox/flox}$ mice were composed of pups with mixed genotypes with respect to SPC-rtTA transgene. Their genotypic ratios were in accordance with Mendelian inheritance as demonstrated by genotyping (Fig. 2.1B). Analysis of these ratios from litters studied (N=30 litters and 190 pups) confirmed no *in utero* mortalities (data not shown). In the absence of doxycycline treatment, pups were phenotypically indistinguishable between litters. The functionality of the doxycyline treatment was demonstrated by the significant decrease in HIF1α mRNA as measured by qRT-PCR (Fig. 2.1C) and loss of HIF1α protein by Western blot analysis (Fig. 2.1D)

Lung-specific deletion of HIF1α causes lethal phenotype: To determine if *in utero* loss of HIF1α influenced litter size or the Mendelian distribution of pups, dams carrying triple transgenic embryos were exposed to doxycyline through feed and water for various lengths of time prior to parturition (i.e. 2, 4, 6, 8, 10, 12, and 14 days). Our findings indicate pups exposed to doxycyline *in utero* for more than 8 days prior to parturition had a 100% mortality rate, while those receiving the drug for 4-6 days prior to parturition had approximately a 15% chance of survival (Fig. 2.2A). Following parturition, HIF1α$^{Δ/Δ}$ pups [doxycyline-induced] developed respiratory distress, severe cyanosis, and died within an hour of birth (range of 10-60 minutes) (Fig. 2.2B). At necropsy, the lungs from HIF1α$^{Δ/Δ}$ pups were dark red and atelectic, in contrast to pink, aerated lungs from control (in the absence of doxycycline treatment) pups. Excised lung lobes from HIF1α$^{Δ/Δ}$ pups weighed slightly

more than the lungs from control mice and sank to the bottom of a saline-filled vial in contrast to the lungs from control littermates which floated in saline (Figs. 2.2C and 2.2D). At birth, the average total body weights of control littermate and HIF1α$^{\Delta/\Delta}$ were 1.318 ± 0.018 (SEM) and 1.288 ± 0.024 grams, respectively.

Defective lung morphology: The lungs of HIF1α$^{\Delta/\Delta}$ pups had histologic and ultrastructural features that indicate an impairment of normal *in utero* differentiation of alveolar epithelium, with a related loss of lung surfactant proteins that are essential for preventing collapse of individual alveoli and ensuring proper gas exchange to maintain life. Lungs of HIF1α$^{\Delta/\Delta}$ pups at birth had abnormally thickened alveolar septa (Fig 2.3C) lined by undifferentiated cuboidal epithelial cells (immature pneumocytes) containing large amounts of intracytoplasmic periodic acid Schiff (PAS)-positive material (Fig 2.3D) that was ultrastructurally identified, via transmission electron microscopy, as glycogen (Figs. 2.4C and 2.4D). There was a marked reduction of alveolar airspaces in the lungs of these mice due in part to the thickened septa and to focal areas of atelectasis. In contrast, the lungs of control mice at birth had uniformly dilated alveolar airspaces with much thinner alveolar septa that were lined by more differentiated surface epithelium containing much less PAS-positive glycogen (Figs. 2.3A and 2.3B).

Figure 2.2. Effects of lung specific deletion of HIF1α .

Graph of the percent viability of pups at birth versus intrauterine doxycycline treatment days. Doxycycline-induced lethality was more pronounced when the drug was delivered more than 4 days before parturition (circles). No lethality was observed in control group (no doxycyline, squares) or other possible genotype controls (data not shown). **(B)** At birth $HIF1\alpha^{\Delta/\Delta}$ pups were cyanotic (right) compared to normal, pink well oxygenated controls (left). **(C)** Mean lung weights of control (black bar) and $HIF1\alpha^{\Delta/\Delta}$ pups (white bar). The asterisk indicates a significant difference (*P* value < 0.05) based on a two-tailed *t* test for samples of unequal variance. The *P* value is indicated. **(D)** Vial containing excised lungs from newborn pups. Lungs from $HIF1\alpha^{\Delta/\Delta}$ (**Δ/Δ**) pups sink whereas control (**Ctrl**) lungs float in saline. "Images in this dissertation are presented in color."

A

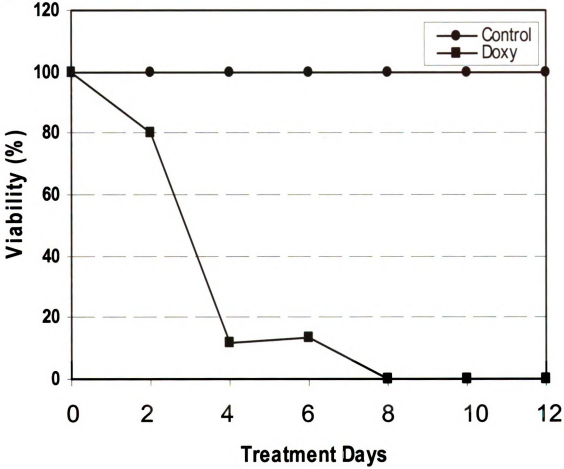

B

Control HIF1α$^{\Delta/\Delta}$

Figure 2.2. Continued.

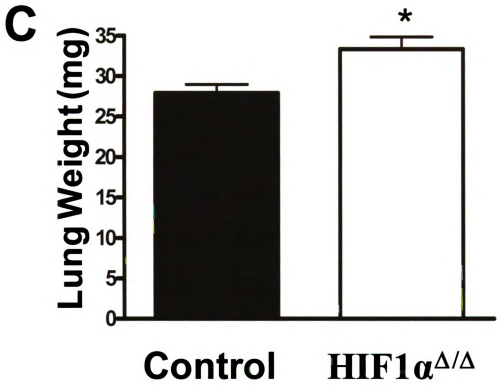

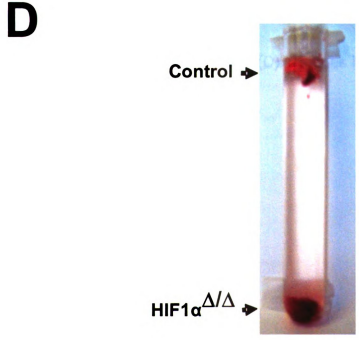

Figure 2.3. Pulmonary Histopathology of Lungs.

Light photomicrographs of hematoxylin and eosin stained lung sections from control (**A**) and HIF1α$^{\Delta/\Delta}$ (**C**) pups. Lung from HIF1α$^{\Delta/\Delta}$ pup has less alveolar airspace (a) and thicker alveolar septa (S) compared to control. Large cuboidal epithelial cells line the alveolar septa of HIF1α$^{\Delta/\Delta}$ pup while the alveolar septa of control pup is lined primarily by squamous epithelial cells (type 1) and only a few widely scattered cuboidal cells (type II). Periodic acid Schiff (PAS) stained lung sections from control (**B**) and HIF1α$^{\Delta/\Delta}$ (**D**) pups. Cuboidal epithelium lining alveolar septa in HIF1α$^{\Delta/\Delta}$ pup has greater PAS-stained glycogen (arrows) than that of the control pup (D). "Images in this dissertation are presented in color."

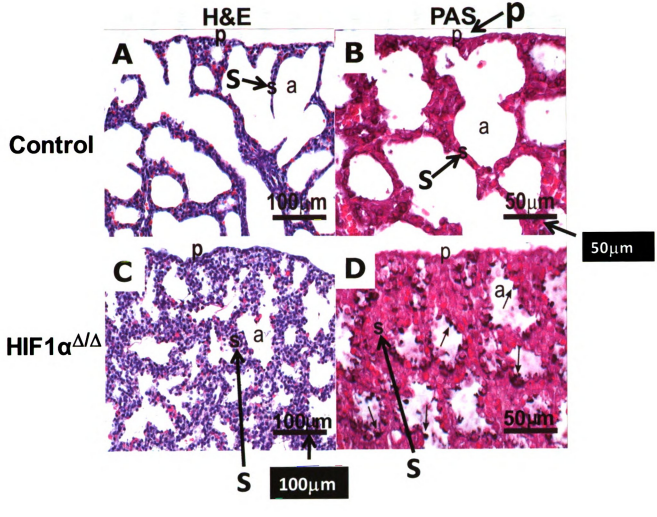
H&E
PAS
p
A
B
Control
S
a
100μm
50μm
C
D
HIF1α$^{\Delta/\Delta}$
100μm
50μm

Figure 2.4. Electron photomicrographs of alveolar epithelium of newborn pups.

Lung from control pup (A, B) has a well differentiated alveolar epithelium containing both type I and II cells (B). Stipled arrow indicates thin, squamoid, type I cells and solid arrows indicate tubular myelin figures (secreted surfactant) within the alveolar airspace of control pup. Type II cells have numerous intracytoplasmic lamellar bodies (lb) and apical microvilli (mv). In contrast the alveolar surface in HIF1α$^{\Delta/\Delta}$ pup (C, D) is lined by large undifferentiated cuboidal epithelial cells The cytoplasm of these epithelial cells are primarily filled with glycogen (*). No lamellar bodies are present in these cells. C, Capillary; rbc, red blood cells; II, type II alveolar epithelial cell; I, type I alveolar epithelial cell; if, interstitial fibroblast; *, glycogen; n, nucleus; 1, mitochondrion; 2, rough endoplasmic reticulum; pl, pleural surface; solid black arrows, tubular myelin; stipled arrow, type I cells. "Images in this dissertation are presented in color."

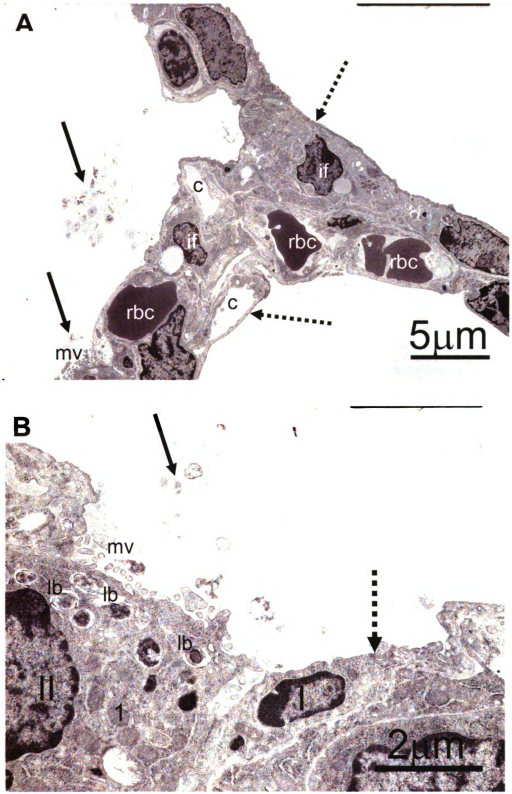
A
c
if
if
rbc
rbc
rbc
c
mv
5µm
B
mv
lb
lb
lb
ll
l
l
2µm

Figure 2.4 Continued.

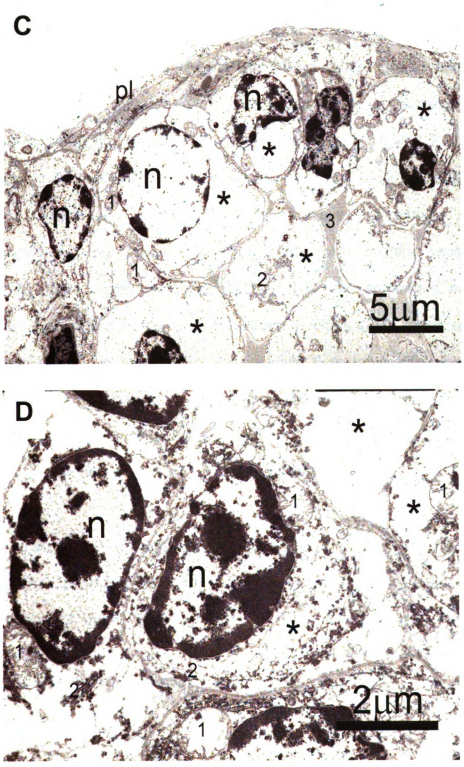

Ultrastructurally the luminal epithelium lining the alveolar airspace of control pups consisted of both alveolar type I and II cells (differentiated pneumocytes). Distinctive lamellar bodies were present in the apical cytoplasm of alveolar type II cells along with tubular myelin and secreted lamellar material (ultrastructural features of secreted surfactant) widely scattered along the alveolar luminal surface (Figs. 2.4A and 2.4B). These distinctive cuboidal epithelial cells also had a round to ovoid nucleus, an apical luminal surface lined by short microvilli, and numerous cytoplasmic organelles consisting of mitochondria, rough endoplasmic reticulum, and lysosomes. In contrast, Type I cells were identified by their thin squamous morphology containing few organelles and a fusiform nucleus (Figs. 2.4A and 2.4B). Interestingly, there were no microscopically detectable differences in the morphology of intrapulmonary conducting airways (preterminal and terminal bronchioles), lined principally by ciliated cells and nonciliated cuboidal (Clara) cells, between control and HIF1$\alpha^{\Delta/\Delta}$ pups at birth.

Altered surfactant metabolism:

qRT-PCR analysis of the genes for surfactant proteins show a decreased expression of SP-A, SP-B, and SP-C in the HIF1$\alpha^{\Delta/\Delta}$ mice compared to control pups (Fig. 2.5A). SP-D mRNA expression was not significantly different between the two genotypes.

Figure 2.5. Surfactant protein expression.

(A) mRNA levels for Surfactant associated proteins (SP-A, SP-B, SP-C and SP-D). Each expression level is expressed relative to HGPRT. **(B)** Immunoblot analysis of surfactant associated proteins (SP-A, SP-B, SP-C, and SP-D) in lung homogenates from control and HIF1α$^{\Delta/\Delta}$ pups (n=3). β-actin (actin) was used as loading control. (**C**) Immunohistochemical staining of SP-B (left panels) and SP-C (right panels) in lung sections from control **(upper panels)** and HIF1α$^{\Delta/\Delta}$ **(lower panels)** pups. HIF1α$^{\Delta/\Delta}$ pups show decreased expression of SP-B and SP-C as compared to control littermates. The asterisk indicates a significant difference (*P* value < 0.05) based on a two-tailed *t* test for samples of unequal variance. The *P* values are indicated. "Images in this dissertation are presented in color."

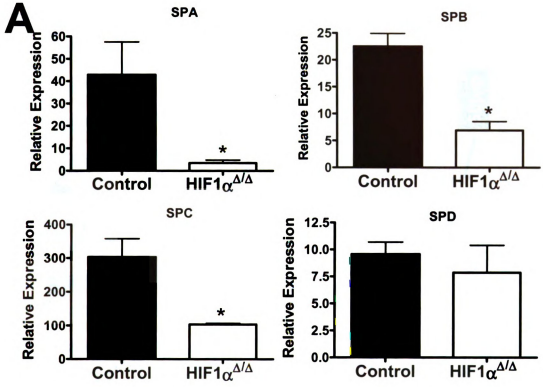
A
SPA
Relative Expression
60
50
40
30
20
10
0
*
Control
HIF1α Δ/Δ
SPB
Relative Expression
25
20
15
10
5
0
*
Control
HIF1α Δ/Δ
SPC
Relative Expression
400
300
200
100
0
*
Control
HIF1α Δ/Δ
SPD
Relative Expression
12.5
10.0
7.5
5.0
2.5
0.0
Control
HIF1α Δ/Δ

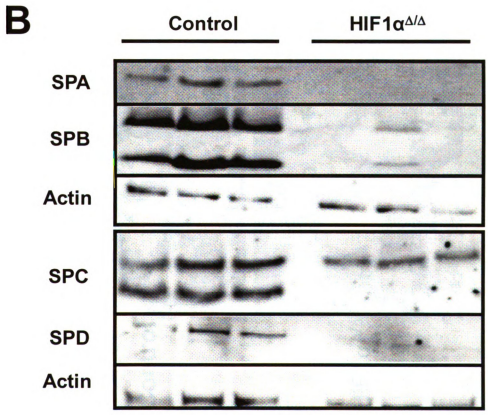
B
Control
HIF1α Δ/Δ
SPA
SPB
Actin
SPC
SPD
Actin

Figure 2.5. Continued.

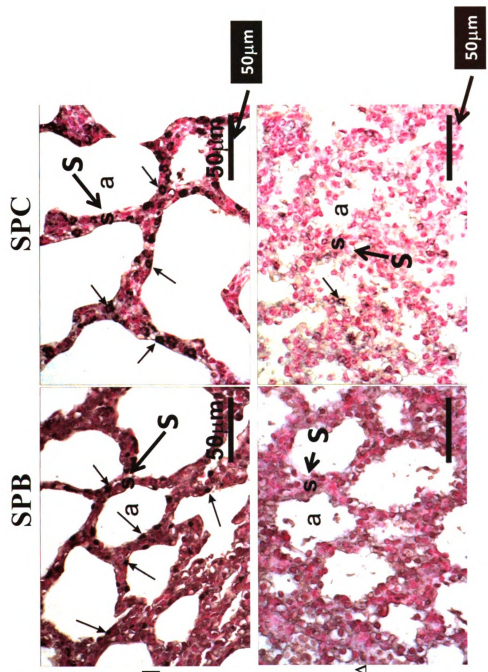

Western blot analysis of protein extract from HIF1α$^{\Delta/\Delta}$ and control animals was also performed to determine if surfactant protein levels were similar to gene expression patterns. All four surfactants displayed a substantial reduction in protein levels in the HIF1α$^{\Delta/\Delta}$ mice as compared to control pups (Fig. 2.5B). Immunohistochemical staining on lung sections confirmed the reduced levels of SP-B and SP-C in the HIF1α$^{\Delta/\Delta}$ compared to control pups (Fig. 2.5C). The reduced levels of surfactant mRNA and protein expression were consistent with the lack of alveolar epithelial differentiation and respiratory distress in the HIF1α$^{\Delta/\Delta}$ pups.

Altered Gene expression: To begin to understand how loss of HIF1α induced changes in lung morphology, qRT-PCR was performed on several critical genes known to be involved in lung development. These genes include β-catenin, clara cell secretory protein (CCSP), forkhead box A2 (Foxa2), forkhead box protein A1 (Foxa1, also known as HNF3α), thyroid transcription factor 1 (TTF-1), GATA binding protein 6 (Gata6), ATP-binding cassette, sub-family A (ABC1 member 3 (ABCA3), and CCAAT/enhancer binding protein alpha (CEBPα). There were no significant differences in the expression levels of Foxa2, ABCA3, CEBPα, TTF-1, Foxa1, or GATA, suggesting that HIF1α is not required for their normal expression and is most likely involved in later events in lung development (Fig. 2.6). However, lower levels of β-catenin,

Figure

Quantit

various

expres

a signif

sample

Figure 2.6. Expression of developmentally important genes.
Quantitative real time PCR was used to measure the mRNA levels of various genes known to play a role in lung development. Each expression level is expressed relative to HGPRT. The asterisk indicates a significant difference (*P* value < 0.05) based on a two-tailed *t* test for samples of unequal variance. The *P* values are indicated.

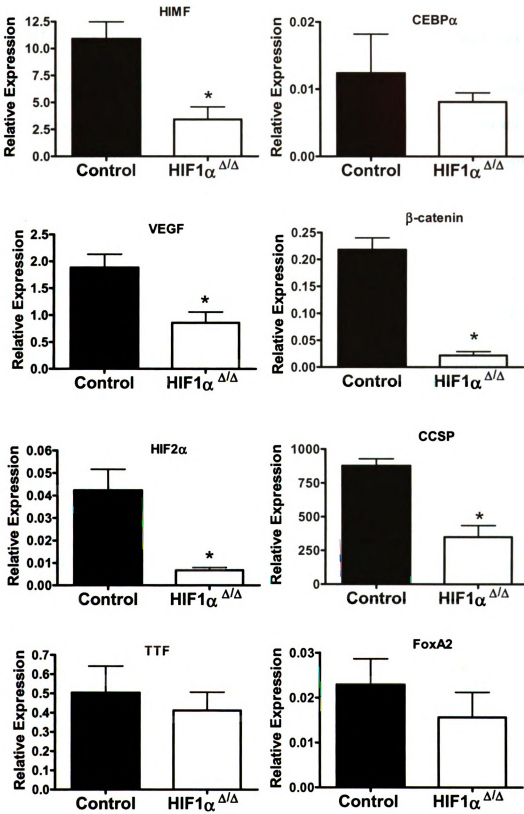
HIMF
Relative Expression
12.5
10.0
7.5
5.0
2.5
0.0
*
Control
HIF1α Δ/Δ
CEBPα
Relative Expression
0.02
0.01
0.00
Control
HIF1α Δ/Δ
VEGF
Relative Expression
2.5
2.0
1.5
1.0
0.5
0.0
*
Control
HIF1α Δ/Δ
β-catenin
Relative Expression
0.25
0.20
0.15
0.10
0.05
0.00
*
Control
HIF1α Δ/Δ
HIF2α
Relative Expression
0.06
0.05
0.04
0.03
0.02
0.01
0.00
*
Control
HIF1α Δ/Δ
CCSP
Relative Expression
1000
750
500
250
0
*
Control
HIF1α Δ/Δ
TTF
Relative Expression
0.7
0.6
0.5
0.4
0.3
0.2
0.1
0.0
Control
HIF1α Δ/Δ
FoxA2
Relative Expression
0.03
0.02
0.01
0.00
Control
HIF1α Δ/Δ

CCSP, HIMF, VEGF and HIF2α mRNA in neonatal HIF1α$^{\Delta/\Delta}$ pups compared to control littermates suggest that HIF1α plays a role in controlling their expression during maturation of the lung [15, 22]. Given the established role of these factors in regulating lung development, our data suggest that HIF1α is centrally located in the transcriptional network that is necessary for proper lung morphogenesis.

The previously described role of HIF2α in lung development, the similarity in phenotype between the HIF2α knockout survivors and HIF1α lung deletion strains, and the loss of HIF2α expression in the HIF1α$^{\Delta/\Delta}$ pups led us to determine the level of HIF2α expression at the protein level using immunohistochemistry [15]. In the presence of doxycyline there was a pronounced expression of Cre recombinase in all cell types of the lung (Fig. 2.7D). There was a corresponding loss in HIF1α expression in the alveolar tissue (Fig. 2.7E). Though HIF1α is not expressed ubiquitously throughout the lung, its cell specific expression was abrogated upon doxycycline treatment in the triple transgenic animal (Fig. 2.7). Surprisingly, the increased Cre recombinase and subsequent loss of HIF1α expression also led to a drastic decline in HIF2α levels in the lung (Figs. 2.7C and 2.7F).

Figure 2.7. Immunohistochemistry for Cre recombinase, HIF1α, and HIF2α.

Lung sections from control (A,B,C) and HIF1α$^{\Delta/\Delta}$ pups (D,E,F) were immunostained for Cre recombinase (A,D), HIF1α (B,E) and HIF2α (C,F). Immunohistochemistry for Cre recombinase shows strong staining of HIF1α$^{\Delta/\Delta}$ mouse alveolar epithelial cells (D, brown color). Positively stained cells for HIF1α and HIF2α are depicted by solid arrows. HIF1α$^{\Delta/\Delta}$ pups show decreased expression of HIF1α and HIF2α as compared to control littermates. a, air space; p, pleural surface; s, septa. "Images in this dissertation are presented in color."

Cre Recombinase
HIF1α
HIF2α
Control
HIF 1α Δ/Δ
A
B
C
D
E
F
p
S
a
50µm

Table 2.1: Primers for PCR-genotyping.

Allele	Forward Primer (5'-3')	Reverse Primer (5'-3')
HIF 1α	gca gtt aag agc act agt tg	gga gct atc tct cta gac c
Cre	tgc cac gac caa gtg aca gca atg	aga gac gga aat cca tcg ctc g
rtTA	gac aca tat aag acc ctg gtc a	aaa atc ttg cca gct ttc ccc

Table 2.2: Primers for real-time RT-PCR.

Gene	Forward Primer (5'-3')	Reverse Primer (5'-3')
SPA	gct gtc agt ggg gga taa ag	ctt tgt aat gct tgc gat gg
SPB	ctt gtc ctc cga tgt tcc ac	ggc ctg gtt gat cac aga ct
SPC	cag ctc cag gaa cct act gc	gct tag agg tgg gtg tgg ag
SPD	gag gtt gcc ttc tcc cac ta	agc ctg ttt gca cat ctc ct
HIF1-α	tgg ctc cct ata tcc caa tg	ggt ctg ctg gaa ccc agt aa
HIF2-α	gag caa gcc ttc caa gac ac	ttc gca ctg atg gtc ttg tc
β-catenin	ggc agc agc agt ctt act tg	aag gac tgg gaa aag cct tg
VEGF	tca cca aag cca gca cat ag	aat gct ttc tcc gct ctg aa
CCSP	cat cat gaa gct cac gga ga	gag aca cag ggc agt gac aa
FoxA2	gcc agc gag tta aag tat gc	tca tgt tgc tca cgg aag ag
HNF 3-α	ccc ttt ctc cct ttc act cc	gtg gtg ggc cta aca aca ac
TTF-1	gct ggc ctt tca gaa aat tg	gga cta ggg act ggg act gg
CEBPa	gca agc cag gac tag gag at	cgg aaa gtc tct cgg tct ca
HGPRT	aag cct aag atg agc gca ag	tta cta ggc aga tgg cca ca
PPI-A	agc ata cag gtc ctg gca tc	ttc acc ttc cca aag acc ac
ABCA3	gag ctt tgc cca cct aca ac	gaa act ggg agg gag agg ac
GATA 6	caa aag ctt gct ccg gta ac	ctg agg tgg tcg ctt gtg ta
Retnlα	tat gaa cag atg ggc ctc ct	ggt cca gtc aac gag taa gca

Discussion

Mammalian lung development and successful transition to extrauterine respiration involves a wide battery of biochemical, cellular and ultrastructural changes. This complex process begins at embryonic day E9.5 with most of the alveolar epithelial differentiation events starting at embryonic day E17.5. Several transcription factors control the temporal and positional epithelial differentiation process, as well as, the function of these differentiated cells. When the function of these critical factors is disrupted during development, lung function is compromised, leading to respiratory distress at birth. Our results have added HIF1α to this list of transcription factors that are critical for lung development. We have also demonstrated that loss of HIF1α during development leads to changes in the expression of other critical factors, such as HIF2α, VEGF and α-catenin [23].

HIFs are a class of transcription factors that play a critical role in oxygen sensing and the metabolic adaptations to hypoxia. Previous studies have shown that HIF1α levels are predominant during lung development until day E13.5, at which time, HIF2α becomes the major HIF in this tissue [24, 25]. Targeted gene disruption of the HIF1α locus results in the embryonic lethality due to cardiovascular defects [12]. Mice partially deficient for HIF1α alleles showed normal development but were physiologically compromised as they exhibited impaired pulmonary vascular remodeling under chronic hypoxic stress. In addition, the heterozygote was used to show that partial loss of

HIF1α alleles results in impaired pulmonary arterial myocyte electrophysiological responses under hypoxic stress [13, 25, 26]. The study presented here has shown that the lung-specific loss of HIF1α leads to neonatal respiratory distress syndrome due to impaired alveolar epithelial differentiation. Interestingly, the lungs of HIF1α$^{\Delta/\Delta}$ pups had normal morphogenesis of conducting airways with phenotypic alterations restricted to the alveolar parenchyma. These results suggest that HIF1α is involved in the late events of lung morphogenesis and alveolar epithelial differentiation but not in the early lung biogenesis and airway branching morphogenesis.

Respiratory distress syndrome and associated histopathology are phenotypic hallmarks of targeted deletion of several transcription factors, such as Foxa2, CEBPα, GATA-6, SMAD3, Calcineurin b1, and thyroid transcription factor-1, suggesting an intricate network of transcriptional regulation governing the complex ultrastructural maturation of lungs [8, 27-30]. Expression analysis demonstrated that the levels of Foxa2, Foxa1, CEBPα, and GATA-6 are comparable among pups with and without HIF1α (Fig. 2.6). This suggests that HIF1α acts either downstream or independent of these transcription factors. In contrast, the loss of HIF1α led to a decreased expression of other critical factors, including CCSP, β-catenin, HIMF, VEGF, and HIF2α (Fig. 2.6). Recently, the loss of HIF2α and subsequent decrease in VEGF has been linked to respiratory distress syndrome [15]. These experiments involved a subset of HIF2α$^{-/-}$ mice that were viable up to parturition and displayed similar

pathology to the HIF1α$^{\Delta/\Delta}$ mice described here. Delivery of VEGF, either intrauterine or postnatal intratracheal instillation protected the HIF2α$^{-/-}$ mice from symptoms of respiratory distress syndrome. Given that HIF2α expression is abrogated in the HIF1α$^{\Delta/\Delta}$ pups suggests that HIF1α regulates HIF2α early in lung development and the subsequent loss of VEGF might explain the pathology of the HIF1α$^{\Delta/\Delta}$ pups. It remains to be seen if the decrease in VEGF expression is due to direct loss of HIF1α or indirectly through the loss of HIF2α expression. More importantly, the pathophysiology of the HIF1α$^{\Delta/\Delta}$ mouse resembles that of the HIF2α$^{-/-}$ mouse in relation to the lack of differentiation of type II pneumocytes and increased septal thickness. In addition, the HIF1α$^{\Delta/\Delta}$ pups display large glycogen stores with concurrent loss of surfactant protein expression.

In conclusion, these studies provide evidence that HIF1α plays an important role in lung development. The respiratory failure induced by lung-specific deletion of HIF1α, suggests that hypoxia and HIF1α-regulated genes play an essential role in lung maturation, especially proper differentiation of type II alveolar cells. HIF1α's potential upstream regulatory function of HIF2α and VEGF expression, directly or indirectly, offers a mechanism of action for the phenotypic observations. Finally, the results suggest that the hypoxia signaling cascade is important during the later stages of lung development but

not essential in the initial patterning of the tissue. HIFs seem to play a later role in directing cell differentiation and regulating growth factors necessary for lung remodeling required for sustaining life extrauterine. Understanding the pathways necessary for proper HIF expression and function and the downstream pathways influenced by these factors will impact our ability to treat RDS and other diseases of the lung.

REFERENCES

1 Webster, W. S. and Abela, D. (2007) The effect of hypoxia in development. Birth Defects Res C Embryo Today. **81**, 215-228

2 Giaccia, A. J., Simon, M. C. and Johnson, R. (2004) The biology of hypoxia: the role of oxygen sensing in development, normal function, and disease. Genes Dev. **18**, 2183-2194

3 James Metcalfe, H. B., Waldemar Moll. (1967) Gas Exchange in the Pregnant Uterus. Physiol. Rev. **47**, 782-838.

4 Groenman, F., Unger, S. and Post, M. (2005) The molecular basis for abnormal human lung development. Biology of the Neonate. **87**, 164-177

5 Cassel, T. N., Suske, G. and Nord, M. (2000) C/EBP alpha and TTF-1 synergistically transactivate the Clara cell secretory protein gene. Annals of the New York Academy of Sciences. **923**, 300-302

6 deFelice, M., et al. (2003) TTF-1 phosphorylation is required for peripheral lung morphogenesis, perinatal survival, and tissue-specific gene expression. Journal of Biological Chemistry. **278**, 35574-35583

7 Mucenski, M. L., et al. (2003) beta-Catenin is required for specification of proximal/distal cell fate during lung morphogenesis. J Biol Chem **278**, 40231-40238

8 Wan, H. J., et al. (2004) Foxa2 is required for transition to air breathing at birth. Proceedings of the National Academy of Sciences of the United States of America. **101**, 14449-14454

9 Semenza, G. L. (2000) HIF-1: mediator of physiological and pathophysiological responses to hypoxia. Journal of Applied Physiology. **88**, 1474-1480

10 Ryan, H. E., Lo, J. and Johnson, R. S. (1998) HIF-1 alpha is required for solid tumor formation and embryonic vascularization. Embo Journal. **17**, 3005-3015

11 Kotch, L. E., Iyer, N. V., Laughner, E. and Semenza, G. L. (1999) Defective vascularization of HIF-1 alpha-null embryos is not associated with VEGF deficiency but with mesenchymal cell death. Developmental Biology. **209**, 254-267

12 Iyer, N. V., et al. (1998) Cellular and developmental control of O_2 homeostasis by hypoxia-inducible factor 1 alpha. Genes & Development. **12**, 149-162

13 Yu, A. Y., et al. (1999) Impaired physiological responses to chronic hypoxia in mice partially deficient for hypoxia-inducible factor 1alpha. J Clin Invest. **103**, 691-696

14 Asikainen, T. M., et al. (2006) Improved lung growth and function through hypoxia-inducible factor in primate chronic lung disease of prematurity. Faseb Journal. **20**, (E986-E994) 1698-1700

15 Compernolle, V., et al. (2002) Loss of HIF-2alpha and inhibition of VEGF impair fetal lung maturation, whereas treatment with VEGF prevents fatal respiratory distress in premature mice. Nat Med. **8**, 702-710

16 Tomita, S., et al. (2003) Defective brain development in mice lacking the Hif-1alpha gene in neural cells. Mol Cell Biol. **23**, 6739-6749

17 Ryan, H. E., et al. (2000) Hypoxia-inducible factor-1 alpha is a positive factor in solid tumor growth. Cancer Research. **60**, 4010-4015

18 Perl, A. K., et al. (2002) Early restriction of peripheral and proximal cell lineages during formation of the lung. Proc Natl Acad Sci U S A. **99**, 10482-10487

19 Lobe, C. G., et al. (1999) Z/AP, a double reporter for cre-mediated recombination. Dev Biol. **208**, 281-292

20 Bradford, M. M. (1976) A rapid and sensitive method for the quantitation of microgram quantities of protein utilizing the principle of protein-dye binding. Analytical biochemistry. **72**, 248-254

21 Vengellur, A. and LaPres, J. J. (2004) The role of hypoxia inducible factor 1 alpha in cobalt chloride induced cell death in mouse embryonic fibroblasts. Toxicological Sciences. **82**, 638-646

22 Mucenski, M. L., et al. (2003) beta-catenin is required for specification of proximal/distal cell fate during lung morphogenesis. Journal of Biological Chemistry. **278**, 40231-40238

23 Maeda, Y., Dave, V. and Whitsett, J. A. (2007) Transcriptional control of lung morphogenesis. Physiological reviews. **87**, 219-244

24 Ema, M., et al. (1997) A novel bHLH-PAS factor with close sequence similarity to hypoxia-inducible factor 1alpha regulates the VEGF expression and is potentially involved in lung and vascular development. Proc Natl Acad Sci U S A. **94**, 4273-4278

25 Shimoda, L. A., et al. (2001) Partial HIF-1 alpha deficiency impairs pulmonary arterial myocyte electrophysiological responses to hypoxia. American Journal of Physiology-Lung Cellular and Molecular Physiology. **281**, L202-L208

26 Semenza, G. L. (2005) Pulmonary vascular responses to chronic hypoxia mediated by hypoxia-inducible factor 1. Proceedings of the American Thoracic Society. **2**, 68-70

27 Dave, V., et al. (2006) Calcineurin/Nfat signaling is required for perinatal lung maturation and function. The Journal of clinical investigation. **116**, 2597-2609

28 Devriendt, K., Vanhole, C., Matthijs, G. and de Zegher, F. (1998) Deletion of thyroid transcription factor-1 gene in an infant with neonatal thyroid dysfunction and respiratory failure. New England Journal of Medicine. **338**, 1317-1318

29 Liu, C., Morrisey, E. E. and Whitsett, J. A. (2002) GATA-6 is required for maturation of the lung in late gestation. American Journal of Physiology-Lung Cellular and Molecular Physiology. **283**, L468-L475

30 Martis, P. C., et al. (2006) C/EBP alpha is required for lung maturation at birth. Development. **133**, 1155-1164

Chapter 3

Loss of HIF2α rescues the HIF1α deletion phenotype of neonatal respiratory distress in mice

Abstract

Hypoxia is defined as a state of decreased oxygen reaching the tissues of the body. During normal prenatal development, the fetus is exposed to hypoxic conditions and the fetus' response to these localized occurrences of oxygen deprivation is essential for proper organogenesis and survival. The mammalian response to these decreases in oxygen availability is regulated by the hypoxia-inducible factors (HIFs). HIFs are transcription factors responsible for regulating the cellular adaptation to hypoxia through direct modulation of key genes involved in glycolysis, angiogenesis, and erythropoiesis. HIF1α and HIF2α, two key isoforms, are important in embryonic development, however; their role in lung maturation is not well defined. We have recently shown that the loss of HIF1α early in lung development leads to pups that die within an hour of parturition, exhibiting symptoms similar to neonatal respiratory distress syndrome (RDS). To further investigate the independent role of HIF2α and its ability to alter HIF1α-mediated lung maturation, we generated two additional lung-specific HIFα knockout models (HIF2α and HIF1α+HIF2α). Our current study has shown that the intrauterine loss of HIF2α does not display signs of RDS. More interestingly, survivability observed after the loss HIF1α and HIF2α suggests that the loss of HIF2α is capable of rescuing the neonatal RDS phenotype seen in HIF1α deficient pups. Microarray analyses on the total mRNA from these three genotypes have identified several factors, such as MMP-9, Acot-9, CDS-1, and IL1R-II,

that are differentially regulated by the two isoforms of HIFα. These results suggest that HIFα isoforms are involved in lung maturation and differentiation and further understanding of mechanisms underlying the observed phenotype might explain the pathophysiology of neonatal RDS.

Introduction

During gestation, the oxygen needs of the developing fetus are met via placental gas exchange. Developmental defects specific to the lung fail to manifest until the parturition stage, when placental roles of oxygen and nutrient supply are taken over by the neonate. Thus, proper intrauterine development of the alveolar gas exchange regions of the lung is essential for the newborn's first breath and for sustaining life outside the womb [1]. Lung development, similar to all the other tissues in the fetus, is a highly coordinated series of events involving complex intracellular and extracellular signals that control transcriptional programs leading to proper cellular behavior and morphogenesis.

Lung morphogenesis and alveoli formation processes are regulated through the temporo-spatial expression of a plethora of transcription factors, growth regulators, and environmental signals [2]. Proteins, such as TTF-1, TGF-β, CEBPα, GATA-6, CEBP-α, KLF-5, Foxa1, and Foxa2 have been shown to be critical for proper lung development [3-9]. Alveolar epithelium-specific ablation of these and several other genes compromise lung function and perinatal survivability [6, 10]. Most of these factors function to transduce extracellular signals into developmental outcomes. One important extracellular signal is oxygen availability. A decrease in available oxygen, referred to as hypoxia, is a natural occurring condition within a fetus. Sensing

hypoxia is essential for proper development and mammals use a family of proteins called, the hypoxia inducible factors (HIFs) to perform this task.

There are three cytosolic HIFs, HIF1α, HIF2α, HIF3α, and each is oxygen labile. In the presence of adequate oxygen, these HIFs are modified by prolyl hydroxylases(PHDs), in an oxygen-, iron- and α-ketoglutarate-dependent manner. Upon hydroxylation, the cytosolic HIF becomes a substrate for ubiquitination by the Von Hippel Lindau (VHL) tumor suppressor and thereafter, HIFα is proteasomaly degraded. Under the conditions of oxygen deprivation, PHD activity is inhibited leading to the stabilization and translocation of HIFα into the nucleus and subsequent dimerization with the aryl hydrocarbon nuclear translocator (ARNT, also known as HIF1β). The active dimer binds to the hypoxia responsive element sequence in the promoter region of hypoxia responsive genes [11].

HIF target genes have been shown to play important roles in processes such as glycolysis, angiogenesis, erythropoiesis and development. Studies have suggested that the low oxygen environment in the developing lung is required for HIF-regulated pathways that are essential for proper organogenesis [12, 13]. For example, mice lacking HIF1α, the most ubiquitously expressed HIF, display disorganized yolk sac vascularization and cardiac defects [14]. HIF1α-deficient embryos also exhibited only a few capillaries in the neural fold with complete absence of vascular network and

also reduced size of dorsal aorta [15]. In addition, HIF1$^{+/-}$ mice developed pulmonary hypertension and pulmonary vascular remodeling under hypoxic conditions [16]. Similarly, homozygous deficiency of HIF2α in murine embryo results in vascular disorganization in yolk sac and failure to assemble and maintain vascular tubular structure and leading eventually to death between day E9.5 and E13.5 [17, 18]. The defective phenotype of HIF1α$^{-/-}$ were further aggravated by deleting either or both alleles of HIF2α. HIF1α$^{-/-}$/2α$^{-/-}$ mice showed absence of placental vasculature, increase in trophoblastic giant cells, poor invasive efficiency and defective placental structure thus representing phenocopy of ARNT deficient mice [13]. The mid-gestational lethality of the systemic knockout models has made it challenging to study the role of different HIF proteins in fetal lung development.

Current understanding of the role of HIF signaling in the lung development is limited. It has been shown that the PHD inhibitor, FG-4095, can improve lung growth in prematurely born baboon neonates, predominantly through HIF-mediated enhanced expression of VEGF [19]. In addition, some of the progeny from HIF2α$^{-/-}$ mice within the isogenic 129S6/SvEvTac strain survive to parturition and die shortly after birth from a respiratory distress syndrome-like pathology. The cause of this was linked to loss of VEGF expression that resulted in pulmonary surfactant deficiency [20]. Finally, lung-

specific knockout mice demonstrated that HIF1α is indispensable for lung development and is an important factor in surfactant production and cellular differentiation [21]. Moreover, the lung-specific deletion of HIF1α alters the expression of factors with putative roles in lung development, including HIF2α.

The collective role of HIF1α and HIF2α in lung development, their place in the transcriptional network necessary for proper cellular differentiation, and their potential redundant function in lung development are still unclear. To increase our understanding of the role of these two HIFs in lung development, mice with a lung-specific deletion of HIF1α (termed HIF1α$^{\Delta/\Delta}$), HIF2α (termed HIF2α$^{\Delta/\Delta}$), and both HIF1α and HIF2α (termed HIF1/2α$^{\Delta/\Delta}$) were generated. These studies confirmed that HIF1α is essential for proper lung development. Interestingly, the lung specific deletion of HIF2α did not confirm previous published reports and displayed no lethality upon parturition. More importantly, simultaneous deletion of both isoforms of HIF rescued the respiratory distressed phenotype that was observed after HIF1α deletion. In addition, a battery of genes has been identified that might be related to the described phenotype in each of the genotypes. These results demonstrate a non-redundant function for HIF1α and HIF2α in lung development and establish hypoxia and HIF-mediated signaling pathways that are altered upon their manipulation.

Material and methods

Transgenic mice and genotyping: HIF1α$^{flox/flox}$, HIF2α$^{flox/flox}$ and SPC-rtTA$^{-/tg}$/ (tetO)$_7$-CMV-Cre$^{tg/tg}$ transgenic mice were generous gifts from Randall Johnson (UCSD), M. Celeste Simon (University of Pennsylvania) and Jeffrey Whitsett (Cincinnati Children's Hospital Medical Center), respectively [22-26]. In the present study, we used these three transgenic mice to generate three genotypically different mice lines, SPC-rtTA$^{-/tg}$/(tetO)$_7$-CMV-Cre$^{tg/tg}$/HIF1α$^{flox/flox}$,SPC-rtTA$^{-/tg}$/(tetO)$_7$-CMV-Cre$^{tg/tg}$/HIF2α$^{flox/flox}$, and SPC-rtTA$^{-/tg}$/(tetO)$_7$-CMV-Cre$^{tg/tg}$/HIF1α$^{flox/flox}$/HIF2α$^{flox/flox}$ [21]. All of these three mice lines are capable of respiratory epithelium specific conditional recombination in the floxed HIFα alleles (Fig. 3.1). In this model, depending upon the day doxycycline is administered to the dam, various cell populations within the lung undergo recombination in the floxed alleles [24]. Genotyping screening of the mice progeny was performed by PCR for all the three loci using previously published primer sequences. Genomic DNA extraction from tail clipping was performed using Direct PCR extraction system (Viagen Biotech, CA) via manufacturer's instructions. PCR conditions were standardized for all the three alleles: denaturation at 94˚C for 3 min; 38 cycles of denaturation at 94˚C for 45 sec, annealing at 60˚C for 45 sec and polymerization at 72˚C for 60 sec. followed by a 7 min extension at 72˚C. Size of the amplified products obtained were approx 210 bp for HIF1α (wild type);

244 bp for HIF1α$^{flox/flox}$; 410 bp for HIF2α (wild type); 444bp for HIF2α$^{flox/flox}$; 370 for Cre transgene; 350 for rtTA transgene (Fig. 3.2). Each mouse line was maintained in a mixed C57BL/6:FVB background.

Doxycycline treatment and animal husbandry: Triple and quadruple transgenic pups were exposed to doxycycline *in utero* to generate lung-specific HIF-deficient pups. Dams were maintained on the doxycycline feed (625 mg doxycycline/Kg; Harlan Teklad, Madison, WI) and drinking water (0.8 mg/ml: Sigma chemicals Co.) from day E4.5 until day PN1. All the HIF-deficient pups born from these dams will be referred to as HIF1α$^{\Delta/\Delta}$, HIF2α$^{\Delta/\Delta}$ or HIF1α$^{\Delta/\Delta}$/HIF2α$^{\Delta/\Delta}$. Triple and quadruple transgenic mice that were not exposed to doxycycline will be referred to as controls. All the animal handling and necropsy protocols were approved by the ULAR regulatory unit of Michigan State University. Mice used in this study were kept at the animal housing facility under the strict hygienic and pathogen free conditions approved by the university laboratory animal resource (ULAR) regulatory unit.

Lungs harvesting and processing: Control and HIF1α$^{\Delta/\Delta}$, HIF2α$^{\Delta/\Delta}$ or HIF1α$^{\Delta/\Delta}$/HIF2α$^{\Delta/\Delta}$ pups were either sacrificed within one hour of parturition

Figure 3.1. Lung specific, doxycycline-inducible deletion of HIF1α and HIF2α in triple transgenic mice.

Triple transgenic mice were generated to induce expression of rtTA protein in the epithelial cells of the lung. rtTA expression is controlled by the human *SP-C* promoter. Another transgene is *(tetO)7-CMV-Cre recombinase* transgene in which Cre recombinase expression is controlled by *(tetO)7-CMV* promoter. In the presence of doxycycline, the rtTA protein is produced and activates the expression of the Cre-recombinase. Cre recombinase recognizes the loxP sites flanking exon 2 of the HIF1α and/or HIF2α locus and facilitates homologous recombination and thus inactivation of respective HIFα locus.

"Images in this dissertation are presented in color".

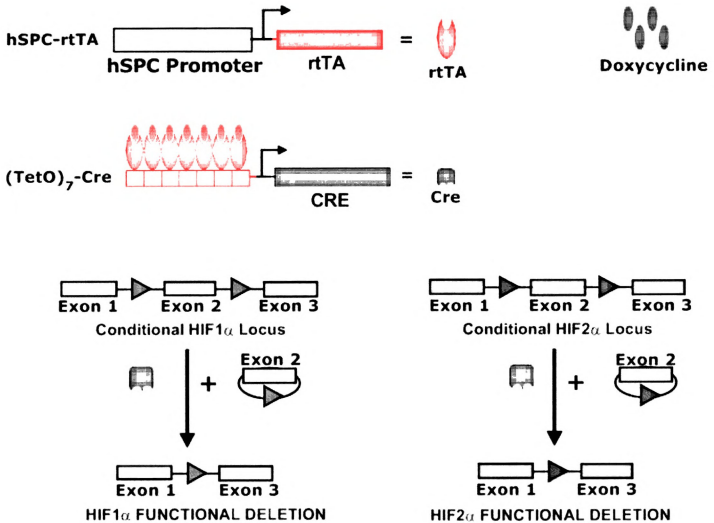
hSPC-rtTA
hSPC Promoter
rtTA
=
rtTA
Doxycycline
(TetO)7-Cre
CRE
=
Cre
Exon 1
Exon 2
Exon 3
Conditional HIF1α Locus
Exon 2
+
Exon 1
Exon 3
HIF1α FUNCTIONAL DELETION
Exon 1
Exon 2
Exon 3
Conditional HIF2α Locus
Exon 2
+
Exon 1
Exon 3
HIF2α FUNCTIONAL DELETION

Figure 3.2. Genotyping of transgenes.

Gel shows the PCR genotyping results for all the combinations of four transgenes. Sizes of the amplified products obtained are: 240 bp for HIF1α (wild type); 274 bp for $HIF1\alpha^{flox/flox}$; 410 bp for HIF2α (wild type); 444bp for $HIF2\alpha^{flox/flox}$; 370 for Cre transgene; 350 for rtTA transgene. One representative sample from each of three generated mice ($SPC\text{-}rtTA^{-/tg}/(tetO)_7\text{-}Cre^{-/tg}/HIF1\alpha^{fl/fl}$ (**Lane 1**), $SPC\text{-}rtTA^{-/tg}/(tetO)_7\text{-}Cre^{-/tg}/HIF2\alpha^{fl/fl}$ mouse (**Lane 2**), and $SPC\text{-}rtTA^{-/tg}/(tetO)_7\text{-}Cre^{-/tg}/HIF1\alpha/2\alpha^{fl/fl}$ (**Lane 3**)) was genotyped for the four transgenes.

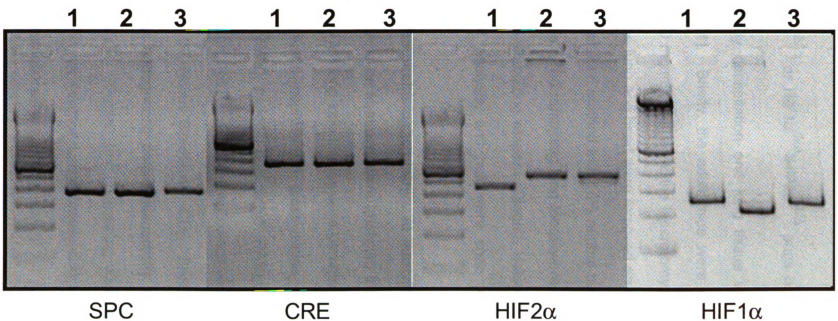
1 2 3
1 2 3
1 2 3
1 2 3
SPC
CRE
HIF2α
HIF1α

or at day PN60 ($HIF2\alpha^{\Delta/\Delta}$ or $HIF1\alpha^{\Delta/\Delta}/HIF2\alpha^{\Delta/\Delta}$ pups only). All neonatal pups were sacrificed by decapitation and lung tissue was harvested as described previously [21]. Briefly, the adult mice were anesthetized with sodium pentobarbital (50 mg/ml), and a midline laparotomy was performed to canulate the trachea. The lung and heart were removed *en bloc.* The left lobe was fixed via perfusion inflation method with 10% neutral buffered formalin for histopathological analysis. The remaining lung lobes were divided: half were stored in RNA*later* RNA stabilizing reagent (Qiagen, Valencia, CA) for RNA isolation and qRT-PCR analysis, and half were snap frozen for protein extraction.

Histopathology and immunohistochemistry: At least four to six pups of each genotype and doxycycline treatment were analyzed for histopathological changes. Formalin fixed left lung lobe tissues were paraffin embedded and 5-micron thick sections were mounted on glass slides and stained with hematoxylin and eosin (H&E), periodic acid Schiff (PAS), or immunostained with HIF1α (1:250 dilution, NB100-479, Novus Biologicals, CO) and HIF2α (1:150 dilution, NB100-122, Novus Biologicals, CO). Briefly, tissue sections were deparaffinized and endogenous peroxidase activity was quenched by incubation with 6% H_2O_2 for 30 min. Immunostaining was performed using Rabbit Vector Elite ABC kit (Vector Laboratories, CA), according to the manufacturer's recommendations.

RNA Isolation

Lung tissue (10 mg) stored in RNA*later* RNA Stabilization Reagent was homogenized in RLT buffer (RNeasy RNA isolation Kit, Qiagen, Maryland) using a Retsch MM200 bead beater system (Retsch, Haan, Germany). Total RNA quantification was performed spectrophotometrically (NanoDrop ND-1000 UV-Vis Spectrophotometer). Isolated RNA was resuspended in RNAase free water, quantified (A_{260}), and concentration was calculated by spectrophotometric methods (A_{260}). Purity was assessed by the A_{260}:A_{280} ratio and by visual inspection of 3 µg on a denaturing gel.

Microarray Experimental Design

The lung RNA samples extracted from HIF1α$^{\Delta/\Delta}$, HIF2α$^{\Delta/\Delta}$ or HIF1/2α$^{\Delta/\Delta}$ and control animals were individually hybridized to 4 x 44K whole mouse genome oligo microarrays (Agilent Technologies, Inc., Santa Clara, CA). Hybridizations were performed with four biological replicates per group, using one-color labeling (Cy3), according to the manufacturer's protocol (Agilent Manual: G4140-90040 v. 5.7). Briefly, 1 µg of total RNA from each sample was reverse-transcribed to cDNA in the presence of RNA One-Color Spike-In mix, T7 Promoter primer, 5X First Strand Buffer, 0.1M DDT, 10 mM dNTP mix, MLV-RT and RNaseOut during 2 h incubation at 40°C. Obtained cDNA was then converted to fluorescently labeled cRNA and amplified using 4X Transcription Buffer, 0.1M DDT, NTP mix, 50% PEG, RNaseOut, Inorganic

pyrophosphatase, T7 RNA Polymerase and Cyanine 3-CTP (Cy3) during second 2 h incubation at 40°C. The cRNA was purified using RNeasy Isolation Kit (Qiagen) and eluted with RNase-free water. Purified cRNA was assessed for Cy3 absorbance and concentration using NanoDrop spectrophometry. Fluorescently labeled cRNA was fragmented using 25X Fragmentation Buffer and 10X Blocking Agent for 30 min at 60°C before samples were hybridized. After 17 h incubation at 65°C, microarray slides were washed and scanned at 532 nm (Cy3) on a GenePix 4000B scanner (Molecular Devices, Union City, CA). Images were analyzed for feature and background intensities using GenePix Pro 6.0 (Molecular Devices). All data were managed in TIMS dbZach data management system [27].

Microarray Analysis and Functional Annotation

All microarray data in this study passed quality assurance protocols [28]. Microarray data were normalized using a semiparametric approach [29] and the posterior probabilities were calculated using an empirical Bayes method based on a per gene and group basis using model-based *t*-values [30]. Gene expression data were ranked and prioritized using a |fold change| ≥1.5 and P1(*t*) values ≥0.95 to identify differentially expressed genes that were used for further investigation and interpretation. Annotation and functional categorization of differentially regulated genes was performed using Database for Annotation, Visualization and Integrated Discovery (DAVID) [31].

RNA isolation and real-time PCR analysis: Lung tissue (10 mg) stored in RNA*later* RNA Stabilization Reagent was homogenized in RLT buffer (RNeasy RNA isolation Kit, Qiagen, Maryland) using a Retsch MM200 bead beater system (Retsch, Haan, Germany). Total RNA quantification was performed spectrophotometrically (NanoDrop ND-1000 UV-Vis Spectrophotometer). Total RNA (1 μg) was reverse transcribed using superscript II reverse transcriptase kit (Invitrogen, CA). Expression level of selected genes involved in surfactant metabolism and lung development were analyzed by Real-Time PCR using SYBR green (Applied Biosystems, Foster City, CA) as previously described [32]. Gene specific primers are listed in Table 3.1. Copy number was determined by comparison with standard curves of the respective genes. This measurement was controlled for RNA quality, quantity, and RT efficiency by normalizing it to the expression level of the hypoxanthine guanine phosphoribosyl transferase (HGPRT) gene. Statistical significance was determined by use of normalized relative changes and ANOVA.

Quantitative analysis: qRT-PCR analysis was performed using unpaired two-tailed Student's *t*-test on GraphPad Prism. Results were considered significant at the 5% level.

Results:

Generation of HIF1α and HIF2α deficient mice and their survivability: Three strains of mice were generated that were capable of inducible lung-specific deletion of HIF1α, HIF2α, or HIF1α/HIF2α as described in materials

Table 3.1. Primers for real-time RT-PCR.

Gene ID	Gene Name	Forward	Reverse
20505	Solute carrier family 34	ttggcactaccactacagcc	agtaggatgcccgagatgtt
84112	Succinate receptor 1	ttaaagaggaggagccagca	tcctcaaattgcgcatgata
234814	Methenyltetrahydrofolate synthetase domain	cccaccagggtcatcactac	atccttcccagcctgtttct
75512	Glutathione peroxidase 6	gcagtatgcaggaaagcaca	caaaaccgtgacgttgaatg
68214	Glutathione S-transferase omega 2	cgcctggacgtatatggact	ttcaagaagcccaggaagac
20464	Single-minded homolog 1 (Drosophila)	tcgtcagcgtcaactacgtc	ccgagatagtgggagtggaa
12000	Arginine vasopressin receptor 2	gccccttgagtggagactaa	ctgttgctgggagagctagg
54710	Heparan sulfate 3-O-sulfotransferase 3B1	attgctggagttcctgcgcgt	atggtgatctgtcccttgagggtt
320376	BCL6 co-repressor-like 1	gggctggactgatatcctga	agcaagagccagatggtttc
237911	BRCA1 interacting protein, helicase 1	tggctactaaaagcccctca	ccaaaagttgggcttgaaga
15357	3-hydroxy-3-methylglutaryl-Co A reductase	gaattgaactccccatcgag	ggatatgcttggcattgacc
12310	Calcitonin/calcitonin-related polypeptide, alpha	aagaagaagttcgcctgctg	tgcaggatctcttctgagca
16178	Interleukin 1 receptor, type II	ctcccctggagacaatacca	agccgagataaacgtgctgt
210766	BRCA1/BRCA2-containing complex, subunit 3	agctgccaaaaatcctgtgt	tgctgacatctgactgcaca
108030	Lin-7 homolog A (C. Elegans)	agcagcaacaacaaccacaa	tttttctgtgtgctgggattc
56360	Acyl-coa thioesterase 9	agacaagctgcgggagatag	tcattttcctcggtggtagg
18145	Niemann Pick type C1	agcgccatttaccatcattc	agcagtcctggcagctacat
245195	Resistin like gamma (FIZZ3)	ggaacttcttgccaatcgag	tagccacaagcacaaccagt
20249	Stearoyl-Coenzyme A desaturase 1	ccgggagaatatcctggttt	gtcgatgaagaacgtggtga
74596	CDP-diacylglycerol synthase 1	ctccctccctccattcctac	gaatccactggcaaagaagc
14866	Glutathione S-transferase, mu 5	acggtacatctgtggggaag	gatggcgttactctgggtga
17395	Matrix metallopeptidase 9	tcgcgtggataaggagttct	ctcatggtccaccttgttca
75646	retinoic acid induced 14	gtcctccccacgatcaataa	cctgcagtactgtcgctcag

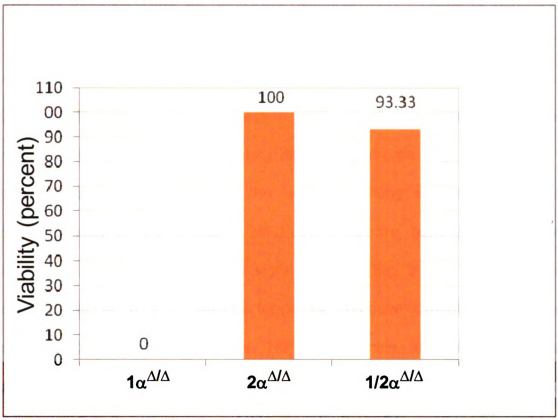

Figure 3.3. Survivability Plot.

Viability of neonatal HIF1αΔ/Δ, HIF2αΔ/Δ and HIF1/2αΔ/Δ pups. All the HIF1αΔ/Δ pups showed signs of respiratory distress whereas all the HIF2αΔ/Δ pups were viable with no signs of respiratory distress. Simultaneous removal of both the form of HIFα resulted in approximately 7% deaths. The data plotted is from n>~300 for HIF1αΔ/Δ, n>~100 for HIF2αΔ/Δ, n= 41 of HIF1/2αΔ/Δ pups.

"Images in this dissertation are presented in color".

and methods. To achieve recombination of the floxed alleles, dams were exposed to doxycycline as previously described [21]. Dams of genotype controls for the triple or quadruple embryos were maintained on regular feed and water. The litters were genotyped via PCR using established primers. Lung-specific deletion of HIF1α leads to 100% lethality upon parturition from a pathology that resembles respiratory distress syndrome (Fig. 3.3) [21]. In contrast, deletion of HIF2α in the developing lung shows no adverse consequences to the animal. HIF2αΔ/Δ mice are born in appropriate Mendelian ratios and display no signs of RDS (Fig. 3.3). These results suggest that HIF2α is not essential for proper lung development as previously reported [20]. Interestingly, the HIF1/2αΔ/Δ mice also displayed little pathology. There was a slight decrease in survivability but otherwise the double deficient pups appeared identical to their littermate and genotype controls (Fig. 3.3). These results suggest that loss of HIF2α can rescue the RDS-like phenotype seen in the HIF1αΔ/Δ mice.

Histopathological analysis of neonatal HIF-deficient mice: Pups were euthanized approximately 1 hour post-parturition and the lungs were examined. HIF1αΔ/Δ mice confirmed previous finding and displayed attenuated alveolar space and thickened septa compared to controls (Fig. 3.4A and 3.4B)[21]. In contrast, the lungs from HIF2α$^{\Delta/\Delta}$ mice displayed thinner septa and larger alveolar space than controls (Fig. 3.4A and 3.4C). Finally, the HIF1/2α$^{\Delta/\Delta}$ pups appeared similar to control pups. They displayed

Figure 3.4. Pulmonary Histopathology.

Light photomicrographs of hematoxylin and eosin stained lung sections from control (**A**) and HIF1α$^{\Delta/\Delta}$ (**B**), HIF2α$^{\Delta/\Delta}$ (**C**), HIF1/2α$^{\Delta/\Delta}$ (**D**) pups. Lung from HIF1α$^{\Delta/\Delta}$ pup has less alveolar airspace (a) and thicker alveolar septa (S) compared to control. The lungs from HIF2α$^{\Delta/\Delta}$ mice displayed thinner septa and larger alveolar space than controls. The lungs from HIF1/2α$^{\Delta/\Delta}$ mice resembled lungs from control in terms of septal thickness and alveolar space. "Images in this dissertation are presented in color."

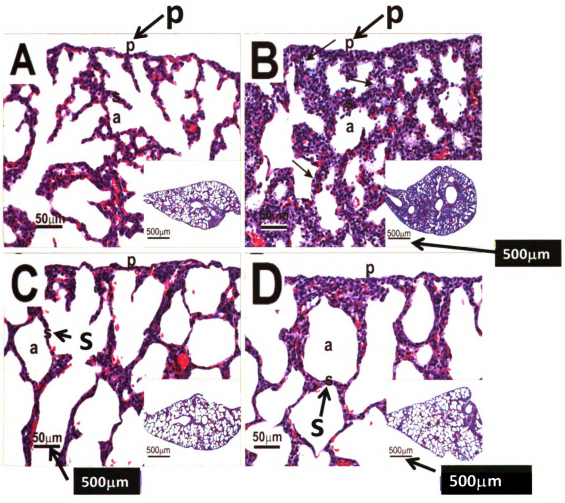
A
B
C
D
p
a
s
50μm
500μm
500μm
500μm
500μm

normal septa and alveolar architecture when compared to controls (Fig. 3.4A and 3.4D).

Expression of HIF1α and HIF2α in the three genoptypes: To access the efficiency of HIF deletion, immunohistochemistry was performed on lung sections from HIF1α$^{\Delta/\Delta}$, HIF2α$^{\Delta/\Delta}$, HIF1/2α$^{\Delta/\Delta}$, and their respective controls. In neonates, the expression of HIF1α is predominantly localized to alveolar and bronchiolar epithelial cells in controls and HIF2α$^{\Delta/\Delta}$ mice (Fig. 3.5A, C, D, and E). The level of HIF1α positive staining was drastically reduced in the HIF1αΔ/Δ and HIF1/2αΔ/Δ mice (Fig. 3.5B and F). The extent of HIF1α staining increased in HIF2α$^{\Delta/\Delta}$ pups at the neonatal stage (Fig. 3.5D).

In neonates, the level of HIF2α staining was attenuated in each of the three deficient genotypes as compared to their controls (Fig. 3.6). This confirmed the recombination at this HIF2α floxed locus in the HIF2αΔ/Δ and HIF1/2αΔ/Δ mice. Moreover, it supports the previous observation that loss of HIF1α leads to a decrease in HIF2α expression (Fig 3.6A and B) [21]. The results confirm the functional deletion of the floxed loci and suggest that there is some level of coordination between the expression of these two hypoxia regulated factors and this coordination plays a role in lung development

During development, the newly differentiated Type II cells use glycogen stores to produce surfactants. Lung sections from HIF1α$^{\Delta/\Delta}$ pups (Fig. 3.7B) had larger reserves of glycogen as compared to HIF2α$^{\Delta/\Delta}$ pups (Fig. 3.7D). In contrast, lung sections from HIF1α$^{\Delta/\Delta}$/HIF2α$^{\Delta/\Delta}$ pups (Fig. 3.7F) were devoid of

Figure 3.5. Immunohistochemistry for HIF1α.

Lung sections from control (**A,C,E**) and HIF1α$^{\Delta/\Delta}$ (**B**), HIF2α$^{\Delta/\Delta}$ (**C**), HIF1/2α$^{\Delta/\Delta}$ (**F**) pups were immunostained for HIF1α as described in "materials and methods". Representative positively stained cells for HIF1α are depicted by solid arrows. "Images in this dissertation are presented in color."

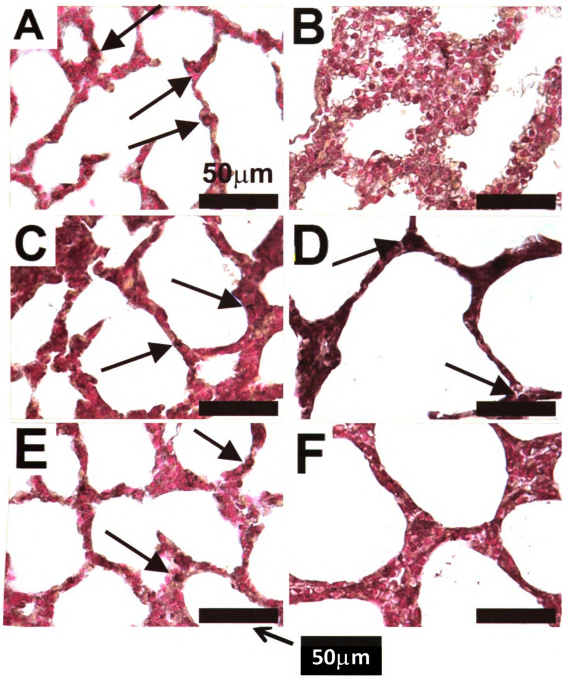
A
B
50μm
C
D
E
F
50μm

Figure 3.6. Immunohistochemistry for HIF2α.

Lung sections from control (**A,C,E**) and HIF1α$^{\Delta/\Delta}$ (**B**), HIF2α$^{\Delta/\Delta}$ (**C**), HIF1/2α$^{\Delta/\Delta}$ (**F**) pups were immunostained for HIF2α as described in "materials and methods" Positively stained cells for HIF2α are depicted by solid arrows. "Images in this dissertation are presented in color."

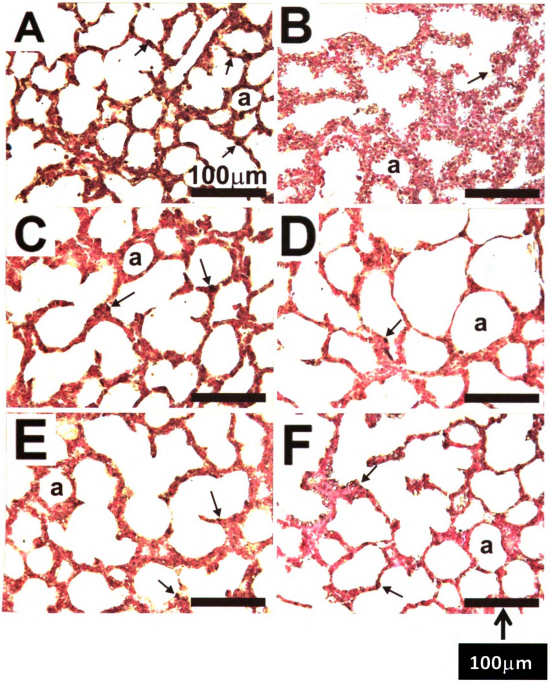
A
a
100μm
B
a
C
a
D
a
E
a
F
a
100μm

Figure 3.7. Periodic acid Schiff (PAS) staining

Periodic acid Schiff (PAS) stained lung sections from control (**B**) and HIF1α$^{\Delta/\Delta}$ (**D**) pups. Cuboidal epithelium lining alveolar septa in HIF1α$^{\Delta/\Delta}$ pup has greater PAS-stained glycogen (arrows) than that of the control pup (**D**). "Images in this dissertation are presented in color."

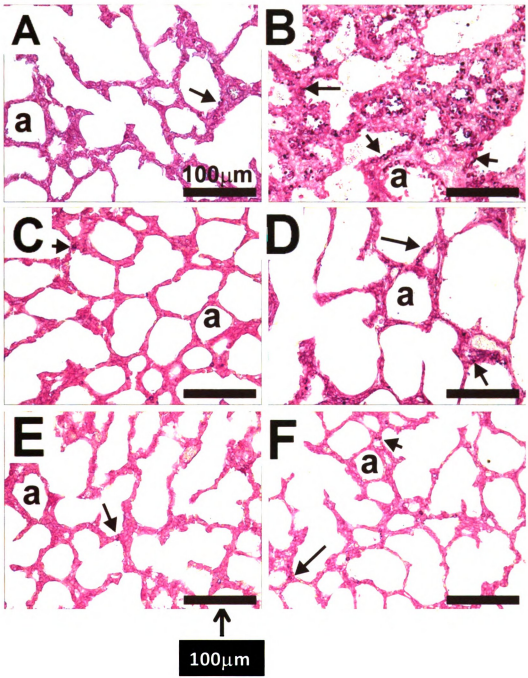
A
a
100μm
B
a
C
a
D
a
E
a
F
a
100μm

PAS-positive cells and were undistinguished from control pups (Fig. 3.7A, 3.7C, 3.7E).

Genomic Response to HIF1α and HIF2α Deletions

To understand the collective roles of HIF1α and HIF2α in the fetal lung development, gene expression was assessed using the 4 × 44 K Mouse Agilent array containing approximately 44,000 oligonucleotide probes, representing 34,204 annotated genes, including approximately 20,969 unique genes. Model-based *t*-values that compared treated and vehicle responses followed by Empirical Bayes analysis identified 1,174 differentially expressed genes based on a p1(*t*) > 0.95 and absolute fold change ≥1.5-fold (Fig. 3.8A). Overall, 632 genes were induced and 439 genes were repressed in the $HIF1\alpha^{\Delta/\Delta}$ as compared to control pups. The change in gene expression in $HIF1\alpha^{\Delta/\Delta}$ ranged from 37.07-fold induction (Solute carrier family 34) to -16.00-fold repression (Stearoyl-Coenzyme A desaturase 1). In $HIF2\alpha^{\Delta/\Delta}$ 102 genes were induced and 45 genes were repressed whereas in $HIF1/2\alpha^{\Delta/\Delta}$ 43 genes were induced and 108 genes were repressed. The changes in gene expression were ranged from 9.00-fold (Fc receptor-like 6) and 5.84-fold (glutathione S-transferase, mu 5) induction to -3.03-fold (olfactory receptor 583) and -6.6-fold (apolipoprotein F) repression in $HIF2\alpha^{\Delta/\Delta}$ and $HIF1/2\alpha^{\Delta/\Delta}$,

Figure 3.8 Differential gene expression between HIF1α$^{\Delta/\Delta}$, HIF2α$^{\Delta/\Delta}$ and HIF1/2α$^{\Delta/\Delta}$.

Identification of differentially regulated genes (**A**). Comparative gene expression analysis between HIF1α$^{\Delta/\Delta}$, HIF2α$^{\Delta/\Delta}$ and HIF1/2α$^{\Delta/\Delta}$ pups. The Venn diagram illustrates common and unique differentially expressed genes (**B**).

"Images in this dissertation are presented in color".

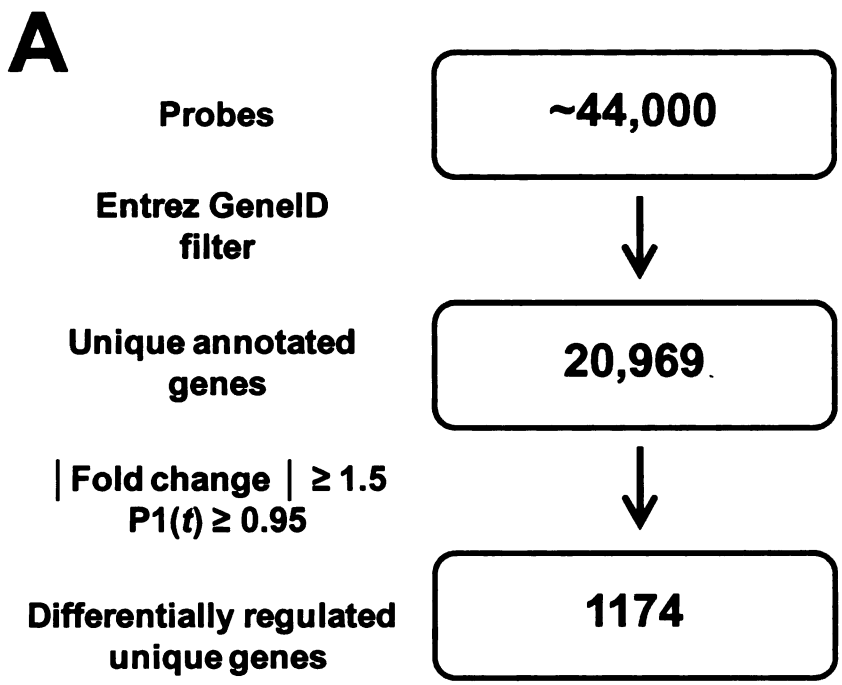
A
Probes
~44,000
Entrez GeneID filter
Unique annotated genes
20,969
| Fold change | ≥ 1.5
P1(t) ≥ 0.95
Differentially regulated unique genes
1174

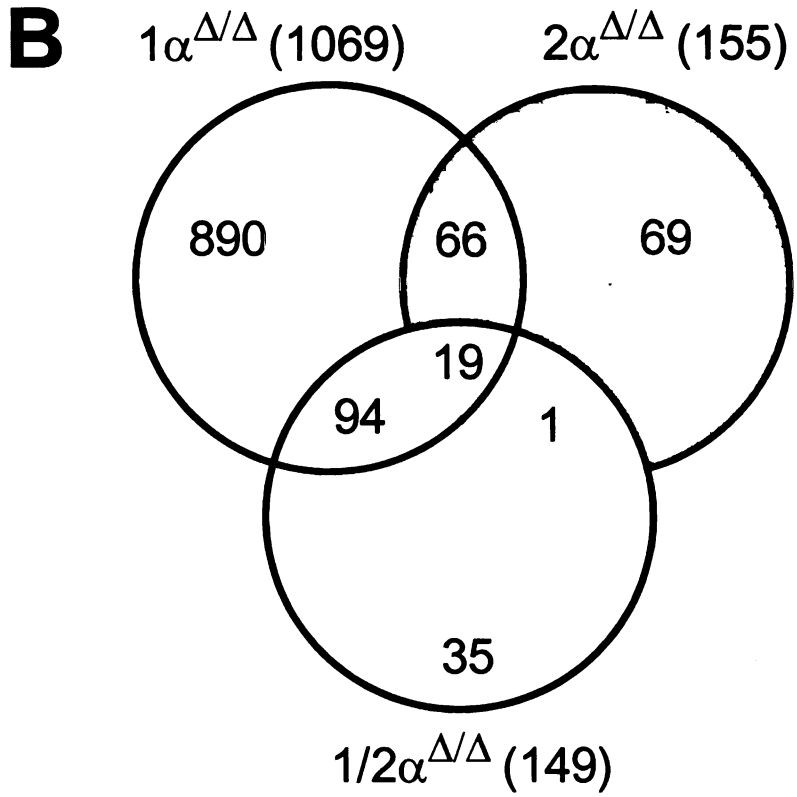
B
1α^Δ/Δ (1069)
2α^Δ/Δ (155)
890
66
69
19
94
1
35
1/2α^Δ/Δ (149)

respectively. List of differentially expressed genes is provided in Appendix Table A.1.

Database for Annotation, Visualization, and Integrated Discovery (DAVID) Analysis

To further investigate the pattern of cellular and physiological impacts of the HIFα deletions, Analysis through DAVID was conducted to allow detection of biological pathways and processes affected due to the deletion of either or both the isoforms of HIFα. Entrez gene ID list of 1174 differentially expressed unique genes were analyzed using all the genes representing mouse genome oligo-microarrays as a background. Given the wide array of biological processes regulated by HIFs and their roles in perinatal development, the effects on biological processes and cellular pathways were determined. Important cellular pathways that were affected include cell cycle and vesicular transport (table 3.2). Gene set enrichment analysis using the differentially expressed genes showed 45 biological processes that were significantly ($p \leq 0.05$) affected by deletions of HIF1α, HIF2α and HIF1/2α (table 3.3).

Surfactant biosynthesis and secretion pathways affected by HIF1α and HIF2α Deletions

An extensive literature search and microarray analysis identified changes in genes known to be involved in surfactants biosynthesis, processing and

Table 3.2. Cellular pathways affected by deletions of HIF1α, HIF2α and HIF1/2α

Cellular pathways affected by deletions of HIF1α, HIF2α and HIF1/2α				
Category	**Pathways**	**Genomic Response**	**Count**	**P-Value**
KEGG Pathways	Cell cycle	Upregulation	8	0.007
KEGG Pathways	SNARE interactions in vesicular transport	Downregulation	5	0.014
Biocarta Pathways	The role of FYVE-finger proteins in vesicle transport	Downregulation	3	0.021
KEGG Pathways	Leukocyte transendothelial migration	Downregulation	8	0.037
KEGG Pathways	Prostate cancer	Downregulation	7	0.046
KEGG Pathways	Butanoate metabolism	Downregulation	5	0.046
KEGG Pathways	ABC transporters - General	Upregulation	4	0.054
KEGG Pathways	Ubiquitin mediated proteolysis	Upregulation	7	0.054
KEGG Pathways	Urea cycle and metabolism of amino groups	Downregulation	4	0.055
KEGG Pathways	Cell Communication	Downregulation	8	0.058
KEGG Pathways	Tight junction	Downregulation	8	0.060
KEGG Pathways	Glycosylphosphatidylinositol(GPI)-anchor biosynthesis	Upregulation	3	0.073
KEGG Pathways	Tryptophan metabolism	Upregulation	4	0.090

Table 3.3. Biological processes affected by deletions of HIF1α, HIF2α and HIF1/2α

	Term	Count	P-Value
1	Biopolymer metabolic process	285	1.48E-05
2	RNA metabolic process	168	5.99E-04
3	Cell division	25	0.0020
4	Macromolecule metabolic process	343	0.0041
5	Intracellular signaling cascade	84	0.0044
6	Small gtpase mediated signal transduction	34	0.0059
7	Intracellular transport	51	0.0068
8	Nucleobase, nucleoside, nucleotide and nucleic acid metabolic process	201	0.0069
9	Biopolymer modification	108	0.0071
10	Primary metabolic process	385	0.0091
11	Intracellular protein transport	35	0.0103
12	Gene expression	184	0.0128
13	Cellular localization	61	0.0136
14	Protein modification process	102	0.0150
15	Post-translational protein modification	90	0.0160
16	Establishment of protein localization	52	0.0173
17	RNA processing	31	0.0194
18	Regulation of transcription, DNA-dependent	130	0.0197
19	Transcription	140	0.0210
20	Protein localization	55	0.0217
21	Cellular component organization and biogenesis	153	0.0218
22	Response to X-ray	4	0.0220
23	Metabolic process	418	0.0232
24	mRNA metabolic process	23	0.0243
25	Regulation of liquid surface tension	3	0.0246
26	Hindgut morphogenesis	3	0.0246
27	Regulation of macrophage activation	3	0.0246
28	Response to ionizing radiation	5	0.0256
29	Establishment of cellular localization	58	0.0263
30	Regulation of cellular process	216	0.0268
31	Biopolymer catabolic process	23	0.0272
32	Macromolecule localization	56	0.0276
33	Transcription, DNA-dependent	130	0.0277
34	RNA biosynthetic process	130	0.0287
35	Protein transport	48	0.0288
36	Mitosis	17	0.0318
37	Rho protein signal transduction	11	0.0320
38	M phase	21	0.0323
39	M phase of mitotic cell cycle	17	0.0332
40	Biological regulation	256	0.0347
41	Regulation of angiogenesis	6	0.0380
42	Regulation of transcription	133	0.0409

Table 3.3. Continued.

	Term	Count	P-Value
43	Embryonic organ development	6	0.0421
44	Cellular metabolic process	376	0.0475
45	Amino acid transport	7	0.0489
46	Regulation of nucleobase, nucleoside, nucleotide and nucleic acid metabolic process	134	0.0551
47	Carboxylic acid transport	8	0.0561
48	Phospholipid biosynthetic process	8	0.0561
49	Membrane lipid biosynthetic process	9	0.0571
50	Organic acid transport	8	0.0599
51	Regulation of cell size	13	0.0602
52	Cellular zinc ion homeostasis	3	0.0620
53	Zinc ion homeostasis	3	0.0620
54	Vacuolar transport	4	0.0647
55	Protein targeting	19	0.0675
56	Regulation of biological process	231	0.0680
57	Dephosphorylation	13	0.0685
58	Cell growth	12	0.0687
59	Regulation of smooth muscle contraction	4	0.0739
60	Negative regulation of angiogenesis	4	0.0739
61	Nucleocytoplasmic transport	11	0.0749
62	Protein-RNA complex assembly	9	0.0760
63	Macrophage activation	3	0.0770
64	Central nervous system neuron axonogenesis	3	0.0770
65	Nuclear transport	11	0.0784
66	Ras protein signal transduction	16	0.0784
67	Regulation of gene expression	138	0.0796
68	Phosphate transport	9	0.0844
69	Transition metal ion transport	7	0.0868
70	Ectodermal gut development	3	0.0930
71	Cerebellar Purkinje cell differentiation	3	0.0930
72	Cerebellar Purkinje cell layer formation	3	0.0930
73	Cerebellar Purkinje cell layer morphogenesis	3	0.0930
74	Lysosomal transport	3	0.0930
75	Ectodermal gut morphogenesis	3	0.0930
76	Pyrimidine nucleotide biosynthetic process	4	0.0941
77	Ubiquitin cycle	33	0.0962

Table 3.4 Genes involved in surfactant metabolism

Gene	Symbol	HIF1α Ratio	HIF2α Ratio	HIF1/2α Ratio
surfactant associated protein B	Sftpb	-2.40	-1.07	-1.81
surfactant associated protein A1	Sftpa1	-4.70	-1.02	-1.47
synaptosomal-associated protein 23	Snap23	-1.50	1.27	-1.13
golgi SNAP receptor complex member 1	Gosr1	-1.54	1.44	-1.19
golgi SNAP receptor complex member 2	Gosr2	-2.02	1.34	-1.25
syntaxin 19	Stx19	-2.14	1.04	-1.10
syntaxin 11	Stx11	-1.98	1.28	-1.06
ATP-binding cassette, sub-family A (ABC1), member 1	Abca1	-1.72	1.16	-1.20
ATP-binding cassette, sub-family A (ABC1), member 6	Abca6	-4.46	1.98	-1.48
acyl-Coenzyme A oxidase 2, branched chain	Acox2	-1.69	1.32	-1.14
stearoyl-Coenzyme A desaturase 1	Scd1	-16.67	-1.08	-3.58
sterol regulatory element binding factor 2	Srebf2	-1.51	1.05	-1.23
low density lipoprotein receptor	Ldlr	-1.33	1.04	-1.09
CDP-diacylglycerol synthase 1	Cds1	-2.30	1.07	-1.39
acyl-CoA thioesterase 1	Acot1	-1.18	1.16	-1.28
acyl-CoA thioesterase 9	Acot9	-2.29	1.12	-1.38
lysophosphatidylcholine acyltransferase 1	Lpcat1	-2.93	-1.04	-2.52
CDP-diacylglycerol synthase (phosphatidate cytidylyltransferase) 2	Cds2	-1.09	1.28	-1.14
phosphatidylethanolamine binding protein 2	Pbp2	-2.91	-1.06	-1.13
inositol polyphosphate-5-phosphatase A	Inpp5a	-1.51	1.17	-1.09
inositol 1,4,5-trisphosphate 3-kinase A	Itpka	-2.38	1.10	1.12
phosphatidylinositol glycan anchor biosynthesis, class A	Piga	-1.27	1.25	1.21
phosphatidylglycerophosphate synthase 1	Pgs1	-1.32	-1.10	-1.28
choline phosphotransferase 1	Chpt1	-1.74	1.27	-1.11
choline kinase alpha	Chka	-1.03	1.03	1.26
1-acylglycerol-3-phosphate O-acyltransferase 3	Agpat3	-1.30	1.02	-1.10
fatty acid synthase	Fasn	-1.34	1.17	-1.28
cAMP responsive element binding protein 5	Creb5	-1.66	1.24	-1.40
cAMP responsive element binding protein 3	Creb3	-2.94	1.10	1.00
syntaxin 6	Stx6	-1.16	1.33	-1.51
syntaxin 3	Stx3	-2.04	1.38	-1.71
syntaxin 5A	Stx5a	-1.41	1.30	-1.18
N-ethylmaleimide sensitive fusion protein	Nsf	-1.47	1.26	-1.23

Figure 3.9 QRTPCR verification of selected microarray gene expression responses.

The same RNA used for cDNA microarrays was examined by QRTPCR. All fold changes were calculated relative to controls. Bars (left y-axis) and lines (right y-axis) represent QRT-PCR and microarray data, respectively. Expression levels are expressed relative to HGPRT. "a" means statistically different from $2\alpha^{\Delta/\Delta}$, "b" means statistically different from $1\alpha^{\Delta/\Delta}$,"c" means statistically different from $1/2\alpha^{\Delta/\Delta}$. a, b and c designate statistical significance at $p \leq 0.05$.

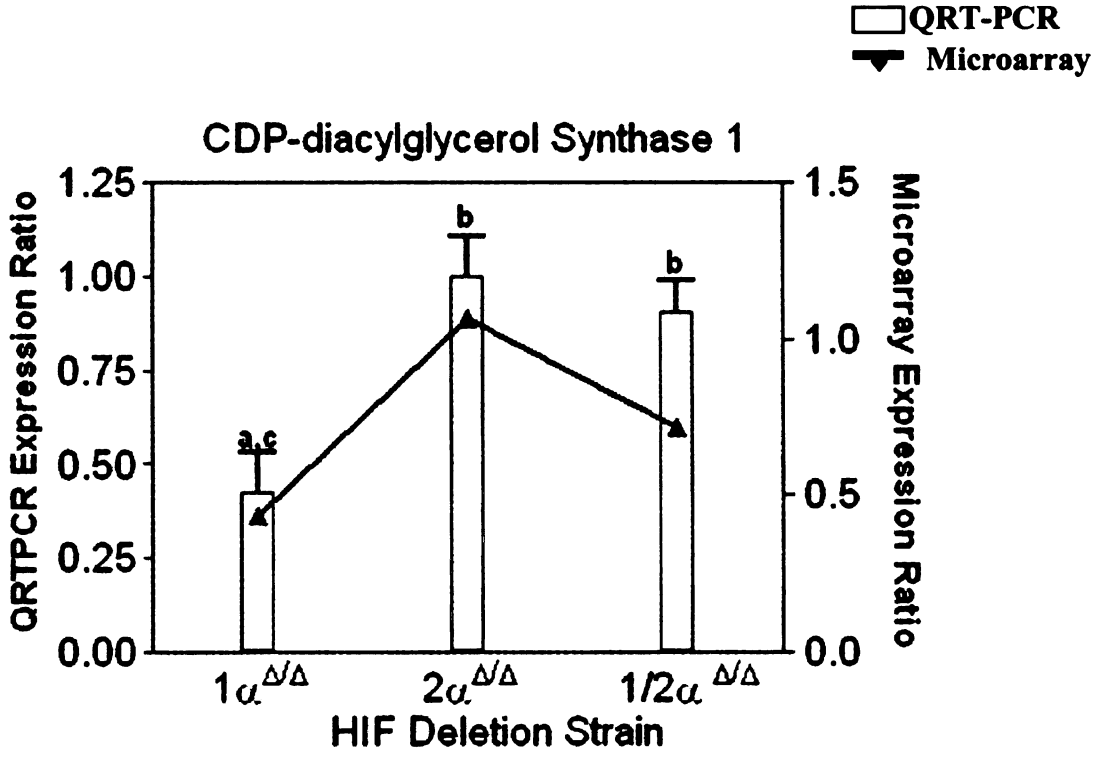
QRT-PCR
Microarray
CDP-diacylglycerol Synthase 1
QRTPCR Expression Ratio
Microarray Expression Ratio
1.25
1.00
0.75
0.50
0.25
0.00
1.5
1.0
0.5
0.0
a,c
b
b
1α Δ/Δ
2α Δ/Δ
1/2α Δ/Δ
HIF Deletion Strain

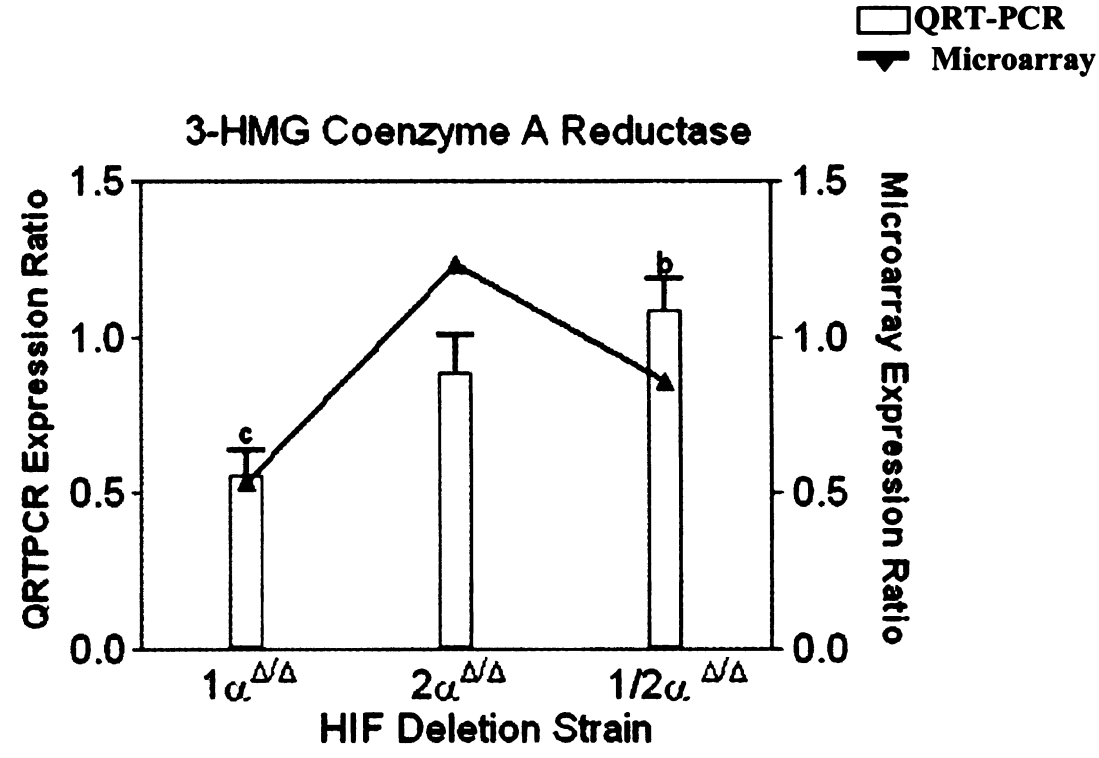
QRT-PCR
Microarray
3-HMG Coenzyme A Reductase
QRTPCR Expression Ratio
Microarray Expression Ratio
1.5
1.0
0.5
0.0
c
b
1α Δ/Δ
2α Δ/Δ
1/2α Δ/Δ
HIF Deletion Strain

Figure 3.9. Continued.

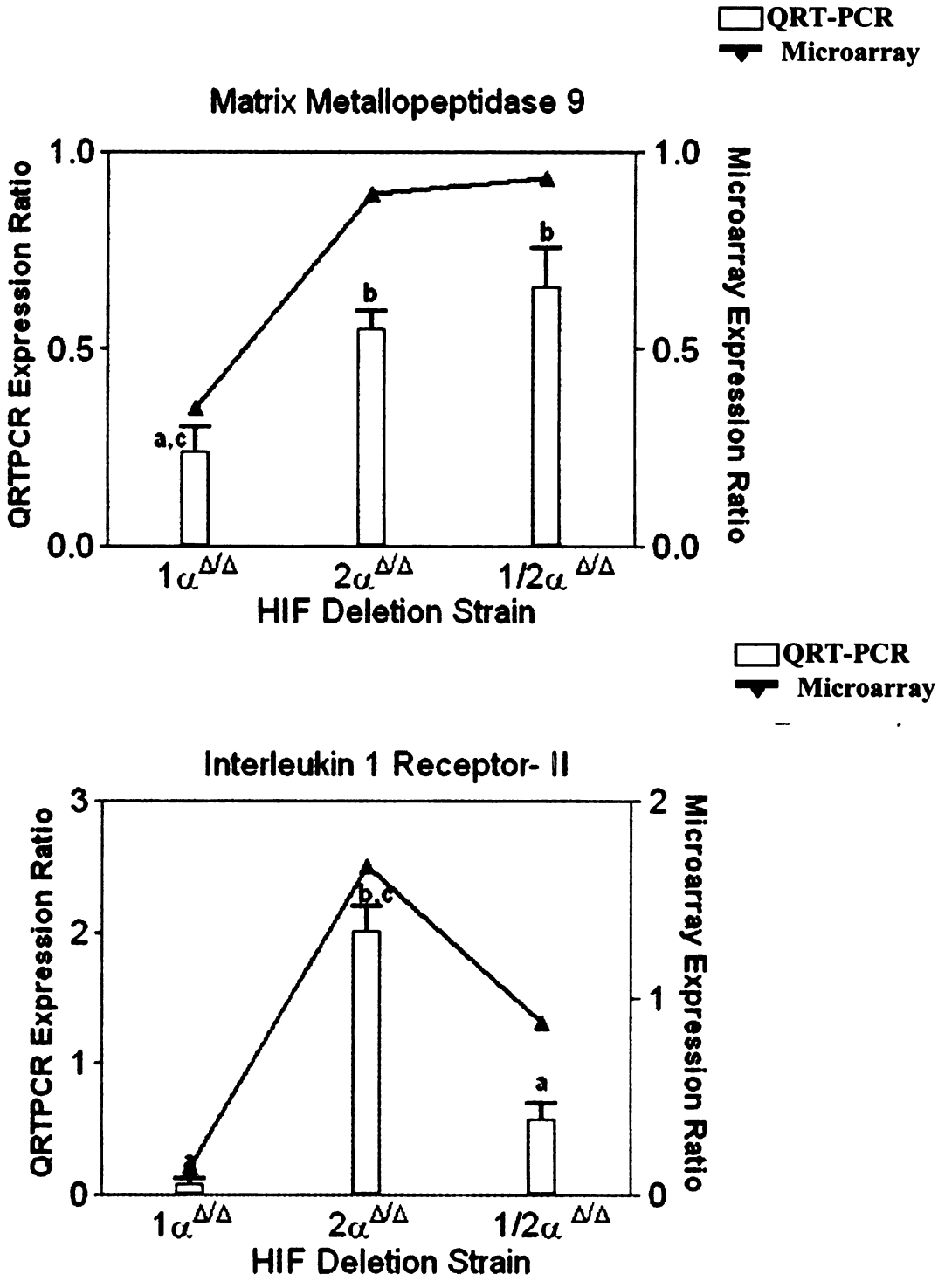

Figure 3.9. Continued.

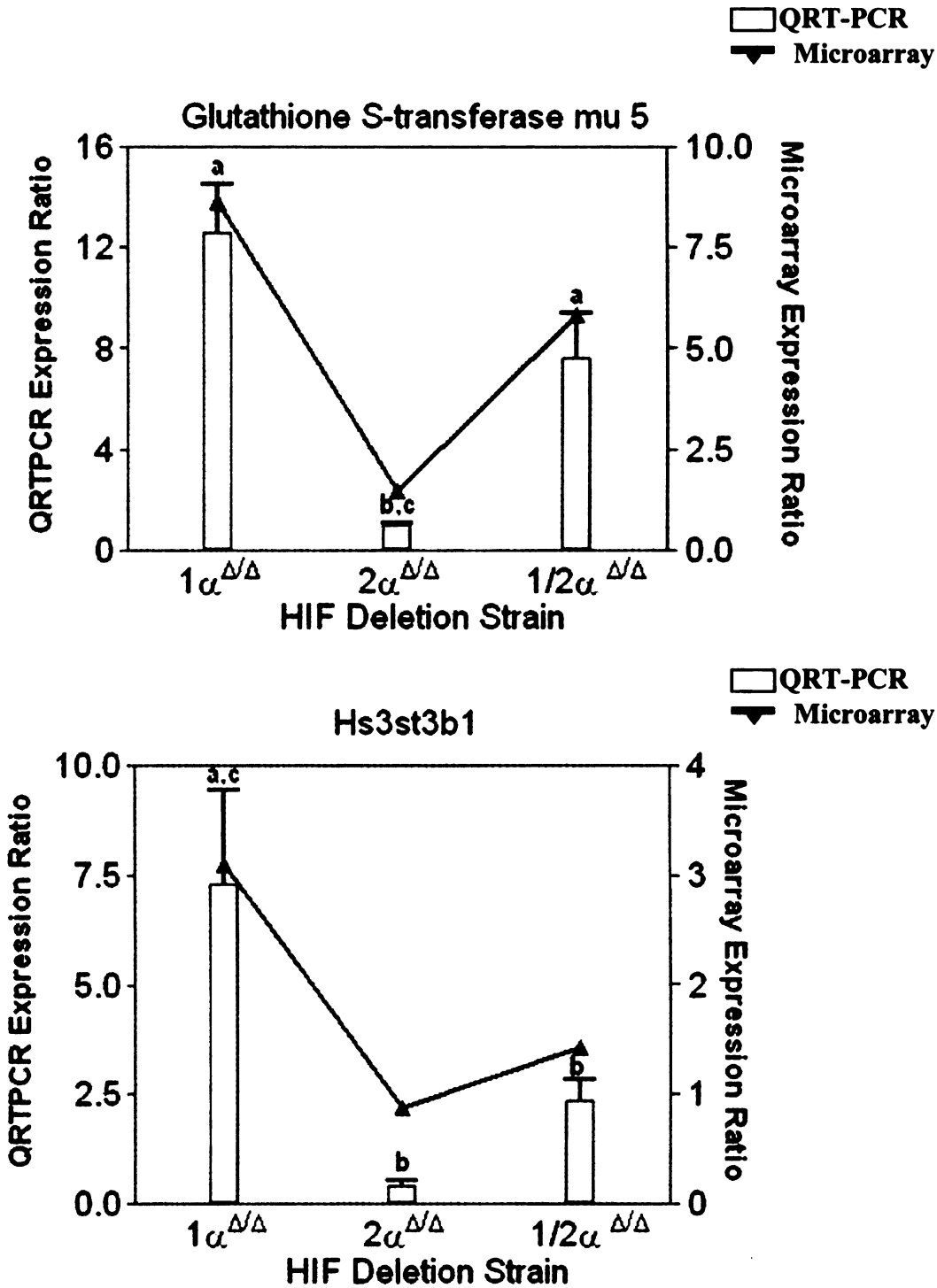

Figure 3.9. Continued.

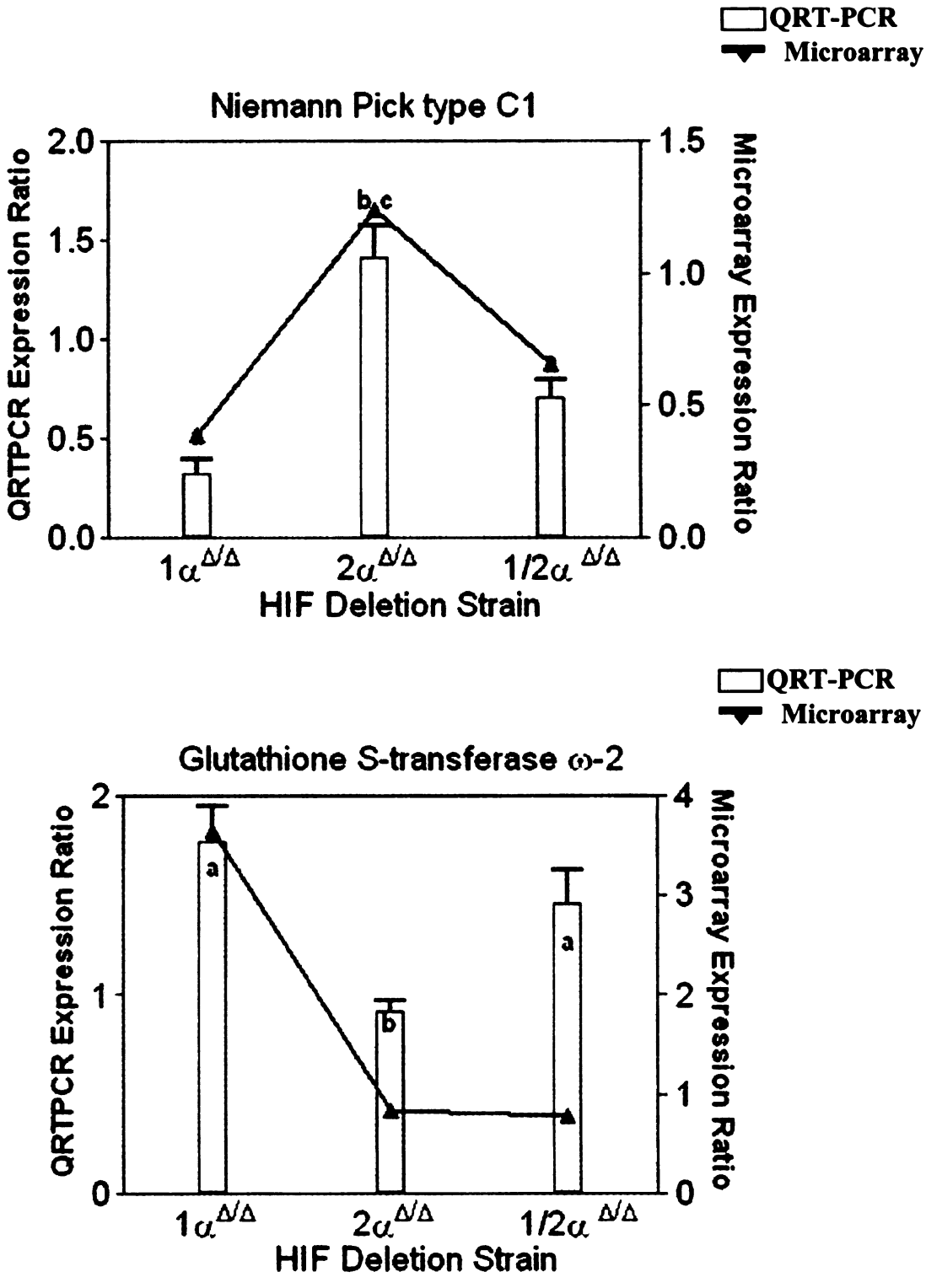

secretion pathways. The comparison of HIF1αΔ/Δ expression patterns and those of HIF1/2αΔ/Δ identified several genes that showed rescued expression upon loss of both HIF isoforms. These genes are important in lipid biosynthesis (e.g. acyl-CoA thioesterase 9, sterol regulatory element binding factor 2) or surfactant transport and secretions (e.g. golgi SNAP receptor complex member 2, SNAP 23). Interestingly, some of the genes such as stearoyl- Coenzyme A desaturase 1 and surfactant protein B did not exhibit significantly increased expression after accompanied deletion of HIF2α.

QRTPCR verification of selected microarray gene expression responses. Quantitative real-time PCR (QRT-PCR) was used to verify the differential expression for a selected subset of differentially expressed genes representing different response profiles and functions (table 3.1). In general, there was a good agreement in the level of differential expression when comparing microarray and QRT-PCR data (Fig. 3.9).

Discussion

Normal prenatal lung development is essential for the smooth transition of the placental gas transport to an air breathing at the birth. This complex process is characterized by biochemical, cellular and ultrastructural changes that are precisely controlled by the spatiotemporal pattern of expression (or activity) of large number of transcriptional and paracrine factors. Several

transcription factors including KLF5, Foxa2, CEBPα, GATA-6, β-catenin and thyroid transcription factor-1 have already been added to the list of indispensables for lung development [3-7, 9]. However, further testing for the other developmentally critical transcriptional factors, individually or collectively, will provide a broader understanding on the intricate networks and cascades involved in lung development.

HIFs are a class of transcription factors that play a critical role in oxygen sensing and the metabolic adaptations to hypoxia. HIF1α is a most widely expressed isoform of HIFs. Previous studies have shown that targeted gene disruption of the HIF1α locus results in the mid-gestational lethality due to cardiovascular defects [15, 33]. Mice partially deficient for HIF1α alleles showed normal development but were physiologically compromised as they exhibited impaired pulmonary vascular remodeling under chronic hypoxic stress [16, 34]. Similarly, targeted disruption of HIF2α, another pulmonary isoform of HIFs, have shown that reduced VEGF expression leads to respiratory distress at birth [20].

Recently, using a lung-specific HIF1α deficient mouse model, epithelial-derived HIF1α deletion led to compromised lung development and altered surfactant metabolism [21]. The epithelial-specific loss of HIF1α leads to neonatal respiratory distress syndrome due to impaired alveolar epithelial differentiation. Morphogenesis of conducting airways, however, was unaffected, suggesting the involvement of HIF1α in late events in lung

morphogenesis rather than in the early lung biogenesis and airway branching morphogenesis.

To further investigate the role of HIF2α in lung development, lung-specific HIF2α deficient and HIF1α/2α deficient mice were generated. The results suggest that lung-specific loss of HIF2α does not result in the respiratory distress. The difference between these results and previously published reports most likely stems from genotype and strain differences of the mice used [20]. The previously published report used traditional HIF2α knockout mice generated in a specific genetic background and the conclusions were based on a percentage of mice that survived until parturition. These differences in genetic background, genotype, and the loss of HIF2α from other organs, most notably the cardiac tissue, are potentially confounding factors. The data presented here suggests that loss of HIF2α specifically from the lungs leads to no overt phenotype and actually might lead to more developed lungs when compared to genotype controls (Fig. 3.4).

The simultaneous deletion of HIF1α and HIF2α isoforms rescues the respiratory distress phenotype that was observed in HIF1α deficient mice. To investigate the mechanisms underlying these interesting, microarray analysis was performed to identify differentially expressed genes. Extensive data mining and literature search revealed that the deficiency of HIF1a protein results in the differential expression of 1069 unique genes whereas the

deficiency of HIF2a protein affected the expression of only 155 genes. Interestingly, after HIF1α/2α deficiency the list of differentially expressed genes was reduced to only 149 out of which 113 genes overlapped with HIF1α deficient mice (Fig. 3.8B). Out of 1069 genes, the expression patterns of 890 genes were specifically disturbed in HIF1α deficient mice. Previous study on the characterization of the respiratory distress phenotype in HIF1α deficient mice highlighted the altered surfactant proteins expression and the expression of developmentally critical genes [21]. However, the screening for the biological processes affected by the deletion of HIF1α returned a list of wide variety processes such as biopolymer metabolic processes, RNA metabolism, cell division, intracellular signaling cascades and intracellular protein sorting (Table 3.3). Further search for the cellular pathways affected revealed the perturbation of vesicular transport pathways and cell cycle pathways (Table 3.2). Proper functioning and regulation of vesicular transportation is an important step in the processing and secretion of surfactants and associated proteins.

Pulmonary surfactants are modified in the golgi apparatus and are then released from the *trans* golgi network into secretory vesicles, known as composite bodies, the immediate precursors of lamellar bodies. The lamellar body-bound surfactants are released via exocytosis into the lumen alveolar lumen where it forms a lattice-like network known as tubular myelin. The processes involving intracellular sorting (golgi transport, vesicular fusion) and

surfactant biosynthesis (fatty acid metabolism, cholesterol sythesis, plospholipids biosynthesis) are specifically affected in HIF1α deficient mice (Table 3.4).

Genes involved in vesicular transport such as Gosr2, SNAP-23, Syntaxins are downregulated in HIF1α deficient mice but were restored to normal levels in HIF1α/2α deficient mice [35]. Similarly, levels of expressions of genes involved in lipid metabolism such as Acot9, CDS-1, SCD-1, Acox2, CDS-2, Chpt-1, Itpka were increased in HIF1α/2α deficient mice [36, 37]. PAS staining for glycogen deposition also suggested the complete utilization of glycogen in HIF2α and HIF1α/2α deficient mice (Fig.3.7). Taken together, these findings suggest the global alteration of the surfactant metabolism starting from the phospholipids and protein biosynthesis to the final exocytosis of packaged surfactants into the alveolar space upon perturbation of the hypoxia signaling cascade in the lungs.

Interestingly, genes involved in cellular processes such as cell cycle and biopolymer metabolism showed differential gene expression pattern. The first category includes genes such as interleukin 1 receptor type II (IL1-RII) that are minimally expressed in from HIF1α$^{\Delta/\Delta}$ lungs but show higher expression in HIF1/2α$^{\Delta/\Delta}$ lungs. The second category includes genes such as heparan sulfate (glucosamine) 3-O-sulfotransferase 3A1 (Hs3st3a1) that are

highly expressed in HIF1α$^{\Delta/\Delta}$ lungs but show lower expression in HIF1/2α$^{\Delta/\Delta}$ lungs (Fig. 3.9). Interleukin 1 (IL1α and IL1β) has been shown to promote lung function and surfactant biosynthesis [38]. Similarly, heparan sulphate proteoglycans are required for various signaling pathways critical in the lung development [39].

In conclusion, the present study provides evidence that HIF1α plays an important role in multiple processes including surfactant metabolism, metabolic pathways, signal transduction cascades and vesicular trafficking. The lung-specific deletion of HIF2α alone, however, is not lethal to the neonatal pups and there was no sign of observable pathology. Interestingly, the rescue of respiratory distress was observed after simultaneous deletion of both the isoforms of HIFs. Microarray analysis of the lungs has identified interesting genes that might be the focus of further investigation.

REFERENCES

1 James Metcalfe, H. B., Waldemar Moll. (1967) Gas Exchange in the Pregnant Uterus. Physiol. Rev. **47**, 782-838.

2 Groenman, F., Unger, S. and Post, M. (2005) The molecular basis for abnormal human lung development. Biology of the Neonate. **87**, 164-177

3 DeFelice, M., et al. (2003) TTF-1 phosphorylation is required for peripheral lung morphogenesis, perinatal survival, and tissue-specific gene expression. The Journal of biological chemistry. **278**, 35574-35583

4 Liu, C., Morrisey, E. E. and Whitsett, J. A. (2002) GATA-6 is required for maturation of the lung in late gestation. Am J Physiol Lung Cell Mol Physiol. **283**, L468-475

5 Martis, P. C., et al. (2006) C/EBPalpha is required for lung maturation at birth. Development (Cambridge, England). **133**, 1155-1164

6 Mucenski, M. L., et al. (2003) beta-Catenin is required for specification of proximal/distal cell fate during lung morphogenesis. The Journal of biological chemistry. **278**, 40231-40238

7 Wan, H., et al. (2004) Foxa2 is required for transition to air breathing at birth. Proceedings of the National Academy of Sciences of the United States of America. **101**, 14449-14454

8 Yang, H., et al. (2002) GATA6 regulates differentiation of distal lung epithelium. Development (Cambridge, England). **129**, 2233-2246

9 Wan, H., et al. (2008) Kruppel-like factor 5 is required for perinatal lung morphogenesis and function. Development (Cambridge, England). **135**, 2563-2572

10 Dave, V., et al. (2006) Calcineurin/Nfat signaling is required for perinatal lung maturation and function. The Journal of clinical investigation. **116**, 2597-2609

11 Semenza, G. L. (2000) HIF-1: mediator of physiological and pathophysiological responses to hypoxia. J Appl Physiol. **88**, 1474-1480

12 Groenman, F., et al. (2007) Hypoxia-inducible factors in the first trimester human lung. J Histochem Cytochem. **55**, 355-363

13 Cowden Dahl, K. D., et al. (2005) Hypoxia-inducible factors 1 alpha and 2 alpha regulate trophoblast differentiation. Molecular and cellular biology. **25**, 10479-10491

14 Compernolle, V., et al. (2003) Cardia bifida, defective heart development and abnormal neural crest migration in embryos lacking hypoxia-inducible factor-1alpha. Cardiovascular research. **60**, 569-579

15 Ryan, H. E., Lo, J. and Johnson, R. S. (1998) HIF-1 alpha is required for solid tumor formation and embryonic vascularization. The EMBO journal. **17**, 3005-3015

16 Yu, A. Y., et al. (1999) Impaired physiological responses to chronic hypoxia in mice partially deficient for hypoxia-inducible factor 1alpha. The Journal of clinical investigation. **103**, 691-696

17 Peng, J., Zhang, L., Drysdale, L. and Fong, G. H. (2000) The transcription factor EPAS-1/hypoxia-inducible factor 2alpha plays an important role in vascular remodeling. Proceedings of the National Academy of Sciences of the United States of America. **97**, 8386-8391

18 Patel, S. A. and Simon, M. C. (2008) Biology of hypoxia-inducible factor-2alpha in development and disease. Cell death and differentiation. **15**, 628-634

19 Asikainen, T. M., et al. (2006) Improved lung growth and function through hypoxia-inducible factor in primate chronic lung disease of prematurity. Faseb Journal. **20**, (E986-E994) 1698-1700

20 Compernolle, V., et al. (2002) Loss of HIF-2alpha and inhibition of VEGF impair fetal lung maturation, whereas treatment with VEGF prevents fatal respiratory distress in premature mice. Nature medicine. **8**, 702-710

21 Saini, Y., Harkema, J. R. and LaPres, J. J. (2008) HIF1alpha is essential for normal intrauterine differentiation of alveolar epithelium and surfactant production in the newborn lung of mice. The Journal of biological chemistry. **283**, 33650-33657

22 Ryan, H. E., Lo, J. and Johnson, R. S. (1998) HIF-1 alpha is required for solid tumor formation and embryonic vascularization. Embo Journal. **17**, 3005-3015

23 Ryan, H. E., et al. (2000) Hypoxia-inducible factor-1 alpha is a positive factor in solid tumor growth. Cancer Research. **60**, 4010-4015

24 Perl, A. K., et al. (2002) Early restriction of peripheral and proximal cell lineages during formation of the lung. Proc Natl Acad Sci U S A. **99**, 10482-10487

25 Lobe, C. G., et al. (1999) Z/AP, a double reporter for cre-mediated recombination. Dev Biol. **208**, 281-292

26 Gruber, M., et al. (2007) Acute postnatal ablation of Hif-2alpha results in anemia. Proceedings of the National Academy of Sciences of the United States of America. **104**, 2301-2306

27 Burgoon, L. D. and Zacharewski, T. R. (2007) dbZach toxicogenomic information management system. Pharmacogenomics. **8**, 287-291

28 Burgoon, L. D., et al. (2005) Protocols for the assurance of microarray data quality and process control. Nucleic acids research. **33**, e172

29 Eckel, J. E., et al. (2005) Normalization of two-channel microarray experiments: a semiparametric approach. Bioinformatics (Oxford, England). **21**, 1078-1083

30 Eckel, J. E., et al. (2004) Empirical bayes gene screening tool for time-course or dose-response microarray data. Journal of biopharmaceutical statistics. **14**, 647-670

31 Dennis, G., Jr., et al. (2003) DAVID: Database for Annotation, Visualization, and Integrated Discovery. Genome biology. **4**, P3

32 Vengellur, A. and LaPres, J. J. (2004) The role of hypoxia inducible factor 1 alpha in cobalt chloride induced cell death in mouse embryonic fibroblasts. Toxicological Sciences. **82**, 638-646

33 Iyer, N. V., et al. (1998) Cellular and developmental control of O_2 homeostasis by hypoxia-inducible factor 1 alpha. Genes & Development. **12**, 149-162

34 Semenza, G. L. (2005) Pulmonary vascular responses to chronic hypoxia mediated by hypoxia-inducible factor 1. Proceedings of the American Thoracic Society. **2**, 68-70

35 Abonyo, B. O., et al. (2004) Syntaxin 2 and SNAP-23 are required for regulated surfactant secretion. Biochemistry. **43**, 3499-3506

36 Zhang, F., Pan, T., Nielsen, L. D. and Mason, R. J. (2004) Lipogenesis in fetal rat lung: importance of C/EBPalpha, SREBP-1c, and stearoyl-CoA desaturase. American journal of respiratory cell and molecular biology. **30**, 174-183

37 Batenburg, J. J. and Haagsman, H. P. (1998) The lipids of pulmonary surfactant: dynamics and interactions with proteins. Progress in lipid research. **37**, 235-276

38 Willet, K. E., et al. (2002) Intra-amniotic injection of IL-1 induces inflammation and maturation in fetal sheep lung. Am J Physiol Lung Cell Mol Physiol. **282**, L411-420

39 Hu, Z., et al. (2009) NDST1-dependent heparan sulfate regulates BMP signaling and internalization in lung development. Journal of cell science. **122**, 1145-1154

Chapter 4

The Role of Hypoxia Inducible Factor 1α (HIF1α) in Modulating Cobalt-Induced Lung Inflammation

This chapter is the edited version of a research article that was published in American Journal of Physiology, Lung Cellular and Molecular Physiology. 2009 Nov 13.

Authors: Yogesh Saini, Kyung Y. Kim, Ryan Lewandowski, Lori A. Bramble, Jack R Harkema, John J. LaPres

ABSTRACT

Hypoxia plays an important role in development, cellular homeostasis, and pathological conditions, such as cancer and stroke. There is also growing evidence that hypoxia is an important modulator of the inflammatory process. Hypoxia inducible factors (HIFs) are a family of proteins that regulate the cellular response to oxygen deficit and loss of HIFs impairs inflammatory cell function. There is little known, however, about the role of epithelial-derived HIF signaling in modulating inflammation. Cobalt is capable of eliciting an allergic response and promoting HIF signaling. To characterize the inflammatory function of epithelial derived HIF in response to inhaled cobalt, a conditional lung specific HIF1α deletion mouse was created. Wild type mice showed classic signs of metal-induced injury following cobalt exposure, including fibrosis and neutrophil infiltration. In contrast, HIF1α deficient mice displayed a Th2 response that resembled asthma, including increased eosinophilic infiltration, mucus cell metaplasia, and chitinase-like protein expression. The results suggest that epithelial derived HIF signaling has a critical role in establishing a tissue's inflammatory response, and compromised HIF1α signaling biases the tissue towards a Th2-mediated reaction.

INTRODUCTION

Lung diseases, including chronic obstructive pulmonary disease and asthma, involve a large inflammatory component. The lung's response to allergens involves a complex interplay between resident inflammatory and epithelial cells, cytokine signaling, and the environmental conditions within the tissue. One of the critical environmental features that can impact the inflammatory process is hypoxia.

Hypoxia, a decrease in available oxygen reaching the tissues of the body, has profound cellular and metabolic consequences. The cellular response to hypoxia is regulated by a family of transcription factors called the hypoxia inducible factors (HIFs) [1]. HIFs are primarily regulated at the level of protein stability by a family of prolyl hydroxylases. These prolyl hydroxylase domain (PHDs) proteins are members of a broader family of non-heme, iron- and 2-oxoglutarate dependent dioxygenases [2]. Cobalt has been shown to inhibit PHDs and this inhibition causes very similar transcriptional outputs to that of hypoxia [3, 4]. Recent research using human peripheral blood mononuclear cells has shown that this transcriptional overlap applies to tungsten carbide-cobalt particles, linking hard metal lung disease to hypoxia signaling [5].

HIF1α is the most ubiquitously expressed and widely studied HIF isoform. HIF1α heterodimerizes with the aryl hydrocarbon receptor nuclear translocator (ARNT, also known as HIF1β) forming the functional transcription factor HIF1.

HIF1 regulates the expression of over one hundred genes, including genes for glycolytic enzymes, sugar transporters, and pro-angiogenic and inflammatory factors [6-9]. Moreover, HIF1α has also been shown to modulate inflammation indirectly by influencing the NFκB signaling pathway [8, 10]. Given the relationship between cobalt, HIF1α, and inflammation, it seems likely that HIF1α will impact cobalt-induced injury *in vivo*. More specifically, it is hypothesized that cobalt-induced HIF1-mediated transcription will impact cobalt-related asthma and/or hard metal lung disease [5].

Cobalt (or hard metal) asthma is one of three occupational respiratory diseases associated with exposure to the transition metal. The other two are hypersensitivity pneumonitis and interstitial lung disease with fibrosis. These diseases are caused by the inhalation of hard metal particles and are characterized by airway constriction, alveolitis, fibrosis and associated giant cell interstitial pneumonitis [11]. Asthma associated with cobalt exposure most likely involves an allergic response and has variable latency periods following initial sensitization [12-14]. Cobalt-specific immunoglobulin isotype E (IgE), has been characterized in workers with signs of cobalt asthma, and their symptoms can be relieved upon removal from the contaminated environment [12]. Besides acting as a pro-oxidant and sensitizer in the lung and skin, cobalt has also been characterized as a hypoxia mimic [4].

To characterize the role of HIF1α in cobalt-induced lung injury, a lung specific HIF1α knock out mouse model was created. *In utero* deletion of HIF1α led to lethality due to respiratory distress upon parturition [15]. In the present study, post-natal deletion of HIF1α from Type II and Clara cells had no observable pathology. In order to elucidate the role of epithelial derived-HIF1α signaling in cobalt-induced lung injury, these mice were exposed to cobalt chloride via oropharyngeal aspiration. Compared to control mice, mice that were HIF1α deficient in their lungs (HIF1αΔ/Δ) exhibited airway infiltration of eosinophils associated with airway epithelial changes, including mucus cell metaplasia and increased levels of the chitinase-like proteins YM1 and YM2. Mice deficient in HIF1α also showed a drastic change in cytokine profiles in their lavage fluid when compared to their control. These results suggest that loss of HIF1α from alveolar Type II epithelial and Clara cells of the lungs leads to cellular and molecular processes that are associated with asthma following cobalt exposure and that airway epithelial-derived HIF1α plays a critical role in modulating the inflammatory response of the lung.

MATERIALS AND METHODS

Description of mice: Triple transgenic mice were created by mating HIF1α$^{flox/flox}$ (a generous gift of Randall Johnson, Univ. California-San Diego) and SP-C-rtTA$^{-/tg}$/(tetO)$_7$-CMV-Cre$^{tg/tg}$ transgenic mice (a generous gifts of

Jeffrey A. Whitsett Cincinnati Children's Hospital Medical Center) [16-19]. The generated mice, SP-C-rtTA$^{-/tg}$/(tetO)$_7$-CMV-Cre$^{tg/tg}$/HIF1α$^{flox/flox}$, are capable of respiratory epithelium specific conditional recombination in the floxed HIF1α gene upon exposure to doxycycline [18]. In addition to the triple transgenic controls, four additional genotypes were employed to rule out effects of any one locus in the presence and absence of doxycycline. These include, SP-C-rtTA$^{-/tg}$/(tetO)$_7$-CMV-Cre$^{-/-}$/HIF1α$^{+/+}$ (sTH), SP-C-rtTA$^{-/-}$/(tetO)$_7$-CMV-Cre$^{tg/tg}$/HIF1α$^{+/+}$ (StH), SP-C-rtTA$^{-/tg}$/(tetO)$_7$-CMV-Cre$^{tg/tg}$/HIF1α$^{+/+}$ (stH) and SP-C-rtTA$^{-/-}$/(tetO)$_7$-CMV-Cre$^{-/-}$/HIF1α$^{flox/flox}$ (STh). The HIF1α$^{flox/flox}$ were originally maintained in a C57BL/6 background, whereas the SP-C-rtTA$^{-/tg}$/(tetO)$_7$-CMV-Cre$^{tg/tg}$ were generated in an FVB/N genetic background. These parental strains were carefully mated to acquire the necessary genotypes for the described experiments and all of the mice used in this study have been maintained in this mixed C57BL/6 and FVB/N background. Genotyping of the mice was performed by PCR for all the three loci as previously described [15].

Doxycycline treatment and animal husbandry: *In utero* exposure to doxycycline in the triple transgenic mice led to lethality upon parturition [15]. Postnatal recombination was carried out by exposing lactating dams to doxycycline containing feed (625 mg doxycycline/Kg; Harlan Teklad, Madison,

WI) and drinking water (0.8 mg/ml: Sigma chemicals Co.) until weaning. Triple transgenic mice were then maintained on the same doxycycline containing food and water until they were approximately 7 weeks of age. Doxycycline treatment was terminated 7-10 days prior to first exposure to metals. These mice will be referred to as HIF1α deficient or HIF1αΔ/Δ throughout the chapter. Control animals used in the study were triple transgenic (SP-C-rtTA$^{-/tg}$/(tetO)$_7$-CMV-Cre$^{tg/tg}$/HIF1α$^{flox/flox}$) mice that were maintained on normal food and water *ad libitum*. All of the remaining genotype control lines described above were exposed to doxycycline for the same 7 week paradigm when appropriate. Mice used in this study were kept at the animal housing facility under the strict hygienic and pathogen free conditions approved by the university laboratory animal resource (ULAR) regulatory unit. All the animal handling and necropsy protocols were approved by the ULAR regulatory unit of Michigan State University.

Cobalt exposure, tissue harvesting and processing: 18 mice from each genotype were randomly assigned to one of three groups. Mice were treated with saline, 5 mM, or 10 mM cobalt chloride in 25 μL volume by oropharyngeal aspiration. These cobalt concentrations correspond to 30 and 60 μg daily exposure, respectively. Mice were treated for 5 days on, 2 days off, 5 days on and then euthanized 72 hours after the last exposure. Mice were assessed for total body weight prior to first treatment and assessed again prior to sacrifice. Following exposure, mice were anesthetized with sodium pentobarbital (50

mg/ml), and a midline laparotomy was performed. The trachea was exposed and cannulated. The lung and heart were removed *en bloc* and the lungs were lavaged with two successive 1 ml volumes of sterile saline. These fractions were combined and total cell counts were performed using a hemocytometer. Differential cell counts were performed in cytospin samples using Diff-Quik reagent (Baxter, FL). The remaining BALF was frozen for cytokine profiling. The right lung lobe was removed and stored in RNA*later* RNA stabilizing reagent (Qiagen, Valencia, CA) for RNA isolation. The left lobe was perfusion inflated and fixed in 10% neutral buffered formalin for histopathological analysis.

Histopathology and immunohistochemistry: At least four to six mice from each genotype and treatment group were analyzed for histopathological changes. Formalin fixed left lung lobe tissues were paraffin embedded and 5-micron thick sections were mounted on glass slides and stained with hematoxylin and eosin (H&E) or immunostained with HIF1α (1: 500 dilution, NB100-479, Novus Biologicals, Littleton, CO), major basic protein (1:500 dilution, Mayo Clinic, AZ), or YM1 (1:100 dilution, AB24608; Abcam, Cambridge, MA) as previously described [15]. Other lung sections were histochemically treated with picro-sirius red solution for interstitial collagen staining to identify areas of pulmonary fibrosis or with Alcian Blue (pH 2.5)/Periodic Acid Schiff (AB-PAS) stain to identify mucosubstances in mucous cells.

RNA isolation and quantitative real-time PCR (qRT-PCR) analysis: Lung tissue (10 mg) stored in RNA*later* RNA Stabilization Reagent was homogenized in RLT buffer (RNeasy RNA isolation Kit, Qiagen, Maryland) using a Retsch MM200 bead beater system (Retsch, Haan, Germany). Total RNA quantification was performed spectrophotometrically (NanoDrop ND-1000 UV-Vis Spectrophotometer). Total RNA (1 μg) was reverse transcribed using superscript II reverse transcriptase kit (Invitrogen, CA). cDNAs from each experimental group were pooled and quantitative real-time PCR array analysis reactions were carried out in duplicate on an ABI Prism 7900HT 384-well block using *Taq*Man assays (ABI, Applied Biosytems, Foster City, CA). The complete table of the genes analyzed is listed in table 4.1. Changes in gene expression were calculated using the $2^{-\Delta\Delta Ct}$ method. An average of the number of cycles of three housekeeping genes, GAPDH, Actin-β, and 18S, was used to normalize the expression between samples. Genes that had greater than a 2 fold change in expression level when compared to the control group were further analyzed by qRT-PCR using individual samples run in duplicate to confirm the PCR array results. Samples exhibiting Ct values greater than 40 were deemed undetermined and removed from subsequent analysis. Outliers were removed by Grubbs test and averages compared. The fold changes for these genes are listed in Table 4.2.

Determination of cytokine levels by Bead array: Bronchoalveolar lavage fluid was analyzed for IL-1β, Eotaxin, KC, IL-6, IL-10, IL-12, IL-4,IL-5, IL-13, IL-

2, Rantes, GM-CSF, INF-γ, TNF-α, MCP-1, VEGF, MIP-2, MIP-1α using a Bio-Plex 200 system and reagents (Bio-Rad Laboratories Inc., Hercules, CA, USA) according to manufacturer's instructions. Briefly, cytokine specific antibody coupled color-coded beads are allowed to react with the cytokines present in the sample. Following extensive washing, a biotinylated detection antibody is added to the cytokine bound beads. The sandwich complex formation is detected by the addition of streptavidin-phycoerythrin. Cytokines are identified and quantitated based on bead color and fluorescence. Cytokine levels are calculated by system-specific software (Bio-Plex Manager™) using a standard curve derived from a recombinant cytokine standard. A multiplex assay was performed by mixing beads specific to each of above listed cytokines and incubating them with 50 µl of undiluted BALF in the provided 96 well filter plate. Following washing, all the respective detection antibodies were added to wells followed by addition of streptavidin-phycoerythrin. Values from blank wells for each cytokine were subtracted from the corresponding cytokine values in each sample. Negative values were set to zero. Outliers were removed by Grubbs' Test, averages were calculated, and significance determined by ANOVA followed by Tukey's HSD test.

Quantitative analysis: All cell counts and cytokine and gene expression data were analyzed by ANOVA followed by a Tukey's HSD test. All the data from the study was presented as standard error of the mean (SEM). Statistical difference of P value less than 0.05 was considered as significant.

RESULTS:

Post-natal deletion of HIF1α: The initial description of the lung specific cre recombinase model had very little data regarding post-natal deletion, however, it can be assumed that doxy-induced cre expression will be restricted to Clara and Type II cells since SPC expression is restricted to these cells types in the adult animal [18]. To determine if prolonged exposure to doxycyline (Dox) could induce recombination within the conditional HIF1α locus, mice were exposed to Dox for approximately 7 weeks starting on post-natal day 4 (PN4). Initially, they received the drug through their mother's milk, and then through their food and water. These mice will be referred to as HIF1α deficient or HIF1αΔ/Δ. The mice referred to as controls throughout the studies are triple transgenic (SP-C-rtTA$^{-/tg}$/(tetO)$_7$-CMV-Cre$^{tg/tg}$/HIF1α$^{flox/flox}$) mice that were maintained on regular feed and water. The lungs of control and Dox treated mice were then removed and analyzed for HIF1α expression via immunohistochemistry (IHC). Control mice showed pronounced HIF1α expression in the Clara cells lining the bronchiolar airway and Type II cells of the alveoli (Figs. 4.1A and 4.1B). In contrast, the HIF1αΔ/Δ mice showed a marked decrease in expression in these cells, with only minor staining visible in the bronchiolar airway lining cells and little or no staining in the alveoli (Figs. 4.1C and 4.1D).

Figure 4.1. HIF1α immunohistochemistry of lungs from control and doxycycline treated mice

Lung tissue sections from control **(A and B)** and HIF1α Δ/Δ (**C and D**) were analyzed by immunohistochemistry using a HIF1α-specific antibody. Control (**A and B**) and doxycycline (**C and D**) treated mice were compared. HIF1α staining is prominent in the epithelial cell (e) lining the bronchiolar airway (BA) and type II cells (Solid arrow) in the alveolar duct (AD) and alveolus (a). Staining is greatly reduced in the postnatally doxycycline treated animals (**C and D**).

"Images in this dissertation are presented in color."

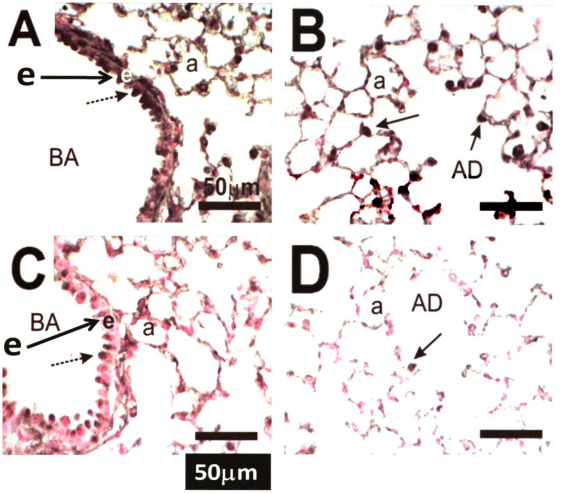
A
e
e
a
BA
50μm
B
a
AD
C
BA
e
e
a
50μm
D
a
AD

The results suggest that postnatal exposure to Dox can induce significant recombination of the HIF1α locus and that the triple transgenic mouse is a viable model to test the role of HIF1α in cobalt-induced lung injury.

Body weight change and cell counts in lavage fluid: To characterize the role of HIF1α in cobalt-induced lung injury, control and HIF1αΔ/Δ mice were randomly assigned to three groups. Individual groups received, sterile saline, 30, or 60 μg cobalt chloride by oropharyngeal aspiration per day using a two week protocol, 5 days on, 2 days off, 5 days on, and 2 days off. Total body weight of some of the control mice rose slightly during the course of the exposure however the body weight gain remained largely unchanged. In contrast, the HIF1αΔ/Δ mice lost weight in a dose dependent fashion (Fig. 4.2A). Though this decrease was not significant, it was the first indication that the HIF1α deficient mice responded differently to cobalt challenge. After the final 2-day incubation, mice were euthanized, BALF was collected, and lung tissue was processed for light microscopic examination, IHC, and RNA isolation. HIF1α-deficient mice treated with 60 μg cobalt chloride showed significant increase in total BALF cells as compared to 60 μg cobalt chloride treated control mice suggesting that loss of HIF1α in the Clara and Type II cells made the mice more susceptible to injury (Fig. 4.2B). Specific cellularity within the BALF was also different between the two genotypes.

Figure 4.2. Weight change and cell counts from cobalt challenged control and HIF1α Δ/Δ mice.

Mice were exposed to saline, 30 μg (5 mM) or 60 μg (10 mM) $CoCl_2$ for 2 week, 5 days/week paradigm. Total animal weight change (**A**) in control (**white bars**) and HIF1α Δ/Δ (**black bars**) were calculated by subtracting animal weight on the day of sacrifice from weight at the start of exposure. Total cell counts from BALF (**B**) were assessed from all of the mice and averaged. Cell differential counts were performed for macrophages (**C**), lymphocytes (**D**), neutrophils (**E**), and eosinophils (**F**). N>5 mice/group. * = Significance (p values noted).

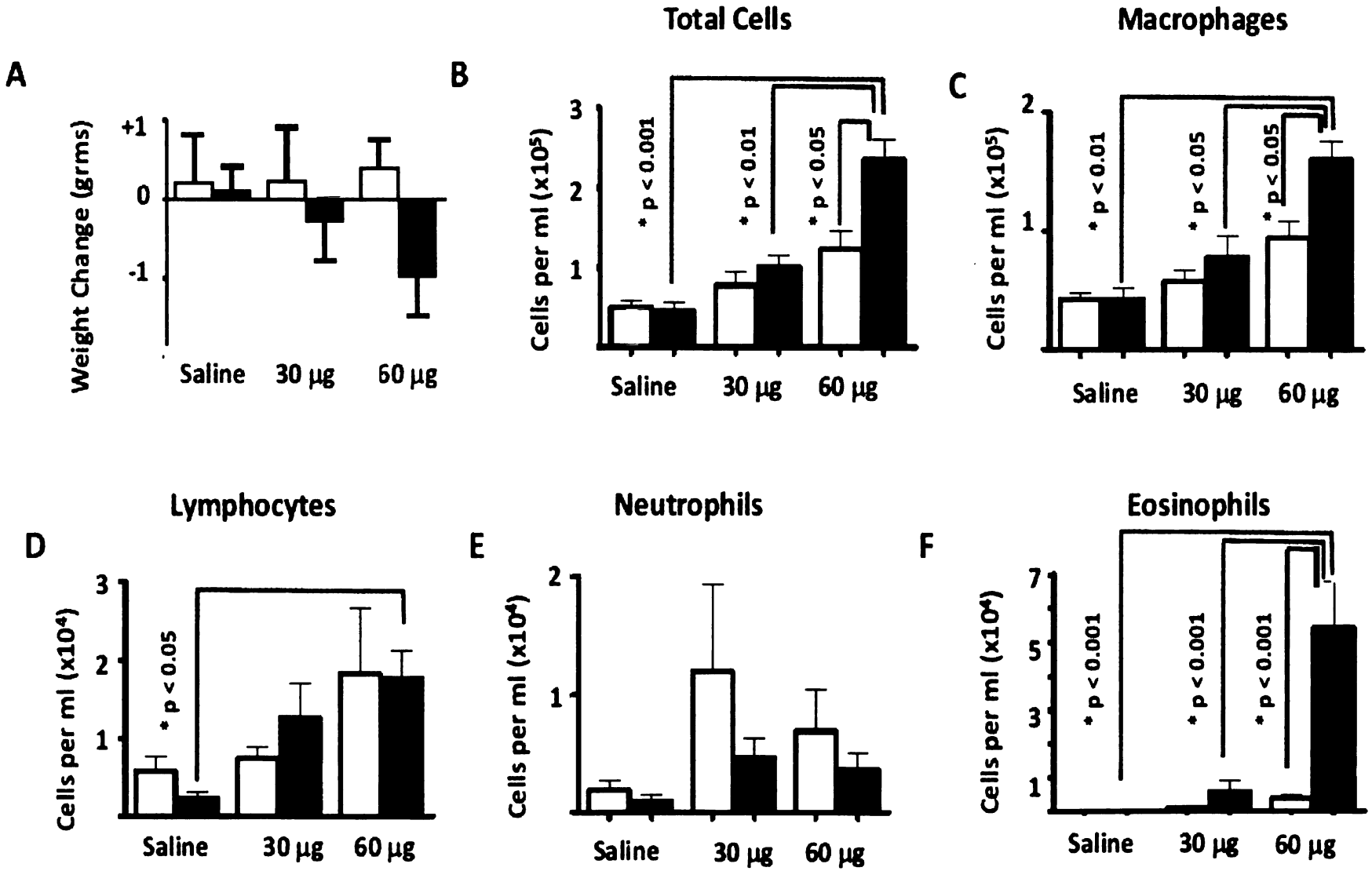
A
Weight Change (grms)
+1
0
-1
Saline
30 µg
60 µg
B
Total Cells
Cells per ml (x10⁵)
* p < 0.001
* p < 0.01
* p < 0.05
Saline
30 µg
60 µg
C
Macrophages
Cells per ml (x10⁵)
* p < 0.01
* p < 0.05
* p < 0.05
Saline
30 µg
60 µg
D
Lymphocytes
Cells per ml (x10⁴)
* p < 0.05
Saline
30 µg
60 µg
E
Neutrophils
Cells per ml (x10⁴)
Saline
30 µg
60 µg
F
Eosinophils
Cells per ml (x10⁴)
* p < 0.001
* p < 0.001
* p < 0.001
Saline
30 µg
60 µg

Cobalt-treated control and HIF1αΔ/Δ mice showed dose-dependent increases in lymphocytes and macrophages, however, only HIF1αΔ/Δ mice treated with 60 μg cobalt was significant when compared to saline (macrophages and lymphocytes) and 30 μg (macrophages only) treated HIF1αΔ/Δ mice (Figs. 4.2C and 4.2D). Moreover, the 60 μg treated HIF1αΔ/Δ mice displayed a significant increase in macrophages as compared to control mice treated with 60 μg cobalt. Lymphocytes and neutrophils displayed no significant changes when control and HIF1αΔ/Δ mice were compared within treatment groups. Control mice displayed a non-significant increase in neutrophils compared to HIF1α deficient mice (Fig. 4.2E). In contrast, the HIF1αΔ/Δ mice following cobalt (60 μg) exposure displayed a significant increase in eosinophils when compared to all other groups, suggesting that HIF1α plays a role in modulating the lung's inflammatory response to metals (Fig. 4.2F). These changes were specific to the loss of HIF1α and not due to Dox treatment or the SPC-rtTA or tet-Cre transgenes as different doxycycline treated monotransgenic and bitransgenic (SP-C-rtTA$^{-/tg}$/(tetO)$_7$-CMV-Cre$^{-/-}$/HIF1α$^{+/+}$ (sTH), SP-C-rtTA$^{-/-}$/(tetO)$_7$-CMV-Cre$^{tg/tg}$/HIF1α$^{+/+}$ (StH), SP-C-rtTA$^{-/tg}$/(tetO)$_7$-CMV-Cre$^{tg/tg}$/HIF1α$^{+/+}$ (stH) and SP-C-rtTA$^{-/-}$/(tetO)$_7$-CMV- Cre$^{-/-}$/HIF1α$^{flox/flox}$ (STh)) mice behaved similar to control mice (SP-C-rtTA$^{-/tg}$/(tetO)$_7$-CMV-Cre$^{tg/tg}$/HIF1α$^{flox/flox}$ (sth) (Fig. 4.3).

Table 4.1. List of genes analyzed qRT-PCR

Gene Symbol	Gene Description	*Taq*Man Assay ID
18S	18S	4352930E
Actb	Beta Actin	4352933E
Arbp	acidic ribosomal phosphoprotein P0	Mm01974474_gH
Gapd	Glyceraldehyde 3phosphate dehydrogenase	4352932E
Gusb	glucuronidase, beta	Mm00446953_m1
Atf4	activating transcription factor 4	Mm00515324_m1
Cat	catalase	Mm00437992_m1
Ccl2	Monocyte chemotactic protein-1	Mm00441242_m1
Ccl3	Macrophage inflammatory protein 1 alpha	Mm00441258_m1
Ccl4	Macrophage inflammatory protein 1 beta	Mm00443111_m1
Ccl5	Regulated upon activation, normal T cell expressed and secreted	Mm01302427_m1
Ccl11	Eotaxin	Mm00441238_m1
Chi3l3	chitinase 3-like 3 (YM1)	Mm00657889_mH
Chi3l4	chitinase 3-like 4 (YM2)	Mm00840870_m1
Clca3	chloride channel calcium activated 3 (Gob-5)	Mm00489959_m1
Crp	C-reactive protein, pentraxin-related	Mm00432680_g1
Cxcl1	Cxcl1 keratinocyte chemoattractant	Mm00433859_m1
Cxcl2	Cxcl2 macrophage-inflammatory protein-2	Mm00436450_m1
Cyp2e1	cytochrome P450, family2, subfamily e, polypeptide1	Mm00491127_m1
Egfr	epidermal growth factor receptor	Mm00433023_m1
F2r	coagulation factor II (thrombin) receptor	Mm00438851_m1
fgf9	fibroblast growth factor 9	Mm00442795_m1
fgf10	fibroblast growth factor 10	Mm00433275_m1
fgf18	fibroblast growth factor 18	Mm00433286_m1
Foxa1	forkhead box A1	Mm00484713_m1
Foxa2	forkhead box A2	Mm00839704_mH
Foxp3	forkhead box P3	Mm00475165_m1
Gata3	GATA binding protein 3	Mm00484683_m1
Gclc	glutamate-cysteine ligase, catalytic subunit	Mm00802655_m1
Gclm	glutamate-cysteine ligase, modifer subunit	Mm00514996_m1
Gstk1	glutathione S-transferase kappa 1	Mm00504022_m1
Gstm1	glutathione S-transferase, mu 1	Mm00833915_g1
Gstp1	glutathione S-transferase, pi 1	Mm00496606_m1
Hmox	heme oxygenase (decycling) 1	Mm00516004_m1
Ifng	interferon gamma	Mm00801778_m1
IL1b	interleukin 1 beta	Mm00434228_m1
Il1rn	interleukin 1 receptor antagonist	Mm01337566_m1
IL2	interleukin 2	Mm00434256_m1
IL4	interleukin 4	Mm00445259_m1
IL5	interleukin 5	Mm00439646_m1
IL6	interleukin 6	Mm00446190_m1
IL10	interleukin 10	Mm00439616_m1
IL-13	interleukin 13	Mm00434204_m1

Table 4.1. Continued.

Gene Symbol	Gene Description	*Taq*Man Assay ID
IL23a	interleukin 23, alpha subunit p19	Mm00518984_m1
Mt1	metallothionein 1	Mm00496660_g1
Muc5ac	mucin 5, subtypes A & C, tracheobronchial/gastric	Mm01276725_g1
Nfe2l2	nuclear factor, erythroid derived 2, like 2	Mm00477784_m1
Nos2	nitric oxide synthase 2, inducible	Mm00440485_m1
Nqo1	NAD(P)H dehydrogenase, quinone 1	Mm00500821_m1
Pcna	proliferating cell nuclear antigen	Mm00448100_g1
Pdgfrb	platelet derived growth factor receptor, beta polypeptide	Mm01262489_m1
Pparg	peroxisome proliferator activated receptor gamma	Mm00440945_m1
Ptgs2	prostaglandin-endoperoxide synthase 2	Mm00478374_m1
Saa3	serum amyloid A3	Mm00441203_m1
Scgb1a1	secretoglobin, family 1A, member 1 (uteroglobin)	Mm00442046_m1
Serpine1	serine (or cysteine) peptidase inhibitor, clade E, member 1	Mm01204469_m1
Sftpc	surfactant associated protein C	Mm00488144_m1
Sftpd	surfactant associated protein D	Mm00486060_m1
Socs3	suppressor of cytokine signaling 3	Mm00545913_s1
Sod1	superoxide dismutase 1, soluble	Mm01344233_g1
Sod2	superoxide dismutase 2, mitochondrial	Mm00449726_m1
Stat6	signal transducer and activator of transcription 6	Mm01160477_m1
Tfpi2	tissue factor pathway inhibitor 2	Mm00436948_m1
Tgfb1	transforming growth factor, beta 1	Mm01178820_m1
Tnfa	tumor necrosis factor(TNF superfamily, member 2)	Mm00443258_m1
Vegfa	vascular endothelial growth factor A	Mm01281447_m1

Figure 4.3. Cell counts from genotype and treatment controls.

Genotypic control mice were exposed to saline or 60 μg (10 mM) $CoCl_2$ for 2 week, 5 days/week paradigm. Total cell counts from BALF (**A**) were assessed from all of the mice and averaged. Cell differential counts were performed for macrophages **(B),** neutrophils **(C),** lymphocytes **(D),** and eosinophils **(E).** N>5 mice/group.

"Images in this dissertation are presented in color."

Figure 4.3. Cell counts from genotype and treatment controls.

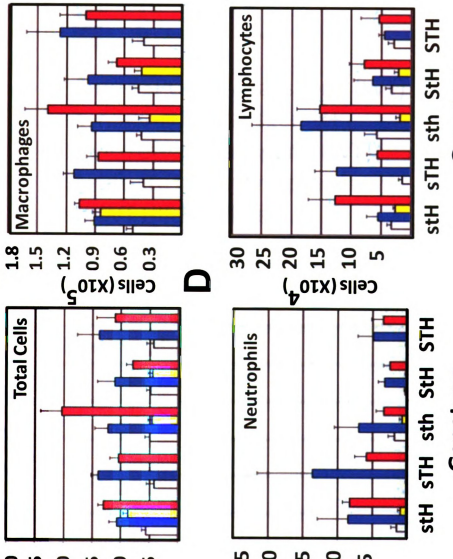

Figure 4.3. Continued.

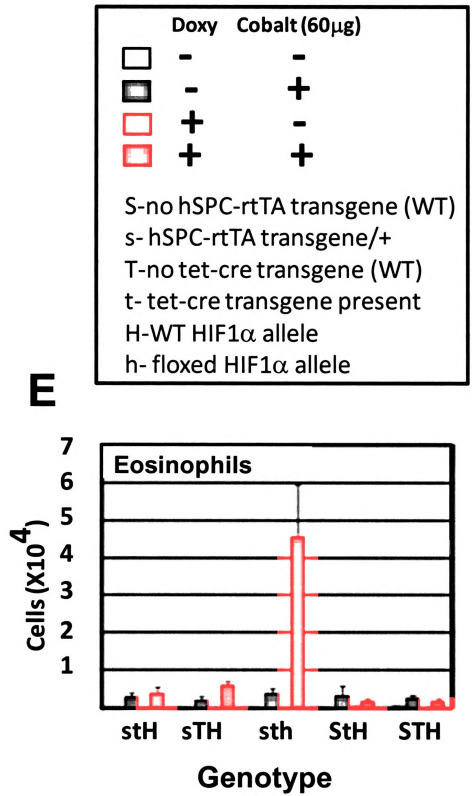

Histopathology of Cobalt-induced injury: Histologically, no pulmonary lesions were found in control or HIF1αΔ/Δ mice that were instilled with saline alone. In contrast, control mice repeatedly instilled with cobalt had a mild-moderate chronic bronchopneumonia that was histologically characterized by a mononuclear cell infiltrate (mainly small and large lymphocytes, monocytes, and occasional plasma cells) admixed with lesser numbers of neutrophils and eosinophils in the interstitial tissues surrounding large- and small-diameter conducting airways (i.e., axial, preterminal and terminal bronchioles) and extending into the centriacinar regions of the lung (alveolar ducts and adjacent alveoli) (Figs. 4.4A and 4.4B). Interstitial fibrosis was a prominent remodeling feature of the alveolar septa in affected parenchymal regions along with minimal to mild hyperplasia of alveolar type II cells and accumulation of mildly hypertrophic macrophages and varying numbers of inflammatory cells (lymphocytes and neutrophils) in alveolar airspaces (Figs. 4.4C and 4.4D). These cobalt-induced airway and alveolar changes were dose-dependent and were more consistently found in the hilar rather than the distal aspects of the lung lobe.

A similar mild-moderate chronic bronchopneumonia with peribronchiolar lymphoplasmacytic inflammation and variable amounts of interstitial alveolar fibrosis airway was present in the lung lobes of cobalt-exposed HIF1αΔ/Δ mice (data not shown). There were, however, marked differences in the character

Figure 4.4. Histopathology and picro-sirius staining control and cobalt-treated control mice

Light photomicrographs of the lungs of control mice instilled with saline (**A and C**) or cobalt (**B and D**). Lung sections in A and B were stained with hematoxylin and eosin, while sections in C and D were histochemically treated with picro-sirius red solution that stains interstitial collagen (red chromagen in interstitial tissues in the alveolar septa and around bronchiolar airways). In cobalt-treated lungs (**B and D**), there is marked inflammation and interstitial fibrosis (asterisk in B) around pre-terminal bronchioles (ptb) and terminal bronchioles (tb) and extending distally into alveolar ducts (ad) and adjacent alveoli (a). There is increased picro-sirius red stained collagen (solid arrows) in the alveolar septa of the cobalt-treated mouse (**D**) compared to that in the saline-treated control mouse (**C**). p, pulmonary pleura; e, bronchiolar epithelium; stippled arrow, mixed inflammatory cell infiltrate. "Images in this dissertation are presented in color."

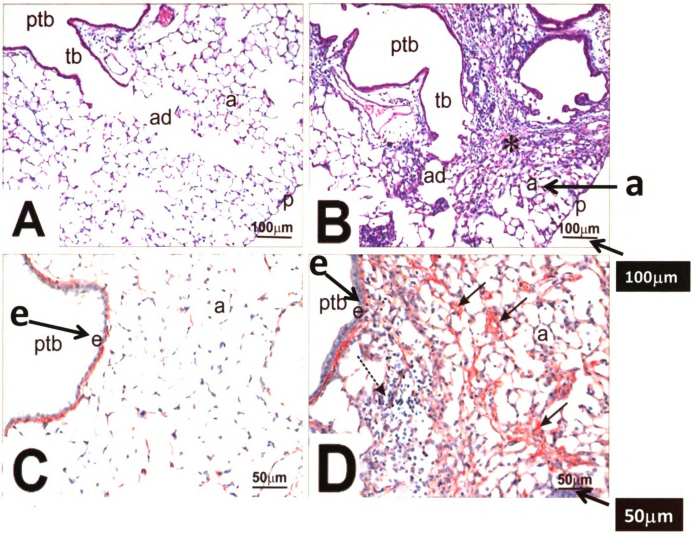
ptb
tb
ad
a
p
100μm
A
ptb
tb
ad
*
a
a
p
100μm
B
100μm
e
ptb
e
a
C
e
ptb
e
a
50μm
D
50μm

of the inflammatory, airway epithelial, and alveolar macrophage changes in the lungs of these transgenic mice compared to their control counterparts. Along with the lymphocytes and plasma cells, there were markedly more eosinophils in the peribronchiolar and alveolar mixed inflammatory cell influxes in HIF1αΔ/Δ mice compared to those of control mice (Fig. 4.5D). Another distinctive change found only in HIF1αΔ/Δ mice was mucous cell metaplasia in the airway epithelium lining axial and preterminal bronchioles. This airway epithelial lesion in large-diameter bronchioles consisted of numerous Alcian Blue/Periodic Acid Schiff stained mucous goblet cells in bronchiolar epithelium that is normally devoid of these mucus-secreting cells in mice (Figs. 4.6A and 4.6B). These areas of epithelial mucous cell metaplasia in cobalt-treated HIF1αΔ/Δ mice were also immunohistochemically positive for YM1/2 chitinase-like proteins (Figs. 4.6C and 4.6D).

Characterization of eosinophils and YM1/2 Expression: In addition to these unique eosinophil and epithelial responses, alveolar macrophages accumulating in alveolar airspaces of cobalt-exposed mice were larger and more eosinophilic in the HIF1αΔ/Δ mice compared to those in similarly exposed control mice (Figs. 4.7A and 4.7B). Immunohistochemically, the cytoplasm of these phenotypically distinctive macrophages stained positive for YM1/2 protein similar to the mucous goblet cells in the metaplastic bronchiolar epithelium of HIF1αΔ/Δ mice (Figs. 4.6C and 4.6D).

Figure 4.5. Major Basic Protein Staining in lungs from control and HIF1αΔ/Δ mice.

Light photomicrographs of the lungs of saline (**A and C**) or cobalt-instilled (**B and D**) control (**A and B**) and HIF1α Δ/Δ (**C and D**) mice. All lung sections were immunohistochemically stained for major basic protein to identify infiltrating eosinophils (red chromagen; arrows) and counterstained with hematoxylin. A mixed inflammatory infiltrate consisting of mononuclear leukocytes, eosinophils and lesser numbers of neutrophils are restricted to the lungs in cobalt-treated mice (**B and D**). Markedly more eosinophils are present in the peribronchiolar and alveolar regions of the cobalt-treated HIF1α Δ/Δ mouse (**D**) compared to that of the cobalt-treated control mouse (**B**). ptb, pre-terminal bronchiole; pa, pulmonary arteriole, a, alveolar airspace; e, bronchiolar epithelium. "Images in this dissertation are presented in color."

A
B
C
D
ptb
e
pa
a
50µm

Variably sized needle-shaped or rectangular refractile eosinophic crystals were also present within these alveolar macrophages or free in the alveolar airspaces (Fig. 4.7B). These crystals also stained positive for YM1/2 (Fig. 4.7D). Multinucleated giant cells were also more frequently observed in the cobalt-induced alveolitis of HIF1αΔ/Δ mice compared to those of control mice.

Cobalt-induced gene expression changes: The differences in cobalt-induced pulmonary pathology between the control and HIF1αΔ/Δ suggested an alteration in the stress response upon loss of HIF1α. To begin characterizing this difference, the expression of 63 key genes involved in immunity, inflammation, oxidative stress, and other stress pathways, was assessed by quantitative real time PCR (qRT-PCR) (table 4.1). Initially, samples from each treatment group and genotype were pooled and screened. Those genes that showed a difference when compared to untreated controls within a genotype or between genotypes were characterized as individual samples (table 4.2). Six of these genes showed significant changes in expression when compared between genotype and within treatment or within genotype and between treatments (Fig. 4.8). Two other genes, Ym1 and IL6, were near significance (0.069 and 0.055 respectively). The expression of Ym2 in the HIF1α deficient mice was significantly increased following challenge with 60 μg cobalt compared to the saline treated HIF1αΔ/Δ mice and the 60 μg cobalt treated control animal.

Figure 4.6. Alcian Blue/Periodic Acid Schiff Stain and YM1/2 IHC

Light photomicrographs of pre-terminal bronchioles (ptb) of cobalt-instilled control (**A and C**) and HIF1α Δ/Δ (**B and D**) mice. Tissues were stained with Alcian Blue (pH 2.5)/Periodic Acid Schiff (AB/PAS; **A and B**) to identify acidic and neutral mucosubstances (magenta stain; arrows) in mucous cells within the bronchiolar epithelium (e). Numerous AB/PAS-stained mucous cells are present only in the airway epithelium lining the pre-terminal bronchiole in the cobalt-treated HIF1α Δ/Δ mouse (**B**). Tissues in C and D were immunohistochemically stained for YM1/2 protein (brown chromagen; arrows) and counterstained with hematoxylin. YM1/2 proteins were present only in the bronchiolar epithelium of the cobalt-treated HIF1α Δ/Δ mouse (**D**). Arrow in C identifies a few alveolar macrophages that were positive for YM1/2 proteins. "Images in this dissertation are presented in color."

A
ptb
e
a
100µm
B
a
ptb
e
a
100µm
100µm
C
ptb
e
e
50µm
D
ptb
e
e
50µm
50µm

Figure 4.7. H&E staining and YM1/2 IHC of cobalt treated control and HIF1αΔ/Δ mice

Light photomicrographs of alveolar macrophages in cobalt-instilled control (**A and C**) and HIF1α Δ/Δ (**B and D**) mice. Lung tissues were histochemically stained with hematoxylin and eosin (H&E; **A and B**) or immunohistochemically for YM1/2 proteins (**C and D**). H&E-stained alveolar macrophages in the cobalt-instilled HIF1α Δ/Δ mouse (**B**) are larger (hypertrophic) and more eosinophilic than the similarly stained lung section from the cobalt-instilled control mouse (**A**). In **B**, a group of macrophages are surrounding an extracellular aggregate of eosinophilic crystals (arrow). In addition, more alveolar macrophages with immunohistochemically staining for YM1/2 proteins (solid arrows) are present in lung section from the cobalt-instilled HIF1α Δ/Δ mouse (**D**) as compared to that of the cobalt-instilled control mouse (**C**). Stippled arrow in C, alveolar macrophage with no detectable YM1/2 proteins. "Images in this dissertation are presented in color."

A
B
C
D
a
100μm
50μm

Gob5 expression followed a similar pattern of expression as that of Ym2; however, its expression was only significantly changed when the 60 μg cobalt treated HIF1αΔ/Δ animals were compared to the 30 μg treated ones. Muc5ac and IL5 showed dose dependent changes in expression within genotypes and in the case of IL5, expression was significantly elevated in saline treated HIF1αΔ/Δ mice compared to saline treated controls. Eotaxin was also significantly elevated in the HIF1αΔ/Δ mice when the saline treated mice were compared. Moreover, eotaxin was also significantly different between the genotypes in the 60 μg cobalt treated mice.

Cytokine profiling: The pathology of the lung and the gene expression patterns suggested a change in the inflammatory response upon loss of HIF1α from Type II and Clara cells. To determine if the changes in cytokine gene expression led to changes in the chemoattractants found in the BALF, profiling of 18 cytokines was performed using a bead array (BioRad). Of the 18 characterized, 10 showed significant difference when compared across genotype or within treatment groups (Table 4.3). Interestingly, several of these were different when the saline treated groups of the control and HIF1αΔ/Δ mice were compared (i.e. IL-1β, IL-5, IL-12, GM-CSF, RANTES, TNFα and VEGF [Table 4.3]). This suggests that loss of HIF1α from Type II and Clara cells alters the tissue's native cytokine profile. Moreover, cobalt exposure caused a more pronounced phenotype in the HIF1αΔ/Δ animals with respect to cytokine changes.

Figure 4.8. Gene expression results

The expression of 63 genes was analyzed by qRT-PCR. Those genes that showed a difference as pooled samples were further analyzed as independent replicates. White bars represent control groups and black bars represent HIF1α deficient groups. Expression levels were normalized to the saline treated control animal and expressed as fold change. a = $p < 0.07$, * = $p < 0.05$, ** = $p < 0.01$

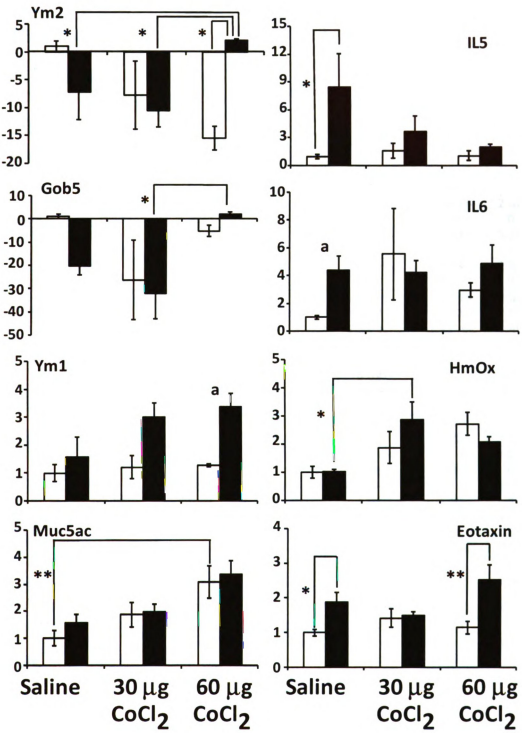
Ym2
Gob5
Ym1
Muc5ac
IL5
IL6
HmOx
Eotaxin
Saline
30 µg CoCl2
60 µg CoCl2
Saline
30 µg CoCl2
60 µg CoCl2

Table 4.2 Gene Expression Changes

	Control			HIF1αΔ/Δ		
Gene	Saline	30 µg	60 µg	Saline	30 µg	60 µg
18S	1.00 +/- 0.04	1.04 +/- 0.03	1.06 +/- 0.04	1.15 +/- 0.05	1.07 +/- 0.02	1.02 +/- 0.03
β-Actin	1.00 +/- 0.05	-1.14 +/- 0.05	-1.13 +/- 0.03	-1.05 +/- 0.02	-1.08 +/- 0.04	-1.06 +/- 0.02
GAPDH	1.00 +/- 0.05	1.08 +/- 0.07	1.05 +/- 0.03	-1.10 +/- 0.05	-1.01 +/- 0.04	1.02 +/- 0.02
MCP	1.00 +/- 0.35	1.70 +/- 0.96	1.18 +/- 0.48	2.38 +/- 1.03	1.10 +/- 0.27	-1.62 +/- 0.40
MIP1a	1.00 +/- 0.21	1.79 +/- 0.46	2.40 +/- 0.62	2.39 +/- 0.56	2.19 +/- 1.83	2.43 +/- 0.34
Eotaxin	1.00 +/- 0.08	1.42 +/- 0.23	1.15 +/- 0.15	1.88 +/- 0.23	1.49 +/- 0.10	2.52 +/- 0.36
Ym1	1.00 +/- 0.25	1.21 +/- 0.36	1.88 +/- 0.51	1.56 +/- 0.62	3.00 +/- 0.42	3.38 +/- 0.41
Ym2	1.00 +/- 0.80	-5.88 +/- 3.99	-3.36 +/- 1.82	-4.46 +/- 2.58	2.04 +/- 1.63	2.82 +/- 0.63
GOB5	1.00 +/- 0.60	-34.02 +/- 16.99	-6.91 +/- 2.93	-2.30 +/- 1.54	2.19 +/- 1.83	2.03 +/- 0.75
KC	1.00 +/- 0.45	2.82 +/- 1.73	-1.11 +/- 0.17	2.92 +/- 1.03	2.21 +/- 1.02	1.40 +/- 0.26
HmOx	1.00 +/- 0.19	1.88 +/- 0.48	2.72 +/- 0.34	1.02 +/- 0.09	2.87 +/- 0.54	2.08 +/- 0.16
IFNγ	1.00 +/- 0.48	1.55 +/- 0.82	3.37 +/- 2.32	-1.90 +/- 0.41	-1.51 +/- 0.40	-2.34 +/- 0.29
IL1β	1.00 +/- 0.43	1.30 +/- 0.32	-2.50 +/- 0.41	1.24 +/- 0.30	-1.16 +/- 0.22	-1.69 +/- 0.62
IL4	1.00 +/- 0.22	-1.03 +/- 0.14	1.31 +/- 0.17	1.05 +/- 0.28	1.34 +/- 0.40	1.27 +/- 0.24
IL5	1.00 +/- 0.19	1.60 +/- 0.67	1.09 +/- 0.46	8.44 +/- 3.02	3.71 +/- 1.36	2.02 +/- 0.23
IL6	1.00 +/- 0.48	2.43 +/- 1.22	1.29 +/- 0.19	1.93 +/- 0.37	1.86 +/- 0.31	2.13 +/- 0.50
IL10	1.00 +/- 0.67	1.11 +/- 0.51	1.89 +/- 1.23	-2.65 +/- 0.47	-1.46 +/- 0.50	-1.26 +/- 0.32
IL13	1.00 +/- 0.41	-1.73 +/- 0.22	-1.18 +/- 0.37	1.34 +/- 0.34	1.40 +/- 0.44	2.46 +/- 0.51
MUC5ac	1.00 +/- 0.24	1.87 +/- 0.39	3.08 +/- 0.50	1.56 +/- 0.27	1.98 +/- 0.23	3.36 +/- 0.41
iNOS	1.00 +/- 0.14	1.91 +/- 0.72	2.59 +/- 1.49	-1.23 +/- 0.22	-1.01 +/- 0.18	1.15 +/- 0.12
SAA3	1.00 +/- 0.73	1.46 +/- 0.69	3.47 +/- 2.13	-1.18 +/- 0.17	-1.17 +/- 0.41	1.09 +/- 0.58
SPC	1.00 +/- 0.22	-1.10 +/- 0.23	1.40 +/- 0.29	-1.01 +/- 0.22	1.72 +/- 0.19	1.48 +/- 0.05
TNFα	1.00 +/- 0.17	1.48 +/- 0.28	2.11 +/- 0.70	1.21 +/- 0.11	1.07 +/- 0.17	1.02 +/- 0.13
VEGF	1.00 +/- 0.08	-1.10 +/- 0.12	-1.47 +/- 0.24	1.13 +/- 0.13	-1.31 +/- 0.05	-1.51 +/- 0.14

DISCUSSION:

The research describes a model for the post-natal deletion of HIF1α from Clara and Type II cells of the lung with the intention of determining the role of the transcription factor in cobalt-induced injury. Control mice repeatedly exposed to cobalt via aspiration had classic signs of metal-induced injury, including increased neutrophils, peribronchial inflammation, and fibrotic lesions. In contrast, the mice deficient in HIF1α in their Clara and Type II cells exhibited a Th2-mediated response in response to cobalt challenge. In fact, these HIF1αΔ/Δ mice displayed a pathology that can be described as asthma-like, including increased eosinophilic infiltration, increased chitinase-like protein expression, and mucus cell metaplasia. In addition, these HIF1α deficient mice expressed an altered panel of cytokines in the absence and presence of cobalt. These results suggest that alveolar epithelium-derived HIF1α plays a critical role in determining the inflammatory response to cobalt challenge and loss of this critical transcription factor can alter the lung's ability to cope with the toxicant insults.

Attempts to study cobalt-induced injury in animal models have successfully mimicked some facets of hard metal lung disease (HMLD). For example, rabbits exposed to low doses of cobalt chloride (0.4 and 2 mg/m^3) for 14-16 weeks (6 hrs/day) displayed increased macrophages and lysozyme activity in BALF, interstitial inflammation, and the presence of large vacuolated macrophages [20-22].

Table 4.3. Cytokine Profiles

Control and HIF1α Δ/Δ mice were exposed to saline, 30 μg, or 60 μg $CoCl_2$ for 2 week, 5 days/week paradigm. The levels of cytokines in BALF were assessed using the Bio-Rad Bio-Plex cytokine suspension array system. N>5 mice/group. Yellow = $p<0.05$, when HIF1α Δ/Δ saline is compared to control saline. Blue = $p<0.05$ compared to genotype matched control. ** = $p<0.05$ when similar treatments are compared between genotypes.

Black shade = significance at 0.05 when compared to saline control between genotypes
= significance at 0.05 when compared to saline treated mice within genotype
** = significance at 0.05 when compared between *genotypes and within treatment group

Table 4.3. Cytokine Profiles

	Control			HIF1α Δ/Δ		
	Saline	30 μg	60 μg	Saline	30 μg	60 μg
IL-1β	0.00 +/- 0.00	0.00 +/- 0.00	0.40 +/- 0.29	7.60 +/- 3.91	0.00 +/- 0.00$^{\#}$	0.00 +/- 0.00$^{\#}$
IL-2	0.00 +/- 0.00	0.00 +/- 0.00	0.00 +/- 0.00	0.00 +/- 0.00	0.00 +/- 0.00	0.00 +/- 0.00
IL-4	0.00 +/- 0.00	0.00 +/- 0.00	0.00 +/- 0.00	0.00 +/- 0.00	2.71 +/- 1.44$^{**,\#}$	0.00 +/- 0.00
IL-5	0.00 +/- 0.00	2.33 +/- 1.67	0.20 +/- 0.20	18.30 +/- 10.61	3.00 +/- 1.21$^{\#}$	0.00 +/- 0.000$^{\#}$
IL-6	1.80 +/- 0.81	1.95 +/- 0.97	5.00 +/- 2.53	3.81 +/- 2.38	3.04 +/- 2.06	5.75 +/- 2.18
IL-10	0.00 +/- 0.00	0.10 +/- 0.06	0.10 +/- 0.06	0.00 +/- 0.00	0.39 +/- 0.22	0.13 +/- 0.06
IL-12	0.00 +/- 0.00	0.00 +/- 0.00	0.00 +/- 0.00	3.10 +/- 1.12	1.86 +/- 0.83	1.58 +/- 0.76
IL-13	1.00 +/- 0.22	0.33 +/- 0.110$^{\#}$	1.17 +/- 0.21	1.00 +/- 0.32	0.79 +/- 0.18	1.00 +/- 0.22
Eotaxin	3.75 +/- 0.55	3.13 +/- 0.80	2.13 +/- 0.52	4.25 +/- 0.29	2.96 +/- 1.04	2.96 +/- 0.88
GM-CSF	0.00 +/- 0.00	1.92 +/- 0.99	2.33 +/- 1.02	5.40 +/- 3.48	2.29 +/- 0.52	1.17 +/- 0.65
IFNγ	0.85 +/- 0.40	1.80 +/- 0.63	2.13 +/- 0.58	2.50 +/- 1.31	1.71 +/- 0.53	1.50 +/- 0.36
KC	31.10 +/- 8.40	46.10 +/- 13.80	42.58 +/- 8.59	59.38 +/- 6.02	37.58 +/- 7.53	118.75 +/- 33.82$^{**,\#}$
MCP1	0.00 +/- 0.00	1.30 +/- 0.58	2.83 +/- 1.49	2.00 +/- 0.71	0.83 +/- 0.31	2.83 +/- 1.08
RANTES	3.00 +/- 1.08	25.25 +/- 7.610$^{\#}$	47.75 +/- 21.390$^{\#}$	8.50 +/- 3.07	17.07 +/- 6.31	18.08 +/- 3.04
TNFα	0.00 +/- 0.00	0.00 +/- 0.00	0.00 +/- 0.00	24.05 +/- 12.47	0.29 +/- 0.290$^{\#}$	0.00 +/- 0.000$^{\#}$
MIP2	45.40 +/- 9.7	65.67 +/- 13.96	75.17 +/- 27.54	82.63 +/- 28.57	30.83 +/- 5.53	90.67 +/- 29.76
VEGF	370.20 +/- 16.3	383.50 +/- 56.75	349.20 +/- 16.56	624.00 +/- 138.97	399.93 +/- 44.040$^{\#}$	538.25 +/- 43.06**
MIP1a	3.40 +/- 1.98	5.00 +/- 1.75	1.30 +/- 0.72	5.50 +/- 1.59	1.92 +/- 1.18	8.83 +/- 2.39**

The values are represents cytokine concentrations (pg/ml) in BALF.

Guinea pigs exposed to 2.4 mg/m^3 of cobalt chloride for 2 weeks (6 hrs/day) had a higher rate of BALF neutrophilic and eosinophilic infiltration when presensitized to the metal [23]. The National Toxicology Program exposed rats and mice to cobalt sulfate heptahydrate at doses ranging from 0.3 to 30 mg/m^3 for 13 weeks (6 hrs/day) and described interstitial fibrosis, epithelial hyperplasia, and lesions in the upper airways that were more pronounced in the rats [24, 25]. Finally, hamsters instilled with cobalt chloride (1-1000 μg/kg) displayed signs of oxidative stress, including increased GSSG (oxidized glutathione) :GSH (reduced glutathione) ratio [26]. To the best of our knowledge, none of these models described chronic eosinophilic infiltration, mucous cell metaplasia, or the increase in chitinase-like proteins as seen in the HIF1αΔ/Δ mice. It has been suggested that an animal model is needed that combines the toxic properties of cobalt with its allergenic potential [11]. The HIF1αΔ/Δ mice might be this model. In the presence of cobalt, HIF1αΔ/Δ mice respond with an asthma-like phenotype (i.e. eosinophil infiltration and mucus cell metaplasia) and increased expression of the chitinase-like proteins, Ym1 and Ym2.

Chitins are acetylated glucosamine biopolymer not found in mammalian systems and chitinase and chitinase-like proteins are believed to function as protection against chitin containing organisms. Ym1 and Ym2 are chitinase-like proteins that share considerable protein homology to the human protein,

YKL-40 (also known as human cartilage glycoprotein 39 and chitinase 3-like 1). YKL-40 has recently been identified in the lungs and circulation of asthmatics [27]. Not only was there a correlation with the presence of YKL-40 and asthma, the levels also correlated with the severity of the disease and the thickening of the subepithelial basement membrane [27]. The biological relationship between these enzymes and the etiology of asthma has not been characterized. What is known, however, is that chitinase and chitinase-like proteins are upregulated in asthma models and in the case of chitinase proteins, this induction is dependent upon IL13. IL13 gene expression is slightly elevated in the cobalt treated HIF1αΔ/Δ mice and its lack of significance is most likely due to the timing of analysis (i.e 14 days after the start of exposure). Increased chitinase expression is required for the subsequent eosinophilia and lymphocytic infiltration [28]. Ym2 was significantly increased in the 60 μg treated HIF1αΔ/Δ mice when compared to the 60 μg treated control mice. Moreover, Ym1 expression was approaching significance ($p < 0.07$) when a similar comparison was made. In contrast, Ym2 show a cobalt-induced decrease in expression in the control animals, and Ym1 is unchanged by cobalt treatment in these control mice. These results suggest that cobalt exposure in the HIF1αΔ/Δ mice induces a series of events within the lungs that resembles the progression of asthma in other asthma models, including increased IL13, subsequent increases in Ym1 and Ym2 expression, and the recruitment of eosinophils.

The results suggest that the ability of Type II and Clara cells to respond to hypoxia is necessary for the proper lung inflammatory response to metal-induced stress. It is important to point out that this response is not due to loss of HIF1α in resident macrophages. HIF1α expression is still strong in these cells following post-natal doxycycline exposure and confirms that the SPC promoter confines the expression of cre recombinase to Type II and Clara cells (data not shown). In addition, it implies that the observed inflammatory response is not due to the previously established role of HIF1α in myeloid cell mediated inflammation [29]. Taken together, the results suggest a model for the inflammatory differences between the control and HIF1α deficient mice following metal exposure. Initially, the cobalt challenge leads to damage within the lung, either at Type I or II cells. This damage is communicated to the remaining viable Type II cells of the parenchyma directly or through resident macrophages. In control lungs, HIF1α will regulate the expression of classic hypoxia target genes as well as others involved in the inflammatory response. This HIF1-regulated transcription will dictate the lung's inflammatory response to the metal challenge. The modest increases in cytokines, such as IFNγ, and the resulting pathology suggest a Th1 mediated response. Loss of HIF1α in the remaining viable Type II cells of the HIF1αΔ/Δ mice would lead to an alteration in the cell's ability to respond to the incoming signals from the cobalt damaged cells. The decreased levels of HIF1α would compromise the lung's ability to respond to cobalt as a toxicant and putative allergen. Ultimately, this difference in epithelium derived HIF1α alters the

pattern of released cytokines and presumably leads to the differential expression of Th2 chemokines, such as IL4, IL5, IL10, and IL13. These changes in cytokines will promote the expression of the chitinase and chitinase-like proteins, such as Ym2 and this would lead to the eosinophilic infiltration seen in the HIF1αΔ/Δ mice following cobalt challenge (Fig. 4.7). This proposed model explains the difference in the inflammatory response between the control and HIF1αΔ/Δ mice; however, it is based on collected data at the end of cobalt exposure. Validation of the model will require a detailed dose and time course response to cobalt challenge.

The striking differences observed following cobalt exposure in these two mice genotypes suggests that they will be a powerful tool to understand the relationship between allergy-induced asthma, hypoxia, and inflammation. More importantly, direct comparison of the responses of the control and HIF1αΔ/Δ mice in other asthma models (e.g. ovalbumin challenge) and to other inflammatory inhalants (e.g. ozone) will correlate this relationship to specific cytokines. The research also raises several important questions: Does the loss of HIF1α alter an organism's susceptibility to asthma using other allergens? What role does HIF1α derived from other cell types (e.g. infiltrating inflammatory cells and Type I cells) play in modulating this inflammatory response? Does post-natal deletion of HIF1α alter HIF2α and if so, what impact does this have on the inflammatory response [15]? Most importantly, does a decrease in HIF1α functionality lead to an increased

susceptibility to asthma in humans? More specifically, is it possible that loss or decrease in HIF1α function biases the lung towards a Th2 immune polarization and this increases the susceptibility of individuals towards extrinsic asthma? Even with these unanswered questions, the HIF1αΔ/Δ mice offer an important step forward in understanding the role of the HIF1α signaling cascade in allergy-induced asthma. Finally, it established epithelial-derived HIF1α as a major regulator of the lung's response to allergenic compounds and creates a new tool to help understand the relationship between inflammation and asthma progression.

REFERENCES

1 Bunn, H. F. and Poyton, R. O. (1996) Oxygen sensing and molecular adaptation to hypoxia. Phys. Rev. **76**, 839-885

2 Epstein, A. C., et al. (2001) C. elegans EGL-9 and mammalian homologs define a family of dioxygenases that regulate HIF by prolyl hydroxylation. Cell. **107**, 43-54.

3 Salnikow, K., et al. (2004) Depletion of intracellular ascorbate by the carcinogenic metals nickel and cobalt results in the induction of hypoxic stress. J Biol Chem. **279,** 40337-44.

4 Vengellur, A., Phillips, J. M., Hogenesch, J. B. and LaPres, J. J. (2005) Gene expression profiling of hypoxia signaling in human hepatocellular carcinoma cells. Physiol. Genomics. **22**, 308-318

5 Lombaert, N., Lison, D., Van Hummelen, P. and Kirsch-Volders, M. (2008) In vitro expression of hard metal dust (WC-Co)--responsive genes in human peripheral blood mononucleated cells. Toxicol Appl Pharmacol. **227**, 299-312

6 Semenza, G. L., Roth, P. H., Fang, H. M. and Wang, G. L. (1994) Transcriptional regulation of genes encoding glycolytic enzymes by hypoxia-inducible factor 1. J. Biol. Chem. **269**, 23757-23763

7 Forsythe, J. A., et al. (1996) Activation of vascular endothelial growth factor gene transcription by hypoxia-inducible factor 1. Mol. Cell. Biol. **16**, 4604-4613

8 Jung, Y., et al. (2003) Hypoxia-inducible factor induction by tumour necrosis factor in normoxic cells requires receptor-interacting protein-dependent nuclear factor kappa B activation. Biochem J. **370**, 1011-1017.

9 Mojsilovic-Petrovic, J., et al. (2007) Hypoxia-inducible factor-1 (HIF-1) is involved in the regulation of hypoxia-stimulated expression of monocyte chemoattractant protein-1 (MCP-1/CCL2) and MCP-5 (Ccl12) in astrocytes. J Neuroinflamm. **4**, 12

10 Rius, J., et al. (2008) NF-kappaB links innate immunity to the hypoxic response through transcriptional regulation of HIF-1alpha. Nature. **453**, 807-811

11 Lison, D., Lauwerys, R., Demedts, M. and Nemery, B. (1996) Experimental research into the pathogenesis of cobalt/hard metal lung disease. Eur Respir J. **9**, 1024-1028

12 Shirakawa, T., et al. (1988) The existence of specific antibodies to cobalt in hard metal asthma. Clin Allergy. **18**, 451-460

13 Gheysens, B., Auwerx, J., Van den Eeckhout, A. and Demedts, M. (1985) Cobalt-induced bronchial asthma in diamond polishers. Chest. **88**, 740-744

14 Shirakawa, T., et al. (1989) Occupational asthma from cobalt sensitivity in workers exposed to hard metal dust. Chest. **95**, 29-37

15 Saini, Y., Harkema, J. R. and LaPres, J. J. (2008) HIF1{alpha} Is Essential for Normal Intrauterine Differentiation of Alveolar Epithelium and Surfactant Production in the Newborn Lung of Mice. J. Biol. Chem. **283**, 33650-33657

16 Ryan, H. E., Lo, J. and Johnson, R. S. (1998) HIF-1 alpha is required for solid tumor formation and embryonic vascularization. EMBO Journal. **17**, 3005-3015

17 Ryan, H. E., et al. (2000) Hypoxia-inducible factor-1alpha is a positive factor in solid tumor growth. Cancer Res. **60**, 4010-4015

18 Perl, A. K., et al. (2002) Early restriction of peripheral and proximal cell lineages during formation of the lung. Proc Natl Acad Sci U S A. **99**, 10482-10487.

19 Lobe, C. G., et al. (1999) Z/AP, a double reporter for cre-mediated recombination. Dev Biol. **208**, 281-292.

20 Johansson, A., et al. (1986) Rabbit alveolar macrophages after long-term inhalation of soluble cobalt. Environ Res. **41**, 488-496

21 Johansson, A., Robertson, B. and Camner, P. (1987) Nodular accumulation of type II cells and inflammatory lesions caused by inhalation of low cobalt concentrations. Environmental research. **43**, 227-243

22 Johansson, A., Camner, P., Jarstrand, C. and Wiernik, A. (1983) Rabbit alveolar macrophages after inhalation of soluble cadmium, cobalt, and copper: a comparison with the effects of soluble nickel. Environ Res. **31**, 340-354

23 Camner, P., et al. (1993) Inhalation of cobalt by sensitised guinea pigs: effects on the lungs. Br J Ind Med. **50**, 753-757

24 Bucher, J. R., et al. (1990) Inhalation toxicity studies of cobalt sulfate in F344/N rats and B6C3F1 mice. Fundam Appl Toxicol. **15**, 357-372

25 Bucher, J. R., et al. (1999) Inhalation toxicity and carcinogenicity studies of cobalt sulfate. Toxicol Sci. **49**, 56-67.

26 Lewis, C. P., Demedts, M. and Nemery, B. (1991) Indices of oxidative stress in hamster lung following exposure to cobalt(II) ions: in vivo and in vitro studies. Am J Respir Cell Mol Biol. **5**, 163-169

27 Chupp, G. L., et al. (2007) A Chitinase-like Protein in the Lung and Circulation of Patients with Severe Asthma. N Engl J Med. **357**, 2016-2027

28 Zhu, Z., et al. (2004) Acidic mammalian chitinase in asthmatic Th2 inflammation and IL-13 pathway activation. Science. **304**, 1678-1682

29 Cramer, T., et al. (2003) HIF-1± Is Essential for Myeloid Cell-Mediated Inflammation. Cell. **112**, 645-657

Chapter 5

The Role of Hypoxia Inducible Factor 1α (HIF1α) in Modulating Cobalt-Induced Lung Inflammation: An Acute Study

ABSTRACT:

Air pollution is a critical factor in the development and exacerbation of pulmonary diseases. Ozone, automobile exhaust, cigarette smoke, and metallic dust are among the potentially harmful pollution components that are linked to disease progression. Transition metals, such as cobalt have been identified at significant levels in air pollution. Cobalt exerts numerous biological effects, including mimicking hypoxia. Similar to hypoxia, cobalt exposure results in the stabilization of hypoxia inducible factors (HIFs). HIFs are a family of proteins that regulate the cellular response to oxygen deficit. HIFs also play an important role in innate immunity and inflammatory processes. Moreover, epithelial-derived HIF signaling has been shown to modulate the lung's inflammatory response to subchronic exposure to cobalt and biased the tissue towards a Th2-mediated response. To further understand the role of HIF1α, the most ubiquitously expressed HIF, in establishing the lung's inflammatory response to cobalt, a series of acute studies was performed. An inducible lung-specific HIF1α deletion model was employed to characterize the inflammatory function of epithelial derived HIF in response to inhaled cobalt. Control mice showed classical sign of metal-induced injury following cobalt exposure, including neutrophilic infiltration and induction of Th1 cytokines. In contrast, HIF1α deficient mice exhibited pronounced eosinophil counts in BALF and lung tissue complemented with Th2 cytokine induction. These results suggests that the loss of epithelial-derived HIF1α result in an asthma-like phenotype following

acute cobalt exposure and that HIF1α is an important mediator in establishing the lung's inflammatory response.

INTRODUCTION

Postnatal lungs require pollution free ambient air for proper function and development. Air pollution is also a critical factor in the occurrence and exacerbation of lung pathological conditions, such as airway hypersensitivity, asthma, chronic obstructive pulmonary disease (COPD) and lung cancer. A plethora of airborne particles are injected into the environment through anthropogenic activities.

The first line of defense against airborne particles is innate immunity. Various lung diseases, such as asthma and COPD, occur due to detrimental effects of these particles on epithelial integrity, resident macrophages activations and recruitment of inflammatory cells. Airborne pollutants, such as smoke, dust particles, ozone, noxious gases, automobile exhausts, and metals can induce lung injury with a strong inflammatory component. Depending upon the degree of exposure and tissue injury, inflammatory reactions facilitate repair and remodeling processes.

Hard metal lung disease (HMLD) and cobalt asthma are occupational respiratory diseases affecting workers involved in the manufacture and maintenance of hard metals (material consisting of tungsten carbide cemented in a matrix of cobalt), diamond polishing, and coal mining. These workers are exposed to cobalt dust and manifest airway constriction, alveolitis, fibrosis and associated giant cell interstitial pneumonitis [1]. The mechanism for the

cobalt-induced pathology remains largely unknown, however, several possibilities have been proposed. One of these possibilities is that ability of cobalt to promote a hypoxic-like response in cells. Given the link between hypoxia and inflammation, cobalt-induced hypoxia mimickry offers a logical link between metal exposure and the observed pathologies of HMLD and cobalt asthma [2, 3].

Hypoxia, a decrease in available oxygen reaching the tissues of the body, can influence the processes such as normal cellular homeostasis, repair, and inflammation. The cellular response to hypoxia is regulated by a family of transcription factors called the hypoxia inducible factors (HIFs) [4]. HIFs are primarily regulated at the level of protein stability by a family of prolyl hydroxylases. These prolyl hydroxylase domain (PHDs) proteins are members of a broader family of non-heme, ferrous ion- and 2-oxoglutarate dependent dioxygenases [5]. Upon exposure to decreases in oxygen availability PHDs become inhibited and HIF1α the most ubiquitously expressed isoform of HIFs, becomes stabilized. Once stable, HIF1α translocates to the nucleus and heterodimerizes with the aryl hydrocarbon receptor nuclear translocator (ARNT, also known as HIF1β) forming the functional transcription factor HIF1. HIF1 regulates the expression of over one hundred genes, including ones involved in energy metabolism, matrix/barrier function, angiogenesis, and inflammation [6-9]. Similar to hypoxia, cobalt has been shown to inhibit PHDs and this inhibition causes very

similar transcriptional outputs to that of hypoxia [2, 10, 11]. Recent study in human peripheral blood mononuclear cells has shown similar transcriptional overlap upon tungsten carbide-cobalt particles treatment, linking hard metal lung disease to hypoxia signaling [12].

Recently, using a lung-specific HIF1α deficient mouse model, a compromised HIF signaling system was shown to alter the tissue's response to subchronic cobalt exposure. The loss of HIF1α from type II and Clara cells was shown to bias the lung's inflammatory response towards a Th2-mediated process. Moreover, these HIF1α-deficient mice displayed an asthma-like phenotype, including pronounced eosinophil infiltration, mucus cell metaplasia of airway epithelium, and increased levels of the chitinase-like proteins YM1 and YM2 following cobalt challenge. These results suggest that airway epithelial-derived HIF1α plays a critical role in modulating the inflammatory response of the lung. However, to understand the progression of cobalt-induced lung injury, further investigation on the role of HIF1α in cobalt-induced acute inflammation is required. In the present study, control and HIF1α deficient mice were exposed to cobalt daily for 1, 2, or 5 days. Bronchoalveolar lavage fluid (BALF) cellularity from HIF1α deficient mice displays a progressive eosinophilic infiltration whereas control mice displayed a transient increase in neutrophils. Histological analysis revealed accelerated tissue injury following acute cobalt challenge in HIF1α deficient mice. Finally, BALF cytokine analysis showed IL-5 elevation specific to cobalt-treated HIF1α

deficient mice. In contrast, control mice showed specific induction of IL-6 and tumor necrosis factor α (TNFα) following cobalt treatment. These results suggests that epithelial-derived HIF1α is essential for regulating early inflammatory events following cobalt challenge and loss of this regulation biases the lung towards a Th2 mediated process and an asthma-like pathology following metal exposure.

MATERIALS AND METHODS:

Description of mice: The mice used in these studies were created by mating HIF1 $\alpha^{flox/flox}$ (a generous gift of Dr. Randall Johnson, Univ. California-San Diego) and SP-C-rtTA$^{-/tg}$/(tetO)$_7$-CMV-Cre$^{tg/tg}$ transgenic mice (a generous gifts of Dr. Jeffrey A. Whitsett, Cincinnati Children's Hospital Medical Center) [13-16]. The generated triple transgenic mice, SP-C-rtTA$^{-/tg}$/(tetO)$_7$-CMV-Cre$^{tg/tg}$/HIF1$\alpha^{flox/flox}$, are capable of respiratory epithelium specific conditional recombination in the floxed HIF1α gene upon exposure to doxycycline (20). All the mice genotypes used in this study have been maintained in a mixed C57/BL6 and FVB/N background. Genotyping of the mice was performed by PCR for the three loci as previously described [17].

Figure 5.1. Experimental Design. HIF1αΔ/Δ mice were generated through postnatal doxycycline treatment paradigm (doxycycline given from PN4 to PN42). Control (n=36) and HIF1αΔ/Δ (n=36) male mice randomly assigned to three different treatment groups (24, 48, and 120 hrs). For each time point, mice were challenged with saline (n=6) or cobalt chloride (60 μg, n=6) via oropharyngeal aspiration. Animals were euthanized 24 hours after their first dose (24 hrs treatment group), second dose (48 hrs treatment group) or fifth dose (120 hrs treatment group).

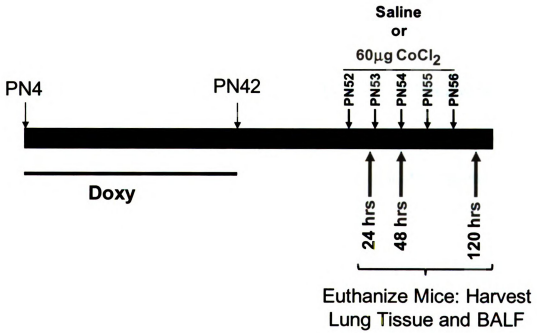
Saline
or
60μg CoCl2
PN4
PN42
PN52
PN53
PN54
PN55
PN56
Doxy
24 hrs
48 hrs
120 hrs
Euthanize Mice: Harvest
Lung Tissue and BALF

Doxycycline treatment and animal husbandry: Postnatal recombination was carried out by exposing lactating dams to doxycycline feed (625 mg doxycycline/Kg; Harlan Teklad, Madison, WI) and drinking water (0.8 mg/ml: Sigma chemicals Co.) until weaning. Triple transgenic mice were then maintained on the same food and water until they were approximately 7 weeks of age. In order to eliminate the effects of doxycycline, the treatment was terminated 7-10 days prior to first exposure to metals. These mice will be referred to as HIF1α deficient or HIF1αΔ/Δ. Genotypic designation of these mice is SP-C-rtTA$^{-/tg}$/ (tetO)$_7$-CMV-Cre$^{tg/tg}$/HIF1α$^{\Delta/\Delta}$. Control animals used in the study were of the same genotype that were maintained on normal food and water *ad libitum*. Mice used in this study were kept at the animal housing facility under the strict hygienic and pathogen free conditions approved by the university laboratory animal resource (ULAR) regulatory unit. All the animal handling and necropsy protocols were approved by the ULAR regulatory unit of Michigan State University.

Cobalt exposure, tissue harvesting and processing: Control and HIF1αΔ/Δ male mice were randomly assigned to one of 6 groups. Mice were treated with saline, or 10 mM cobaltous chloride in 25 μL volume by oropharyngeal aspiration daily for 1, 2 or 5 days. The 10 mM cobalt chloride concentrations correspond to daily exposure of 60 μg of $CoCl_2$. Animals were sacrificed 24 hours following the final exposure. In the case of the one day

treatment group, a single dose of cobalt was administered and mice were sacrificed 24 hours later. For the two day time point, two doses were delivered at 24 hours interval and animals were sacrificed 24 hours after second dose. Finally, for five days time point, five doses were delivered at 24 hours intervals and animals were sacrificed 24 hours after fifth dose. Following exposure, mice were anesthetized with sodium pentobarbital (50 mg/ml), and a midline laparotomy was performed. The trachea was exposed and cannulated. The lung and heart were removed *en bloc* and the lungs were lavaged with two successive one ml volumes of sterile saline. These fractions were combined and total cell counts were performed using a hemocytometer. Differential cell counts were performed in cytospin samples using Diff-Quik reagent (Baxter, FL). The remaining BALF was frozen for cytokine profiling. The right lung lobe was removed and stored in RNA*later* RNA stabilizing reagent (Qiagen, Valencia, CA) for protein and RNA isolation. The left lobe was fixed in 10% neutral buffered formalin for histopathological analysis.

Protein Assay: The total amount of protein in the BALF was quantified using the Bradford assay [18]. Briefly, BALF sample were diluted in distilled water and mixed with dye reagent via manufacturer's instructions (Bio-Rad, Hercules, CA). Absorbance was read at 595 nm using spectrophotometer (GeneQuant 100, GE Heatlthcare Piscataway, NJ). Protein concentrations were determined by comparison to a standard curve created from serially diluted bovine serum albumin standards of known concentrations.

Histopathology and immunohistochemistry: At least four to six mice from each genotype and treatment group were analyzed for histopathological changes. Formalin fixed left lung lobe tissues were paraffin embedded and 5-micron thick sections were mounted on glass slides and stained with hematoxylin and eosin (H&E) or major basic protein (1:500 dilution, Mayo Clinic, AZ), 40kDa antigen of neutrophils (MCA771GA 1:100 dilution, Serotec, Raleigh, NC) as previously described [17].

Determination of cytokine levels by Bead array: Levels of cytokines from acellular BALF samples were measured using BD CBA Mouse Soluble Protein Flex Sets and FACSCalibur flow cytometer according to the manufacturer's instruction (CBA; BD Biosciences, San Diego, CA). Cytokines measured were IL-2, KC, IL-4, IL-5, IL-13, TNFα, IL-6, IL-10, INF-γ and Rantes. Briefly, BALF was mixed with capture beads and incubated for 1 hour at room temperature. Subsequently, PE detection reagent was added and incubation for 1 hours at room temperature. Following extensive washing, samples were analyzed on a BD FACSArray bioanalyzer (BD Biosciences) according to the manufacturer's instruction.

Quantitative analysis: All cell counts and cytokine and gene expression data were analyzed by ANOVA followed by a Bonferroni posttest. All the data from the study was presented as standard error of the mean (SEM). Statistical difference of P value less than 0.05 was considered as significant.

Figure 5.2. BALF proteins and total cell counts from control and HIF1α Δ/Δ mice.

Total protein concentrations **(A)** and cell counts **(B)** were assessed from BALF of saline (**white bars**),and cobalt (**hatched bars**) treated control mice and saline (**checkered bars**) and cobalt (**black bars**) treated HIF1αΔ/Δ mice as described in materials and methods. N>5 mice/group. Data are expressed as mean±SE. * = P ≤0.05.

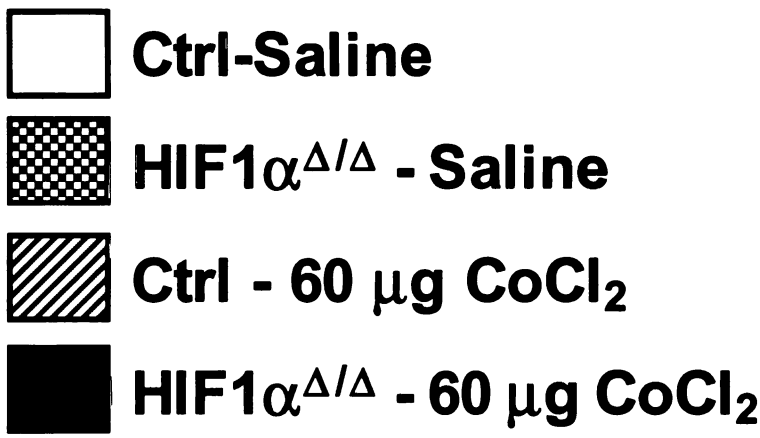

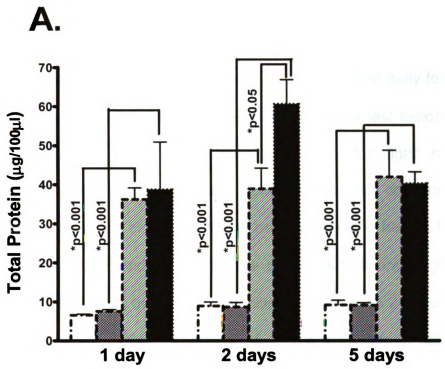
A.
Total Protein (µg/100µl)
70
60
50
40
30
20
10
0
*p<0.001
*p<0.001
*p<0.001
*p<0.001
*p<0.05
*p<0.001
*p<0.001
1 day
2 days
5 days

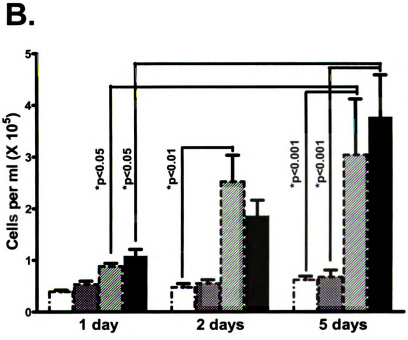
B.
Cells per ml (X 10^5)
5
4
3
2
1
0
*p<0.05
*p<0.05
*p<0.01
*p<0.001
*p<0.001
1 day
2 days
5 days

RESULTS:

BALF protein exudation and cellularity: To characterize the role of HIF1α in cobalt-induced lung injury, control and HIF1αΔ/Δ mice were randomly assigned to saline-or cobalt-treated groups. Individual groups received sterile saline or 60 μg cobalt chloride by oropharyngeal aspiration daily for 1, 2, or 5 days (Fig. 5.1). Mice were euthanized 24 hours after last exposure, BALF was collected and lung tissue was processed for light microscopic examination, IHC, and RNA isolation. Total BALF protein concentration was measured as an index of lung epithelial permeability and hence, lung injury. Cobalt-treated control and HIF1αΔ/Δ mice showed significantly higher protein concentration indicating that lung injury initiates as soon as 24 hours after the initial exposure (Fig. 5.2A). The level of protein exudation in cobalt-treated control mice remained within narrow range of 35-45 μg/100μl at all the three time points. In contrast, cobalt-treated HIF1αΔ/Δ mice showed significantly higher protein exudation (60.71±6.2) at the 48 hours time point as compared to respective control (38.9±5.3) counterparts (Fig. 5.2A), suggesting these mice are more prone to metal-induced lung injury. The total cell count from BALF was also measured to follow the progression of injury. Total cells in BALF showed a significant increase in both control and HIF1αΔ/Δ mice following 5 days of cobalt exposure. There was no difference between control and HIF1αΔ/Δ mice at any time point. These results suggest that acute cobalt-induced changes in total cell infiltration in the lung are not affected by loss of HIF1α.

Figure 5.3. Effect of cobalt treatment on inflammatory cells recovered in bronchoalveolar lavage fluid.

Differential cell counts were performed for macrophages (**A**), lymphocytes (**B**), neutrophils (**C**), and eosinophils **(D)** from BALF of saline (**white bars**), and cobalt (**hatched bars**) treated control mice and saline (**checkered bars**) and cobalt (**black bars**) treated HIF1αΔ/Δ mice. N>5 mice/group. Data are expressed as mean±SE. * = P≤0.05.

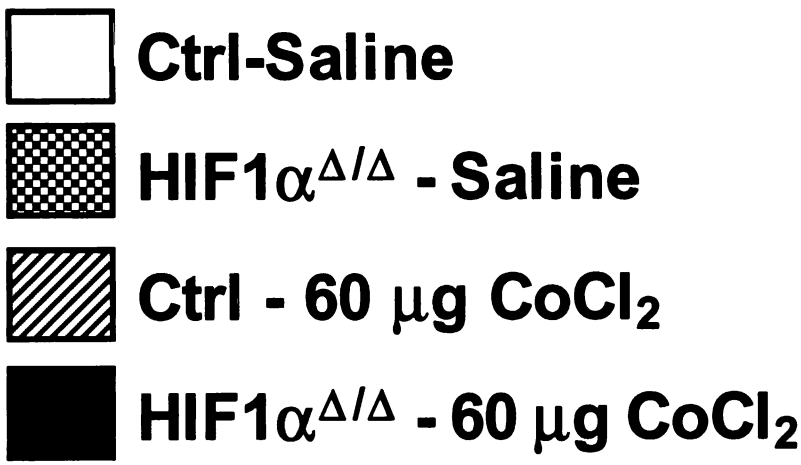

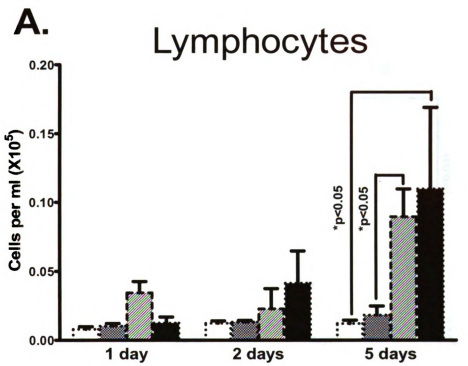
A.
Lymphocytes
Cells per ml (X10^5)
0.20
0.15
0.10
0.05
0.00
1 day
2 days
5 days
*p<0.05
*p<0.05

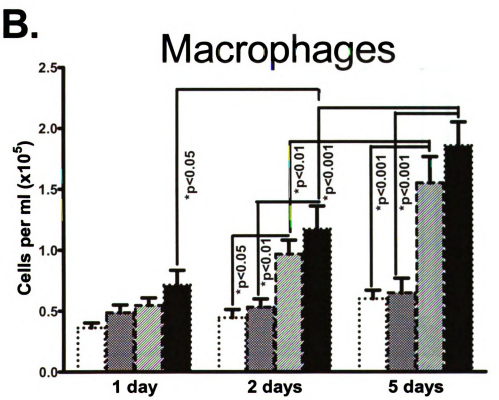
B.
Macrophages
Cells per ml (x10^5)
2.5
2.0
1.5
1.0
0.5
0.0
1 day
2 days
5 days
*p<0.05
*p<0.05
*p<0.01
*p<0.01
*p<0.001
*p<0.001
*p<0.001

Figure 5.3. Continued.

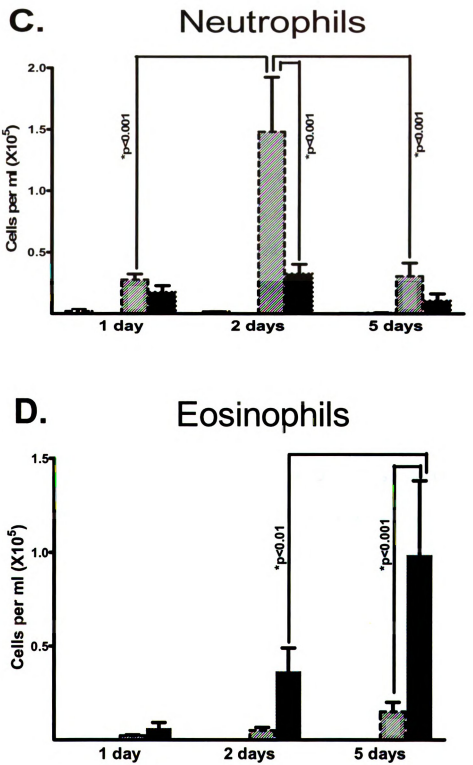

To characterize the types of inflammatory cell infiltration that made up the total cells in BALF, differential cell counts was performed. Similar to total cell counts, total macrophages and lymphocytes showed time dependent increase in numbers, however, no significance difference was noticed between cobalt-treated control and HIF1αΔ/Δ mice at any of the three time points (Fig. 5.3A and 5.3B). In contrast, there was a distinct difference between the two genotypes in the numbers of neutrophils and eosinophils found in the BALF. The control mice displayed a significant increase in neutrophils following cobalt exposure at the 48 hour time point that was not seen in the HIF1α deficient mice. Moreover, this increase was resolved by the 5 day treatment time (Fig. 5.3C). The HIF1αΔ/Δ mice displayed a large and sustained increase in eosinophil infiltration into the lung following cobalt exposure. This increase was observed as early as 2 days post-treatment and reached significance by 5 days of treatment (Fig. 5.3D). These genotype-specific inflammatory cells infiltrations suggest that epithelium-derived HIF1α is an important regulator in the inflammatory responses to metal insults.

Histopathology of Cobalt-induced injury: Histologically, no pulmonary lesions were found in control (Fig 5.4A) or HIF1αΔ/Δ (Fig 5.4E) mice that were

Figure 5.4. Histopathology staining of control and cobalt-treated control mice.

H & E stained lung sections from control (**A-D**) and HIF1αΔ/Δ (**E-H**) mice that were either saline-treated (A and E) or treated with one (**B and E**), two (**C and G**) or 5 consecuitive (**D and H**) doses of cobalt (60μg). bronchiolar airway (BA), terminal bronchioles (tb), alveolar ducts and adjacent alveoli (a). "Images in this dissertation are presented in color."

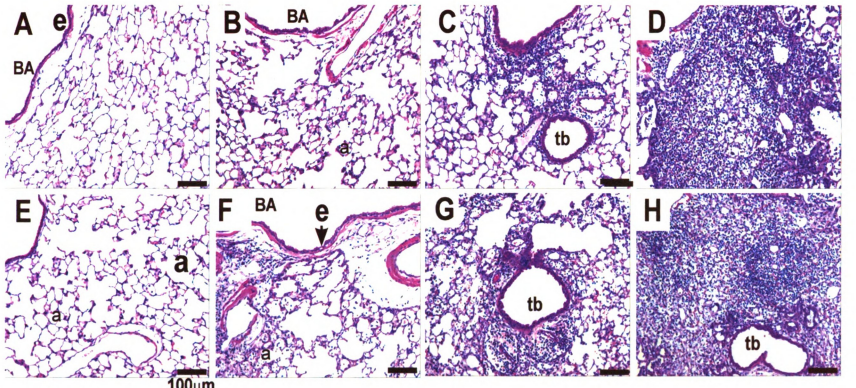
A
e
BA
B
BA
a
C
tb
D
E
a
av
F
BA
e
a
G
tb
H
tb
100μm

instilled with saline alone. Cobalt-treatment induced time-dependent increase in lung damage that appeared slightly more pronounced in the HIF1αΔ/Δ mice (Fig. 5.4B-D and 5.4F-G). To verify the cell infiltration, lung tissues from control and HIF1αΔ/Δ mice were analyzed via immunohistochemistry using an antibody specific to major basic protein, an eosinophilic specific marker. No eosinophils were observed in saline treated mice of either genotype (data not shown). Control mice, following a single dose of cobalt showed a modest increase in MBP positive cells in the interstitium of proximal lung (Fig. 5.5A). This staining was absent in the 2 and 5 days lung section of control mice (Figs. 5.5C and E). In contrast, HIF1α deficient mice showed a pronounced and prolonged eosinophilia following cobalt exposure (Figs. 5.5B, D, and F). The level of neutrophilic infiltration was also assessed using immunohistochemistry. Again, there was little PMN positive staining observed in either control or HIF1αΔ/Δ saline treated mice (data not shown). In control mice, there was substantial PMN positive staining as early as 24 hours after the first cobalt exposure (Fig. 5.6A), This staining remained following 2 days of cobalt exposure, however, it was slightly diminished. Following 5 days of exposure, control mice still displayed some neutrophil positive staining but it restricted to peribronchial regions. HIF1αΔ/Δ mice also showed strong PMN positive staining following a single dose of cobalt (Fig. 5.6B). In contrast to the control mice, this PMN infiltration was absent in the 2 and 5 day treated HIF1α deficient mice. These results are in agreement with the differential cell counts

Figure 5.5. Major Basic Protein (MBP) immunohistochemistry in lungs from control and HIF1αΔ/Δ mice.

Lung sections from control (A, C and E) and HIF1αΔ/Δ mice (B, D and F) following exposure to cobalt (60 μg) for 24 hrs (**A and B**), 48 hrs (**C and D**), or 120 hrs (**E and F**) were immunohistochemically stained for MBP, an eosinophil-specific marker, to identify infiltrating eosinophils (red chromagen) and counterstained with hematoxylin. "Images in this dissertation are presented in color."

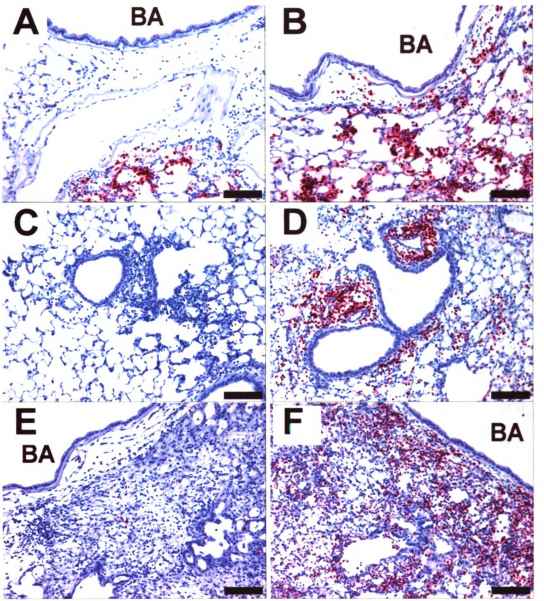
A
BA
B
BA
C
D
E
BA
F
BA
100μm

Figure 5.6. Neutrophil (PMN) immunohistochemistry in lungs from control and HIF1αΔ/Δ mice. Lung sections from control (A, C and E) and HIF1αΔ/Δ mice (B, D and F) following exposure to cobalt (60 μg) for 24 hrs (**A and B**), 48 hrs (**C and D**), or 120 hrs (**E and F**) were immunohistochemically stained for a 40 kDa antigen, a neutrophil-specific marker, to identify infiltrating neutrophils (red chromagen) and counterstained with hematoxylin. "Images in this dissertation are presented in color."

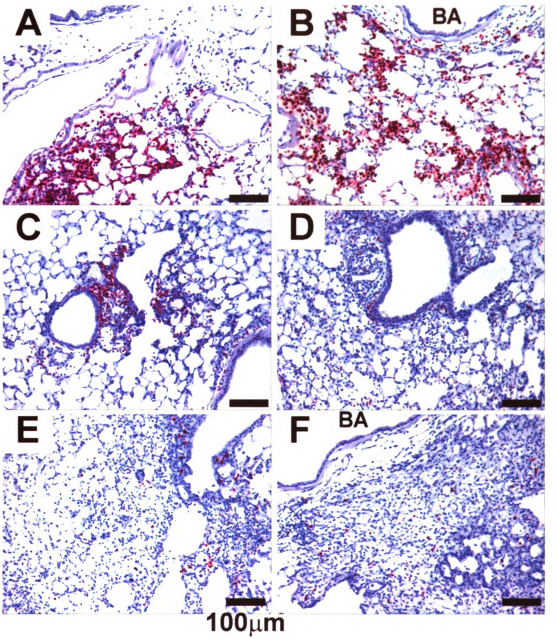
A
B
BA
C
D
E
F
BA
100μm

and suggest that a compromised HIF1α causes a shift in the inflammatory response of the lungs following cobalt exposure. The repeated instillation of cobalt in control (Fig 5.4D) as well as HIF1αΔ/Δ (Fig 5.4H) mice for five consecutive days resulted in marked bronchopneumonia characterized by a mononuclear cell infiltrate (heteromorphic lymphocytes, monocytes, and occasional plasma cells). However, these lesions were infiltrated with numerous eosinophils specifically in HIF1αΔ/Δ mice (Fig. 5.6F) and displayed PMN positive staining specifically in the control mice.

Cytokine profiling: The pathology of the lung and the BALF cellularity patterns suggested a change in the inflammatory response upon loss of HIF1α from Type II and Clara cells. To determine the mechanism underlying these patterns, 10 cytokines (viz. IL-2, KC, IL-4, IL-5, IL-13, TNFα, IL-6, IL-10, INF-γ, Rantes) were profiled in the cell-free BALF. Out of these profiled cytokines four showed significant difference when compared across genotype or within treatment groups (Fig. 5.7). IL-5, a key mediator in eosinophil activation, was significantly elevated in BALF collected from mice following 1 and 2 day cobalt exposure to HIF1αΔ/Δ mice as compared to control mice (Fig. 5.7A). On the other hand, cobalt treated control mice had significantly higher levels of IL-6 and TNF-α at 48 hours time point suggesting their proinflammatory involvement in cobalt induced acute inflammation and further transition to chronic inflammation (Fig 5.7B and 5.7C). .

Figure 5.7. Cytokine levels in BALF from cobalt-treated control and HIF1α Δ/Δ mice.

Control and HIF1αΔ/Δ mice were exposed to saline or 60 μg $CoCl_2$. The levels of cytokines in BALF were assessed using BD CBA Mouse Soluble Protein Flex Sets and FACSCalibur flow cytometer. N>5 mice/group. Outliers were removed by Grubb's test and ANOVA was performed with Boneferroni posttest. Asterisks indicate significant difference between cobalt-treated control mice and cobalt-treated HIF1α deficient mice. * =P < 0.05, ** =P < 0.01, *** =P < 0.001

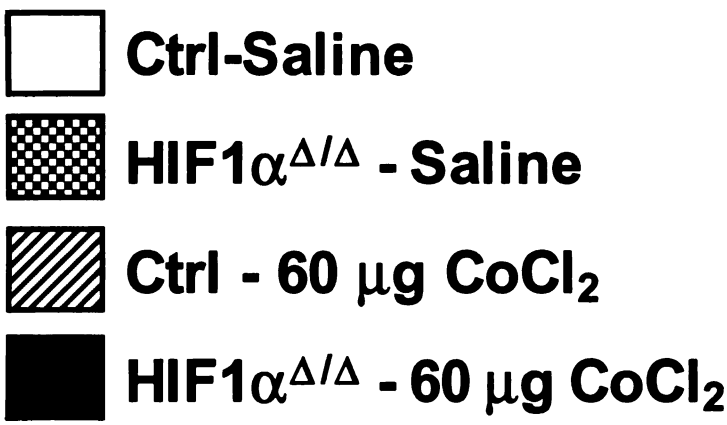

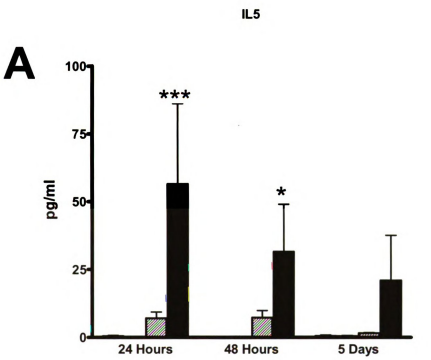
IL5
A
100
75
50
25
0
pg/ml
***
*
24 Hours
48 Hours
5 Days

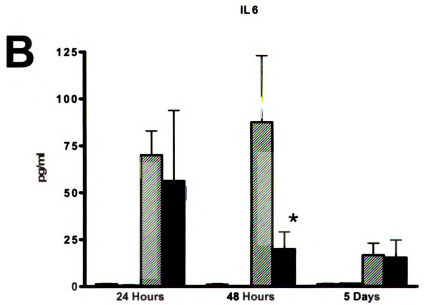
IL6
B
125
100
75
50
25
0
pg/ml
*
24 Hours
48 Hours
5 Days

Figure 5.7. Continued.

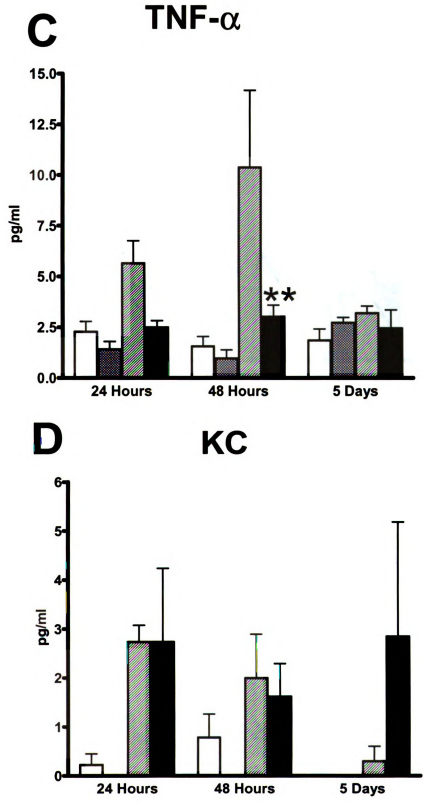

Figure 5.7. Continued.

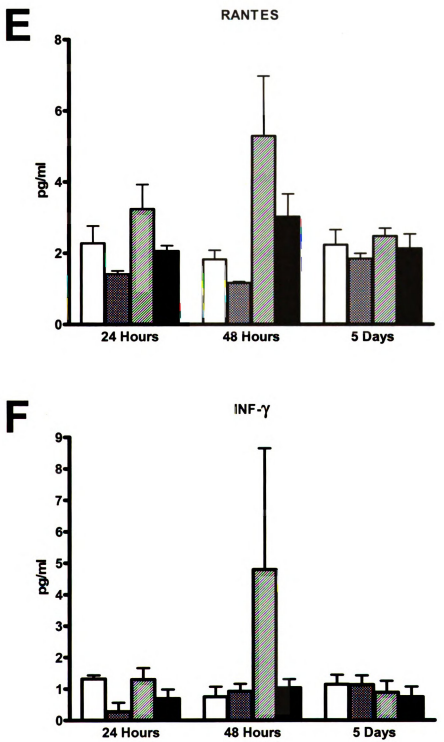

DISCUSSION:

Hard metal lung disease (HMLD) and cobalt asthma are occupational respiratory diseases affecting workers involved in manufacture and maintenance of hard metals (material consisting of tungsten carbide cemented in a matrix of cobalt), diamond polishing, and coal mining. The incidence of HMLD in diamond polishers who were exposed to cobalt-containing dust suggests cobalt as a sole etiological agent in HMLD [1]. These workers manifested airway constriction, alveolitis, fibrosis and associated giant cell interstitial pneumonitis [1]. Despite the countless incidences of cobalt induced toxicities, a complete mechanistic understanding is still lacking.

Several *in vitro* studies have shown that cobalt acts as a stabilizer of HIFs. Hypoxia-like cellular responses have also been observed following cobalt exposure [19, 20]. In addition, a defined role for HIFs in inflammation and tissue injury has been established. HIF1α target genes such as VEGF and MMPs have been shown to be unregulated in inflammatory conditions [21]. Similarly, hypoxia induced activation of genes involved in inflammatory processes suggests links between hypoxia and inflammation [22]. Based on the links between cobalt and hypoxia as well as hypoxia and inflammation, cobalt-induced HIF1α stabilization might be an important player in inflammatory manifestations of metal-induced lung disease.

To characterize the progression of cobalt induced inflammation, we performed short-term cobalt exposure studies in a lung epithelium-specific HIF1α deficient mice model. Subchronic cobalt exposure in the same model has elucidated the role of HIF1α in modulation of lung inflammation. These results suggest that airway epithelial-derived HIF1α plays a critical role in modulating the inflammatory response of the lung, however, the signals necessary to instigate the differences in inflammatory response could not be discerned from the single time point tested. The results presented in this study suggest that loss of epithelial derived HIF1α signaling is necessary for establishing the proper Th1 response to cobalt challenge.

In recent years, Clinical and experimental studies have generated evidences highlighting various pathological changes in the lungs of exposed humans as well as experimental animals. The pathology observed in cobalt-induced inhalation toxicity includes degeneration of the olfactory epithelium, hyperplasia and squamous metaplasia in the epithelium of the respiratory turbinates and larynx, hemorrhage, macrophage infiltration in the alveolar spaces, lung edema [23] and fibrosing alveolitis [24]. In clinical case of cobalt-fume exposure, positive correlation between TNFα and cobalt pneumoconiosis has been reported that suggests TNFα's has a potential role in the pathogenesis of interstitial lung disease [25]. However, the similar elevation of TNFα was not seen in rat alveolar macrophage culture as well as in *in vivo* intranasal exposure studies in rats [26]. Interestingly, levels of TNFα

are specifically higher in control mice after 1 and 2 days of cobalt chloride treatments that was not observed in their HIF1$\alpha^{\Delta/\Delta}$ counterparts (Fig. 5.7). These results suggest that HIF1α is capable of regulating the cytokines correlated with manifestations of lung disease.

Early in the course of injury, similar to the classical responses to cobalt exposure, neutrophils are seen in cobalt-treated HIF1α deficient as well as cobalt-treated control mice 24 hours after first exposure (Figs. 5.6A and 5.6B). This finding suggests that the initial acute inflammatory events in response to the cobalt exposure are similar between control and HIF1α deficient mice. Cobalt-treated HIF1α deficient mice exhibited less neutrophilic infiltration upon repeated exposure (Figs. 5.6C and 5.6D). The possibility of early removal of neutrophils from cobalt-treated HIF1α deficient mice explains the significant reduction of BALF neutrophils 24 hours after second exposure (Fig. 5.3C). Neutrophilic influx in to the lung and alveolar space is the characteristic feature of the acute lung injury (ALI) where they act as a key player in the pathogenesis of the injury. Mice deficient in CXCR2, a neutrophil membrane receptor for CXC chemokines KC/CXCL1 and MIP-2/CXCL2/3, showed marked reduction in neutrophilic reduction in response to ventilator-induced lung injury [27]. Neutrophil recruitment is mediated by KC in conjunction with several other factors such as CXC chemokines (Fig 5.7D). Although important for the immune response, neutrophil-predominant inflammatory responses are involved in diffused alveolar tissue damage through the release of proteases

(MMPs, protease 3, neutrophil elastase, cathepsin G) and reactive oxygen metabolites (hydrogen peroxide, hypohalous acids, hydroxyl radicals) [28]. Neutrophils generate chemotactic signals that regulate the recruitment of monocytes and dictate macrophage differentiation towards pro- or anti-inflammatory state [29]. Similar to activated alveolar macrophages, alveolar epithelial cells also produced cytokines and chemokines. It has been shown, similar to macrophages, LPS exposed type II cells also act as an important source of cytokines such as MCP-1 and IL-8 [30]. Given the growing evidence of the inflammatory roles of HIFs, It is possible that the loss of HIF1α from the type II cells result in their altered response to the signals received from inflammatory cells such as neutrophils and activated macrophages.

All three time points tested in the present study have shown significant interstitial eosinophil infiltration in cobalt-treated HIF1α deficient mice as compared to cobalt-treated control mice (Figs. 5.5B, 5.5D and 5.5F). However, the BALF eosinophilia cobalt-treated HIF1α deficient mice reached significance only after 5 exposures (Fig. 5.3D). Interestingly, interstitial eosinophilic infiltration was present in cobalt-treated control mice that were exposed to one dose but the degree of infiltration was remarkably less as compared to cobalt-treated HIF1α deficient mice (Fig. 5.5A). Eosinophils are differentiated from myeloid precursor cells under the influence of interleukin IL-3, granulocyte-macrophage colony-stimulating factor (GM-CSF), and IL-5. These cells are selectively recruited into the airways through Th2 cytokines.

HIF1α deficient mice specific recruitment of eosinophils suggests the epithelial origin of the inflammatory switch. To date, the role of HIFs in eosinophilic inflammation is unclear. Moreover, the role of epithelial-derived mediators as modulator of inflammatory responses has not been examined directly. Taken together, the findings from the current study supplements the data collected in the recent study and suggests critical role of epithelial-derived HIF1α in the observed inflammatory switch. However, further investigation on the chemical signals released by the HIF1α deficient type II and Clara cells will further help us to understand the mechanism underlying the recruitment of eosinophils and other downstream events.

The BALF cytokine analyses for IL-2, KC, IL-4, IL-5, IL-13, TNFα, IL-6, IL-10, INF-γ and Rantes have shown the genotype specific changes after cobalt exposure. Control mice showed significant induction of TNFα, a Th1 cytokine secreted by activated macrophages, as well as INF-γ (Figs. 5.7C and 5.7F). In accordance to the finding that TNF-α and INF-γ stimulates Rantes production, the levels of Rantes in cobalt-treated control mice followed TNFα like pattern (Fig. 5.7E) [31]. IL-6 cytokine that promotes Th2 cells differentiation is elevated in the cobalt-treated control mice (Fig. 5.7B). In contrast to control mice, cobalt-treated HIF1α deficient mice had significantly increased IL-5 that mediates Th2 cytokine-producing capacity of eosinophils (Fig. 5.7A). These changes in the cytokine levels further suggest that the loss of HIF1α in lung

epithelial cells of the HIF1α deficient mice results in an alteration in the cell's ability to respond to the incoming signals from the cobalt damaged cells.

Taken together, the data collected from the current study consolidates our understanding of the course and nature of cobalt induced inflammation. In conclusion, the data supports a model in which epithelial-derived HIF1α activity regulates the lung's response to metal challenge by controlling the expression of cytokines necessary to recruit the proper inflammatory response. Loss of this regulatory mechanism leads to the tissue being biased towards a Th2-mediated inflammation. The mechanism that leads to this alteration in the inflammatory response remains unknown and is the focus of new investigations.

Acknowledgements: The authors appreciate the gift of the conditional HIF1α mice from Dr. Randall Johnson (University of California San Diego) and the SP-C-rtTA/(tetO)7-CMV-Cre transgenic from Dr. Jeffrey A. Whitsett (Cincinnati Children's Hospital Medical Center).

Grants: This work was supported by funds from the National Institutes of Health (NIH) R01-ES12186 and P42 ES04911-17

REFERENCES

1 Lison, D., Lauwerys, R., Demedts, M. and Nemery, B. (1996) Experimental research into the pathogenesis of cobalt/hard metal lung disease. Eur Respir J. **9**, 1024-1028

2 Vengellur, A., Phillips, J. M., Hogenesch, J. B. and LaPres, J. J. (2005) Gene expression profiling of hypoxia signaling in human hepatocellular carcinoma cells. Physiol. Genomics. **22**, 308-318

3 Jain, M. and Sznajder, J. I. (2005) Effects of hypoxia on the alveolar epithelium. Proceedings of the American Thoracic Society. **2**, 202-205

4 Bunn, H. F. and Poyton, R. O. (1996) Oxygen sensing and molecular adaptation to hypoxia. Phys. Rev. **76**, 839-885

5 Epstein, A. C., et al. (2001) C. elegans EGL-9 and mammalian homologs define a family of dioxygenases that regulate HIF by prolyl hydroxylation. Cell. **107**, 43-54.

6 Semenza, G. L., Roth, P. H., Fang, H. M. and Wang, G. L. (1994) Transcriptional regulation of genes encoding glycolytic enzymes by hypoxia-inducible factor 1. J. Biol. Chem. **269**, 23757-23763

7 Forsythe, J. A., et al. (1996) Activation of vascular endothelial growth factor gene transcription by hypoxia-inducible factor 1. Mol. Cell. Biol. **16**, 4604-4613

8 Jung, Y., et al. (2003) Hypoxia-inducible factor induction by tumour necrosis factor in normoxic cells requires receptor-interacting protein-dependent nuclear factor kappa B activation. Biochem J. **370**, 1011-1017.

9 Mojsilovic-Petrovic, J., et al. (2007) Hypoxia-inducible factor-1 (HIF-1) is involved in the regulation of hypoxia-stimulated expression of monocyte chemoattractant protein-1 (MCP-1/CCL2) and MCP-5 (Ccl12) in astrocytes. J Neuroinflamm. **4**, 12

10 Salnikow, K., et al. (2004) Depletion of intracellular ascorbate by the carcinogenic metals nickel and cobalt results in the induction of hypoxic stress. J Biol Chem

11 Vengellur, A., Phillips, J. M., Hogenesch, J. B. and LaPres, J. J. (2005) Gene expression profiling of hypoxia signaling in human hepatocellular carcinoma cells. Physiological genomics. **22**, 308-318

12 Lombaert, N., Lison, D., Van Hummelen, P. and Kirsch-Volders, M. (2008) In vitro expression of hard metal dust (WC-Co)--responsive genes in human peripheral blood mononucleated cells. Toxicol Appl Pharmacol. **227**, 299-312

13 Ryan, H. E., Lo, J. and Johnson, R. S. (1998) HIF-1 alpha is required for solid tumor formation and embryonic vascularization. EMBO Journal. **17**, 3005-3015

14 Ryan, H. E., et al. (2000) Hypoxia-inducible factor-1alpha is a positive factor in solid tumor growth. Cancer Res. **60**, 4010-4015

15 Perl, A. K., et al. (2002) Early restriction of peripheral and proximal cell lineages during formation of the lung. Proc Natl Acad Sci U S A. **99**, 10482-10487.

16 Lobe, C. G., et al. (1999) Z/AP, a double reporter for cre-mediated recombination. Dev Biol. **208**, 281-292.

17 Saini, Y., Harkema, J. R. and LaPres, J. J. (2008) HIF1{alpha} Is Essential for Normal Intrauterine Differentiation of Alveolar Epithelium and Surfactant Production in the Newborn Lung of Mice. J. Biol. Chem. **283**, 33650-33657

18 Bradford, M. M. (1976) A rapid and sensitive method for the quantitation of microgram quantities of protein utilizing the principle of protein-dye binding. Analytical biochemistry. **72**, 248-254

19 Vengellur, A. and LaPres, J. J. (2004) The role of hypoxia inducible factor 1alpha in cobalt chloride induced cell death in mouse embryonic fibroblasts. Toxicol Sci. **82**, 638-646

20 Karovic, O., et al. (2007) Toxic effects of cobalt in primary cultures of mouse astrocytes. Similarities with hypoxia and role of HIF-1alpha. Biochemical pharmacology. **73**, 694-708

21 Elson, D. A., et al. (2000) Coordinate up-regulation of hypoxia inducible factor (HIF)-1alpha and HIF-1 target genes during multi-stage epidermal carcinogenesis and wound healing. Cancer research. **60**, 6189-6195

22 Walmsley, S. R., Cadwallader, K. A. and Chilvers, E. R. (2005) The role of HIF-1alpha in myeloid cell inflammation. Trends in immunology. **26**, 434-439

23 Bucher, J. (1991) NTP technical report on the toxicity studies of Cobalt Sulfate Heptahydrate in F344/N Rats and B6C3F1 Mice (Inhalation Studies) (CAS No. 10026-24-1). Toxicity report series. **5**, 1-38

24 Lison, D. (1996) Human toxicity of cobalt-containing dust and experimental studies on the mechanism of interstitial lung disease (hard metal disease). Critical Reviews in Toxicology. **26**, 585-616

25 Rolfe, M. W., Paine, R., Davenport, R. B. and Strieter, R. M. (1992) Hard metal pneumoconiosis and the association of tumor necrosis factor-alpha. The American review of respiratory disease. **146**, 1600-1602

26 Huaux, F., Lasfargues, G., Lauwerys, R. and Lison, D. (1995) Lung toxicity of hard metal particles and production of interleukin-1, tumor necrosis factor-alpha, fibronectin, and cystatin-c by lung phagocytes. Toxicology and applied pharmacology. **132**, 53-62

27 Belperio, J. A., et al. (2002) Critical role for CXCR2 and CXCR2 ligands during the pathogenesis of ventilator-induced lung injury. The Journal of clinical investigation. **110**, 1703-1716

28 Nathan, C. (2006) Neutrophils and immunity: challenges and opportunities. Nat Rev Immunol. **6**, 173-182

29 Bennouna, S., Bliss, S. K., Curiel, T. J. and Denkers, E. Y. (2003) Cross-talk in the innate immune system: neutrophils instruct recruitment

and activation of dendritic cells during microbial infection. J Immunol. **171**, 6052-6058

30 Thorley, A. J., et al. (2007) Differential regulation of cytokine release and leukocyte migration by lipopolysaccharide-stimulated primary human lung alveolar type II epithelial cells and macrophages. J Immunol. **178**, 463-473

31 Teran, L. M., et al. (1999) Th1- and Th2-type cytokines regulate the expression and production of eotaxin and RANTES by human lung fibroblasts. American journal of respiratory cell and molecular biology. **20**, 777-786

CHAPTER 6

CONCLUSIONS

The increasing use of disposable electronics and growing industrialization of nation's economies have drastically raised the risk of exposure to toxic metals. Mining operations, the burning of fossil fuels and globalization have pushed metals into close proximities of neighborhoods and the general population. The most "at risk" group, however, remains workers in various industrial settings, including large-scale smelting operations and alloy manufacturers.

One of these metals, cobalt, is used as a coloring agent for ceramics and the production of alloys. Cobalt is used widely in several industries involved in the production of coloring agent for ceramics, hard metal alloys, sintered carbides, drilling and grinding tools. The people who manufacture these metals and use the end products are at particular risk for exposure. It has been estimated that more than 1 million workers in the United States are exposed to cobalt due to the nature of their work. Moreover, cobalt is present in 426 of the 1,636 National Priorities List (NPL) hazardous waste sites identified by the Environmental Protection Agency (EPA). Finally, the correlation of high environmental cobalt levels to a cluster of lung diseases makes the understanding of cobalt-induced signaling and toxicity important to workers and the public at large.

Workers exposed to cobalt dust from welding, grinding, or diamond polishing operations have displayed multiple lung pathologies. Cobalt (or hard metal) asthma is one of three occupational respiratory diseases associated with exposure to the transition metal. The other two are hypersensitivity pneumonitis and interstitial lung disease with fibrosis. These diseases are caused by the inhalation of hard metal particles and are characterized by airway constriction, alveolitis, fibrosis and associated giant cell interstitial pneumonitis. Therefore, mechanistic understanding of the toxicities of cobalt and related metals such as nickel is important to devise treatment strategies. The characterizations of these toxicities demands comprehensive understanding of the effects of toxicants on the cell signaling and the downstream changes in the gene expression. It is well established that cobalt is a hypoxia mimic due to its ability to induce hypoxia-like gene expression responses. To enhance our understanding on the involvement of hypoxia-mimicking properties of cobalt in its toxic responses, we developed and used a mouse model system. This mouse model is an inducible lung-specific HIF1α deficient system based on Cre-LoxP recombination strategy.

HIFs are the most widely studied family of hypoxia responsive transcription factors and they directly influence the expression of more than 150 genes. Among three known HIFα's, oxygen labile isoforms, HIF1α is most widely expressed isoform that has been studied extensively. Previous studies in our lab, using an immortalized mouse embryonic fibroblast (MEFs)

cell line lacking HIF1α, established the correlation between HIF1α removal and protection against $CoCl_2$ toxicity. Validation of our *in vitro* understanding of cobalt-induced HIFs signaling necessitates the *in vivo* studies of cobalt toxicity in HIFs null animals.

Our attempt to generate the inducible lung-specific HIF1α deficient mice model led us to an interesting investigation on the roles of HIF1α in lung development. Lung specific embryonic deletion of HIF1α earlier than 3 days prior to parturition led to HIF1α deficient neonates exhibiting cyanosis and respiratory failure soon after birth. The expression of surfactant proteins was significantly lower in HIF1α deficient neonates as compared to littermate control pups. Examination of the lungs from HIF1α deficient neonates via light and transmission electron microscopy confirmed defects in both alveolar epithelial differentiation and septal development that resulted in the observed respiratory distress. It was interesting to note the decreased expression of HIF2α, another prominent form of HIFα in lungs, in HIF1α deficient neonates that led us to further investigate the roles of both HIF isoforms, individually and collectively.

The attempts to generate viable HIF2α mice revealed that the removal of this isoform from the lung does not affect the viability of neonates. However, the removal of both the isoforms from the lungs revealed an interesting rescue phenotype. Microarray analysis of the lungs from HIF1αΔ/Δ, HIF2 αΔ/Δ and HIF1/2 αΔ/Δ mice identified genes and cellular pathways. The majority of these pathways, such as surfactant metabolism and vesicular trafficking, were

specifically affected in the HIF1αΔ/Δ neonates. However, the expression profile of some genes, such as IL1R-II and CDS-1, were significantly reduced in the HIF1α deficient mice and regained their expression levels after the simultaneous removal of HIF1α and HIF2 α. Further studies to understand the intricate network of developmentally important factors relative to HIFs necessitates conducting future experiments using rescue or complementation strategies.

Given the extremely complex developmental network involved in the lung development, it would be rational to approach to investigate the observed findings through multidimensional approach specific to each of the affected cellular pathway. The upregulation of genes involved in cell cycle processes suggests the shift from cell differentiation pathways to more cell proliferation pathways. This is in agreement with the pathology in which the HIF1α deficient mice exhibited signs of stalled differentiation of immature cuboidal alveolar epithelial cells. It is assumed that these immature cuboidal alveolar epithelial cells are the precursors of differentiated alveolar type II cells that, in turn, differentiate into type I cells. The most striking function of type II cells in the developing lungs is surfactant biosynthesis which necessitates the cell-specific upregulation of genes involved in fatty acid synthesis, cholesterol biosynthesis, surfactant proteins biosynthesis and the specialized vesicular transport system. Surfactant biosynthesis and their vesicular transportation to the cell membrane are characteristic of alveolar type II cells. It is clearly a cell-specific temporal mode of expression of genes involved in these processes.

In addition to the cell cycle processes, the genes involved in the vesicular transport and surfactant pathways are downregulated in HIF1α deficient mice. There could be two possible explanation of these observed expression pattern. First, the stalled differentiation might be the consequence of the deletion of HIF1α that leads to the perturbation of the downstream developmentally critical cascades. This effect could be explained by the observed gene expression pattern of transcriptional factors such as β-catenin that were significantly downregulated upon HIF1α deletion. It is quite possible that some other developmentally critical (transcriptional) factors fall directly or indirectly downstream of HIF1α in the cellular differentiation cascades. Thus, the altered expression of the surfactants might be the consequence of stalled differentiation process. The second possible explanation of the respiratory distress phenotype observed in HIF1α deficient mice might be more intimately related to the surfactant metabolism. The genes involved in the surfactant metabolism are still not well studied for their hypoxia responsiveness. Further studies on the selected genes will certainly provide avenues for the development of treatment strategies to combat neonatal distress syndrome.

The lethality following *in utero* deletion of HIF1α, led us to adopt postnatal strategy of doxycycline treatment and functional deletion of HIF1α. The post-natal deletion of HIF1α from Type II and Clara cells had no observable pathology. In order to elucidate the role of epithelial derived-HIF1α signaling in cobalt-induced lung injury these mice were exposed to cobalt chloride via oropharyngeal aspiration. Compared to control mice, mice

that were HIF1α deficient in their lungs exhibited airway infiltration of eosinophils and airway epithelial changes, including mucus cell metaplasia and increased levels of the chitinase-like proteins YM1 and YM2. Mice deficient in HIF1α also showed a drastic change in cytokine profiles in their lavage fluid when compared to their control.

These results suggested that loss of HIF1α from alveolar Type II epithelial and Clara cells of the lungs leads to cellular and molecular processes that are associated with asthma following cobalt exposure. Moreover, the results suggest that airway epithelial-derived HIF1α plays a critical role in modulating the inflammatory response of the lung. These results also suggested a difference in the inflammatory response between the control and HIF1αΔ/Δ mice; however, it is based on collected data at a single time point following two weeks of cobalt exposure. Thus, to consolidate our understanding on the course and nature of cobalt induced inflammation further time course studies were planned.

In the time course studies, control and HIF1α deficient mice were exposed to cobalt daily for 1, 2, or 5 days. Bronchoalveolar lavage fluid (BALF) cellularity from HIF1α deficient mice displayed a progressive eosinophilic infiltration whereas control mice displayed a transient increase in neutrophils. Histological analysis revealed accelerated tissue injury following acute cobalt challenge in HIF1α deficient mice. Finally, BALF cytokine analysis showed IL-5 elevation specific to cobalt-treated HIF1α deficient mice. In contrast, control mice showed specific induction of IL-6 and tumor necrosis

factor α (TNFα) following cobalt treatment. These results suggests that epithelial-derived HIF1α is essential for regulating early inflammatory events following cobalt challenge and loss of this regulation biases the lung towards a Th2-mediated process and an asthma-like pathology following metal exposure.

Taken together, the striking differences observed following cobalt exposure in the two mice suggests that they will be a powerful tool to help understand the relationship between allergy-induced asthma, hypoxia, and inflammation. More importantly, direct comparison of the responses of the control and HIF1αΔ/Δ mice in other asthma models (e.g. ovalbumin challenge) and to other inflammatory inhalants will correlate this relationship to specific cytokines. The research also raises several important questions: Does the loss of HIF1α alter an organism's susceptibility to asthma using other allergens? What role does HIF1α derived from other cell types (e.g. infiltrating inflammatory cells and Type I cells) play in modulating this inflammatory response. Does post-natal deletion of HIF1α alter HIF2α and if so, what impact does this have on the inflammatory response. Most importantly, does a decrease in HIF1α functionality lead to an increased susceptibility to asthma in humans? More specifically, is it possible that loss or decrease in HIF1α function biases the lung towards a Th2 immune polarization and this increases the susceptibility of individuals towards extrinsic asthma?

Table A.1. List of differentially expressed genes

GeneID	Gene Name	HIF1 ratio	HIF2 ratio	HIF1/2 ratio
20505	Solute carrier family 34 (sodium phosphate), member 1	37.07	-1.00	-1.19
546994	Similar to Ankyrin repeat domain-containing protein 26	28.05	-1.00	-1.02
15395	Homeo box A10	21.62	2.30	1.24
56183	Neuromedin U	16.00	1.27	5.62
212070	Clarin 3	13.84	-1.19	-1.09
15378	Hepatic nuclear factor 4, alpha	13.40	1.08	-1.82
84112	Succinate receptor 1	11.10	1.40	1.06
228491	Zinc finger protein 770	10.52	-1.16	1.10
14866	Glutathione S-transferase, mu 5	8.64	1.48	5.84
17748	Metallothionein 1	8.42	4.34	3.44
241516	Fibrous sheath-interacting protein 2	6.46	-1.13	1.47
13653	Early growth response 1	6.25	-1.30	2.35
215627	Zinc finger and BTB domain containing 8	5.54	1.33	2.20
654824	Ankyrin repeat domain 37	5.31	1.04	2.14
75656	RIKEN cdna 1700020A23 gene	5.13	1.22	2.54
230766	Cdna sequence BC030183	4.80	1.10	1.37
66261	Transmembrane 4 L six family member 20	4.23	-1.11	1.27
234814	Methenyltetrahydrofolate synthetase domain containing	3.88	-1.52	1.24
75512	Glutathione peroxidase 6	3.85	1.12	-1.04
20423	Sonic hedgehog	3.74	1.35	1.08
71389	Chromodomain helicase DNA binding protein 6	3.72	-1.19	1.24
72650	RIKEN cdna 2810006K23 gene	3.69	1.00	1.13
13099	Cytochrome P450, family 2, subfamily c, polypeptide 40	3.68	1.51	-1.79
239250	SLIT and NTRK-like family, member 6	3.65	-1.03	1.39
68214	Glutathione S-transferase omega 2	3.64	-1.20	-1.29
58909	RIKEN cdna D430015B01 gene	3.62	1.08	1.34
67951	Tubulin, beta 6	3.37	1.03	1.46
19434	Retina and anterior neural fold homeobox	3.36	-1.00	-1.31
232339	Ankyrin repeat domain 26	3.32	-1.48	1.23
20464	Single-minded homolog 1 (Drosophila)	3.31	-1.06	-1.02
53601	Protocadherin 12	3.27	1.28	1.01
12000	Arginine vasopressin receptor 2	3.25	-1.35	-1.00
13193	Doublecortin	3.24	-1.00	1.05

GeneID	Gene name	HIF1 ratio	HIF2 ratio	HIF1/2 ratio
207742	Ring finger protein 43	3.14	-1.09	1.03
380773	RIKEN cdna 1810035L17 gene	3.13	-1.52	1.07
54710	Heparan sulfate (glucosamine) 3-O-sulfotransferase 3B1	3.10	-1.13	1.42
66950	Transmembrane protein 206	3.09	-1.17	1.07
72748	Haloacid dehalogenase-like hydrolase domain containing 3	3.09	1.04	1.10
320803	RIKEN cdna C130022M03 gene	3.06	-1.08	1.31
72080	RIKEN cdna 2010317E24 gene	3.04	1.41	1.14
22295	Cadherin 23 (otocadherin)	3.04	1.74	-2.20
56742	Proline/serine-rich coiled-coil 1	3.02	1.57	2.66
68750	Ras responsive element binding protein 1	3.01	1.14	1.22
74043	Peroxisome biogenesis factor 26	3.00	1.20	1.55
18762	Protein kinase C, zeta	2.98	-1.02	1.47
216829	Cdna sequence BC025076	2.96	-1.21	1.34
208117	Anterior pharynx defective 1b homolog (C. Elegans)	2.92	1.47	1.63
15438	Homeo box D9	2.88	-1.20	-1.17
215693	Zinc finger, matrin type 1	2.88	-1.22	1.31
13841	Eph receptor A7	2.87	1.32	1.19
78320	RIKEN cdna 2210415I11 gene	2.87	1.06	1.83
71263	Maestro	2.87	1.59	1.49
56742	Proline/serine-rich coiled-coil 1	2.84	1.60	2.03
18828	Phospholipid scramblase 2	2.84	1.13	1.28
232441	RAS-like, estrogen-regulated, growth-inhibitor	2.84	-1.43	-1.14
16182	Interleukin 18 receptor 1	2.82	-1.25	1.65
18510	Paired box gene 8	2.81	-1.05	1.11
329650	Mediator of RNA polymerase II transcription	2.80	1.03	1.29
18828	Phospholipid scramblase 2	2.80	1.14	1.40
328425	Deleted in lymphocytic leukemia, 2	2.78	1.16	1.47
55946	Adaptor-related protein complex 3, mu 1 subunit	2.77	-1.07	1.33
98685	RIKEN cdna 1190005F20 gene	2.77	1.02	1.12
103573	Exportin 1, CRM1 homolog (yeast)	2.76	1.06	1.41
215494	Expressed sequence C85492	2.75	-1.23	1.51
100177	Zinc finger, MYM-type 6	2.74	-1.00	-2.39
218763	Leucine rich repeat containing 3B	2.73	-1.00	1.09
69260	Inhibitor of growth family, member 2	2.73	-1.07	1.38

GeneID	Gene name	HIF1 ratio	HIF2 ratio	HIF1/2 ratio
171282	Acyl-coa thioesterase 4	2.70	1.14	1.07
433940	Cdna sequence BC057022	2.70	-1.52	1.20
66315	SUMO1/sentrin specific peptidase 7	2.70	1.03	1.20
12160	Bone morphogenetic protein 5	2.69	1.52	1.11
244071	ATP/GTP binding protein-like 1	2.68	-1.00	-1.08
320573	RIKEN cdna C130024J02 gene	2.68	-1.09	1.08
77418	RIKEN cdna C030015A19 gene	2.67	-1.62	1.31
83486	RNA binding motif protein 5	2.67	-1.26	1.06
66274	RIKEN cdna 1810012P15 gene	2.65	1.15	1.48
330256	Hypothetical protein 9530028C05	2.64	1.46	1.36
56742	Proline/serine-rich coiled-coil 1	2.64	1.63	1.77
228880	Protein kinase C binding protein 1 .	2.64	1.00	1.21
22163	Tumor necrosis factor receptor superfamily, member 4	2.64	1.12	1.48
216877	DEAH (Asp-Glu-Ala-His) box polypeptide 33	2.64	1.10	-1.22
72852	RIKEN cdna 2900024O10 gene	2.64	1.07	1.55
78004	Proline rich 15	2.63	1.37	1.22
67892	RIKEN cdna 1810063B05 gene	2.63	-1.40	1.19
381853	Gastric inhibitory polypeptide receptor	2.63	1.59	1.67
21683	Tectorin alpha	2.63	-1.06	-1.30
218100	Zinc finger protein 322a	2.63	-1.16	1.20
791282	Predicted gene, ENSMUSG00000057802	2.61	1.03	-1.01
434179	Predicted gene, EG434179	2.60	1.29	1.34
13423	Deoxyribonuclease II alpha	2.58	-1.23	1.42
71599	SUMO/sentrin specific peptidase 8	2.58	-1.10	1.43
67790	RAB39B, member RAS oncogene family	2.58	-1.18	1.33
77609	RIKEN cdna C330001K17 gene	2.56	1.58	1.16
217716	Mutl homolog 3 (E coli)	2.56	1.16	1.03
68281	RIKEN cdna 4930430F08 gene	2.56	-1.12	1.24
56335	Methyltransferase-like 3	2.55	-1.04	1.07
16428	IL2-inducible T-cell kinase	2.55	1.02	1.28
68134	UPF3 regulator of nonsense transcripts homolog B (yeast)	2.55	1.34	1.31
193736	Zinc finger and BTB domain containing 12	2.54	-1.11	1.22
109136	Methylmalonic aciduria (cobalamin deficiency) type A	2.53	-1.04	1.28
14211	Structural maintenance of chromosomes 2	2.52	1.09	1.47
67283	Solute carrier family 25 , member 19	2.52	-1.13	1.26

GeneID	Gene name	HIF1 ratio	HIF2 ratio	HIF1/2 ratio
218850	DNA segment, Chr 14, Abbott 1 expressed	2.51	-1.10	-1.09
66816	THAP domain containing, apoptosis associated protein 2	2.50	-1.34	1.21
72397	RNA binding motif protein 12B	2.50	1.48	-1.09
72789	Ventricular zone expressed PH domain homolog 1 (zebrafish)	2.49	-1.05	1.63
22635	Zonadhesin	2.49	1.09	1.10
75387	Sirtuin 4 (S. Cerevisiae)	2.49	-1.03	1.42
66522	Pyroglutamyl-peptidase I	2.47	-1.29	-1.04
50780	Regulator of G-protein signaling 3	2.47	-1.04	1.04
30838	F-box and WD-40 domain protein 4	2.46	-1.15	-1.04
235442	RAB8B, member RAS oncogene family	2.46	-1.04	1.20
77857	RIKEN cdna 9430065F17 gene	2.45	-1.04	1.22
73094	SH3-domain GRB2-like (endophilin) interacting protein 1	2.45	-1.12	-1.08
108078	Oxidized low density lipoprotein (lectin-like) receptor 1	2.43	-1.53	-1.16
625963	Hypothetical protein LOC625963	2.42	1.20	1.36
268853	Gene model 671, (NCBI)	2.41	-1.12	1.01
13176	Deleted in colorectal carcinoma	2.40	-1.17	-1.12
58240	HCLS1 binding protein 3	2.39	1.02	1.21
58894	RIKEN cdna 4732460K03 gene	2.38	-1.58	1.68
75787	RIKEN cdna 4930471M09 gene	2.38	-1.18	1.05
21808	Transforming growth factor, beta 2	2.38	1.05	1.09
93871	Bromodomain and WD repeat domain containing 1	2.38	1.28	1.24
107338	Golgi-specific brefeldin A-resistance factor 1	2.38	1.05	1.27
74455	NOL1/NOP2/Sun domain family 6	2.37	1.11	1.14
228880	Protein kinase C binding protein 1	2.37	1.09	1.15
57432	Zinc finger CCCH type containing 8	2.37	-1.01	1.23
434234	RIKEN cdna 2610020H08 gene	2.36	-1.00	1.30
67382	Bromodomain containing 3	2.35	-1.35	1.07
225283	Cdna sequence BC021395	2.35	-1.26	1.36
17997	Neural precursor cell expressed, developmentally down-regulated gene 1	2.34	-1.12	1.16
21848	Tripartite motif-containing 24	2.33	-1.25	-1.10
94281	Sideroflexin 4	2.33	-1.08	1.49
72739	Zinc finger with KRAB and SCAN domains 3	2.32	1.09	1.20
77940	RIKEN cdna A930004D18 gene	2.31	-1.12	-1.12
78004	Proline rich 15	2.31	-1.02	1.07

GeneID	Gene name	HIF1 ratio	HIF2 ratio	HIF1/2 ratio
72103	RIKEN cdna 2010301N04 gene	2.31	-1.25	-1.03
11994	Protocadherin 15	2.30	-1.21	1.07
77519	RIKEN cdna 5730601F06 gene	2.29	-1.08	1.23
73242	RIKEN cdna 2610110G12 gene	2.28	1.10	1.27
66821	BCS1-like (yeast)	2.28	-1.00	1.26
69008	Calcium binding protein 39-like	2.27	1.00	1.29
70551	Transmembrane and tetratricopeptide repeat containing 4	2.27	1.04	1.38
434179	Predicted gene, EG434179	2.27	1.27	1.44
240641	Kinesin family member 20B	2.26	1.05	1.12
213649	Rho guanine nucleotide exchange factor (GEF) 19	2.26	1.37	1.28
109731	Monoamine oxidase B	2.24	1.18	1.27
26404	Mitogen-activated protein kinase kinase kinase 12	2.24	1.04	1.24
74087	Solute carrier family 7, member 13	2.24	1.02	-1.21
26414	Mitogen-activated protein kinase 10	2.24	-1.10	-1.00
18205	Neurotrophin 3	2.23	-1.21	1.20
268822	Aarf domain containing kinase 5	2.23	-1.00	1.44
231832	Transmembrane protein 184a	2.23	1.25	1.27
338320	Melanoma inhibitory activity 2	2.23	-1.09	-1.14
76742	Sorting nexin family member 27	2.23	-1.14	1.09
387334	Defensin beta 50	2.22	-1.11	1.07
19331	RAB19, member RAS oncogene family	2.22	-1.01	1.25
230073	DEAD (Asp-Glu-Ala-Asp) box polypeptide 58	2.21	1.17	1.22
67856	Enoyl Coenzyme A hydratase domain containing 3	2.20	1.26	1.25
320376	BCL6 co-repressor-like 1	2.20	-1.26	1.05
113854	Vomeronasal 1 receptor, B4	2.19	-1.03	1.15
52335	Ataxin 1-like	2.19	-1.08	1.08
268480	Rap guanine nucleotide exchange factor (GEF)-like 1	2.19	-1.03	1.40
12858	Cytochrome c oxidase, subunit Va	2.19	1.04	1.16
22117	Thiosulfate sulfurtransferase, mitochondrial	2.19	1.28	1.46
280645	Beta-1,3-glucuronyltransferase 2 (glucuronosyltransferase S)	2.19	-1.06	1.31
114654	Lymphocyte antigen 6 complex, locus G6D	2.18	-1.08	1.27
240638	Solute carrier family 16 , member 12	2.18	1.20	1.42
245886	Ankyrin repeat domain 27 (VPS9 domain)	2.18	-1.17	1.03

GeneID	Gene name	HIF1 ratio	HIF2 ratio	HIF1/2 ratio
77634	Small nuclear RNA activating complex, polypeptide 3	2.18	-1.01	-1.18
78887	Sfi1 homolog, spindle assembly associated (yeast)	2.18	1.00	1.09
21778	Testis expressed gene 9	2.17	1.47	1.10
215008	Vezatin, adherens junctions transmembrane protein	2.17	1.08	1.25
75763	RIKEN cdna 4833418A01 gene	2.17	-1.01	1.08
101187	Poly (ADP-ribose) polymerase family, member 11	2.16	-1.33	1.22
30054	Ring finger protein 17	2.16	-1.00	1.18
12009	5-azacytidine induced gene 1	2.16	1.02	1.07
269023	Zinc finger protein 608	2.15	1.04	1.23
22718	Zinc finger protein 60	2.15	-1.58	1.13
26450	Retinoblastoma binding protein 9	2.15	1.31	1.52
57276	V-set and immunoglobulin domain containing 2	2.15	1.24	1.26
18044	Nuclear transcription factor-Y alpha	2.14	-1.54	-1.15
381293	Kinesin family member 14	2.14	1.23	1.07
320488	RIKEN cdna D130039L10 gene	2.14	-1.12	-1.07
20689	Sal-like 3 (Drosophila)	2.14	-1.00	-1.14
67118	Bifunctional apoptosis regulator	2.14	1.04	1.30
225283	Cdna sequence BC021395	2.14	-1.01	1.18
67459	Nuclear VCP-like	2.13	-1.13	1.15
13639	Ephrin A4	2.13	1.11	1.16
224055	Receptor transporter protein 2	2.13	-1.20	-1.09
28019	Inhibitor of growth family, member 4	2.13	1.12	1.05
19650	Retinoblastoma-like 1 (p107)	2.13	1.16	1.28
27369	Deoxyguanosine kinase	2.13	-1.02	1.10
74760	RAB3A interacting protein (rabin3)-like 1	2.13	1.11	1.44
78745	RIKEN cdna 9530097N15 gene	2.12	1.12	-1.03
20585	Helicase-like transcription factor	2.12	1.08	1.34
53861	Zinc finger, RAN-binding domain containing 2	2.12	-1.06	1.45
100177	Zinc finger, MYM-type 6	2.12	1.03	1.28
66660	SAFB-like, transcription modulator	2.12	1.03	1.29
231807	Cdna sequence BC037034	2.11	-1.20	1.01
72739	Zinc finger with KRAB and SCAN domains 3	2.11	1.05	1.13
212919	Potassium channel tetramerisation domain containing 7	2.11	-1.02	-1.06

GeneID	Gene name	HIF1 ratio	HIF2 ratio	HIF1/2 ratio
110809	Splicing factor, arginine/serine-rich 1 (ASF/SF2)	2.10	-1.03	1.04
237465	Coiled-coil domain containing 38	2.10	-1.31	1.02
57869	Aarf domain containing kinase 2	2.10	-1.03	1.15
77593	Ubiquitin specific petidase 45	2.10	-1.11	1.12
320575	RIKEN cdna C230057H02 gene	2.10	-1.05	-1.00
211329	Nuclear receptor coactivator 7	2.09	-1.32	-1.67
230848	Zinc finger and BTB domain containing 40	2.09	-1.11	1.02
320720	FAST kinase domains 1	2.09	1.05	1.10
19364	RAD51-like 3 (S. Cerevisiae)	2.09	1.16	1.12
240028	Leucyl/cystinyl aminopeptidase	2.09	-1.57	1.08
11512	Adenylate cyclase 6	2.09	1.17	1.04
57277	Secreted Ly6/Plaur domain containing 1	2.09	1.13	1.17
72615	Ankyrin repeat and sterile alpha motif domain containing 3	2.09	1.01	-1.02
54678	Zinc finger protein 108	2.09	-1.03	1.17
17763	Mature T-cell proliferation 1	2.08	1.03	1.35
67288	SFRS12-interacting protein 1	2.08	-1.08	1.13
17268	Meis homeobox 1	2.08	-1.02	1.12
66921	PRP38 pre-mrna processing factor 38 (yeast) domain containing B	2.08	1.12	1.29
12349	Carbonic anhydrase 2	2.08	1.24	1.12
77015	Metallophosphoesterase domain containing 2	2.08	1.17	1.23
30051	SAM pointed domain containing ets transcription factor	2.08	-1.54	1.84
242297	RIKEN cdna 1700012H17 gene	2.07	1.29	1.36
494448	Chromobox homolog 6	2.07	-1.00	-1.03
52592	Breast cancer metastasis-suppressor 1-like	2.07	-1.02	1.20
209176	Indoleamine-pyrrole 2,3 dioxygenase-like 1	2.07	-1.05	1.13
237911	BRCA1 interacting protein C-terminal helicase 1	2.07	-1.18	1.04
16924	Ligand of numb-protein X 1	2.06	1.23	1.68
258472	Olfactory receptor 899	2.06	1.57	1.12
108015	Cholinergic receptor, nicotinic, beta polypeptide 4	2.06	1.18	-1.05
331535	Serine (or cysteine) peptidase inhibitor, clade A, member 7	2.05	-1.13	2.53
675815	Similar to quaking type II	2.05	-1.52	1.06
30840	F-box and leucine-rich repeat protein 6	2.05	1.10	1.11
69847	WNK lysine deficient protein kinase 4	2.05	1.12	1.19
230098	RIKEN cdna E130306D19 gene	2.05	1.25	1.22

GeneID	Gene name	HIF1 ratio	HIF2 ratio	HIF1/2 ratio
73683	Autophagy related 16 like 2 (S. Cerevisiae)	2.05	-1.06	-1.03
108912	Cell division cycle associated 2	2.05	1.14	1.11
16634	Killer cell lectin-like receptor, subfamily A, member 3	2.04	-1.00	-1.06
76432	RIKEN cdna 2310001H17 gene	2.04	1.05	-1.07
434903	Expressed sequence CN716893	2.04	-1.05	1.04
103733	Tubulin, gamma 1	2.04	1.00	1.23
98463	Expressed sequence AI851716	2.04	1.17	1.12
353165	Taste receptor, type 2, member 136	2.04	-1.29	-1.09
71774	Shroom family member 1	2.04	-1.01	-1.04
237073	RNA binding motif protein 41	2.04	-1.08	-2.02
78808	Syntaxin binding protein 5 (tomosyn)	2.04	-1.14	-1.10
22619	Sialic acid acetylesterase	2.04	1.17	1.15
494448	Chromobox homolog 6	2.04	-1.08	1.10
68490	Zinc finger protein 579	2.03	1.02	1.33
23955	NIMA (never in mitosis gene a)-related expressed kinase 4	2.03	-1.07	1.14
12638	Cystic fibrosis transmembrane conductance regulator homolog	2.03	-2.26	1.11
229487	PET112-like (yeast)	2.03	1.48	1.41
19653	RNA binding motif protein 4	2.03	-1.06	-1.03
215641	Melanoma antigen family B, 18	2.03	-1.00	1.27
240595	Potassium channel, subfamily V, member 2	2.02	-1.00	-1.22
56229	Thrombospondin, type I, domain 1	2.02	1.02	-1.29
14149	Ferredoxin reductase	2.02	1.07	1.56
68607	Serine hydrolase-like	2.02	1.44	1.36
56711	Pleiomorphic adenoma gene 1	2.01	-1.16	-1.17
76511	RIKEN cdna 2010004M13 gene	2.01	-1.00	1.33
23894	General transcription factor II H, polypeptide 2	2.01	1.07	1.05
68837	Forkhead box K2	2.01	1.01	-1.09
237211	Fanconi anemia, complementation group B	2.01	-1.24	1.03
93728	Poly A binding protein, cytoplasmic 5	2.01	1.16	1.48
54141	Sperm associated antigen 5	2.01	1.61	1.03
67454	RIKEN cdna 1200009F10 gene	2.00	1.02	1.33
225283	Cdna sequence BC021395	2.00	-1.01	1.23
21843	Tia1 cytotoxic granule-associated RNA binding protein-like 1	2.00	-1.12	1.21
69754	F-box protein 7	1.99	1.00	-1.01
101563	Expressed sequence AI426330	1.99	1.01	1.23

GeneID	Gene name	HIF1 ratio	HIF2 ratio	HIF1/2 ratio
68053	RIKEN cdna 3110003A22 gene	1.99	1.07	1.41
207474	Potassium channel tetramerisation domain containing 12b	1.99	1.06	1.22
78248	Armadillo repeat containing, X-linked 1	1.99	-1.04	-1.02
234686	Formin homology 2 domain containing 1	1.99	-1.15	-1.02
114889	Visual system homeobox 1 homolog (zebrafish)	1.99	-1.06	-1.32
67493	Methyltransferase 10 domain containing	1.98	-1.30	1.20
208982	3-hydroxymethyl-3-methylglutaryl-Coenzyme A lyase-like 1	1.98	-1.16	1.50
71807	Threonyl-trna synthetase 2, mitochondrial (putative)	1.98	-1.12	1.13
14302	Fyn-related kinase	1.98	-1.26	-1.02
64176	Synaptic vesicle glycoprotein 2 b	1.97	1.03	1.13
13494	Developmentally regulated GTP binding protein 1	1.97	-1.36	-1.04
72852	RIKEN cdna 2900024O10 gene	1.97	1.14	1.16
246293	Kelch-like 8 (Drosophila)	1.97	-1.10	-1.00
74042	RIKEN cdna 4921501E09 gene	1.97	-1.02	-1.07
22222	Ubiquitin protein ligase E3 component n-recognin 1	1.97	-1.05	1.08
68364	RIKEN cdna 0610030E20 gene	1.96	1.03	1.13
20454	ST3 beta-galactoside alpha-2,3-sialyltransferase 5	1.96	-1.02	1.10
74498	Golgi reassembly stacking protein 1	1.96	1.12	1.09
213409	LEM domain containing 1	1.96	-1.10	1.20
319806	RIKEN cdna D630022N01 gene	1.96	-1.01	1.13
233424	Transmembrane channel-like gene family 3	1.96	-1.30	-1.55
21390	Thromboxane A2 receptor	1.96	-1.04	-1.08
320230	RIKEN cdna C130023O10 gene	1.95	-1.00	1.19
668173	Peroxisome biogenesis factor 10	1.95	1.49	1.13
13829	Erythrocyte protein band 4.9	1.95	-1.17	-1.34
104248	Calcineurin binding protein 1	1.95	-1.10	-1.11
225608	SH3 domain and tetratricopeptide repeats 2	1.95	1.04	-1.05
103161	Apolipoprotein F	1.94	1.08	-6.60
16353	Imprinted gene in the Prader-Willi syndrome region	1.94	-1.47	-1.12
57249	Gamma-aminobutyric acid (GABA-A) receptor, subunit theta	1.94	-1.00	-1.01
17684	Cbp/p300-interacting transactivator, 2	1.94	-1.03	1.62
68082	Dual specificity phosphatase 19	1.94	1.09	1.34
246104	Rhomboid, veinlet-like 3 (Drosophila)	1.94	-1.23	1.06

GeneID	Gene name	HIF1 ratio	HIF2 ratio	HIF1/2 ratio
245638	TBC1 domain family, member 8B	1.94	1.22	1.18
68366	Transmembrane protein 129	1.93	1.01	-1.15
192663	ATP-binding cassette, sub-family G (WHITE), member 4	1.93	-1.31	1.01
218734	RIKEN cdna 3830406C13 gene	1.93	1.01	1.12
231642	Alkb, alkylation repair homolog 2 (E. Coli)	1.92	-1.03	1.08
54721	Tyrosine kinase 2	1.92	1.23	-1.04
113859	Vomeronasal 1 receptor, C2	1.92	1.07	-1.06
17690	Musashi homolog 1 (Drosophila)	1.92	-1.20	-1.20
27059	SH3 domain protein D19	1.92	-1.15	1.00
109019	Oligonucleotide/oligosaccharide-binding fold containing 2A	1.92	-1.11	1.37
140500	Centaurin, beta 5	1.92	1.09	-1.01
232237	FYVE, rhogef and PH domain containing 5	1.92	1.07	1.03
18120	Mitochondrial ribosomal protein L49	1.92	1.27	1.04
77781	EPM2A (laforin) interacting protein 1	1.91	1.08	-1.07
277463	G protein-coupled receptor 107	1.91	1.12	-1.02
21684	Tectorin beta	1.91	-1.26	-1.26
75425	RIKEN cdna 2610036D13 gene	1.91	1.28	1.08
17222	Anaphase promoting complex subunit 1	1.91	-1.00	1.09
231214	Coiled-coil and C2 domain containing 2A	1.91	1.14	1.28
229776	CDC14 cell division cycle 14 homolog A (S. Cerevisiae)	1.91	-1.25	-1.00
20420	Src homology 2 domain-containing transforming protein D	1.90	1.38	1.05
52563	CDC23 (cell division cycle 23, yeast, homolog)	1.90	1.02	-1.11
17714	Grpe-like 2, mitochondrial	1.90	1.36	1.85
213006	Major facilitator superfamily domain containing 4	1.90	-1.20	-1.01
71389	Chromodomain helicase DNA binding protein 6	1.90	-1.07	1.02
73373	Phosphatase, orphan 2	1.90	-1.00	-1.05
71718	TEL2, telomere maintenance 2, homolog (S. Cerevisiae)	1.90	-1.10	-1.01
106794	DEAH (Asp-Glu-Ala-Asp/His) box polypeptide 57	1.89	-1.21	1.06
72915	RIKEN cdna 2900017F05 gene	1.89	-1.07	1.08
623046	Fibrous sheath CABYR binding protein	1.89	-1.00	-1.08
328801	Zinc finger protein 414	1.89	-1.11	1.12
233545	RIKEN cdna 2210018M11 gene	1.89	-1.27	1.18

GeneID	Gene name	HIF1 ratio	HIF2 ratio	HIF1/2 ratio
224111	UBX domain containing 7	1.88	-1.04	1.14
70359	GTP binding protein 3	1.88	1.14	1.08
102323	DCN1, defective in cullin neddylation 1, domain containing 2	1.88	-1.09	1.07
233335	Desmuslin	1.88	-1.46	1.19
20540	Solute carrier family 7, member 7	1.88	-1.07	1.37
101700	Tripartite motif-containing 68	1.88	-1.03	1.07
19213	Pancreas specific transcription factor, 1a	1.87	-1.06	-1.08
56032	Tumor suppressor candidate 4	1.87	1.10	1.15
19769	Ras-like without CAAX 1	1.87	-1.06	1.04
235606	Acylpeptide hydrolase	1.86	1.03	1.34
50915	Growth factor receptor bound protein 14	1.86	1.14	1.41
83563	Ubiquitin specific peptidase 26	1.86	-1.04	-1.00
67569	Mannosyl (alpha-1,3-)-glycoprotein beta-1,4-NAG transferase	1.86	-1.24	-1.06
57890	Interleukin 17 receptor E	1.86	-1.29	-1.20
100929	Trna-yw synthesizing protein 1 homolog (S. Cerevisiae)	1.86	1.01	-1.04
105351	Expressed sequence AW209491	1.86	-1.09	-1.02
23966	Odd Oz/ten-m homolog 4 (Drosophila)	1.86	1.10	1.01
225912	Cytochrome b, ascorbate dependent 3	1.86	-1.04	1.24
16351	IAP promoted placental gene	1.85	1.10	1.15
71609	TNFRSF1A-associated via death domain	1.85	-1.16	-1.03
102323	DCN1, defective in cullin neddylation 1, domain containing 2 (S. Cerevisiae)	1.85	1.04	1.07
83946	Pleckstrin homology domain interacting protein	1.85	1.24	1.37
73238	RIKEN cdna 3110049I03 gene	1.85	-1.05	1.07
217026	HEAT repeat containing 6	1.85	-1.10	1.29
105000	Dynein, axonemal, light chain 1	1.85	-1.13	1.29
106064	Expressed sequence AW549877	1.85	1.09	1.36
215789	Phosphatase and actin regulator 2	1.85	1.21	1.33
208760	Aquaporin 12	1.85	-1.23	1.14
18582	Phosphodiesterase 6D, cgmp-specific, rod, delta	1.84	1.10	1.05
67725	Nudix (nucleoside diphosphate linked moiety X)-type motif 13	1.84	1.15	1.19
74356	RIKEN cdna 4931428F04 gene	1.84	-1.07	1.16
241989	Poly(A) binding protein, cytoplasmic 4-like	1.84	1.10	1.07
213988	Trinucleotide repeat containing 6b	1.84	-1.05	-1.08
27059	SH3 domain protein D19	1.84	1.09	-1.07

GeneID	Gene name	HIF1 ratio	HIF2 ratio	HIF1/2 ratio
246317	Neuropilin (NRP) and tolloid (TLL)-like 1	1.83	-1.08	-1.20
80890	Tripartite motif-containing 2	1.83	1.12	1.18
101214	Transformer 2 alpha homolog (Drosophila)	1.83	-1.18	1.25
76265	Trna splicing endonuclease 54 homolog (SEN54, S. Cerevisiae)	1.83	-1.11	1.03
107375	Solute carrier family 25, member 45	1.83	1.04	-1.05
226153	Progressive external ophthalmoplegia 1 (human)	1.82	1.08	1.03
240186	Zinc finger protein 438	1.82	1.04	1.52
12412	Chromobox homolog 1 (Drosophila HP1 beta)	1.82	1.08	-1.13
69401	PLAC8-like 1	1.82	-1.02	-1.17
624633	Similar to Spetex-2E protein	1.82	1.13	-1.01
13829	Erythrocyte protein band 4.9	1.81	-1.01	-1.10
67544	RIKEN cdna 4932442K08 gene	1.81	-1.29	1.14
72656	Integrator complex subunit 8	1.81	1.08	-1.06
13866	V-erb-b2 erythroblastic leukemia viral oncogene homolog 2	1.81	1.01	1.10
328801	Zinc finger protein 414	1.81	-1.08	1.21
20452	ST8 alpha-N-acetyl-neuraminide alpha-2,8-sialyltransferase 4	1.80	1.19	1.17
26895	COP9 (homolog, subunit 7b (Arabidopsis thaliana)	1.80	-1.11	1.17
235283	GRAM domain containing 1B	1.80	1.21	-1.18
16551	Kinesin family member 11	1.80	-1.07	-1.18
52463	Tet oncogene 1	1.80	1.08	-1.06
14625	Glycerol kinase-like 1	1.80	1.03	1.05
12041	Branched chain ketoacid dehydrogenase kinase	1.80	1.19	-1.09
215951	Lactation elevated 1	1.80	1.19	1.24
52231	Ankyrin repeat and zinc finger domain containing 1	1.80	1.01	1.12
109674	Adenosine monophosphate deaminase 2 (isoform L)	1.79	-1.21	1.07
212442	Lactamase, beta 2	1.79	1.41	1.14
108689	Oligonucleotide/oligosaccharide-binding fold containing 1	1.79	1.08	1.07
52231	Ankyrin repeat and zinc finger domain containing 1	1.79	1.37	-1.08
215819	NHS-like 1	1.79	1.13	1.21
192976	Cdna sequence BC046404	1.79	1.14	-1.23
66336	Centromere protein P	1.79	-1.01	1.02

GeneID	Gene name	HIF1 ratio	HIF2 ratio	HIF1/2 ratio
228812	Phosphatidylinositol glycan anchor biosynthesis, class U	1.79	1.07	1.15
69369	RIKEN cdna 1700017D01 gene	1.78	-1.69	1.12
238023	Hexosaminidase (glycosyl hydrolase family 20, catalytic domain) containing	1.78	1.17	1.05
69807	Tripartite motif-containing 32	1.78	1.11	1.24
69089	Oxidase assembly 1-like	1.78	1.08	1.23
194744	Solute carrier family 25, member 43	1.78	-1.03	-1.13
229759	Olfactomedin 3	1.78	1.11	-1.00
208098	Pannexin 3	1.78	-1.02	-1.35
56771	Mediator complex subunit 20	1.78	1.05	-1.04
72472	Solute carrier family 16 (monocarboxylic acid transporters), member 10	1.78	-1.12	1.02
26378	2-4-dienoyl-Coenzyme A reductase 2, peroxisomal	1.78	1.24	1.07
100473	Expressed sequence BB031773	1.78	1.03	1.53
226539	Aspartyl-trna synthetase 2 (mitochondrial)	1.78	1.04	1.27
66977	NUF2, NDC80 kinetochore complex component, homolog (S. Cerevisiae)	1.77	-1.14	1.08
13175	Doublecortin-like kinase 1	1.77	1.30	1.00
116848	Bromodomain adjacent to zinc finger domain, 2A	1.77	-1.07	-1.05
51886	Far upstream element (FUSE) binding protein 1	1.77	-1.18	1.02
24071	Synaptojanin 2 binding protein	1.77	1.01	1.30
224630	BCL2/adenovirus E1B interacting protein 1, NIP1	1.76	1.35	1.06
56771	Mediator complex subunit 20	1.76	1.21	1.03
56695	Paroxysmal nonkinesiogenic dyskinesia	1.76	1.24	1.29
59035	Coactivator-associated arginine methyltransferase 1	1.76	-1.08	1.11
171254	Vomeronasal 1 receptor, I3	1.76	1.06	1.26
80890	Tripartite motif-containing 2	1.76	1.11	1.00
227624	RIKEN cdna B230208H17 gene	1.76	1.01	1.05
242406	RGP1 retrograde golgi transport homolog (S. Cerevisiae)	1.76	-1.04	1.03
67155	SWI/SNF related, matrix associated, subfamily a, member 2	1.76	-1.38	1.08
54201	Zinc finger protein 316	1.76	1.21	1.21
207213	TD and POZ domain containing 1	1.75	-1.08	-1.10
74610	ATP-binding cassette, sub-family B (MDR/TAP), member 8	1.75	1.40	1.03
17222	Anaphase promoting complex subunit 1	1.75	1.07	1.22

GeneID	Gene name	HIF1 ratio	HIF2 ratio	HIF1/2 ratio
494448	Chromobox homolog 6	1.74	-1.01	1.09
76547	Transmembrane protein 101	1.74	1.16	1.02
22169	Cytidine monophosphate (UMP-CMP) kinase 2, mitochondrial	1.74	1.22	1.09
380669	Lin-28 homolog B (C. Elegans)	1.74	-1.18	-1.18
68364	RIKEN cdna 0610030E20 gene	1.74	-1.05	1.11
21685	Thyrotroph embryonic factor	1.73	1.46	1.27
74653	RIKEN cdna 4930444A02 gene	1.73	1.00	1.27
234371	Transmembrane protein 161A	1.73	-1.07	1.11
210035	Transmembrane protein 194	1.73	1.15	1.21
258872	Olfactory receptor 908	1.73	-1.01	-1.00
67230	Zinc finger protein 329	1.73	1.06	-1.19
226422	RAB7, member RAS oncogene family-like 1	1.73	-1.14	1.09
52710	G protein-coupled receptor 172B	1.72	-1.06	1.18
217232	Cell division cycle 27 homolog (S. Cerevisiae)	1.72	-1.06	-1.06
73747	RIKEN cdna 1110034G24 gene	1.72	1.02	1.10
78323	RIKEN cdna 2310046O06 gene	1.72	-1.03	1.04
245638	TBC1 domain family, member 8B	1.72	-1.07	1.12
76089	Rap guanine nucleotide exchange factor (GEF) 2	1.72	1.00	-1.11
258752	Olfactory receptor 583	1.72	-3.03	1.18
331195	RIKEN cdna A430089I19 gene	1.71	1.18	-1.00
76429	RIKEN cdna 2310007H09 gene	1.71	-1.02	1.14
14105	FUS interacting protein (serine-arginine rich) 1	1.71	-1.26	1.10
76788	RIKEN cdna 2410127E18 gene	1.71	1.05	-1.02
215615	Arginyl aminopeptidase (aminopeptidase B)	1.71	1.03	1.33
108899	RIKEN cdna 2700081O15 gene	1.71	-1.06	-1.07
70325	Phosphatidylinositol glycan anchor biosynthesis, class W	1.71	1.14	-1.09
78913	Zinc finger protein 294	1.71	-1.05	1.11
66449	Mitochondria-associated protein involved in GM-CSF signal transduction	1.71	-1.01	1.27
208198	BTB (POZ) domain containing 2	1.70	1.01	1.09
17433	Myelin-associated oligodendrocytic basic protein	1.70	1.02	-1.12
19155	Aminopeptidase puromycin sensitive	1.70	1.06	1.20
56187	Rab geranylgeranyl transferase, a subunit	1.70	1.10	1.11
13185	Down syndrome critical region gene 3	1.70	-1.01	1.08
320727	Importin 8	1.70	-1.05	1.02

GeneID	Gene name	HIF1 ratio	HIF2 ratio	HIF1/2 ratio
65102	Ngg1 interacting factor 3-like 1 (S. Pombe)	1.70	-1.18	1.03
171235	Vomeronasal 1 receptor, F4	1.70	-1.16	-1.07
102098	Rho/rac guanine nucleotide exchange factor (GEF) 18	1.70	-1.00	1.05
68936	RIKEN cdna 1190017O12 gene	1.69	-1.08	1.08
17532	Muscle and microspikes RAS	1.69	-1.21	1.25
237636	NPC1-like 1	1.69	-1.01	1.01
14050	Eyes absent 3 homolog (Drosophila)	1.69	1.04	1.05
83679	Phosphodiesterase 4D interacting protein (myomegalin)	1.69	-1.06	1.07
104709	Phosphoinositide-3-kinase, regulatory subunit 6	1.69	1.04	-1.17
170753	Zinc finger protein 704	1.69	-1.34	-1.02
67105	RIKEN cdna 1700034H14 gene	1.69	-1.01	1.13
214498	Cell division cycle 73	1.69	-1.16	1.04
66979	Polymerase (DNA-directed), epsilon 4 (p12 subunit)	1.69	-1.19	1.15
54131	Interferon regulatory factor 3	1.68	-1.28	-1.11
56513	Par-6 (partitioning defective 6,) homolog alpha (C. Elegans)	1.68	1.01	1.06
29808	MAX gene associated	1.68	1.02	-1.01
117109	Processing of precursor 5, ribonuclease P/MRP family (S. Cerevisiae)	1.68	-1.11	1.01
240899	Leucine rich repeat containing 52	1.68	-1.26	-2.55
277562	Olfactory receptor 1286	1.67	-1.00	-1.18
71701	Polyribonucleotide nucleotidyltransferase 1	1.67	1.12	1.20
76784	Mitochondrial translational initiation factor 2	1.67	1.20	1.03
76894	Methyltransferase 5 domain containing 1	1.67	1.17	1.29
59015	Nucleoporin 160	1.67	-1.01	-1.08
20534	Solute carrier family 4 (anion exchanger), member 1, adaptor protein	1.67	-1.04	-1.13
224630	BCL2/adenovirus E1B interacting protein 1, NIP1	1.67	1.13	1.08
320563	Immunoglobulin superfamily containing leucine-rich repeat 2	1.67	-1.52	-1.13
13859	Epidermal growth factor receptor pathway substrate 15-like 1	1.66	-1.03	-1.03
210148	Solute carrier family 30 (zinc transporter), member 6	1.66	-1.14	1.16
217031	Transcriptional adaptor 2 (ADA2 homolog, yeast)-like	1.66	-1.01	1.11
103012	RIKEN cdna 6720401G13 gene	1.66	1.32	1.16
78408	RIKEN cdna 2900046G09 gene	1.66	-1.01	1.22

GeneID	Gene name	HIF1 ratio	HIF2 ratio	HIF1/2 ratio
69757	Leukocyte receptor cluster (LRC) member 1	1.65	1.16	1.15
23897	HCLS1 associated X-1	1.65	-1.04	1.00
26407	Mitogen-activated protein kinase kinase kinase 4	1.65	-1.07	1.12
66574	RIKEN cdna 2510017J16 gene	1.65	1.48	-1.05
13644	Embryonal Fyn-associated substrate	1.64	-1.04	1.25
18854	Promyelocytic leukemia	1.64	1.06	1.12
244895	RIKEN cdna C230081A13 gene	1.64	1.11	1.01
78785	CAP-GLY domain containing linker protein family, member 4	1.64	1.46	1.12
258409	Olfactory receptor 1431	1.64	-1.00	-1.02
74114	Carnitine O-octanoyltransferase	1.64	1.09	1.07
268281	SNF2 histone linker PHD RING helicase	1.64	-1.03	1.09
56695	Paroxysmal nonkinesiogenic dyskinesia	1.64	1.22	1.13
236732	RNA binding motif protein 10	1.63	-1.07	-1.06
71382	Peroxisome biogenesis factor 1	1.63	-1.06	1.04
78323	RIKEN cdna 2310046O06 gene	1.63	-1.03	-1.13
547150	Similar to p47 protein	1.63	-1.10	1.24
210766	BRCA1/BRCA2-containing complex, subunit 3	1.63	1.03	1.16
18174	Solute carrier family 11 , member 2	1.63	-1.33	1.13
330963	Predicted gene, EG330963	1.63	1.11	1.23
66050	RIKEN cdna 0610009B22 gene	1.63	1.04	1.18
26371	Cytosolic iron-sulfur protein assembly 1 homolog (S. Cerevisiae)	1.63	-1.02	-1.07
72016	RIKEN cdna 1600002H07 gene	1.63	-1.05	-1.11
12338	Calpain 6	1.62	1.66	1.02
66609	Crystallin, zeta (quinone reductase)-like 1	1.62	1.27	1.09
17101	Lysosomal trafficking regulator	1.62	-1.07	1.01
94223	Digeorge syndrome critical region gene 8	1.62	-1.00	-1.10
319953	Tubulin tyrosine ligase-like 1	1.62	1.09	1.12
223483	Hypothetical protein A830021M18	1.62	-1.16	-1.25
15468	Protein arginine N-methyltransferase 2	1.62	-1.24	1.06
239318	Phosphatidylinositol-specific phospholipase C, X domain containing 3	1.62	-1.20	-1.05
67892	RIKEN cdna 1810063B05 gene	1.61	1.01	1.20
23954	NIMA (never in mitosis gene a)-related expressed kinase 3	1.60	1.14	1.03
30057	Translocase of inner mitochondrial membrane 8 homolog b (yeast)	1.60	1.05	1.23
330050	Expressed sequence AI847670	1.60	1.18	1.22

GeneID	Gene name	HIF1 ratio	HIF2 ratio	HIF1/2 ratio
209707	Ligand dependent nuclear receptor corepressor-like	1.60	-1.03	1.02
66454	Nicotinamide nucleotide adenylyltransferase 1	1.60	-1.07	1.11
193796	Jumonji domain containing 2B	1.60	1.18	-1.17
72320	RIKEN cdna 2510003E04 gene	1.60	-1.03	1.11
18749	Protein kinase, camp dependent, catalytic, beta	1.60	-1.02	1.13
72904	RIKEN cdna 2900034E22 gene	1.59	-1.13	-1.04
442825	RIKEN cdna A230083G16 gene	1.59	1.10	1.00
140486	Insulin-like growth factor 2 mrna binding protein 1	1.59	1.19	-1.01
68223	RIKEN cdna 1700063I17 gene	1.59	-1.22	-2.83
209462	HECT domain and ankyrin repeat containing, E3 ubiquitin protein ligase 1	1.59	1.01	1.31
52856	GTP binding protein 5	1.58	1.16	-1.07
74385	RIKEN cdna 4932432K03 gene	1.58	1.01	1.21
68033	COX19 cytochrome c oxidase assembly homolog (S. Cerevisiae)	1.58	-1.09	1.00
12530	Cell division cycle 25 homolog A (S. Pombe)	1.58	1.03	1.11
73412	Thioredoxin domain containing 3 (spermatozoa)	1.58	1.13	-1.10
20892	Stimulated by retinoic acid 13	1.58	1.08	1.15
22184	Zinc finger (CCCH type), RNA binding motif and serine/arginine rich 2	1.58	1.14	1.16
79264	KRIT1, ankyrin repeat containing	1.58	-1.21	-1.16
269608	Pleckstrin homology domain containing, member 5	1.58	1.14	-1.01
58805	MLX interacting protein-like	1.57	1.42	1.03
171236	Vomeronasal 1 receptor, F5	1.57	-1.00	-1.00
57443	F-box protein 3	1.57	-1.04	1.11
67667	Alkb, alkylation repair homolog 8 (E. Coli)	1.57	1.09	-1.11
75632	RIKEN cdna 1700003O11 gene	1.57	-1.46	1.01
68691	RIKEN cdna 1110028C15 gene	1.57	-1.11	1.26
78910	Ankyrin repeat and SOCS box-containing protein 15	1.56	-1.04	-1.00
241556	Tetraspanin 18	1.56	1.07	2.29
70733	RIKEN cdna 6330411E07 gene	1.56	-1.17	-1.15
22061	Transformation related protein 63	1.56	-1.40	-1.08
244417	Gene model 501, (NCBI)	1.56	1.04	-1.19
68033	COX19 cytochrome c oxidase assembly homolog (S. Cerevisiae)	1.56	-1.08	1.13

GeneID	Gene name	HIF1 ratio	HIF2 ratio	HIF1/2 ratio
67784	Plexin D1	1.55	1.28	-1.13
16882	Ligase III, DNA, ATP-dependent	1.55	-1.16	-1.18
18701	Phosphatidylinositol glycan anchor biosynthesis, class F	1.55	-1.10	1.16
260302	Golgi associated, gamma adaptin ear containing, ARF binding protein 3	1.55	-1.12	1.22
26428	Origin recognition complex, subunit 4-like (S. Cerevisiae)	1.55	1.11	1.26
18106	CD244 natural killer cell receptor 2B4	1.55	-1.27	-1.15
26407	Mitogen-activated protein kinase kinase kinase 4	1.55	-1.07	1.18
76686	CAP-GLY domain containing linker protein 3	1.55	1.21	1.34
75458	Chemokine-like factor	1.55	-1.14	1.06
225372	Amyloid beta (A4) precursor protein-binding, family B, member 3	1.55	1.10	-1.04
21853	Timeless homolog (Drosophila)	1.55	1.24	-1.11
68114	Melanoma associated antigen (mutated) 1	1.55	-1.11	-1.08
16650	Karyopherin (importin) alpha 6	1.54	-1.04	1.06
227327	UDP-glcnac:betagal beta-1,3-N-acetylglucosaminyltransferase 7	1.54	1.10	-1.39
68347	RIKEN cdna 0610011F06 gene	1.54	1.13	1.12
66880	Arginine/serine-rich coiled-coil 1	1.54	1.02	1.06
83429	Cystinosis, nephropathic	1.54	1.04	-1.12
258334	Olfactory receptor 1396	1.54	1.84	1.02
12724	Chloride channel 2	1.53	-1.14	1.05
104859	RIKEN cdna 4930573I19 gene	1.53	-1.10	-1.02
13728	MAP/microtubule affinity-regulating kinase 2	1.53	-1.02	-1.04
1E+08	Predicted gene, ENSMUSG00000052469	1.53	1.02	-1.20
57837	Era (G-protein)-like 1 (E. Coli)	1.53	1.07	-1.05
22702	Zinc finger protein 42	1.53	-1.08	1.19
75339	M-phase phosphoprotein 8	1.53	1.15	1.10
258402	Olfactory receptor 1079	1.53	-1.00	-1.80
170762	Nucleoporin 155	1.53	1.01	-1.04
67707	Mitochondrial ribosomal protein L24	1.53	1.25	1.30
56700	RIKEN cdna 0610031J06 gene	1.52	1.03	1.10
677296	Fc receptor-like 6	1.52	9.00	1.09
73327	RIKEN cdna 1700040I03 gene	1.52	1.18	1.04
321006	Vpr (HIV-1) binding protein	1.52	-1.19	1.05
1E+08	Butyrophilin-like 1	1.52	-1.18	-1.08

GeneID	Gene name	HIF1 ratio	HIF2 ratio	HIF1/2 ratio
227154	Amyotrophic lateral sclerosis 2 (juvenile)	1.52	1.01	1.22
223646	Nicotinate phosphoribosyltransferase domain containing 1	1.51	1.27	1.26
59125	NIMA (never in mitosis gene a)-related expressed kinase 7	1.51	1.35	-1.03
103677	Smg-6 homolog, nonsense mediated mrna decay factor (C. Elegans)	1.51	1.00	-1.00
320816	Ankyrin repeat domain 16	1.51	1.25	1.36
71989	RNA pseudouridylate synthase domain containing 4	1.51	-1.06	1.10
237943	G patch domain containing 8	1.51	-1.02	1.11
72519	Transmembrane protein 55A	1.51	1.06	1.05
12828	Collagen, type IV, alpha 3	1.51	1.98	1.35
60364	Downstream neighbor of SON	1.51	-1.04	-1.02
227326	G protein-coupled receptor 55	1.51	1.03	1.29
67706	Transmembrane protein 179B	1.51	-1.02	1.00
328580	Tubulin, gamma complex associated protein 6	1.50	1.07	1.03
231003	Kelch-like 17 (Drosophila)	1.50	1.06	1.07
216578	Poly(A) polymerase gamma	1.50	1.15	-1.56
216119	RIKEN cdna A130042E20 gene	1.50	1.05	-1.06
12810	Coagulation factor C homolog (Limulus polyphemus)	1.50	1.54	1.10
225998	RAR-related orphan receptor beta	1.48	1.85	1.14
258457	Olfactory receptor 108	1.47	1.86	-1.16
210417	Thrombospondin, type I, domain containing 7B	1.43	-1.00	-1.98
14654	Glycine receptor, alpha 1 subunit	1.43	-1.02	1.83
72892	RIKEN cdna 2900018K06 gene	1.43	1.98	-1.11
70950	RIKEN cdna 4921528I01 gene	1.38	1.96	1.09
71248	RIKEN cdna 4933428M09 gene	1.38	-1.17	-1.82
75506	RIKEN cdna 1700017I07 gene	1.38	-1.88	1.17
229707	RIKEN cdna 6330569M22 gene	1.37	-1.69	-1.21
13491	Dopamine receptor 4	1.36	-1.90	1.02
68126	Fumarylacetoacetate hydrolase domain containing 2A	1.36	1.60	1.30
258973	Olfactory receptor 1228	1.35	-2.55	-1.11
93790	Non imprinted in Prader-Willi/Angelman syndrome 2 homolog (human)	1.35	-1.14	1.55
69928	Apoptosis-inducing, TAF9-like domain 1	1.33	2.04	1.11
24057	Sh3 domain YSC-like 1	1.33	1.05	2.51
239368	Cdna sequence BC030476	1.30	1.14	-2.05

GeneID	Gene name	HIF1 ratio	HIF2 ratio	HIF1/2 ratio
27389	Dual specificity phosphatase 13	1.27	-1.51	1.05
258562	Olfactory receptor 1014	1.27	-2.27	-1.03
12788	Cyclic nucleotide gated channel alpha 1	1.27	-1.73	-1.33
74967	RIKEN cdna 4930474H20 gene	1.26	1.23	-2.21
67944	RIKEN cdna 1700025D03 gene	1.26	-1.12	2.89
13176	Deleted in colorectal carcinoma	1.25	2.20	-1.04
320899	RIKEN cdna A430110C17 gene	1.24	1.75	1.15
170725	Calpain 8	1.23	1.58	-1.00
170654	Keratin associated protein 16-4	1.23	-1.67	-1.02
67286	RAB, member of RAS oncogene family-like 5	1.23	1.63	1.05
237310	Interleukin 22 receptor, alpha 2	1.22	-1.18	2.25
19264	Protein tyrosine phosphatase, receptor type, C	1.22	-2.29	1.07
14177	Fibroblast growth factor 6	1.22	-1.16	-2.17
71229	RIKEN cdna 4933428P19 gene	1.22	1.06	2.56
328918	RIKEN cdna C230097I24 gene	1.21	-1.76	1.21
80986	Cytoskeleton associated protein 2	1.21	1.76	1.01
102060	Growth arrest and DNA-damage-inducible, gamma interacting protein 1	1.21	1.38	-1.95
77945	Retinitis pigmentosa gtpase regulator interacting protein 1	1.21	1.55	-1.08
27883	DNA segment, Chr 16, human D22S680E, expressed	1.20	1.54	1.15
224480	NADPH oxidase 3	1.19	-1.59	-1.21
16184	Interleukin 2 receptor, alpha chain	1.19	-1.24	1.59
67579	Cytoplasmic polyadenylation element binding protein 4	1.19	-2.11	1.04
16508	Potassium voltage-gated channel, Shal-related family, member 2	1.19	2.35	1.39
71701	Polyribonucleotide nucleotidyltransferase 1	1.19	2.35	1.08
382059	Defensin related cryptdin 22	1.18	2.01	1.13
111174	Trace amine-associated receptor 1	1.18	-1.32	-2.33
258356	Olfactory receptor 564	1.18	1.06	-2.74
80861	DEXH (Asp-Glu-X-His) box polypeptide 58	1.17	1.05	-2.47
27403	ATP-binding cassette, sub-family A (ABC1), member 7	1.17	-1.78	1.01
71388	RIKEN cdna 5530401A14 gene	1.17	-2.03	-1.04
319720	RIKEN cdna 9630028I04 gene	1.15	1.04	-1.74
241656	P21 (CDKN1A)-activated kinase 7	1.14	1.92	-1.09
258555	Olfactory receptor 862	1.12	2.06	1.19

GeneID	Gene name	HIF1 ratio	HIF2 ratio	HIF1/2 ratio
56790	DNA segment, Chr 3, ERATO Doi 300, expressed	1.11	-1.00	-2.13
74438	Retinaldehyde binding protein 1-like 1	1.11	-1.10	-1.63
70147	RIKEN cdna 2210019I11 gene	1.09	-1.14	-1.56
381072	ATP-binding cassette, sub-family A (ABC1), member 17	1.09	5.12	1.17
229521	Synaptotagmin XI	1.09	-1.98	-1.11
101533	Kallikrein related-peptidase 9	1.08	-1.38	1.79
110606	Farnesyltransferase, CAAX box, beta	1.06	1.87	1.14
245847	Amidohydrolase domain containing 2	1.05	2.46	1.29
328839	Predicted gene, EG328839	1.05	-1.85	1.10
14057	Sideroflexin 1	1.04	-1.62	-2.00
70954	RIKEN cdna 4922502B01 gene	1.04	-1.00	-1.69
12417	Chromobox homolog 3 (Drosophila HP1 gamma)	1.04	-2.57	-1.03
258822	Olfactory receptor 39	1.04	1.36	2.62
258944	Olfactory receptor 351	1.03	-1.84	1.02
100647	Uroplakin 3B	1.02	1.15	-1.52
258393	Olfactory receptor 1325	1.02	-1.01	1.52
20234	Spermine binding protein	1.02	1.93	1.10
226646	NADH dehydrogenase (ubiquinone) Fe-S protein 2	1.01	1.71	1.01
76633	RIKEN cdna 1700112E06 gene	1.00	-2.39	1.07
269587	Erythrocyte protein band 4.1	-1.01	-1.08	-1.72
13110	Cytochrome P450, family 2, subfamily j, polypeptide 6	-1.02	1.57	-1.05
231413	G-rich RNA sequence binding factor 1	-1.02	1.57	1.06
74916	RIKEN cdna 1700066O22 gene	-1.04	-1.85	-1.03
75231	RIKEN cdna 4930529I22 gene	-1.04	3.03	-1.21
117606	Biregional cell adhesion molecule-related binding protein	-1.06	1.51	1.01
12411	Cystathionine beta-synthase	-1.06	1.72	1.17
16675	Keratin 27	-1.08	-2.71	1.03
21673	Deoxynucleotidyltransferase, terminal	-1.08	-2.26	-1.24
77900	RIKEN cdna 6720473M11 gene	-1.08	1.34	-1.93
69113	Alkb, alkylation repair homolog 3 (E. Coli)	-1.09	1.61	-1.14
11898	Argininosuccinate synthetase 1	-1.12	1.61	1.20
19177	Proteasome (prosome, macropain) subunit, beta type 7	-1.12	1.69	1.10
21366	Solute carrier family 6 (neurotransmitter transporter, taurine), member 6	-1.13	1.11	-1.69

GeneID	Gene name	HIF1 ratio	HIF2 ratio	HIF1/2 ratio
76117	Rho gtpase activating protein 15	-1.16	-2.13	-1.00
277414	Transformation related protein 53 inducible protein 11	-1.17	2.04	-1.07
75089	UHRF1 (ICBP90) binding protein 1-like	-1.17	-1.19	-1.53
74841	Ubiquitin specific peptidase 38	-1.18	1.19	-1.75
76937	RIKEN cdna 2810429I04 gene	-1.18	-1.71	-1.05
17339	Major intrinsic protein of eye lens fiber	-1.18	-1.23	1.79
93747	Enoyl Coenzyme A hydratase, short chain, 1, mitochondrial	-1.19	1.52	-1.17
320500	RIKEN cdna A930001M12 gene	-1.21	1.06	-1.95
56451	Succinate-coa ligase, GDP-forming, alpha subunit	-1.21	1.64	1.00
170788	Crumbs homolog 1 (Drosophila)	-1.22	-2.56	-1.05
109054	Prefoldin 4	-1.26	1.51	1.29
381062	RIKEN cdna 2210404J11 gene	-1.29	1.70	-1.07
107747	Aldehyde dehydrogenase 1 family, member L1	-1.30	1.83	-1.17
56461	Kv channel interacting protein 3, calsenilin	-1.31	1.98	1.11
102527	RIKEN cdna 6720458D17 gene	-1.31	-1.13	-1.76
69354	Solute carrier family 38, member 4	-1.35	2.14	-1.19
548632	Cdna sequence BC023719	-1.35	3.09	1.27
66898	BAI1-associated protein 2-like 1	-1.39	1.64	-1.13
234875	Tetratricopeptide repeat domain 13	-1.50	1.14	-1.31
20403	Intersectin 2	-1.50	1.12	-1.24
20788	Sterol regulatory element binding factor 2	-1.51	1.05	-1.23
14390	GA repeat binding protein, alpha	-1.51	1.13	-1.13
66368	RNA terminal phosphate cyclase domain 1	-1.51	1.10	-1.11
212111	Inositol polyphosphate-5-phosphatase A	-1.51	1.17	-1.09
66860	Tetratricopeptide repeat, ankyrin repeat and coiled-coil containing 1	-1.51	1.36	-1.35
216164	Downstream of Stk11	-1.52	1.12	-1.04
171580	Microtubule associated monoxygenase, 1	-1.53	-1.12	-1.27
18321	Olfactory receptor 23	-1.53	2.05	1.00
75608	Chromatin modifying protein 4B	-1.53	-1.02	-1.10
11566	Adenylosuccinate synthetase, non muscle	-1.53	1.07	-1.16
80914	Uridine-cytidine kinase 2	-1.53	-1.22	-1.08
53334	Golgi SNAP receptor complex member 1	-1.54	1.44	-1.19
28185	Translocase of outer mitochondrial membrane 70 homolog A (yeast)	-1.54	1.24	-1.25
21985	Tumor protein D52	-1.54	1.21	-1.16

GeneID	Gene name	HIF1 ratio	HIF2 ratio	HIF1/2 ratio
20317	Serine (or cysteine) peptidase inhibitor, clade F, member 1	-1.55	1.11	-1.32
21353	TRAF family member-associated Nf-kappa B activator	-1.55	1.13	-1.04
100273	Oxysterol binding protein-like 9	-1.55	1.65	-1.32
75007	RIKEN cdna 4930504E06 gene	-1.56	1.18	-1.47
51792	Protein phosphatase 2 (formerly 2A),alpha isoform	-1.56	1.38	-1.17
13612	EGF-like repeats and discoidin I-like domains 3	-1.56	-1.00	1.02
56532	Receptor-interacting serine-threonine kinase 3	-1.56	-1.07	-1.27
93737	Par-6 partitioning defective 6 homolog gamma (C. Elegans)	-1.56	1.17	-1.26
78808	Syntaxin binding protein 5 (tomosyn)	-1.56	1.13	-1.26
108121	U2 small nuclear ribonucleoprotein auxiliary factor (U2AF) 1	-1.57	1.21	-1.09
76273	Nedd4 family interacting protein 2	-1.57	1.21	-1.19
94088	Tripartite motif-containing 6	-1.57	1.57	1.55
76479	Survival motor neuron domain containing 1	-1.57	1.15	-1.08
234967	Solute carrier family 36 (proton/amino acid symporter), member 4	-1.58	1.17	-1.15
225888	Suppressor of variegation 4-20 homolog 1 (Drosophila)	-1.58	1.01	-1.26
11908	Activating transcription factor 1	-1.58	1.15	-1.22
52440	Tax1 (human T-cell leukemia virus type I) binding protein 1	-1.58	1.39	-1.22
50754	F-box and WD-40 domain protein 7, archipelago homolog (Drosophila)	-1.58	1.23	-1.29
57912	CDC42 small effector 1	-1.59	1.15	-1.33
66711	Shwachman-Bodian-Diamond syndrome homolog (human)	-1.60	1.41	-1.30
70834	Sperm associated antigen 9	-1.60	1.03	-1.49
214547	Src homology 2 domain-containing transforming protein E	-1.60	1.07	-1.55
77929	Yip1 domain family, member 6	-1.60	1.20	-1.07
71472	Ubiquitin specific peptidase 19	-1.60	1.27	-1.24
50770	Atpase, class VI, type 11A	-1.61	-1.04	-1.40
66674	RIKEN cdna 6330409N04 gene	-1.61	1.17	-1.09
233315	Myotubularin related protein 10	-1.61	1.01	-1.23
26443	Proteasome (prosome, macropain) subunit, alpha type 6	-1.61	1.17	-1.08
74159	Acyl-Coenzyme A binding domain containing 5	-1.62	-1.00	-1.13

GeneID	Gene name	HIF1 ratio	HIF2 ratio	HIF1/2 ratio
14118	Fibrillin 1	-1.63	1.12	1.04
224691	Zinc finger protein 472	-1.64	1.19	-1.13
69329	RIKEN cdna 1700003M02 gene	-1.64	1.26	1.03
66249	Partner of NOB1 homolog (S. Cerevisiae)	-1.64	-1.03	-1.21
66461	Protein tyrosine phosphatase, mitochondrial 1	-1.64	1.01	-1.08
20277	Sodium channel, nonvoltage-gated 1 beta	-1.64	1.36	-1.19
208449	Sphingomyelin synthase 1	-1.64	1.15	-1.29
16803	Lipopolysaccharide binding protein	-1.65	1.33	-1.44
76267	Fatty acid desaturase 1	-1.65	1.43	-1.17
12913	Camp responsive element binding protein 3	-1.66	1.24	-1.40
19043	Protein phosphatase 1B, magnesium dependent, beta isoform	-1.66	1.35	-1.42
69743	Castor homolog 1, zinc finger (Drosophila)	-1.66	-1.06	-1.27
242691	G patch domain containing 3	-1.66	1.18	-1.23
27984	EF hand domain containing 2	-1.66	1.17	-1.28
56389	Syntaxin 5A	-1.66	1.26	-1.34
59028	RNA terminal phosphate cyclase-like 1	-1.66	1.04	-1.55
228859	RIKEN cdna D930001I22 gene	-1.67	1.00	-1.30
16923	SH2B adaptor protein 3	-1.67	1.09	-1.29
98238	Leucine rich repeat containing 59	-1.67	1.22	-1.45
55963	Solute carrier family 1 , member 4	-1.67	1.16	-1.25
68705	General transcription factor IIF, polypeptide 2	-1.67	1.15	-1.22
18570	Programmed cell death 6	-1.67	1.14	-1.20
68098	Ring finger and CHY zinc finger domain containing 1	-1.67	1.11	-1.15
79555	Cdna sequence BC005537	-1.68	1.12	-1.27
210529	RIKEN cdna G430022H21 gene	-1.68	-1.00	1.32
70354	RIKEN cdna 3110001I20 gene	-1.68	1.16	-1.45
12834	Collagen, type VI, alpha 2	-1.69	-1.20	-1.05
22688	Zinc finger protein 26	-1.69	1.03	-1.01
19725	Regulatory factor X, 2 (influences HLA class II expression)	-1.69	-1.07	-1.06
77446	HEG homolog 1 (zebrafish)	-1.69	1.15	-1.50
226352	Erythrocyte protein band 4.1-like 5	-1.69	1.21	-1.29
258908	Olfactory receptor 853	-1.70	-1.30	-1.29
66193	RIKEN cdna 1110049F12 gene	-1.70	1.29	-1.11
22022	Protein-tyrosine sulfotransferase 2	-1.70	1.12	-1.24

GeneID	Gene name	HIF1 ratio	HIF2 ratio	HIF1/2 ratio
232807	Protein phosphatase 1, regulatory (inhibitor) subunit 12C	-1.70	1.25	-1.31
215449	RAS related protein 1b	-1.71	1.07	-1.10
15007	Histocompatibility 2, Q region locus 10	-1.71	1.44	-1.38
98758	Heterogeneous nuclear ribonucleoprotein F	-1.71	1.23	-1.27
54170	Ras-related GTP binding C	-1.71	1.36	-1.43
19042	Protein phosphatase 1A, magnesium dependent, alpha isoform	-1.72	1.30	-1.49
56494	Golgi SNAP receptor complex member 2	-1.72	1.26	-1.44
258573	Olfactory receptor 1020	-1.72	-1.00	-1.03
214968	Sema domain, transmembrane domain (TM), (semaphorin) 6D	-1.72	1.24	-1.60
105014	Retinol dehydrogenase 14 (all-trans and 9-cis)	-1.72	-1.13	-1.18
78893	CCR4-NOT transcription complex, subunit 10	-1.73	1.59	-1.13
100494	Zinc finger, AN1-type domain 2A	-1.73	1.08	-1.14
69860	Eukaryotic translation initiation factor 1A domain containing	-1.73	1.36	-1.51
56722	LPS-induced TN factor	-1.73	1.25	-1.23
19267	Protein tyrosine phosphatase, receptor type, E	-1.74	-1.28	-1.39
225020	Fasciculation and elongation protein zeta 2 (zygin II)	-1.74	1.45	-1.43
20437	Seven in absentia 1A	-1.74	1.37	-1.06
233908	Fusion, derived from t(12;16) malignant liposarcoma (human)	-1.74	1.57	-1.30
18613	Platelet/endothelial cell adhesion molecule 1	-1.76	1.33	-1.43
68904	Abhydrolase domain containing 13	-1.76	1.35	-1.41
110351	Rap1 gtpase-activating protein	-1.76	1.35	-1.46
223455	Membrane-associated ring finger (C3HC4) 6	-1.76	1.37	-1.11
108030	Lin-7 homolog A (C. Elegans)	-1.76	-1.17	1.02
56200	DEAD (Asp-Glu-Ala-Asp) box polypeptide 21	-1.77	-1.01	-1.29
208659	Cdna sequence BC029169	-1.77	-1.08	-1.25
67187	Zinc finger, MYND domain containing 19	-1.77	1.06	-1.50
242418	WD repeat domain 32	-1.78	1.09	-1.43
217410	Tribbles homolog 2 (Drosophila)	-1.78	1.17	-1.57
192897	Integrin beta 4	-1.78	-1.24	-1.08
70611	F-box protein 33	-1.78	-1.06	-1.31
239217	Potassium channel tetramerisation domain containing 12	-1.79	1.03	-1.07

GeneID	Gene name	HIF1 ratio	HIF2 ratio	HIF1/2 ratio
22156	Tuftelin 1	-1.79	1.28	-1.21
110651	Ribosomal protein S6 kinase polypeptide 3	-1.79	1.30	-1.35
74504	RIKEN cdna 2410018C17 gene	-1.80	1.20	-1.32
223827	Glycosyltransferase 8 domain containing 3	-1.80	-1.10	1.03
67010	RNA binding motif protein 7	-1.80	1.08	-1.28
17912	Myosin IB	-1.80	1.35	-1.20
232989	Heterogeneous nuclear ribonucleoprotein U-like 1	-1.80	1.29	-1.08
12616	Centromere protein B	-1.81	1.37	-1.46
66105	Ubiquitin-conjugating enzyme E2D 3 (UBC4/5 homolog, yeast)	-1.81	1.25	-1.22
18196	Neuron specific gene family member 1	-1.81	-1.08	-1.44
28035	Ubiquitin specific peptidase 39	-1.81	1.28	-1.22
20527	Solute carrier family 2 (facilitated glucose transporter), member 3	-1.81	1.12	-1.18
19087	Protein kinase, camp dependent regulatory, type II alpha	-1.82	1.14	-1.13
98985	CLP1, cleavage and polyadenylation factor I subunit, homolog	-1.82	1.21	-1.40
56550	Ubiquitin-conjugating enzyme E2D 2	-1.82	1.19	-1.08
50528	Transmembrane protease, serine 2	-1.82	1.08	-1.53
67557	La ribonucleoprotein domain family, member 6	-1.82	-1.22	-1.08
107702	Ribonuclease/angiogenin inhibitor 1	-1.82	1.16	-1.19
22034	Tnf receptor-associated factor 6	-1.83	1.08	-1.13
27965	Spastic paraplegia 21 homolog (human)	-1.83	1.67	-1.27
21985	Tumor protein D52	-1.83	1.09	-1.19
75909	Transmembrane protein 49	-1.84	1.41	-1.56
59069	Tropomyosin 3, gamma	-1.84	1.42	-1.19
16885	LIM-domain containing, protein kinase	-1.84	-1.22	-1.38
228790	Additional sex combs like 1 (Drosophila)	-1.84	1.12	-1.28
20224	SAR1 gene homolog A (S. Cerevisiae)	-1.84	1.11	-1.14
170736	Parvin, beta	-1.84	1.20	-1.48
69368	WD repeat and FYVE domain containing 1	-1.85	-1.02	-1.31
83431	Nuclear distribution gene E-like homolog 1 (A. Nidulans)	-1.85	1.40	-1.40
19042	Protein phosphatase 1A, magnesium dependent, alpha isoform	-1.85	1.25	-1.37
15006	Histocompatibility 2, Q region locus 1	-1.85	1.70	-1.29
16012	Insulin-like growth factor binding protein 6	-1.85	1.57	-1.14
56462	Mitochondrial carrier homolog 1 (C. Elegans)	-1.85	1.37	-1.28

GeneID	Gene name	HIF1 ratio	HIF2 ratio	HIF1/2 ratio
74596	CDP-diacylglycerol synthase 1	-1.86	1.31	-1.38
12343	Capping protein (actin filament) muscle Z-line, alpha 2	-1.86	1.26	-1.10
72508	Ribosomal protein S6 kinase, polypeptide 1	-1.86	1.39	-1.32
16190	Interleukin 4 receptor, alpha	-1.86	1.18	-1.46
66105	Ubiquitin-conjugating enzyme E2D 3 (UBC4/5 homolog, yeast)	-1.86	1.27	-1.26
15357	3-hydroxy-3-methylglutaryl-Coenzyme A reductase	-1.87	1.23	-1.17
223433	Cdna sequence BC052328	-1.87	1.32	-1.38
11308	Abl-interactor 1	-1.87	1.29	-1.30
67951	Tubulin, beta 6	-1.87	-1.05	-1.25
109163	RIKEN cdna 3010003L21 gene	-1.87	-1.14	-1.58
66930	Fibronectin type 3 and ankyrin repeat domains 1	-1.87	1.07	-1.03
57439	Transmembrane protein 183A	-1.87	1.07	-1.40
69718	Inositol polyphosphate multikinase	-1.87	-1.02	-1.14
225280	RIKEN cdna D030070L09 gene	-1.88	1.32	-1.37
22433	X-box binding protein 1	-1.88	1.19	-1.33
192897	Integrin beta 4	-1.88	-1.42	1.03
74325	Clathrin, light polypeptide (Lcb)	-1.88	1.14	-1.25
52014	Nuclear undecaprenyl pyrophosphate synthase 1 homolog	-1.88	1.07	-1.41
67946	Spermatogenesis associated 6	-1.89	1.51	-1.28
107566	ADP-ribosylation factor-like 2 binding protein	-1.89	1.23	-1.47
15467	Eukaryotic translation initiation factor 2 alpha kinase 1	-1.89	-1.06	-1.05
208659	Cdna sequence BC029169	-1.89	-1.09	-1.27
29809	RAB gtpase activating protein 1-like	-1.89	1.14	-1.48
66500	Solute carrier family 30 (zinc transporter), member 7	-1.89	1.19	-1.24
18008	Nestin	-1.90	-1.27	-1.56
218518	MARVEL (membrane-associating) domain containing 2	-1.90	-1.01	-1.35
15502	Dnaj (Hsp40) homolog, subfamily A, member 1	-1.90	1.20	-1.24
215449	RAS related protein 1b	-1.90	1.21	-1.17
15502	Dnaj (Hsp40) homolog, subfamily A, member 1	-1.90	1.40	-1.22
14972	Histocompatibility 2, K1, K region	-1.92	1.35	-1.10
50523	Large tumor suppressor 2	-1.92	1.12	-1.21

GeneID	Gene name	HIF1 ratio	HIF2 ratio	HIF1/2 ratio
193670	Ring finger protein 185	-1.92	1.38	-1.36
13136	CD55 antigen	-1.92	-1.31	-1.22
20708	Serine (or cysteine) peptidase inhibitor, clade B, member 6b	-1.92	-1.06	-1.18
233908	Fusion, derived from t(12;16) malignant liposarcoma (human)	-1.92	1.71	-1.38
14155	Feminization 1 homolog b (C. Elegans)	-1.93	1.39	1.12
236794	Solute carrier family 9 (sodium/hydrogen exchanger), member 6	-1.93	1.08	-1.23
14296	Frequently rearranged in advanced T-cell lymphomas	-1.93	1.19	-1.42
12827	Collagen, type IV, alpha 2	-1.93	1.22	-1.28
24128	5'-3' exoribonuclease 2	-1.94	1.46	-1.22
66748	RIKEN cdna 4933404M02 gene	-1.96	1.15	-1.01
26367	CEA-related cell adhesion molecule 2	-1.96	-1.44	-1.39
78655	Eukaryotic translation initiation factor 3, subunit J	-1.97	-1.03	-1.23
239217	Potassium channel tetramerisation domain containing 12	-1.97	1.15	-1.16
74732	Syntaxin 11	-1.98	1.28	-1.06
13723	Embigin	-1.98	-1.02	-1.83
11752	Annexin A8	-1.99	-1.10	-1.13
98267	Serine/threonine kinase 17b (apoptosis-inducing)	-1.99	1.34	-1.08
19159	Pleckstrin homology, Sec7 and coiled-coil domains 3	-1.99	1.33	-1.30
268294	Zinc finger and BTB domain containing 24	-1.99	1.50	-1.12
16891	Lipase, endothelial	-2.00	1.08	-1.08
80907	Lactamase, beta	-2.00	1.42	-1.23
71013	RIKEN cdna 4933400F03 gene	-2.00	-1.01	-1.10
70231	Golgi reassembly stacking protein 2	-2.01	1.21	-1.40
243538	Coiled-coil domain containing 37	-2.01	1.04	-1.11
319622	RIKEN cdna E030018N11 gene	-2.01	1.21	-1.16
381217	Gene model 967, (NCBI)	-2.01	1.19	-1.49
69035	Zinc finger, DHHC domain containing 3	-2.01	1.04	-1.31
75533	Non-metastatic cells 5, (nucleoside-diphosphate kinase)	-2.01	1.20	-1.00
22688	Zinc finger protein 26	-2.01	1.57	-1.17
19697	V-rel reticuloendotheliosis viral oncogene homolog A (avian)	-2.01	1.06	-1.44
330836	Solute carrier family 7 , member 6	-2.02	1.55	-1.40
69863	RIKEN cdna 1810054D07 gene	-2.02	1.15	-1.20

GeneID	Gene name	HIF1 ratio	HIF2 ratio	HIF1/2 ratio
237806	Dynein, axonemal, heavy chain 9	-2.02	-1.00	1.19
13386	Delta-like 1 homolog (Drosophila)	-2.02	1.01	-1.62
21927	Tumor necrosis factor, alpha-induced protein 1 (endothelial)	-2.03	1.27	-1.35
21983	Trophoblast glycoprotein	-2.03	1.47	-1.26
52502	Calcium regulated heat stable protein 1	-2.03	1.08	-1.22
20674	SRY-box containing gene 2	-2.03	-1.14	-1.11
320791	RIKEN cdna A130071D04 gene	-2.04	-1.27	1.16
53312	Negative regulator of ubiquitin-like protein 1	-2.05	1.57	-1.32
94214	Sparc/osteonectin, cwcv and kazal-like domains proteoglycan 2	-2.05	1.24	-1.21
74122	Transmembrane protein 43	-2.05	-1.07	-1.42
94242	Tubulointerstitial nephritis antigen-like	-2.06	1.15	-1.31
58801	Phorbol-12-myristate-13-acetate-induced protein 1	-2.06	1.33	1.08
18263	Ornithine decarboxylase, structural 1	-2.08	1.81	-1.33
16418	Eukaryotic translation initiation factor 6	-2.08	1.16	-1.18
22041	Transferrin	-2.08	-1.12	-1.88
70747	Tetraspanin 2	-2.09	-1.04	-1.09
24109	Ubiquitin-like 3	-2.09	1.25	-1.36
76964	RIKEN cdna 2610028H24 gene	-2.09	1.30	1.03
381511	Protein phosphatase 2C, magnesium dependent, catalytic subunit	-2.09	1.40	-1.05
320982	ADP-ribosylation factor-like 4C	-2.10	1.38	-1.27
15982	Interferon-related developmental regulator 1	-2.10	1.20	-1.14
195733	Grainyhead-like 1 (Drosophila)	-2.10	1.15	1.06
24063	Sprouty homolog 1 (Drosophila)	-2.11	1.04	-1.27
68098	Ring finger and CHY zinc finger domain containing 1	-2.11	1.25	-1.17
66922	Related RAS viral (r-ras) oncogene homolog 2	-2.11	1.23	-1.57
225363	Eukaryotic translation termination factor 1	-2.12	1.19	-1.05
11668	Aldehyde dehydrogenase family 1, subfamily A1	-2.12	1.10	1.01
11911	Activating transcription factor 4	-2.12	1.45	-1.28
19883	RAR-related orphan receptor alpha	-2.13	1.34	-1.29
12953	Cryptochrome 2 (photolyase-like)	-2.13	1.39	-1.36
69131	Cdc2-related kinase, arginine/serine-rich	-2.13	1.07	-1.45
69660	Transmembrane BAX inhibitor motif containing 1	-2.13	1.18	-1.27
68800	RIKEN cdna 1110059M19 gene	-2.13	-1.24	-1.72

GeneID	Gene name	HIF1 ratio	HIF2 ratio	HIF1/2 ratio
13609	Endothelial differentiation sphingolipid G-protein-coupled receptor 1	-2.13	1.25	-1.19
23970	Protein kinase C and casein kinase substrate in neurons 2	-2.13	1.41	-1.65
68159	Syntaxin 19	-2.14	1.04	-1.10
66849	Protein phosphatase 1, regulatory (inhibitor) subunit 2	-2.14	1.01	-1.27
22135	Trans-golgi network protein 2	-2.14	1.01	-1.56
381741	Leucine rich repeat containing 43	-2.14	-1.07	1.00
56403	Synaptotagmin binding, cytoplasmic RNA interacting protein	-2.15	1.16	-1.21
14461	GATA binding protein 2	-2.15	1.08	-1.27
68283	RIKEN cdna 9530077C05 gene	-2.15	-1.30	-1.27
70019	RIKEN cdna 2410039M03 gene	-2.16	-1.00	-1.03
14972	Histocompatibility 2, K1, K region	-2.17	1.22	-1.43
50708	Histone cluster 1, h1c	-2.17	1.99	-1.02
435337	Predicted gene, EG435337	-2.17	1.17	-1.23
110310	Keratin 7	-2.18	1.25	-1.30
269966	Nucleoporin 98	-2.18	1.21	-1.16
22092	Radial spoke head 1 homolog (Chlamydomonas)	-2.18	1.33	1.01
16782	Laminin, gamma 2	-2.18	1.33	-1.43
140579	Engulfment and cell motility 2, ced-12 homolog (C. Elegans)	-2.19	1.25	-1.45
56289	Ras association (ralgds/AF-6) domain family member 1	-2.20	1.12	-1.52
234797	RIKEN cdna 6430548M08 gene	-2.22	1.15	-1.06
219148	Cdna sequence BC065085	-2.22	1.59	-1.23
15357	3-hydroxy-3-methylglutaryl-Coenzyme A reductase	-2.22	1.14	-1.24
114332	Lymphatic vessel endothelial hyaluronan receptor 1	-2.22	1.11	-1.29
67122	Notch-regulated ankyrin repeat protein	-2.23	1.08	-1.33
75564	RIKEN cdna 1700027N10 gene	-2.23	-1.06	1.26
72147	Zinc finger and BTB domain containing 46	-2.23	1.17	-1.19
234734	Alanyl-trna synthetase	-2.23	1.28	-1.39
14570	Rho GDP dissociation inhibitor (GDI) gamma	-2.23	1.29	-1.07
75137	RIKEN cdna 4930535B03 gene	-2.23	1.94	-1.50
22436	Xanthine dehydrogenase	-2.23	1.40	-1.58
330260	Paraoxonase 2	-2.24	1.19	-1.41
68498	Tetraspanin 11	-2.24	-1.02	-1.98

GeneID	Gene name	HIF1 ratio	HIF2 ratio	HIF1/2 ratio
73075	Peptidylprolyl isomerase (cyclophilin)-like 6	-2.25	1.27	1.08
50926	Heterogeneous nuclear ribonucleoprotein D-like	-2.25	1.98	-1.15
58809	Ribonuclease, rnase A family 4	-2.25	-1.12	-1.50
12492	Scavenger receptor class B, member 2	-2.25	1.07	-1.28
64085	Calsyntenin 2	-2.26	-1.09	-1.16
71326	Triggering receptor expressed on myeloid cells-like 1	-2.26	-1.20	-1.38
13831	Enhancer of polycomb homolog 1 (Drosophila)	-2.26	1.05	-1.18
66540	RIKEN cdna 3110001A13 gene	-2.27	1.04	-1.39
75568	Calcyphosine-like	-2.28	1.11	1.18
56360	Acyl-coa thioesterase 9	-2.29	1.12	-1.38
383295	Yippee-like 5 (Drosophila)	-2.29	1.25	-1.24
74596	CDP-diacylglycerol synthase 1	-2.30	1.07	-1.39
69797	RIKEN cdna 1600029I14 gene	-2.30	1.07	1.06
14461	GATA binding protein 2	-2.31	1.23	-1.33
194655	Kruppel-like factor 11	-2.32	-1.15	-1.38
20568	Secretory leukocyte peptidase inhibitor	-2.32	-1.19	-1.22
19153	Periaxin	-2.34	1.18	-1.75
320769	Peroxiredoxin 6, related sequence 1	-2.34	1.08	-1.20
330260	Paraoxonase 2	-2.34	1.26	-1.43
218518	MARVEL (membrane-associating) domain containing 2	-2.35	1.61	-1.41
71667	RIKEN cdna 0610007L01 gene	-2.35	1.10	-1.29
66270	RIKEN cdna 1810015C04 gene	-2.36	1.72	-1.17
17764	Metal response element binding transcription factor 1	-2.36	1.33	-1.36
66629	Golgi phosphoprotein 3	-2.37	1.16	-1.31
20104	Ribosomal protein S6	-2.37	1.09	-1.38
71823	RIKEN cdna 3300002A11 gene	-2.38	-1.11	1.10
12986	Colony stimulating factor 3 receptor (granulocyte)	-2.38	-1.08	-1.07
228550	Inositol 1,4,5-trisphosphate 3-kinase A	-2.38	1.10	1.12
19243	Protein tyrosine phosphatase 4a1	-2.40	1.27	-1.08
22782	Solute carrier family 30 (zinc transporter), member 1	-2.40	1.23	-1.33
20388	Surfactant associated protein B	-2.40	-1.07	-1.81
71648	Optineurin	-2.40	1.50	-1.54
78781	Zinc finger CCCH type, antiviral 1	-2.42	1.48	-1.26
17713	Grpe-like 1, mitochondrial	-2.42	1.59	-1.52

GeneID	Gene name	HIF1 ratio	HIF2 ratio	HIF1/2 ratio
57349	Pro-platelet basic protein	-2.44	-1.62	-1.57
104009	Quiescin Q6 sulfhydryl oxidase 1	-2.45	1.28	-1.23
215449	RAS related protein 1b	-2.45	1.18	-1.14
317757	Gtpase, IMAP family member 5	-2.45	1.33	-1.66
66849	Protein phosphatase 1, regulatory (inhibitor) subunit 2	-2.46	1.45	-1.26
230678	Transmembrane protein 125	-2.46	-1.09	-1.15
74471	RIKEN cdna 4933440N22 gene	-2.47	1.15	-1.60
18286	Outer dense fiber of sperm tails 2	-2.48	1.62	-1.23
11987	Solute carrier family 7 , member 1	-2.48	-1.05	-1.43
69660	Transmembrane BAX inhibitor motif containing 1	-2.48	1.06	-1.21
170706	Transmembrane protein 37	-2.50	2.14	1.16
64898	Lipin 2	-2.50	1.29	-1.53
218215	Ring finger protein 144B	-2.52	1.32	-1.16
72477	Transmembrane protein 87B	-2.52	1.36	-1.16
11758	Peroxiredoxin 6	-2.53	1.14	-1.22
20515	Solute carrier family 20, member 1	-2.54	1.00	-1.27
18791	Plasminogen activator, tissue	-2.56	1.29	-1.72
18145	Niemann Pick type C1	-2.56	1.24	-1.52
74354	Leucine-rich repeats and guanylate kinase domain containing	-2.57	1.08	1.17
13649	Epidermal growth factor receptor	-2.57	-1.16	-1.60
12310	Calcitonin/calcitonin-related polypeptide, alpha	-2.58	1.16	1.02
94242	Tubulointerstitial nephritis antigen-like	-2.58	1.39	-1.27
75646	Retinoic acid induced 14	-2.58	1.02	-1.82
58220	Par-6 (partitioning defective 6) homolog beta (C. Elegans)	-2.59	1.23	-1.32
114332	Lymphatic vessel endothelial hyaluronan receptor 1	-2.63	1.68	-1.66
59043	WD repeat and SOCS box-containing 2	-2.63	1.26	-1.63
67876	Coenzyme Q10 homolog B (S. Cerevisiae)	-2.64	1.28	-1.28
320213	SUMO/sentrin specific peptidase 5	-2.64	1.13	-1.56
14221	Four jointed box 1 (Drosophila)	-2.64	1.21	-1.35
78801	Adenylate kinase 7	-2.66	-1.07	1.22
15982	Interferon-related developmental regulator 1	-2.68	1.33	-1.11
14623	Gap junction protein, beta 6	-2.69	1.23	-1.61
17130	MAD homolog 6 (Drosophila)	-2.70	-1.01	-1.54
13831	Enhancer of polycomb homolog 1 (Drosophila)	-2.70	1.16	-1.10

GeneID	Gene name	HIF1 ratio	HIF2 ratio	HIF1/2 ratio
73472	Spermatogenesis associated 18	-2.72	1.38	-1.24
64085	Calsyntenin 2	-2.73	1.18	-1.27
20278	Sodium channel, nonvoltage-gated 1 gamma	-2.74	1.32	-1.41
50930	Tumor necrosis factor (ligand) superfamily, member 14	-2.75	1.01	-1.34
66070	CWC15 homolog (S. Cerevisiae)	-2.76	-1.28	-1.03
17395	Matrix metallopeptidase 9	-2.77	-1.27	-1.36
236904	Kelch-like 15 (Drosophila)	-2.80	1.21	-1.05
56542	Intestinal cell kinase	-2.81	1.28	-1.20
21414	Transcription factor 7, T-cell specific	-2.81	-1.25	-1.68
101351	RIKEN cdna A130022J15 gene	-2.82	-1.11	-1.24
64833	Acyl-coa thioesterase 10	-2.82	1.26	-1.50
17395	Matrix metallopeptidase 9	-2.84	-1.12	-1.07
66166	S100 calcium binding protein A14	-2.86	-1.12	-1.71
67647	RIKEN cdna 4930523C07 gene	-2.87	1.19	-1.23
56717	FK506 binding protein 12-rapamycin associated protein 1	-2.90	1.63	-1.56
11845	ADP-ribosylation factor 6	-2.92	1.44	-1.63
382137	RIKEN cdna D630004A14 gene	-2.92	1.25	-1.10
11669	Aldehyde dehydrogenase 2, mitochondrial	-2.93	1.43	-1.12
18260	Occludin	-2.93	1.07	-1.55
226844	Feline leukemia virus subgroup C cellular receptor 1	-2.93	-1.14	-1.76
210992	Lysophosphatidylcholine acyltransferase 1	-2.93	-1.04	-2.52
66102	Chemokine (C-X-C motif) ligand 16	-2.93	1.15	-1.82
231991	Camp responsive element binding protein 5	-2.94	1.10	1.00
14102	Fas (TNF receptor superfamily member 6)	-2.95	1.04	-1.30
110911	CDP-diacylglycerol synthase (phosphatidate cytidylyltransferase) 2	-2.97	1.25	-1.58
66270	RIKEN cdna 1810015C04 gene	-2.98	1.56	-1.15
67109	Zinc finger protein 787	-2.99	1.28	-1.21
104263	Jumonji domain containing 1A	-3.01	1.56	-1.15
84004	Melanoma cell adhesion molecule	-3.02	1.36	-1.93
68947	Carbohydrate (N-acetylgalactosamine 4-0) sulfotransferase 8	-3.04	-1.15	-1.00
20863	Stefin A3	-3.10	-1.29	-1.40
20539	Solute carrier family 7 member 5	-3.13	1.41	-1.62
55948	Stratifin	-3.15	1.01	-1.11
66938	RIKEN cdna 1700029G01 gene	-3.16	1.59	-1.67

GeneID	Gene name	HIF1 ratio	HIF2 ratio	HIF1/2 ratio
66161	Processing of precursor 4, ribonuclease P/MRP family, (S. Cerevisiae)	-3.17	1.41	1.26
14674	Guanine nucleotide binding protein, alpha 13	-3.18	1.34	-1.42
69480	Tetratricopeptide repeat domain 9	-3.20	1.34	-1.87
78781	Zinc finger CCCH type, antiviral 1	-3.20	1.23	-1.26
12274	Complement component 6	-3.24	-1.20	-3.52
29815	Breast cancer anti-estrogen resistance 3	-3.26	1.30	-1.13
213208	Interleukin 20 receptor beta	-3.28	1.60	-1.39
20201	S100 calcium binding protein A8 (calgranulin A)	-3.28	-1.05	-1.45
319520	Dual specificity phosphatase 4	-3.30	-1.26	-1.53
56195	Polypyrimidine tract binding protein 2	-3.31	1.36	-1.43
66395	AHNAK nucleoprotein (desmoyokin)	-3.31	1.70	-1.72
20531	Solute carrier family 34 (sodium phosphate), member 2	-3.31	-1.01	-2.13
403205	Anterior gradient homolog 3 (Xenopus laevis)	-3.31	1.10	1.19
1E+08	Cdna sequence BC1179090	-3.32	-1.37	-1.37
74750	RIKEN cdna 5830410O09 gene	-3.33	-1.00	1.19
68603	Phosphomevalonate kinase	-3.38	1.12	-1.99
17474	C-type lectin domain family 4, member d	-3.41	1.11	-1.41
11501	A disintegrin and metallopeptidase domain 8	-3.42	-1.45	-1.01
109272	RIKEN cdna 8030451F13 gene	-3.42	-1.14	-1.37
17394	Matrix metallopeptidase 8	-4.20	1.34	-1.39
228765	Syndecan binding protein (syntenin) 2	-4.26	1.09	-1.86
71908	Claudin 23	-4.29	-1.16	-1.74
66849	Protein phosphatase 1, regulatory (inhibitor) subunit 2	-4.46	1.56	-1.35
76184	ATP-binding cassette, sub-family A (ABC1), member 6	-4.46	1.98	-1.48
75137	RIKEN cdna 4930535B03 gene	-4.73	1.68	-1.58
66895	RIKEN cdna 1300014I06 gene	-5.03	-1.21	-1.94
77914	Keratin associated protein 17-1	-5.12	-1.20	-1.97
268885	Stefin A2 like 1	-5.13	-1.11	-1.34
73389	High mobility group box transcription factor 1	-5.30	1.83	-1.17
56753	Tumor-associated calcium signal transducer 2	-5.62	1.10	-1.86
17879	Myosin, heavy polypeptide 1, skeletal muscle, adult	-5.66	-1.46	1.17
14066	Coagulation factor III	-5.78	1.42	-1.25

GeneID	Gene name	HIF1 ratio	HIF2 ratio	HIF1/2 ratio
13012	Cystatin 8 (cystatin-related epididymal spermatogenic)	-6.32	-1.56	-5.78
12654	Chitinase 3-like 1	-6.44	-1.34	-1.94
72432	Serine peptidase inhibitor, Kazal type 5	-6.77	-2.09	-3.26
16178	Interleukin 1 receptor, type II	-6.85	1.67	-1.14
245195	Resistin like gamma	-9.15	1.06	-1.39
20249	Stearoyl-Coenzyme A desaturase 1	-16.7	-1.08	-3.58